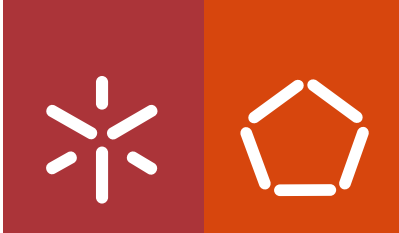**Universidade do Minho**
Escola de Engenharia

Claudia Sofia Lehmann Fernández

Optimization of laminated magnetoelectric structures based on electroactive polymers

January 2015

Universidade do Minho
Escola de Engenharia

Claudia Sofia Lehmann Fernández

Optimization of laminated magnetoelectric structures based on electroactive polymers

Doctoral Dissertation for PhD degree In Materials Engineering

Supervisor:
Professor Doutor Senenxtu Lánceros-Mendez

Co-supervisor:
Professor Doutor Luis Manuel Fernández Rebouta

January 2015

DECLARAÇÃO DE INTEGRIDADE

Declaro ter atuado com integridade na elaboração da presente tese. Confirmo que em todo o trabalho conducente à sua elaboração não recorri à prática de plágio ou a qualquer forma de falsificação de resultados.

Mais declaro que tomei conhecimento integral do Código de Conduta Ética da Universidade do Minho.

Universidade do Minho, _____ de _____ de _____

Nome completo: _____

Assinatura: _____

ACKNOWLEDGMENTS

"Appreciation is a wonderful thing. It makes what is excellent in others belong to us as well".

Voltaire

First of all, I would like to thank my Dad for having me promise to make a PhD in a foreign country after my bachelor graduation. Although taking the flight took me longer than expected, it was a once in a lifetime experience, that gave me more than I ever expected – knowledge, culture, family and friends –. For encouraging me I want to thank my family. For making this possible I would like to thank my advisor Dr. Senentxu Lanceros Méndez -for accepting me, and ERASMUS MUNDUS - VECCEU scholarship program and Academic Vice-Rectory and International Relations office of Minho University for their financial support.

My most deeply gratitude is to my advisor Dr. Senentxu Lanceros-Méndez, for giving me the opportunity to be a part of his exciting and ground-breaking research inside the Electroactive Smart Material Group of Minho University, for his impeccable guidance, supervision, constant support and the allowance of freedom during the entire course of this work. Besides his scientific rigour and devotion to research, I would like to thank him most of all, for his trust and confidence in my abilities, his professional and personable attitude, which guided me into bringing the best out of me and are inspiring qualities that I will embrace throughout my professional and personal life. I am grateful to my co-advisor, Dr. Luis Rebouta Fernandes, for his disposition, confidence and support.

This thesis would not have being possible without the help of Dr. Jon Gutierrez (of the Electricity and Electronic Department of Universidad del País Vasco), I would like to acknowledge him with gratitude for his advices and essential help in the data acquirement, that was crucial in this work. Our discussions have been enlightening and enjoyable.

I also would like to thank all the members of the Physics Department and Electroactive Smart Materials Group (ESMG) of University of Minho for taking me on board and accepting me on their stimulating, productive, professional and familiar research environment, for their help and cooperation. I must mention in particular Pedro Martins for his help, patience and guidance, as well as Marcos Martins, for his help during the early stages of my Ph.D., and finally I want to express my gratitude for working also with Marco Silva, Silvia Reis and Renato Gonçalves.

ABSTRACT

Polymer-based Magnetoelectric (ME) materials are becoming relevant in the development of new technologies for biomedical applications, sensors, actuators and recording devices, among others. The advance of technology has allowed the improvement of the know-how in order to generate new, enhanced and smaller devices. Furthermore, mathematical models and simulations are tools that have become a requirement to reduce costs, optimize features and to acquire fundamental knowledge on material properties to achieve new alternatives to develop these devices. This work is focused on the simulation of polymer-based magnetoelectric laminates, together with spherical, ellipsoidal and fibre composites, to obtain knowledge about the influence of their structure, mechanical, electrical and magnetic properties on the magnetoelectric response, as well as on the dimensional and assembly requirements for optimal functioning. The developed model considers magnetostrictive and electrostrictive domains coupled via strain.

The effect of size, bonding and configuration of poly(vinylidene fluoride) Vitrovac/PVDF laminated composites has been analysed and compared with the simulated response of lead zirconate titanate Vitrovac/PZT composites. Laminates composed by bi-layers, tri-layers and multi-layers have being analysed. It has been established that the elastic properties and amorphous constitution of PVDF is a key parameter governing its magnetoelectric performance, increasing its influence with increasing number of layers in the composite. Although configurations of multi-layers where the laminate is sandwiched between magnetostrictive layers (M-M configurations) presented more stable ME performances, the structural influence of PVDF in the configurations where the multi-layer is sandwiched between piezoelectric layers (P-P configurations) established peaks of ME performance, which should be further studied. Both configurations presented an improved behaviour for piezoelectric thicknesses below 150μm. PZT multi-layer laminates also showed lower ME performance for piezoelectric thicknesses above 200 μm, with an enhanced performance for M-M configurations with respect to P-P configurations with the same number of piezoelectric layers. Finally, configurations with an equal number of magnetostrictive and piezoelectric layers and constant volume (M-P configurations) showed generally an enhanced performance for thinner and larger number of layers than for bulk bi-layers. The effect of the bonding layer characteristics on the ME response of layered

poly(vinylidene fluoride) PVDF/epoxy/Vitrovac composites shows a reduction of the ME voltage coefficient from 53 V/cmOe to 6 V/cmOe with increasing epoxy Young Modulus from 2.7×10^8 Pa to 9.0×10^9 Pa, and an increase of the ME voltage coefficient from 45 V/cmOe to 53 V/cmOe with increasing PVDF thickness from 28 μm to 110 μm in a bi-layer.

Magnetoelectric (ME) spheres, ellipsoids, fibres and piezoelectric composites embedding magnetostrictive spheres all composed by cobalt ferrite ($CoFe_2O_4$, CFO) and PVDF, were also reported. Simulations results established improvement of the ME performance by increasing size or CFO weight concentration (wt.%) of the structures, as well as a direct relation between the maximal operational magnetic field and the normal surface of the structure exposed to the magnetic field, introducing the possibility of modifying the structures operational magnetic field range by changing the sphere´s eccentricity. Sphere´s and ellipsoidal structures with low eccentricity presented operational magnetic fields between 200-2000 Oe, decreasing progressively their operational magnetic field range and increasing their maximal ME performance for higher eccentricity values. Two groups of high eccentric ellipsoidal structures were reported: one that operates with magnetic fields lower than 20 Oe and a group of giant magnetoelectric fibres with an operational magnetic field range above 20 Oe and below 200 Oe. Fibres presented the lowest magnetic field operational range between 0-3 Oe, with the lowest ME coefficient values. For 50 wt.% CFO ME structures, spheres reached a maximal ME coefficient value (α_{ME}) of 182 V/cm with a maximal operational magnetic field of 684 Oe, the giant ME ellipsoidal structure (with eccentricity of 1200 nm) presented an α_{ME} of 4241 V/cm for a magnetic field of 208 Oe, the third group of high eccentricity ellipsoidal structures with eccentricity of 3200 nm presented an α_{ME} of 1601 V/cm for a magnetic field of 30 Oe, the fibres presenting the lowest values for ME coefficient and maximal operational magnetic field, of 14.7 V/cm for 1.3 Oe, respectively. Finally, the simulation of the cylindrical composite of CFO spheres embedded into a PVDF matrix established that the separation of the spheres is a key variable, obtaining higher ME performances and maximal operational magnetic field values for the experiment with 7 nm of separation between the CFO balls - 27.7 V/cm for 19 Oe, respectively-.

RESUMO

Materiais magnetoelétricos (ME) baseados em polímeros eletroativos são fundamentais no desenvolvimento de novas tecnologias em aplicações biomédicas, sensores, atuadores e aparelhos de gravação, entre outros. A evolução da tecnologia tem permitido avançar na transferência de conhecimento para a geração de novos dispositivos, melhorados e de menor dimensão. Além disso, a modelação matemática e as simulações são ferramentas que aparecem como requisito fundamental com vista à redução de custos e alcançar novas alternativas para construir esses dispositivos. Este trabalho de pesquisa foca-se na simulação do efeito ME em laminados, estruturas esféricas e elipsoidais, fibras e compósitos ME baseados em polímeros eletroativos. Tal simulação tem como objetivo primordial estudar o efeito da estrutura, das propriedades mecânicas e dos limites de operação dos materiais ME. O modelo estabelecido articula o funcionamento dos domínios magnetostritivos e piezoelétricos, introduzindo o acoplamento entre eles, através da transmissão de deformações.

No que diz respeito ao efeito ME em laminados, foi realizado um estudo acerca da influência do tamanho, tipo de colagem (entre lâminas magnetostritivas e piezoelétricas), e configuração de compósitos laminados de Poli(fluoreto de vinilideno) (PVDF)/Vitrovac na resposta ME do material. Esta resposta foi ainda comparada com o desempenho simulado de laminados de titanato zirconato de chumbo (PZT)/Vitrovac. Foram analisados compósitos de duas e três camadas e multicamadas. Os resultados estabelecem que a elasticidade e a estrutura amorfa do PVDF são parâmetros fundamentais de comportamento do PVDF. Esta influência torna-se ainda mais evidente quando o laminado é composto por um maior número de camadas. Nas configurações onde as lâminas piezoelétricas são "ensanduichadas" entre camadas magnetostritivas (configurações M-M), apresentaram desempenhos ME mais estáveis. Pelo contrário, nas configurações onde as lâminas magnetostritivas são "ensanduichadas" entre camadas piezoelétricas (configurações P-P), a influência estrutural da composição do PVDF gera picos no comportamento ME pelo que estes materiais deverão ser estudados com mais detalhe. Ambas as configurações mostraram um melhor comportamento para espessuras abaixo dos 150 μm. Laminados de PZT apresentaram um menor desempenho ME para espessuras do material piezoelétrico na ordem dos ≈200 μm, com um melhor desempenho da configuração M-M sobre a configuração P-P. Configurações com uma mesma quantidade de camadas e volume

constante (configurações M-P) são otimizadas com camadas mais finas, consequentemente com um maior número de camadas. O efeito do tipo de colagem na resposta ME de compósitos laminados de PVDF/cola/Vitrovac também foi estudado, tendo-se verificado uma redução de 53 V/cmOe a 6 V/cmOe com o aumento do Módulo de Young da cola de 2.7×10^8 Pa para 9.0×10^9 Pa, e um aumento do coeficiente ME de 45 V/cmOe a 53 V/cmOe quando a espessura do PVDF foi aumentada de 28 μm para 110 μm num compósito de duas camadas.

Estruturas ME de forma esférica e elípsoidal, fibras e compósitos piezoelétricos que incorporam esferas magnetostritivas, de PVDF e ferrita de cobalto ($CoFe_2O_4$, CFO) também foram alvos de estudo. Os resultados das simulações revelam uma tendência de aumento da resposta ME com o aumento do tamanho e da concentração de CFO, e uma relação direta entre a faixa de campo magnético de operação e a área normal da estrutura exposta ao campo magnético, desta forma verificou-se que existe a possibilidade de modificar a faixa de campo magnético de operação com a variação da excentricidade das estruturas elípticas. As estruturas esféricas e elipsoidais de baixa excentricidade apresentam campos magnéticos de operação entre 200-2000 Oe, diminuindo progressivamente o campo magnético ótimo de operação e aumentando o desempenho ME para valores de maior excentricidade. Verificou-se a existência de dois grupos de estruturas elipsoidais de grande excentricidade, relacionadas com os campos magnéticos de operação: o primeiro, com faixa de campo magnético operacional menor do que 20 Oe, e o grupo de grande resposta ME, que possuem uma faixa de campo magnético operacional entre 20 Oe e 200 Oe. As fibras apresentaram a faixa de campo magnético de operação menor, entre 0 e 3 Oe, com baixos coeficientes ME. Relativamente às esferas, as estruturas com 50 wt.% de CFO obtiveram um coeficiente ME máximo (α_{ME}) de 182 V/cm para o campo magnético (H_{max}) de 684 Oe, a elipsoidal de grande resposta ME (excentricidade 1200 nm) apresentou um α_{ME} de 4241 V/cm para um H_{max} de 208 Oe, e o terceiro grupo de excentricidade de 3200 nm apresentou um α_{ME} de 1601 V/cm para um H_{max} de 30 Oe. A fibra mostrou o valor mais baixo de α_{ME}, de 14.7 V/cm para um H_{max} de 1.3 Oe. Finalmente, a simulação do compósito cilíndrico com a inclusão de esferas de CFO numa matriz de PVDF, mostrou que a separação das esferas de CFO é uma variável chave, tendo sido obtidos os maiores valores de α_{ME} e de H_{max} para uma separação de 7 nm -27.7V/cm e 19 Oe, respetivamente-.

TABLE OF CONTENT

x

LIST OF FIGURES

xiv

xxii

LIST OF TABLES

LIST OF ABREVIATIONS

A

AC   alternate current

C

CFO   cobalt ferrite ($CoFe_2O_4$)

D

-D   dimensional (3-D, 2-D)

DC   direct current

E

EFE   electrically floating electrode

F

FEM   finite element method

G

GME   giant magnetoelectric effect

H

H-B curve   magnetic field - magnetic induction curve

L

LCMO $La_{0.7}Ca_{0.3}MnO_3$

LSMO $La_{0.7}Sr_{0.3}MnO_3$

M

ME   magnetoelectric

MEMS	micro-electro-mechanical systems
Metglas	$(Co_{0.93}Fe_{0.07})_{75-x}Cr_xSi_{15}B_{10}$, specific amorphous soft-magnetic alloy
M-M	magnetostrictive -magnetostrictive multi-layer configuration
M-P	magnetostrictive -piezoelectric multi-layer configuration
MPM	magnetostrictive-piezoelectric-magnetostrictive laminate
MPMPM	5 layered M-M structure
MPMPMPM	7 layered M-M structure
MPMPMPMPM	9 layered M-M structure
MS/ms	magnetostrictive

P

P-P	piezoelectric-piezoelectric multi-layer configuration
PMP	piezoelectric-magnetostrictive-piezoelectric laminate
PMPMP	5 layered M-M structure
PMPMPMP	7 layered M-M structure
PMPMPMPMPMP	11 layered M-M structure
PU	polyurethane elastomers
PVDF	polyvinylidene fluoride
P(VDF-TrFE)	poly(vinylidene trifluorethylene)
PZO/pzo	piezoelectric
PZT	Lead Zirconate Titanate $(Pb(ZrTi)O_3)$

S

SNR   signal to noise ratio

T

Terfenol-D $Tb_{1-x}Dy_xFe_2$

V

Vitrovac $(Fe_{39}Ni_{39}Mo_4Si_6B_{12})$ particular amorphous soft-magnetic alloy

LIST OF SYMBOLS

A

a   major axis of ellipsoidal structure

a_{CFO} major axis of magnetostrictive (CFO) ellipsoidal ME structure

a_{PZO} major axis of piezoelectric ellipsoidal ME structure

B

B   magnetic flux density (magnetic induction)

b   minor axis of ellipsoidal structure

b_{CFO} minor axis of magnetostrictive (CFO) ellipsoidal ME structure

b_{PZO} minor axis of piezoelectric ellipsoidal ME structure

B_r remanent magnetic induction

B_s saturation magnetic induction

C

C   structural damping matrix

c_E elasticity matrix

c_E^{-1} compliance matrix

D

D, *D*   electrical displacement field (flux density vector)

d_{33} piezoelectric coefficient

d_{3n} piezoelectric coefficients matrix

d_{im}, d_{jk}	third order piezoelectric strain coefficients
d_{pzo}	piezoelectric thickness (in centimetres)
D_c	thickness of the ME laminate composite
d_ms	magnetostrictive thickness of laminate
d_ms/d_pzo	thickness ratio of laminate
d_pzo	piezoelectric thickness of laminate
d_{sp}	spheres separation distance

E

E, E	local electric field strength, electric field vector
e	ellipsoidal eccentricity
e_s	piezoelectric stress matrix

F

F	Gibb´s free energy of the system
F_0	structural load vector
f	volume fraction
f_v	force per unit volume

H

H, H	magnetic field
H_{AC}	alternating current magnetic field
H_c	coercivity, magnetic coercive field

xxx

H_{DC} direct current magnetic field

H_{max} maximal operational magnetic field

H_s saturation magnetic field

J

J_0 current density

J_e electrical current to induce a magnetic field

K structural stiffness

k, k interface coupling coefficient (bonding)

K_d dielectric conductivity (vectorial notation)

K_z piezoelectric coupling matrix (vectorial notation)

K_σ dielectric permittivity matrix.

L

L interface length of the laminate

L_0 electrical load vector

M

M, M magnetization

M_0 structural mass

$\mathit{M_i}$ magnetization in the i-direction

$\mathit{m_i}$ magnetization direction cosine

M_r remanent magnetization

M_s saturation magnetization

N

N   number of layers

N_pzo number of piezoelectric layers

n-ratio   total magnetostrictive thickness over total piezoelectric thickness of laminates

N_u matrix of displacement shape functions

N_v vector of the electrical potential shape function

P

P, P polarization

Pr   remanent polarization

R

R   external radius of spherical or cylindrical geometries

r   internal radius of spherical or cylindrical geometries

S

S   strain tensor (vector)

S_0 initial strain tensor

S_E compliance coefficients matrix

S_k second order strain tensor

S_{km} fourth order elastic compliance tensor

T

T   temperature

T_m	stress tensor
U	
u, *u*	displacement tensor, vector of nodal displacements
u_c	displacement within element domain in the x, y, z directions
V	
V, *V*	electric potential, vector of nodal electrical potential
V_c	electrical potential within element domain
W	
wt.%	weight percent (concentration)
Y	
Y	Young modulus, elasticity modulus

LIST OF GREEK SYMBOLS

α	magnetoelectric coefficient (as function of thickness)
α_{ij}	magnetoelectric coefficient (second rank tensor)
α_{ME}	magnetoelectric coefficient
α_S	magnetoelectric susceptibility tensor
α_{unit}	unitary magnetoelectric coefficient
β	strain ratio
$\beta_{ijk}(T)$	higher order magnetoelectric coefficient (third rank tensor)
χ	susceptibility
δH_{AC}	AC magnetic field amplitude
$\Delta r, \Delta r_{pzo}$	piezoelectric thickness for spherical and cylindrical structures (R-r)
δV	induced magnetoelectric voltage
ε	dielectric constant, electric permittivity
ε_{ij}	dielectric permittivity (second rank tensor)
$\varepsilon_s, \boldsymbol{\varepsilon_s}$	relative permittivity, dielectric matrix (
φ	electric potential
Γ	displacement vector
γ_{ijk}	higher order magnetoelectric coefficients (third rank tensor)
$\lambda(H)$	induced magnetostrictive strain from the magnetic field

$\lambda_{\parallel}$	magnetostriction that is parallel to the magnetization
$\lambda_{\perp}$	magnetostriction that is perpendicular to the magnetization
λ_i	relative magnetostrictive deformation along the i-th direction
λ_{max}	maximal magnetostriction
λ_s	polycrystalline magnetostriction constant
μ_0	vacuum permeability
μ_{ik}	relative permeability matrix (second rank tensor)
μ_r	relative permeability
ν	Poisson´s ratio
ρ	mass density
ρ_v	free electric charge density
σ	Cauchy stress tensor
σ_0	initial stress tensor
τ	Curie temperature
Ψ	magnetic vector potential

CHAPTER 1: INTRODUCTION TO MAGNETOELECTRIC MATERIALS AND STRUCTURES

1.1. State of the Art

Magnetoelectric (ME) and multiferroic materials are gaining increasing attention from the fundamental and applied points of view. As technology evolves, the size of the devicesis getting smaller in order to achieve higheraccuracy and performance. This implies a growing need of knowledge on the fundamental of devices and their way to operate and a growing knowledge on new materials to achieve the requirements of the smaller and more qualified devices.

Multiferroic materials possess two—or all three—of the so-called 'ferroic' properties (ferroelectricity, ferromagnetism and ferroelasticity). ME coupling describes the influence of a magnetic (electric) field on the polarization (magnetization) of a material, in ME composites it appears indirectly via strain/stress, relating the influence of one material performance in the other.

Single phase materials in which ferromagnetism and ferroelectricity arise independently exist, but are rare (Eerenstein, Mathur, & Scott, 2006), with low ME performance at low temperature (D. a Pan, Bai, Chu, & Qiao, 2008). In order to improve these properties ME composites arise. Thus, composites with magnetostrictive (ms) and piezoelectric (pzo) phases provide the best ME systems available today. Several applications, ranging from magnetic field sensors to actuators, are being developed on the basis of these composite materials(Fuentes, Fuentes, Olivera, & García, 2007).

The use of magnetoelectric materials will allow a wide range of applications, including electrically controlled microwave phase shifters, magnetically controlled electro-optic or piezoelectric devices, broadband magnetic field sensors and memory devices, among others. For the materials to be technologically useful coupling must be achieved. A large effort should be devoted to develop composites with higher magnetoelectric coupling than single phase materials (Ramesh & Spaldin, 2007).

1.1.1. Basic concepts: multiferroic materials and magnetoelectric effect

The link between magnetic and electric properties allows the development of novel devices if the magnetic and electrical orders can be mutually controlled.

A single-phase multiferroic material is one that possesses two—or all three—of the so-called 'ferroic' properties: ferroelectricity, ferromagnetism and ferroelasticity. However, the current trend is to exclude the requirement for ferroelasticity, but to include the possibility of ferrotoroidic and antiferroic order (Eerenstein et al., 2006). Further, this definition has been expanded to include other long-range orders, for instance antiferromagnetism. Magnetoelectric (ME) switching in multiferroics can only be achieved if the magnetization and polarization are strongly coupled, which is a very unusual phenomenon (Seva V. V. Khikhlovsky, 2010).

The area of ME materials uses a complex taxonomy and typically involves not obvious terms. These lead to establish the following concepts (Eerenstein et al., 2006):

- ferroelectric materials possess spontaneous stable polarization that can be switched hysteretically by an applied electric field.

- ferromagnetic materials possess spontaneous stable magnetization that can be switched hysteretically by an applied magnetic field.

- ferroelastic materials possess spontaneous stable deformation that can be switched hysteretically by an applied stress.

- ferrotoroidic materials possess a stable and spontaneous order parameter that is taken to be the curl of a magnetization or polarization. This order parameter may be switchable.

- antiferroelectric materials possess ordered dipole moments that cancel each other completely within each crystallographic unit cell.

- antiferromagnetic materials possess ordered magnetic moments that cancel each other completely within each magnetic unit cell.

- ferrimagnetic materials differ from antiferromagnets because the magnetic moment cancellation is incomplete in such a way that there is a net magnetization that can be switched by an applied magnetic field

- piezoelectricity describes a change in strain as a linear function of applied electric field, or a change in polarization as a linear function of applied stress.

- piezomagnetism describes a change in strain as a linear function of applied magnetic field, or a change in magnetization as a linear function of applied stress.

- electrostriction describes a change in strain as a quadratic function of applied electric field.

- magnetostriction describes a change in strain as a quadratic function of applied magnetic field.

- magnetoelectric coupling: describes the influence of a magnetic (electric) field on the polarization (magnetization) of a material. The ME effect is defined by the electric field (**E**) induced under application of a magnetic field (**H**); or vice versa, by the magnetization variation induced under application of an electric field.

The phenomenon of magnetoelectricity was first proposed in 1894 by Pierre Curie, based on symmetry considerations in non-moving crystals. Already in 1988, Röntgen observed that a dielectric moving in a electric field could magnetize, but the reverse effect was not discovered until 1905, by Wilson, who observed the electrical polarization of a dielectric moving in a magnetic field (Pedro Martins & Lanceros-Méndez, 2013).

ME response has been found in a relatively small number of single-phase materials. General trends show that (Fuentes et al., 2007):

a) as rule, the effect is weaker than for composites;

b) ME coupling at room temperature is rare (practically only by $BiFeO_3$), and;

c) bismuth-layered perovskited, so called Aurivillius phases, are highly interesting materials in this field.

ME coupling may arise directly between the two order parameters or indirectly via strain. In strain-mediated indirect ME coupling, the magnetic and electrical order parameters arise in separate but intimately connected phases (Eerenstein et al., 2006).The research of these materials is practically related to efforts to switch the orientation of magnetic domains by the application of an electric field, and vice versa (Hur et al., 2004; Lottermoser et al., 2004). On these cases, crystal orientations and/or crystallographic textures play an important role in magnetoelectricity (bulk matter and thin films) (Fuentes et al., 2007).

Generally, the ME response of a material is described by the ME voltage coefficient (*α*$_{ME}$), defined as (Junyi Zhai, Xing, Dong, Li, & Viehland, 2008):

$$\alpha_{ME} = \delta E \Big/ \delta H \qquad ,$$ (1.1)

where *α*$_{ME}$ represents the rate of change of the electric field, *E*, induced under application of a magnetic field, *H*.

1.1.1.1. Coupling properties of single phase materials

In 1959 Landau and Lifshitz expressed theoretically the coupling between the magnetic and electric degrees freedom in one material (Landau & Lifshitz, 1959). Such materials show magnetization, which is proportional to an applied electric field and a polarization proportional to the applied magnetic field. This type of coupling is now known as the linear ME effect. It should be noted that only very few single-phase multiferroics are linear MEs (because of strict crystal symmetry requirements), therefore higher-order coupling terms usually dominate (Seva V. V. Khikhlovsky, 2010).

By the Landau theory, the ME effect in a single-phase crystal is described by the Gibbs free energy *F* of the system in terms of an applied magnetic field *H* and electric field *E*, whose *i-th* components are *H*$_i$ and *E*$_i$, respectively, by considering a non-ferroic material, where both, the electrical polarization *P*$_i$*(T)* and the magnetization *M*$_i$*(T)* (temperature, *T*, dependent), are zero in the absence of applied fields, with no hysteresis. An infinite, homogeneous and stress-free medium may be represented by the free energy *F*, under the Einstein summation convention, as (Eerenstein et al., 2006):

4

$$-F(E,H) = \frac{1}{2}\varepsilon_0\varepsilon_{ij}E_iE_j + \frac{1}{2}\mu_0\mu_{ij}H_iH_j + \alpha_{ij}E_iH_j + \frac{\beta_{ijk}}{2}E_iH_jH_k + \frac{\gamma_{ijk}}{2}H_iE_jE_k + \cdots \quad , (1.2)$$

where ε_o represents the permittivity of free space; the relative permittivity, $\varepsilon_{ij}(T)$, is a second-rank tensor; $\mu_{ij}(T)$, is the relative permeability; μ_o, is the permeability of free space, and:

- $\frac{1}{2}\varepsilon_0\varepsilon_{ij}E_iE_j + \frac{1}{2}\mu_0\mu_{ij}H_iH_j$ represents the resulting contribution from the electrical and

magnetic response to an electric and magnetic field, respectively.

- $\alpha_{ij}E_iH_j$ stands for linear ME coupling via $\boldsymbol{\alpha_{ij}(T)}$,

- $\frac{\beta_{ijk}}{2}E_iH_jH_k + \frac{\gamma_{ijk}}{2}H_iE_jE_k + \cdots$ shows the third-rank and higher order (quadratic)

tensors, where $\boldsymbol{\beta_{ijk}(T)}$ and $\boldsymbol{\gamma_{ijk}(T)}$ represent higher-order ME coefficients.

All ME coefficients incorporate the field independent material response functions $\varepsilon_{ij}(T)$ and $\mu_{ij}(T)$. The ME effect can also be established in the form $P_i(H_j)$ or $M_i(E_j)$ by differentiating F with respect to E_i and then setting $E=0$, or, involving H_i, establishing (Eerenstein et al., 2006):

$$P_i = \alpha_{ij}H_j + \frac{\beta_{ijk}}{2}H_jH_k + \cdots \tag{1.3}$$

$$\mu_0 M_i = \alpha_{ij}E_j + \frac{\gamma_{ijk}}{2}E_jE_k + \cdots \tag{1.4}$$

As ferroic materials display field hysteresis, they are better parameterized in terms of resultant rather than applied fields. In this way, it is possible to account for the potentially significant depolarizing/demagnetizing factors infinite media and the coupling constants would be functions only of temperature, as in the standard Landau theory (Eerenstein et al., 2006).

A multiferroic that is ferromagnetic and ferroelectric will often display large linear ME effects, because they normally possess a large permittivity and permeability respectively, and $\boldsymbol{\alpha_{ij}}$ is bounded by the geometric mean of the diagonalized tensors $\varepsilon_{ii}(T)$ and $\mu_{ii}(T)$, which allow the following condition (Eerenstein et al., 2006):

$$\alpha_{ij}^2 \leq \varepsilon_0 \mu_0 \varepsilon_{ii} \mu_{jj} \qquad\qquad (1.5)$$

Equation (1.5) is obtained from equation (1.2) by ignoring higher coupling terms, and forcing the sum of the first three terms to be larger than zero. This represents a stability condition on $\varepsilon_{ii}(T)$ and $\mu_{ii}(T)$. In the case of the coupling becoming too strong, driving a phase transition to a more stable state, then α_{ii}, $\varepsilon_{ii}(T)$ and $\mu_{ii}(T)$ would have to take new values in the new phase (Eerenstein et al., 2006).

Most materials show small values of either $\varepsilon_{ii}(T)$ or $\mu_{ii}(T)$, or both, so the linear ME effect will also be small, given that permittivity and permeability appears as a product in equation (1.5). However, not such restriction applies to higher-order couplings, such as those described by β_{ijk} and γ_{ijk}, and then **nonlinear coupling** will emerge (Eerenstein et al., 2006).

So far, linear and higher-order ME coupling has ignored the effects of strain. Such effects could be significant or even dominant. For example, the inclusion of piezomagnetism (magnetostriction) would generate cross terms in equation (1.2) that are proportional to strain and vary linearly (quadratically) with H_i. Analogous expressions would arise from piezoelectricity or electrostriction. Furthermore, mixed terms involving products of strain, H_i and E_i have been predicted. In two-phase materials, magnetic and electrical properties are strain-coupled by design in the quest for large ME effects. The strength of this **indirect coupling** is not restricted by equation (1.5), and enhancements over single-phase systems of several orders of magnitude have been achieved (Eerenstein et al., 2006).

1.1.1.2. Coupling on two-phase systems and composites

Van Suchtelen (Van Suchtelen, 1972) proposed three types of composite multiferroic materials, the ones with sum properties, those with product properties, and the combination of the two last ones (sum and product properties). A sum property of a composite reflects a weighted sum of the contributions from the individual component phases, proportional to the volume of weight fractions of these phases in the composite. A product property, is reflected in the composite structure but is absent in the individual phases. If one phase exhibits a property A→B (with a proportionality tensor dB/dA = X) and the second phase exhibits a property B→C (with a proportionality tensor dC/dB =Y) , then the composite will exhibit a property A→C which

6

is absent in either of the initial phases and the proportionality tensor dC/dA is the product of the proportionality tensor of the phases, where (Jungho Ryu, Priya, Uchino, & Kim, 2002):

$$\partial C \big/ \partial A = \partial C \big/ \partial B \cdot \partial B \big/ \partial A = Y \cdot X \qquad (1.6)$$

In this way, an alternative strategy for engineering enhanced ME effects is to introduce indirect coupling, via strain (Van Run, Terrell, & Scholing, 1974), between two materials such as a ferromagnet and a ferroelectric, obtaining a resultant material that will, via strain, interact between the magnetic and the electric domains. Each phase may then be independently optimized for room temperature performance.

In 1978, Van den Boomgaard (Van den Boomgaard & Born, 1978) outlined the conceptual issues inherent to the ME effect in composites, which can be summarized as (Jungho Ryu et al., 2002):

i. two individual phases should be in equilibrium;

ii. mismatching between grains should not be present ;

iii. magnitude of the magnetostriction coefficient of the magnetic phase and magnitude of the piezoelectric coefficient of the piezoelectric phase must be high;

iv. accumulated charge must not leak through the piezomagnetic or magnetostrictive phase;

v. the use of deterministic strategy for poling of the composites.

Most ferromagnetic materials show the magnetostrictive effect but not piezomagnetic effect. This means that the strain caused by a magnetic field in these materials is not linearly proportional to the field strength but is related to the square of the magnetic field strength, making the product property, the ME effect in the piezoelectric-magnetostrictive composites a non-linear effect and showing a hysteretic behaviour (Jungho Ryu et al., 2002).

Strain coupling requires intimate contact between a piezomagnetic (or magnetostrictive) material and a piezoelectric (or electrostrictive) material. This can be achieved in the form of (Eerenstein et al., 2006):

i.   composites (C. W. Nan, Liu, et al., 2002; Van Run et al., 1974)

ii. laminates (Jungho Ryu et al., 2001)

iii. epitaxial multi-layers (M. K. Lee, Nath, Eom, Smoak, & Tsui, 2000)

The coupling constant of the multiferroic structures depends on the frequency of the A.C. applied magnetic field (Bichurin, Filippov, et al., 2003a). Epitaxial thin-film heterostructures could allow precise ME studies, since the crystallographic orientation, layer thickness and interfacial roughness may be controlled accurately (Eerenstein et al., 2006).

The most efficient ME transducers are fabricated from magnetostricitve-piezoelectric composites (Fuentes et al., 2007). In multi-layer composite structures consisting of alternate layers of ferromagnetic and piezoelectric materials the ME coupling arises from product-properties of the phases. When the composite is placed in an external magnetic field δH, a deformation of the magnetic layer due to magnetostriction results in a deformation of the piezoelectric layer, leading to a polarization δP. The induced polarization is given by

$$\delta P = \alpha_S \cdot \delta H \qquad , \qquad\qquad (1.7)$$

being α_S the ME susceptibly tensor (Boomgaard, Terrell, Born, & Giller, 1974).

As the ME coupling describes the influence of a magnetic (electric) field on the polarization (magnetization) of a material, in ME composites it appears indirectly via strain/stresses a product tensor property (Van Suchtelen, 1972) that results from the cross interaction between the two phases in the composite, as a result of the product of the magnetostrictive effect (magnetic/mechanical) in the magnetic phase and the piezoelectric effect (mechanical/magnetic) in the piezoelectric phase (Y. Wang, Hu, Lin, & Nan, 2010).

Calculations based on magnetostrictive and piezoelectric parameters of the two phases predict the possibility of even higher ME coefficients (Bichurin, Petrov, & Srinivasan, 2002). The measured values are still relatively small in several systems possibly due to deterioration of magnetic and electrical properties of materials during the fabrication process (Srinivasan, Rasmussen, & Hayes, 2003; Srinivasan, Rasmussen, Bush, et al., 2003). Also, considerations

have to be made about the strain transmission in the interface that can be modified by the bonding properties.

1.2. Multiferroic magnetoelectric materials

In 1957, the linear α_S was predicted to occur in chromium oxide (Cr_2O_3)(Dzyaloshinskii, 1959). Then, in 1960s, α_S was experimentally observed (Astrov, 1960; Folen, Rado, & Stalder, 1961) to be non-zero below the antiferromagnetic Néel temperature of 307K, near which it peaked to a value of $\alpha_S = \partial P / \partial H \approx 0.0314\ Vcm^{-1}Oe^{-1}$ [1]. This work on chromium oxide led to other antiferromagnetic crystals, boracites and phosphates, such as Gd_2CuO_4, Sm_2CuO_4, $KNiPO_4$, $LiCoPO_4$ and $BiFeO_3$. In 1973, the research of ME materials research area reached a saturation point: no improvements were expected in the functionality of the applications of single-phase ME materials, due to no theoretical indications of improvements and weak ME coupling under the need of very low temperatures (Eerenstein et al., 2006; Pedro Martins & Lanceros-Méndez, 2013). However, a renaissance of the interest in ME materials in the 90´s was observed, when multiferroic and ME compounds, with higher ME coupling, appeared. On those materials, the ME coupling is obtained due to the elastic coupling between piezoelectric (electroactive) and magnetostrictive constituent phases, that interact due to elastic coupling (Pedro Martins & Lanceros-Méndez, 2013; C. Nan, Bichurin, Dong, Viehland, & Srinivasan, 2008).

1.2.1. Single-phase multiferroic magnetoelectric materials

In a single-phase material, the symmetry of the crystal is a key factor that determines the existence of ME effect (Srinivasan, 2010). The most widely studied and used ferroelectrics today are perovskite-structure oxides, ABO_3, which possess a cubic structure at high temperature. The cubic perovskite structure is characterized by a small cation, B, at the centre of an octahedron of oxygen anions, with large cations, A, at the unit cell corners. A structural distortion from a high symmetry type to a low symmetry type occurs below the Curie temperature. This distortion is

---

[1]Eerenstein *et al.*(Eerenstein et al., 2006) reported α_S=4.1x10^{-12}s/m. The relationship (s/m)=1.1x10^{-11}*ε_r (V/cmOe) was established to obtain α_S in the practical unit. The dielectric constant was established from Liu*et al.*(Y. Y. Liu, Xie, Jin, & Li, 2009). Other reports (Shuxiang Dong, Zhai, Li, & Viehland, 2006a) establish for Chromium oxide early room temperture magnetoelectric mesurements of α_S =2.67 x10^{-12}s/m=0.01 V/cmOe, as the highest value of single-phase materials.

accompanied by an off-centre shift of the small cation, which is the major factor giving rise to the spontaneous polarization (Seva V. V. Khikhlovsky, 2010). In 1958, Smolensky's group studied weakly ferromagnetic mixed perovskites, such as $(1-x)Pb(Fe_{2/3}W_{1/3})O_3 \cdot _xPb(Mg_{1/2}W_{1/2})O_3$(Smolensky, Isupov, & Agronovskaya, 1959). These were doped to increase resistivity, but boracite was the first highly insulating ferromagnetic ferroelectric to be studied (Ascher, Rieder, Schmid, & Stössel, 1966).

The perovskite $BiMnO_3$ is a low-temperature multiferroic(Chiba, Atou, & Syono, 1997; Sugawara, Iiida, Syono, & Akimoto, 1968). Ferromagnetic ordering below 105K is attributed to orbital ordering of the Mn3+ ions (3d4) and a large magnetization for polycrystalline samples is observed(Chiba et al., 1997). These samples tend to be electrically conducting, with restricted ferroelectricity to low temperatures. Multiferroic behaviour was observed at 80K (Kimura et al., 2003; Moreira dos Santos et al., 2002) which led to research into less-conducting samples..

1.2.2. Single-phase multiferroic magnetoelectric thin films

Single-phase multiferroic thin films of $BiFeO_3$ have been obtained and characterized. Their reported polarization, magnetization, and coupling parameters are higher than those of bulk $BiFeO_3$.The epitaxial films presented room-temperature spontaneous polarization of 50 to 60 $\mu C/cm^2$, nearly one order of magnitude superior than the bulk, of 6.1 $\mu C/cm^2$(J. Wang et al., 2003). Yun (Yun, Ricinschi, Noda, & Okuyama, 2005) finds similar polarization but smaller magnetization. Eerenstein and collaborators (Eerenstein et al., 2005a, 2005b) states that strain do not enhance properties in the way considered by Wang, Son *et al.*(Son, Kim, Kim, & Cho, 2004) describes the process of writing polarization bits on a multiferroic $BiMnO_3$ thin film by means of a Kevin probe force microscope, opening a tangible possibility of using ME thin films for data storage. Zheng *et al.* (H. Zheng, Wang, Lofland, Ma, Zhao, et al., 2004) published the important achievement of self-assembled $BaTiO_3$-$CoFe_2O_4$ multiferroic nanocomposites.

1.2.3. Magnetoelectric composites

The ME effect obtained in composites is more than a hundred times larger than for single-phase magnetoelectric materials such as Co_2O_3 (Jungho Ryu et al., 2002).Until now, three main

type of bulk magnetoelectric composites have been theoretically and experimentally investigated (Pedro Martins & Lanceros-Méndez, 2013), those are:

i. magnetic metals/alloys and piezoelectric ceramics

ii. laminated metals/alloys and piezoelectric polymers

iii. particulate composites of ferrite and piezoelectric ceramics.

The notation 0-3, 2-2, 1-3, etc. is used to describe the possible structures of two-phase composites (Newnham, Skinner, & Cross, 1978), where each number denotes the connectivity of each phase. The common connectivities examined so far include, as seen in Figure 1.1: a) 0-3 particulate nanocomposite films with magnetic particles embedded in a ferroelectric film, b) 2-2 horizontal heterostructures with alternating ferroelectric and magnetic layers, and c) 1-3 vertical heterostructures with one-phase nanopillars embedded in a matrix of another phase.
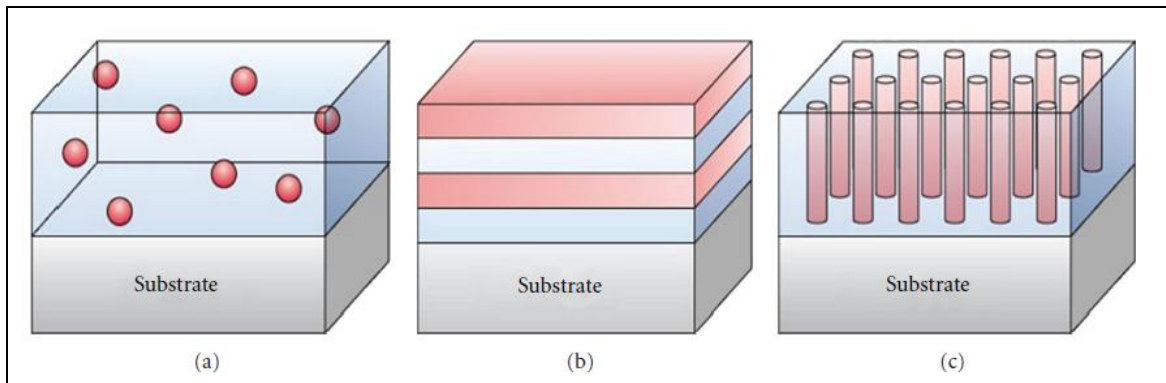
Figure 1.1: Schematic illustration of three ME composites with three common connectivity schemes: (a) Particulate composite, or 0-3, (b) Laminate composite, or 2-2, (c) fibre/rod composites, or 1-3 (Kambale, Jeong, & Ryu, 2012)

In the 1970's, just after the product ME property in composites combining magnetostrictive and piezoelectric phases was proposed by Van Suchtelen (Van Suchtelen, 1972), it was found experimentally(Boomgaard et al., 1974; Van den Boomgaard & Born, 1978)that a large ME effect could be produced in such composites in composites of $BaTiO_3$–$CoFe_2O_4$ prepared by unidirectional solidification of eutectic compositions. In the early 1990s,

Newnham's group (G. Harshe, Dougherty, & Newnham, 1993) and Russian scientists (Bichurin, Korneva, Petrova, & Lisnevskaya, 1997; Lopatin, Lopatin, & Lisnevskaya, 1994; Lupeiko, Lisnevskaya, Chkheidze, & Zvyagintsev, 1995) prepared particulate ceramic composites of ferrites and $BaTiO_3$or $Pb(ZrTi)O_3$ (Lead Zirconate Titanate, **PZT**) by a conventional sintering processing. However, these sintered ceramic composites showed lower ME coefficients than the prior eutectic composites (C. Nan et al., 2008). Srinivas *et al.* (K. Srinivas, Bhimasankaram, & Suryanarayana, 2000) characterized in detail the $PZT-CoFe_2O_3$ system, finding an optimal proportion of components and proposing a "sum rule" for the prediction of the electromechanical coupling coefficient. Srinivasan *et al.* (Srinivasan, Rasmussen, Bush, et al., 2003) studied and optimized, regarding chemical compositions, the influence of Zn substitutions.

In 2001, a breakthrough in the development of ME bulk composites occurred: the appearance of composites containing the giant magnetostrictive rare-earth-iron alloy $Tb_{1-x}Dy_xFe_2$ (**Terfenol-D**) (Shuxiang Dong, Cheng, Li, & Viehland, 2003; C.-W. Nan, Li, & Huang, 2001; J. Ryu, Priya, Carazo, Uchino, & Kim, 2001; Jungho Ryu et al., 2001). Particulate composites with Terfenol-D embedded in a piezoelectric polymer matrix such as polyvinylidene fluoride-trifluorethylene copolymer (P(VDF-TrFE)) or a piezoelectric ceramic matrix such as PZT, and laminate composites of Terfenol-D/P(VDF-TrFE) or Terfenol-D/PZT, were predicted to exhibit a giant ME effect (GME).Since then, Dong and co-workers have reported various laminate composites of Terfenol-D and piezoelectric ceramics (C. Nan et al., 2008). Ryu *et al.* (Jungho Ryu et al., 2002) established that magnetoelectric laminate composites made with Terfenol-D and relaxor-based piezocrystals show superior ME response. Carman and collaborators also obtained high ME voltage coefficients in a Terfenol-D/epoxy and PZT-5H [2-2] composite (Nersesse Nersessian, Or, Member, & Carman, 2004). Later, in order to overcome brittleness and high eddy current loss of the Terfenol-D disks used in two-phase Terfenol-D/piezoceramic composites, three-phase ME bulk composites of Terfenol-D/piezoceramics/polymer have been developed(C. Nan et al., 2008; C. W. Nan, Liu, et al., 2002; J. G. Wan et al., 2003).

1.2.3.1. Composite magnetoelectric thin films

Magnetoelectric films, in comparison to bulk composites, have some unique advantages (Y. Wang et al., 2010):

i. ferroelectric/piezoelectric and magnetostrictive phases could be tuned and controlled at the nanoscale, representing a new scale for exploring ME coupling mechanisms.

ii. the two constituent phases in bulk ME composites are usually combined by co-sintering or adhesive bonding, resulting in loss at the interface. In composite films, the different phases are combined at atomic level and interface losses could be reduced significantly.

iii. by combining different phases with similar crystal lattices, epitaxial or superlattice composite films can be designed, facilitating the understanding of ME coupling at the atomic scale.

The renaissance of multiferroic ME films has recently been accelerated by advances in thin-film growth techniques, such as the work of Zheng *et al.* (H. Zheng, Wang, Lofland, Ma, Mohaddes-Ardabili, et al., 2004). The new growth techniques have provided routes to novel structures and phases and allow the properties of traditional functional materials to be modified by strain engineering (Y. Wang et al., 2010).

The construction of laminated composites have been until now based on co-sintering or mechanical bonding methods (Shuxiang Dong et al., 2003; Shuxiang Dong, Zhai, Bai, Li, & Viehland, 2005; Srinivasan et al., 2001; Srinivasan, Rasmussen, Gallegos, et al., 2002). Although the co-sintering method is easy to perform, there are several limitations that influence the property of composites (Gao, 2013):

i. chemical reaction at higher sintering temperatures;

ii. non-ideal interfacial boundary between the two phases, like porous in ceramics,

iii. limited materials selection.

Although the first two limitations take the ME coefficients for laminated composites fabricated by co-sintering smaller than predicted, the use of mechanical bonding can also present imperfections that can reduce the ME coefficient, as shown by Silva *et al.* (M. Silva et al., 2013). Nevertheless, an epoxy bonding method is much more suitable for magnetic alloy and piezoelectric ceramic based ME laminated composites (Gao, 2013), because materials with

completely different properties can be bonded together mechanically (Shuxiang Dong, Li, & Viehland, 2004; Junyi Zhai, Dong, Xing, Li, & Viehland, 2006). For example, Terfenol-D is a magnetostrictive alloy with extremely high magnetostriction coefficients, but it is impossible to form composites by using the co-sintering method because the high sintering temperature for PZT would oxidize Terfenol-D (Gao, 2013). Mechanical bonding can solve this problem. Dong *et al.* have reported giant ME coefficient in PZT/Terfenol-D laminated composites (Shuxiang Dong, Zhai, Li, & Viehland, 2006b). More investigations on magnetic alloys and ceramic systems have been developed, such as Fe-Ga alloy, Galfenol, or Fe-B as Metglas/Vitrovac and PZT, PMN-PT or PVDF layers (Gao, 2013).

1.2.3.2. Magnetostrictive materials for magnetoelectric composites

Although the magnetostrictive phenomena was found in materials such as nickel, cobalt, iron and their alloys with saturation magnetostrictions on the order of 50 ppm (below 100 ppm) (Chakrabarti, 2011; Ralph C Smith, 2005), in the 1960 two simultaneous events change the course of magnetostrictive material´s research.

The first event occurred in 1963, when "giant" magnetostriction (on the order of 10000 ppm) was found to be exhibited in materials constituted by rare-earth elements (like terbium and dysprosium) at cryogenic temperatures (Chakrabarti, 2011; R C Smith, 1998; Ralph C Smith, 2005). In the 1970´s, the combination of these rare earth alloys with the transition metal iron was achieved (Clark & Belson, 1972; Koon, Schindler, & Carter, 1971; Ralph C Smith, 2005).. They proved to operate with giant magnetostrictive capabilities at room temperature, therefore reaching sufficiently large strain and forces to facilitate their use in actuators and sensors (Ralph C Smith, 1998, 2005). This led to the emergence of the magnetostrictive alloy Terfenol-D (Tb,DyFe, Terbium: Ter; Iron:Fe; Naval Ord. Lab.: NOL; dysprosium:D), which exhibits saturation magnetostriction values up to 1600 ppm with moderate applied fields (2500 Oe) (with values up to 3600 ppm at resonance) at room temperature (Chakrabarti, 2011; Ralph C Smith, 2005). As Terfenol-D is brittle (poor machinability and low tensile strength), with reduced hysteresis and anisotropic, a new magnetostrictive alloy of iron gallium (Galfenol) was developed (Chakrabarti, 2011; Ralph C Smith, 2005). Galfenol combines moderate magnetostriction (around 250 ppm) at lower fields of 125 Oe and steel-like structural properties (Chakrabarti, 2011).

14

The second event, is related to the discovery of amorphous metallic alloys or metallic glasses first in 1957 in a limited number of forms (typically ribbons, foils, or wires) (Klement, Willens, & Duwez, 1960). As consequence of their atomic disorder (with an isotropic and homogeneous structure in the microscopic scale) (Ojovana & Lee, 2010), properties as extremely high hardness and tensile strength, exceptionally good corrosion resistance and very low magnetic losses (in some of these soft magnetic materials) arise as some of the attractive properties associated with amorphous metallic alloys (Chen, 1980; Russell & Lee, 2006; Thomas et al., 2010). In 1976, after vitrification of metallic alloys became possible by using the technique of ultra-rapid quenching of molten alloys on a super-cooled fast-spinning wheel (Libermann & Graham, 1976), an alloy of iron, nickel, phosphorous and boron was synthesized and named Metglas (Roya & Majumdara, 1981). Later, multi-component alloys based on lanthanum, magnesium, zirconium, palladium, iron, copper, and titanium were developed at critical cooling rates between 1K/s to 100K/s (A. Inoue, 2000; S. Inoue, Inoue, Koterazawa, & Mizuuchi, 2003). These amorphous soft-magnetic alloys provide high saturation magnetostriction at low applied fields, low anisotropy energies and coercivity, easy fabrication and low cost (Chen, 1980; Thomas et al., 2010). Commercially available by the trend of Metglas($(Co_{0.93}Fe_{0.07})_{75-x}Cr_xSi_{15}B_{10}$) or Vitrovac ($Fe_{39}Ni_{39}Mo_4Si_6B_{12}$), these soft materials present lower magnetostriction saturation values (up to 60 ppm) but are easier to magnetize, with a saturation induction around 1.5 T (Ralph C Smith, 2005).

Terfenol-D, Metglas and Vitrovac show high saturation inductances but are conductive (Bluhm, 2006; Rafferty, Bakir, Brabazon, & Prescott, 2009), inducing eddy currents and therefore establishing ohmic losses with the consequence of a decrease in the magnetostrictive performance of the material (Engdahl & Mayergoyz, 2000; Rafferty et al., 2009). To overcome this problem, low electrical conductivity magnetostrictive materials can be used.

Cobalt Ferrite ($CoFe_2O_4$, CFO) corresponds to the material category of spinel ferrites, which are represented by the formula unit AB_2O_4. Most spinel ferrites may be described as semiconductor ceramics, which form cubic spinel structures (Brabers, 1995; Muthuselvam & Bhowmik, 2009; Rahman et al., 2013). Because of their potential applications in science and technology and because it is an economic alternative to the existing alloy-based magnetostrictive materials, in the last few decades extensive work has been carried out on certain spinel ferrites,

particularly in CFO and its generic $Co_xF_{3-x}O_{4-Y}$ (Muthuselvam & Bhowmik, 2009; Okuno, Hashimoto, & Inomata, 1992; J. X. Zhang et al., 2009a; Zhao et al., 2008). CFO has almost the largest magnetostrictive coefficients ($\lambda_s=-110 \times 10^{-6}$ at 300 K) among different magnetic oxide materials, with high Curie temperature above 700 K (J. X. Zhang et al., 2009a).

The properties of cobalt ferrite depend strongly on composition, annealing conditions, grain sizes and dopant materials as expressed in the vast literature (Farea et al., 2008; George, Nair, Malini, Joy, & Anantharaman, 2007; Rahman et al., 2013; Shaikh, Kanamadi, & Chougule, 2005; Shinde & Jadhav, 1998).

1.2.3.3. Piezoelectric polymers for magnetoelectric materials

For its high dielectric and piezoelectric responses, moderate costs, and broad range of operating temperatures, lead zirconate titanate (PZT) is the best known piezoceramic; it is widely used as high precision actuator and sensor for a wide range of frequencies, including ultrasonic applications (Piefort, 2001; Ralph C Smith, 2005). Piezopolymers are mainly used as sensors, being polyvinylidene fluoride (PVDF) and its copolymers the ones with the highest piezoelectric responses. PVDF was first studied by Kawai (end of the 60's) and was commercially available in the early 80's (Piefort, 2001)

As organic materials, piezoelectric polymers are softer and generally more flexible than piezoceramics (Cottinet et al., 2004). Strong piezoelectric effects have been observed in a group of commercial synthetic polymers named polyvinylidene fluoride (PVDF or PVF2) and PVDF co-polymers, having the largest piezoelectric coefficient compared with other bulk polymers, followed by amorphous polyimide. Although polyimide (nitrile-group containing polyimide (2.6-bis[3-aminophenoxy] benzonitrile/4.40 oxidiphthalic anhydride, [β-CN] APB/ODPA) shows a lower piezoelectric coefficient, it has the advantage over PVDF of operating at higher temperatures, due to its high glass transition temperature (360–410°C). Other electroactive polymer, Parylene-C, presents lower piezoelectric performance. Because of its biocompatibility, chemical resistance, and its vapour deposition method (that grants conformal coating disregardless of surface´s porosity, it is used commonly as an electrically insulating material in micro-electro-mechanical systems (MEMS), (Ramadan, Sameoto, & Evoy, 2014).In Table 1.1, a

16

comparison of the piezoelectric constants of some commonly used piezoelectric materials is presented.

Table 1.1: Piezoelectric and dielectric properties for different piezoelectric ceramics (*)(Esterly, 2002; Kim, Tadesse, & Priya, 2009) and polymers (**) (Ramadan et al., 2014)

Material	Relative Dielectric Constant (ε_r)	Piezoelectric Constant, $|d_{33}|$ (pC/N)
BaTiO$_3$ (*)	1700	191
Quartz (*)	4.5	2.3
PZT-4 (*)	1300	289
PVDF (**)	12	13-28
P(VDF-TrFE) (**)	12	24-38
Parylene-C (**)	3.15	2.0
PI(β-C)APB/ODPA (**)	4	5.3-16.5

Different fabrication methods and poling conditions used for bulk piezopolymers and piezocomposites may produce variation on the piezoelectric performance of the material (Ramadan et al., 2014), and therefore a range of values is presented in Table 1.1.PVDF presents a lower piezoelectric coefficient compared to the piezoelectric ceramic materials, although general properties of PVDF and PVDF copolymers include stable flexibility, malleability, lightweight, response characteristics in a wide frequency range, low acoustic impedance, high degree of resistance to impact, resistance to moisture absorption, and insensitivity to intense ultraviolet and nuclear radiation, have low manufacturing costs and are easily moulded into any desired shapes (Cottinet et al., 2004; Gandhi & Thompson, 1992; Ren, Liu, Hofmann, & Zhang, 2007; A. M. Vinogradov, Hao, & Filisko, 2002).

1.2.3.4. Poly(vinylidene fluoride) and copolymers

Before 1969 the only materials that received some attention for their ferroelectric or piezoelectric properties were naturally occurring crystals, such as quartz, and ceramics, such as barium titanate (BaTiO$_3$) and lead zirconate titanate (PZT) (Esterly, 2002; Ralph C Smith, 2005). In 1969, Dr. Heiji Kawai discovered the piezoelectric properties of PVDF. Furakawa and Johnson confirmed those results in 1981 (Destruel, Rojas, Tougne, & Hoang-The-Giam, 1984; Esterly, 2002; Furukawa, 1989; Linares & Acosta, 1995; Lovinger, 1982; Marutake, 1995; Rao & Sunar, 1994; A. Vinogradov & Holloway, 1999; Wirsen, 1986). Besides its piezoelectric properties,

poly(vinylidene fluoride), PVDF, is useful due to its chemical stability and resistance to organic solvents and high elastic modulus compared with other polymers. It has high permittivity and dielectric strength and low dissipation factor. Compared to other polymers and other piezoelectric materials in general, PVDF has many benefits, including high rigidity and resists deformation, low glass transition temperature (no transitions between −45° and 170°C), wide range of processing temperatures (185°- 250°C) , resistance to heat and combustion, resistance to ageing, resistance to abrasion, chemically inert, non toxic, chemically resistant (highly polar solvents will cause slight swelling), stability to radiation (UV, X-ray, Gamma), excellent electrical insulator and high Curie point (103°C, for high temperature piezoelectric applications) (Bar-Cohen, Xue, & Lih, 1996; Esterly, 2002; Gregorio & Ueno, 1999; Inderherbergh, 1991; Xu, Shanthi, Bharti, & Zhang, 2000).

Typically, PVDF is a ≈50% amorphous semicrystalline polymer with molecular weight between 60 and 70 Kg/mol (Esterly, 2002; A. M. Vinogradov & Holloway, 2000), that is commonly synthesized through the free radical polymerization of 1,1-difluoroethylene. Its monomer structure is -CH2-CF2-, with the chains mostly in a head to tail configuration. Four different crystals structures for PVDF polymers have been identified. These four crystal phases are referred by α, β, γ and δ (Esterly, 2002; Gregorio & Ueno, 1999; Inderherbergh, 1991; Linares & Acosta, 1995). The amorphous phase of the polymer has the properties of a super-cooled liquid with the glass transition temperature of about -50°C. Permanent dipole polarization of PVDF is obtained through a technological process that involves stretching and polling of extruded thin sheets of the polymer. In general, polarization in PVDF depends on such factors as poling temperature, poling time, poling process, and electrode conditions (Hilczer & Malecki, 1986; Aleksandra Vinogradov, Su, Jenkins, & Bar-Cohen, 2005). Typically, PVDF is produced in the form of thin films with thicknesses ranging from 9 to 800 μm. A thin layer of nickel, silver or copper is deposited on both material surfaces to provide electrical conductivity or to allow measurements of the charge induced by mechanical deformations.

The β-phase has more intermolecular stability while the α-phase is favoured on an intramolecular basis, due to the van der Waals forces acting between the atoms along the carbon backbone and between the molecules of the polymer. These forces govern the structure of PVDF.

18

The β crystal phase of PVDF forms a planar zig-zag, or TT where T represents a trans bond that remains in the same plane as the carbon backbone. The all-trans structure of β-PVDF forces the fluorine atoms along the carbon backbone to come closer together and overlap their van der Waals radii. The simple head to tail organization and planar zigzag structure creates a very organized crystal, allowing tighter packing density, reducing the intermolecular strain and introducing more dipolar alignment, favouring strong piezoelectric properties (Chiang & Chaikin, 1990; Esterly, 2002; Furukawa, 1989; Gregorio & Ueno, 1999; Lovinger, 1982; Tadokoro, 1979; Yang et al., 2000).

The temperature at which PVDF is synthesized determines the number of head-to-head (HH) and tail-to-tail (TT) units that occur in polymer chains, establishing how easily the β-phase will form. Those imperfections allow more space between the fluorine atoms and make the β-phase more stable. The introductions of copolymers such as trifluorethylene and tetrafluoroethylene can take the place of these HH or TT monomers and increase the production of β-PVDF (Esterly, 2002; Furukawa, 1989; Hopfinger, 1973). The addition of the HH and TT defects reduces sufficient stress to stabilize the crystalline structure without interfering with molecular polarity(Esterly, 2002).

Each monomer of PVDF has a dipole formed by the fluorine and hydrogen atoms. Those dipoles are rigidly attached to the carbon backbone and their orientation determines the crystalline structures of PVDF and, therefore if it becomes piezoelectric. The β-phase has a highly polar arrangement of the dipoles, alignment that produce a net polarization of the unit cell, maximizing spontaneous polarization (Bar-Cohen et al., 1996; Esterly, 2002; Furukawa, 1989; Yang et al., 2000). When β -phase of PVDF forms naturally, it has a zero net charge. This is because the dipoles are arranged randomly. During the manufactory, a large electric potential is applied across the material (also known as poling), aligning the dipoles. The direction of the unit cell can be changed when an electric field is applied during the poling process. (Bar-Cohen et al., 1996; Bune et al., 1999; Esterly, 2002; Furukawa, 1989; Riande & Siaz, 1992; Seanor, 1982; A. Vinogradov & Holloway, 1999; Wise, 1998).

1.2.3.5. Polymer –based magnetoelectric composites

Particulate and laminated ME composites such as Terfenol-D/PZT (Shuxiang Dong, Zhai, et al., 2006b)and $NiFe_2O_4$/PZT (Srinivasan et al., 2001)have shown enlarged ME coefficients, experimentally and theoretically(C.-W. Nan et al., 2005, 2001; J. X. Zhang et al., 2009b). Recently, thin films of magnetic and ferroelectric oxides have been developed as nanostructured composites (C. Nan et al., 2008). Potential applications in micro-electro-mechanical systems have led to investigations on 0-3 ME nanocomposite films such as $CoFe_2O_4$/PZT (J. Wan et al., 2006), $CoFe_2O_4$/$BaTiO_3$(J. Wan et al., 2006; J X Zhang et al., 2008), $BiFeO_3$/$NiFe_2O_4$(Zhan et al., 2006)and thin-film heterostructures (J. X. Zhang et al., 2009b).

Oxide based magnetostrictive materials have been suggested for ME nanocomposites (J. X. Zhang et al., 2009b). Since 2004, Zheng *et al.* (H. Zheng, Wang, Lofland, Ma, Zhao, et al., 2004) presented pioneering experiments on nanostructured films composed of $BaTiO_3$/$CoFe_2O_4$ with 1-3 or 2-2 connectivity schemes (C. Nan et al., 2008), $CoFe_2O_4$(CFO) has being important, among different magnetic oxide materials, for applications in magnetic, magneto-optical recording, electromagnetic, and spintronics devices (Rahman et al., 2013; Zhao et al., 2008), since they have the largest magnetostrictive coefficients (λ_s=110x10^{-6} at 300 K) with a high Curie Temperature above 700 K (J. X. Zhang et al., 2009b).

As for the polymer piezoelectric counterpart in the ME structure, the copolymer PVDF presents some advantages when compared to its inorganic piezoelectric pair materials as PZT or PMN-PT, since as a polymer it can stand freely without substrate clamping effect and therefore shapes and sizes can be easily varied by conventional polymer processing, and also shows relatively good voltage sensitivity, high electromechanical properties, low dielectric constant, and low dielectric loss (J. X. Zhang et al., 2009b).

Polymer-based magnetoelectric composites are easy to fabricate by low temperature processing, they can be shaped into a variety of forms (sheets, moulded shapes), they can exhibit enhanced mechanical properties, such as being no brittle and present highly flexibility, and also, some of them can be biocompatible (Pedro Martins & Lanceros-Méndez, 2013; Scott, 2012). Three main types of Polymer-based magnetoelectric composites can be found, as it is presented in Figure 1.2(Pedro Martins & Lanceros-Méndez, 2013):
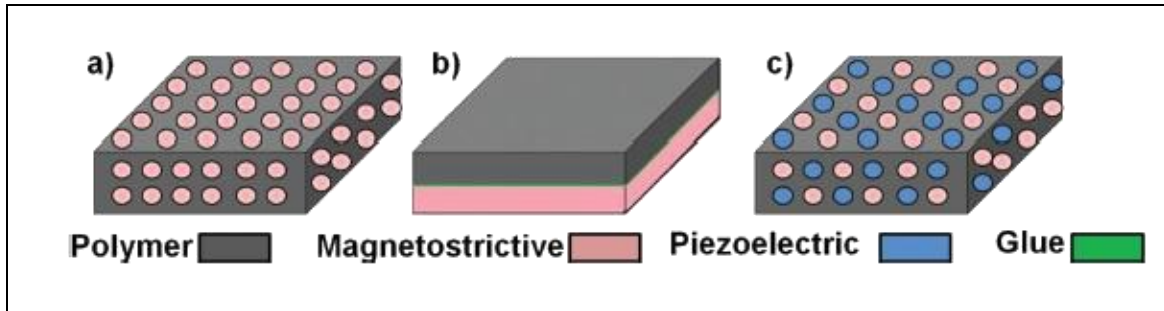
Figure 1.2: Main types of polymer based magnetoelectric composites (Pedro Martins & Lanceros-Méndez, 2013)

a) nanocomposites: electroactive nanoparticles embedded into a polymer electroactive matrix

b) laminated composites: by product property of the materials, the ME effect in laminated composites is established in materials consisting of individual piezomagnetic and piezoelectric phases or individual magnetostrictive and piezoelectric phases (Jungho Ryu et al., 2002).

c) polymer *as a binder*: electro- and magnetostrictive nanoparticles embedded into a polymer matrix, in which cases the polymer is not used as the piezoelectric phase of the ME material but as a binder for the piezoelectric and magnetostrictive particles that keep them together and provides stress coupling between the piezoelectric matrix and the magnetostrictive fillers.

The comparison of the main characteristics of the developed polymer-based nanocomposites, laminated composites and polymer as binder composites materials is presented in Table 1.2.

Table 1.2: Comparison of the main characteristics of the developed polymer-based materials (Pedro Martins & Lanceros-Méndez, 2013)

Type	Constitution	H_{DC} max ME (Oe)	Ref	α (mVcm^{-1}Oe^{-1})	$\alpha_{resonance}$ (mVcm^{-1}Oe^{-1})
Nanocomposites	PE/Fe$_3$O$_4$	0	(Guyomar, Guiffard, Belouadah, & Petit, 2008)	11.4	-
	PE/Nickel	0		6	-
	P(VDF-TrFE)/Ni$_{0.5}$Zn$_{0.5}$Fe$_2$O$_4$	5000	(P. Martins, Moya, et al., 2011)	0.1	1.35
	P(VDF-TrFE)/CoFe$_2$O$_4$	2500	(P. Martins, Lasheras, et al., 2011)	4.1	41.3
		2000	(J. X. Zhang et al., 2009b)	-	40
Laminated Composite	PVDF/Terfenol-D/PZT	4000	(Ning Cai, Nan, Zhai, & Lin, 2004)	80	3000
		4000	(C.-W. Nan et al., 2005)	300	6000
	Spurr epoxy/Terfenol-D/PZT	504	(Hong, Ren-Fa, & Xue-Zhong, 2005)	400	1100
	PE/PVDF/Fe$_3$O$_4$	2000	(Belouadah, Guyomar, Guiffard, & Zhang, 2011)	753	-
	VER/Terfenol-D/PZT	666	(N. Nersessian, Or, & Carman, 2004)	2700	-
	PZT/Terfenol-D/Epoxy	3000	(Shi, Ma, & Nan, 2008)	1310	2790
	Gd crystal/P(VDF-TrFE)/silver conductive epoxy	200	(S. G. Lu et al., 2010)	500	-
	PVDF/Metglas unimorph	8	(Junyi Zhai et al., 2006)	7200	238000
	PVDF/Metglas three-layer	-		-	310000
	PVDF/Metglas	8	(Z. Fang et al., 2009)	21460	-
		3	(X. W. Dong, Wang, Wang, Wan, & Liu, 2009)	400	-
	PVDF-HPFP/Metglas	5	(S. Lu et al., 2011)	12000	-
	Cross-linked P(VDF-TrFE)/Metglas 2605	4	(Jin et al., 2011)	17700	383000
	PVDF/Ni$_{50}$Mn$_{29}$Ga$_{21}$	5100	(Zeng, Or, & Chan, 2010)	1240	-
Polymer as Binder Composites	PVDF/Terfenol-D/PZT	2000	(C. W. Nan, Liu, et al., 2002)	42	-
	PEO/Terfenol-D/PZT	1400	(Chau, Wong, & Shin, 2009)	1.3	-
	Li$^+$PEO/Terfenol-D/PZT	-		3.2	-
	PMMA/Terfenol-D/PZT	-		4.8	-

According to (Pedro Martins & Lanceros-Méndez, 2013), different configuration of particulate polymer-based nanocomposites have being discussed, such as electrostrictive polyurethane (PU)-based magnetoelectric composites (with Terfenol-D, Fe_3O_4 or nickel fillers), with PVDF as the piezoelectric constituent of ME nanocomposites (ferrite/P(VDF-TrFE) nanocomposites). Also, ME polymer-based nanocomposite structures were synthesized using conducting polyaniline and nanosized $BiFeO_3$ particles through in situ sol–gel polymerization (Prabhakaran & Hemalatha, 2008), but the ME response of such nanocomposites has not yet been reported.

In electrostrictive polyurethane elastomers (PU)-based ME composites, the coexistence of both linear and quadratic ME response have been obtained, and it is possible a linear magneto-elasto-electric coupling between fillers and polymer matrix (Guyomar et al., 2008). Other reports show linear voltage ME coefficients, as in Fe_3O_4/PU and nickel/PU composites(D. C. Jiles, Ostenson, Owen, & Chang, 1988; P. Martins, Lasheras, et al., 2011). Experimental observations suggested that the magnetostrictive properties of the material have no influence in the Fe_3O_4/PU and nickel/PU composites, since ME response in PU composites is independent of the magnetostrictive properties of the fillers (Terfenol-D, Fe_3O_4 or Nickel) (Guyomar, Matei, Guiffard, Le, & Belouadah, 2009). These means that the coupling in PU composites is mainly due to the particular nature of the elastomer PU matrix, composed of both rubbery and polar domains (Pedro Martins & Lanceros-Méndez, 2013). Nevertheless, the origin of the ME coupling in such nanocomposites is not yet clearly established (Ma, Hu, Li, & Nan, 2011).

In 2001, Nan *et al.* (C. W. Nan, Li, Feng, & Yu, 2001; C.-W. Nan et al., 2001) reported theoretical calculations of giant ME on ferromagnetic rare-earth-iron-alloys-filled ferroelectric polymers, using PVDF as the piezoelectric constituent of ME nanocomposites. Experimentally, Martins *et al.* introduced $CoFe_2O_4$ and $Ni_{0.5}Zn_{0.5}Fe_2O_4$ferrite nanoparticles into a polymer matrix of (P(VDF-TrFE) (P. Martins, Lasheras, et al., 2011; Sencadas, Lanceros-Mendez, & Mano, 2004). Ferrite/P(VDF-TrFE) nanocomposites exhibit ferroelectric, piezoelectric, magnetic and direct ME effect dependent on the ferrite loading. In the case of $CoFe_2O_4$/P(VDF-TrFE) nanocomposite, the resultant ME films showed saturated hard magnetic properties, improved polarization and

piezoelectric response. For $Ni_{0.5}Zn_{0.5}Fe_2O_4$/P(VDF-TrFE) composites, the ME coefficient increases linearly with applied H_{DC}(P. Martins, Moya, et al., 2011). In contrast to PU based composites, (Guyomar et al., 2009). the ME $CoFe_2O_4$/P(VDF-TrFE) response is strongly influenced by the magnetostriction of the ferrite nanoparticles, as also presented by Zhang *et al.* (J. X. Zhang et al., 2009b), who also studied the effect of $CoFe_2O_4$ nanoparticles on the morphology, ferroelectric, magnetic and ME behaviours of $CoFe_2O_4$/P(VDF-TrFE) nanocomposites, concluding that the ferroelectric and ME responses are strongly influenced by the concentration of ferrite nanoparticles. Both experimental ME voltage coefficients of Martins *et al.* and Zhang *et al.* were theoretical confirmed by a relatively simple model based on those of Wong and Shin, and Zhou and Shin, respectively(Pedro Martins & Lanceros-Méndez, 2013; C. K. Wong & F. G. Shin, 2007; Y. Zhou & Shin, 2006).

b) laminated magnetoelectric composites

A laminate bi-layer or multi-layer configuration for ME composites has other advantages such as avoiding the polarization loss in bulk composites due to leakage currents, that can be overcome in layered structures. The piezoelectric phase can be poled to enhance the ME coupling and it is also possible to vary the poling and applied field directions to achieve maximum ME coupling (Pedro Martins & Lanceros-Méndez, 2013). As presented in Table 1.2, many different configurations of polymer-based laminated ME composites are being studied. The different sheets of the laminate can include particulate nanocomposites, polymer-as binder composites, or just electroactive materials (Pedro Martins & Lanceros-Méndez, 2013).

Piezoelectric particulate layer, of PZT or PVDF, sandwiched between two magnetostrictive particulate composite layers of Terfenol-D, from now on called magnetostrictive-piezoelectric-magnetostrictive laminate (**MPM**)(C.-W. Nan et al., 2005) were also investigated. Although improved, the ME response of such composites is also strongly dependent on the applied bias and on the thickness ratio between the piezoelectric-phase thickness (d_pzo) and the total thickness (D=d_pzo+2*d_ms) of the composite (where d_ms is the magnetostrictive phase thickness). Keeping the thickness of the composite (D) fixed, the d_pzo/D ratio was varied by increasing the thickness of the PZT or PVDF particulate layer (d_pzo) and diminishing the Terfenol-D thickness (d_ms). The ME performance of the composites first increase with d_pzo/D,

which could be attributed to the increase in the effective piezoelectric effect, until an optimal maximal value from which, with further increasing d_pzo/D, the ME sensitivity declines due to the reduction in magnetostrictively induced strain of the laminated composites (Y. H. Lin, Cai, Zhai, Liu, & Nan, 2005).

Ryu *et al.* (Jungho Ryu et al., 2001) established the theoretical expectation for the ME voltage coefficient (dE/dH) as function of the thickness ratio (d_ms/d_pzo) between Terfenol-D and PZT (Figure 1.3 a). They established, that output voltage increases while increasing the thickness ratio, saturating above d_ms/d_pzo=10, as presented in Figure 1.3 (a). Stognij *et al.* (Stognij et al., 2013) achieved similar results by studying the effect of Cobalt Layer Thickness on the magnetoelectric properties of Co/PZT/Co heterostructures, for MPM configurations of 2.5 µm of cobalt thickness and PZT thickness between 270 and 430 µm.
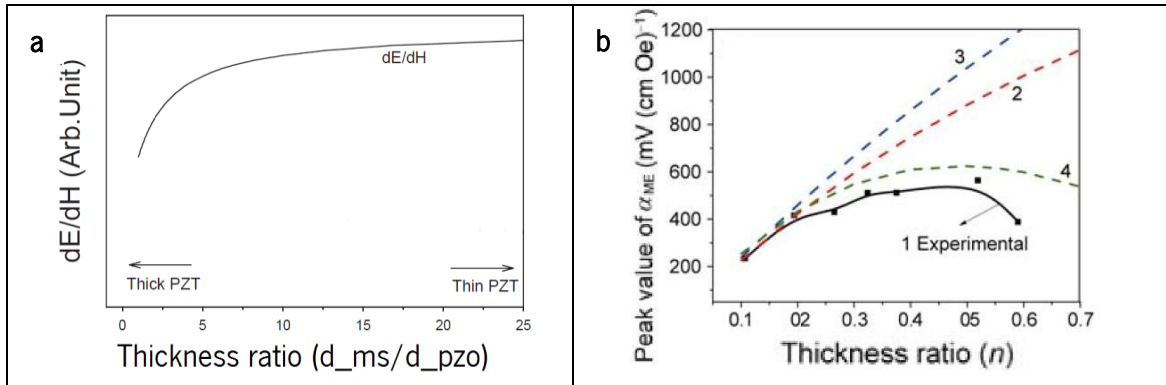
Figure 1.3: Magnetoelectric coefficient as function of the thickness ratio (d_ms/d_pzo) of magnetostrictive and piezoelectric thicknesses (a) and for n-ratio (n=2*d_ms/(2*d_ms+d_pzo) for both PZT and PVDF free magnetostrictive-piezoelectric-magnetostrictive (MPM) configurations. These tendencies are established in literature and data is used as reference (Jungho Ryu et al., 2001) (a), and (F. Fang, Zhao, & Yang, 2011) (b).

Fang (F. Fang et al., 2011) presented peak values of α_{ME} as function of n-ratio (2*d_ms/(2*d_ms+d_pzo)) for Metglas/PZT/Metglas laminates, where Metglas laminates increase its thickness by being glued with an epoxy, confirming tendencies presented by Ryu (Jungho Ryu et al., 2001) and establishing that the ME performance of the laminates, also decrease their performances after a thickness ratio of 0.5, as presented in Figure 1.3 (b).

Magnetostrictive particulate composite layer of Terfenol-D sandwiched between two piezoelectric particulate layers of PZT or PVDF, from now on called piezoelectric-magnetostrictive-

piezoelectric laminate (**PMP**), prepared by hot-moulding technique has been reported (N. Cai, Zhai, Nan, Lin, & Z. Shi, 2003). The polymer phase PVDF is used just as a binder, with no influence on the ME properties of the laminated composite. Experiments show that the ME response of the composite is dependant of the volume fraction of PVDF, f_{PVDF}, and that under a limit value, f_{low}, the low concentration of PVDF leads to low quality of the composites by a poor connection between the three phases and therefore, to low ME performance. The ME properties are improved in the intermediate f_{PVDF} concentration range (over f_{Low} and under f_{up},) and as f_{PVDF} further increases (with a volume fraction of PVDF over f_{up}), the high concentration of inert PVDF causes weak dielectric, magnetostrictive, piezo and ME activity of the three-phased laminated Terfenol-D/PZT/PVDF composites. At high bias, magnetostriction becomes saturated faster under in-plane bias than in out-of-plane bias producing a nearly constant electric field in the PZT, thereby decreasing the ME coupling with increasing bias.

Wong (W. Wong, 2007) compared MPM and PMP configurations by simulating and establishing tendencies for measured α as function of bias magnetic field for MPM (Terfenol-D/PMN-PT/Terfenol-D) and PMP laminates (PMN-PT/Terfenol-D/PMN-PT) with three different thickness ratio, of 0.4, 1.4 and 2.4, as shown in Figure 1.4. The physical models for predicting the quasistatic α_{ME} in each of the laminates under different combinations of dimensions and material properties refined the study, obtaining good agreement with the quasistatic and dynamic characteristics of the laminates that were measured and the quasistatic properties that were predicted by the physical models.
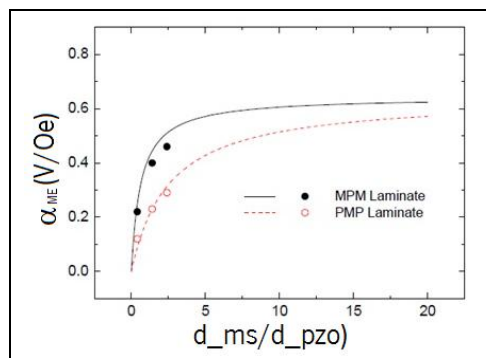
Figure 1.4: Expected magnetoelectric performance for piezoelectric-magnetostrictive-piezoelectric (PMP) and magnetostrictive-piezoelectric-magnetostrictive (MPM) configuration over magnetostrictive/piezoelectric thickness ratio (W. Wong, 2007).

26

Results express that the ME performance of MPM and PMP composites rapidly increase their ME behaviour with increasing thickness ratio until reaching saturation.

Srinivasan *et al.* (Srinivasan, Rasmussen, Levin, & Hayes, 2002) studied the ME effect in bi-layers and multi-layers on thick-film structures of $La_{0.7}Sr_{0.3}MnO_3$ (LSMO)-PZT and $La_{0.7}Ca_{0.3}MnO_3$ (LCMO)-PZT. Their samples were fabricated with an equal number of manganite and PZT layers, between 2 and 8 layers, where N is the number of layers. In all the samples the total thickness of both magnetostrictive and piezoelectric phases remained the same, of 200 μm (for the bi-layer both phases were 200 μm of thickness each; for a multi-layer sample with N=4, the layer thickness was 100 mm, etc.). Their study concluded that low-frequency ME voltage is stronger in LSMO-PZT than in LCMO-PZT, and is weaker in multi-layers compared to bi-layers, in which the transverse ME effect and is a factor of 2 to 3 higher than the longitudinal effect, as presented in Figure 1.5.
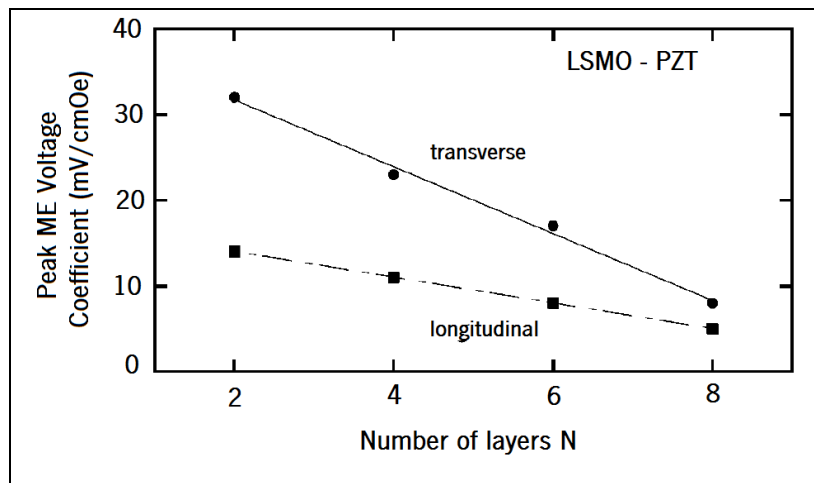
Figure 1.5: Experimental value of peak magnetoelectric voltage coefficient for LSMO-PZT multi-layers and tendency when increasing the numbers of layers, N, of the multi-layer, provided by Srinivasan *et al.* (Srinivasan, Rasmussen, Levin, et al., 2002).

c) Polymer *as a binder* composites

Polymer as a binder ME materials have flexibility, simple fabrication and easy shaping as advantages, but its features are still limited when compared to those of particulate nanocomposites (Pedro Martins & Lanceros-Méndez, 2013).

The first three-phase particulate composites to be studied were those of Tefenol-D alloy, PZT and PVDF (C. W. Nan, Liu, et al., 2002). A small volume fraction, f, of Terfenol-D nanoparticles has to be dispersed in a PZT/PVDF matrix; the obtained dielectric, piezoelectric and ME properties depend of the volume fraction, f, of Terfenol-D: for lower values of $f_{Terfenol-D}$ than a low limit, f_{low}, the composites exhibit good piezoelectric and ME responses. Between this low limit value and the volume fraction when a percolation transition occurs, f_{up}, the piezoelectric and ME response sharply drops and disappears at the percolation threshold, above which the composite becomes a conductor and only respond magnetostrictively (J. Ryu, Carazo, Uchino, & Kim, 2001).This shows that the ME response is mainly determined by the $f_{Terfenol-D}$, but the pre-treatment of the Terfenol-D nanoparticles by the use of surfactants can also change the ME coupling (Hilding, Grulke, Zhang, & F. Lockwood, 2003; Pyun, 2007). On the other hand, in the case of the ferrite-ceramic-composite/PZT, surfactants increase the percolation threshold, leading to two consequences (Pedro Martins & Lanceros-Méndez, 2013):

i. the maximum magnetostrictive filler concentration allowed in the ME nanocomposites is increased, and

ii. a soft and inactive interfacial layer is induced in the Terfenol-D nanoparticles. As the first one allows higher magnetostrictive content in the ME composite, the second one produces a negative effect on both the piezo- and ME- response of the nanocomposites (C. W. Nan, Cai, et al., 2003).

The ME response of this composite can also be improved by increasing the $f_{Terfenol-D}$ and simultaneously ensuring good interfacial contact between phases by optimization the nanocomposite processing.

Other polymers were studied in the ME response of the same kind of magnetoelectric nanocomposites (Chau et al., 2009), as polymer electrolyte polyethylene (PEO) and lithium perchlorate-doped PEO, Lithium perchlorate-doped PEO (Li$^+$ -PEO) and poly(methyl methacrylate) (PMMA). They were mixed separately with Terfenol-D and PZT particles to evaluate the significance of the polymer matrix conductivity, leading to results confirming that samples with higher conductivity exhibit lower ME responses (Pedro Martins & Lanceros-Méndez, 2013; C. W. Nan, Liu, et al., 2002).

Depending upon the interface design, the effective properties of the nanocomposites can be either enhanced or reduced (E. Pan, Wang, & Wang, 2009). These studies were first developed by surface elasticity theory (Cammarata & K. Sieradzki, 1994). As the interfacial stress displays short-range effect on the stress state in nanocomposites, internal stresses are introduced in both the matrix and leads to changes in the displacement field and the stress field created by external loads. Pan *et al.* (E. Pan et al., 2009) concluded that such interface condition exerts a significant influence on the local and overall magneto-electro-elastic responses of the ME composites, in particular when the fillers are at the nanometre-scale. They demonstrated that the ME coefficient can be enhanced when the magnetostrictive fillers are reinforced in a piezoelectric matrix by designing an electrically highly conducting interface. Other theoretical calculations on the mechanical boundary conditions influence over the ME properties were performed for materials that use polymer as binder, particularly in the case PZT/PVDF nanocomposite (Shi, Nan, Liu, Filippov, & Bichurin, 2004).

1.3. Applications of magnetoelectric composites based on electroactive polymers

Electroactive polymers have been used as active elements capable of sensing and responding to external stimuli, reason why they are called "smart structures" or "smart material systems"(Aleksandra Vinogradov et al., 2005).Also, the reason why ME materials in general and polymer-based ME materials in particular are ready for technological applications. Applications include magnetic field sensors, transducers, filters, oscillators, phase shifters, memory devices, and biomedical materials, among others (C. Nan et al., 2008; Scott, 2012). Due to the polymers unique characteristics such as flexibility, lightweight, versatility, low cost and, in some cases biocompatibility, polymer based ME materials can integrate new and enhanced technological applications (Pedro Martins & Lanceros-Méndez, 2013).

Material selection in the design of smart systems involves considerations of factors as maximum achievable strain, stiffness, spatial resolution, frequency bandwidth, temperature sensitivity, between others(Aleksandra Vinogradov et al., 2005).

Applications of ME materials include (Pedro Martins & Lanceros-Méndez, 2013)magnetic field sensors, energy harvester and four-state memory devices, as well as biomedical applications.

1.3.1. Magnetic sensors

Magnetic sensors have been in use for well over 2000 years, for finding directions in navigation. Nowadays, other applications have being developed, driven by the need for improved sensitivity, smaller size, and compatibility with electronic systems (Caruso, Bratland, Smith, & Schneider, 1998). The working principle of magnetic sensing in ME composites can be explained (Petrov, Srinivasan, Bichurin, & Gupta, 2007)as follows: when exposed to a magnetic field, the magnetostrictive phase in the ME composites strains, producing a proportional charge in the piezoelectric phase. High ME coefficients on the ME composites can be highly sensitive magnetic field sensors, detecting ac and/or dc fields (C. Nan et al., 2008).

Traditionally, magnetic sensors (hall sensors, magnetoresistive sensors, etc.) need power supply to operate, and therefore, self-powered magnetic field sensors, that transfer magnetic energy into electric signals directly, such as ME sensors, are of large interest (Giang & Duc, 2009). Nan *et al.* (C.-W. Nan et al., 2001) first suggested to use ferroelectric polymers/rare-earth–iron alloys composites, as magnetic sensors (Bichurin, Petrov, Petrov, et al., 2002). The ME sensor comprised a disk or plate from the ME material (composites containing 95wt.% of yttrium-iron garnet and 5 wt.% of lead PZT and multi-layer composite material consisting of PZT and $Ni_{0.5}Zn_{0.5}Fe_2O_4$) with two electrodes for connecting to the voltage meter. Xing *et al.* (Xing et al., 2008) designed one passive AC magnetic sensor based on charge amplifier circuit, with Terfenol-D/PZT composites on L-T mode. Dong *et al.* (S. X. Dong, Zhai, Li, & Viehland, 2006) developed a lock-in amplifier method, the ME effect in the composites can convert the small DC magnetic field to an electric signal monitored by a lock-in amplifier. Moreover, Zhai *et al.* (J. Y. Zhai, Dong, Xing, Li, & Viehland, 2007) used the similar method to design one geomagnetic detection sensor based on Metglas/PZT laminated composites (Gao, 2013). Other reports present vortex magnetic field sensor based ring-type Terfenol-D/PZT sensors (Bichurin, Petrov, Petrov, et al., 2002; S. X. Dong, Li, & Viehland, 2004; Duc & Giang, 2008; Giang & Duc, 2009; Leung, Or, Zhang, & Ho, 2010; M. Li, Wang, et al., 2012), $Fe_{80}Co_{20})_{78}Si_{12}B_{10}$/PZT laminate ME sensor for

micro-tesla sensitivity and the effect of the mutual inductance on the magnetic field sensitivity of the ME Metglas/PZT laminate (Giang & Duc, 2009; Leung et al., 2010; M. Li, Wang, et al., 2012), respectively. As expressed, numerous reports followed the PZT based ME sensors (Pedro Martins & Lanceros-Méndez, 2013), although the low flexibility, cost, and fragility of PZT do not meet the challenges of future sensor applications (Aoyagi, Beeby, & White, 2002), multiferroic and ME polymer-based composites are good alternatives (Pedro Martins & Lanceros-Méndez, 2013).

One example, given by the ME laminates of Metglas/PVDF magnetic field sensors, that were experimentally studied by Fang *et al.* (Z. Fang, Mokhariwale, Li, Datta, & Zhang, 2011), indicated that the increasing the electrode area (number of layers) of PVDF can enhance the field sensitivity and Signal to Noise Ratio (SNR) (Pedro Martins & Lanceros-Méndez, 2013). A push-pull ME Terfenol-D/PMN-PT/Terfenol-D three-layer laminate was reported by Nan *et al.* (Shuxiang Dong et al., 2003, 2005; C. Nan et al., 2008; Junyi Zhai et al., 2006) as used for AC magnetic field sensor. When those laminates were operated under resonance drive, they demonstrated to have an ultrahigh sensitivity to small ac magnetic field variations. Apart from a bimorph, a multi-layer Terfenol-D/PMN-PT ME configurations has been reported, enabling ultralow frequency detection of magnetic field variations (S. X. Dong, Zhai, Xing, Li, & D. Viehland, 2005; Junyi Zhai et al., 2006). This configuration can improve the low-frequency capability because of its high ME charge coupling and large capacitance (C. Nan et al., 2008). This enhanced performance of the ME sensors show enormous potential as by products related to magnetic sensors: electric current sensors, speed sensors, angular sensors, electronic steering, throttle control, battery management, vehicle transmission, digital compasses and GPS devices, among others (Pedro Martins & Lanceros-Méndez, 2013).

1.3.2. Energy harvesting devices

Power requirement of sensors and devices attracted much attention to energy harvesting technologies (Pedro Martins & Lanceros-Méndez, 2013). For ME bulk and laminated composites it is possible to harvest vibration energy via piezoelectric effect and electromagnetic energy via ME effect. These hybrid harvesters are expected to enhance energy collection and conversion efficiency (Gao, 2013). In particular, the area of the vibration energy based on piezoelectric and

magnetic harvesters has attracted much interest. The optimization of the ME coefficient of laminate composites will increase the ME energy harvesting efficiency (Pedro Martins & Lanceros-Méndez, 2013; S. Priya & Inman, 2009). By using a ME laminated composite attached to a cantilever beam with a tip mass, a multimodal energy harvester was developed, which can harvest energy from both of magnetic field and mechanical vibration(S. X. Dong, Zhai, Li, Viehland, & Priya, 2008).

An electromagnetic energy harvesting scheme by using the Terfenol-D/PZT transducer and a power management circuit was presented by Li *et al.* (P. Li, Wen, Liu, Li, & Jia, 2010). In this transducer, the vibrating wave induced from the magnetostrictive Terfenol-D in the dynamic magnetic field converges using a Be–bronze ultrasonic horn. Therefore, more vibrating energy can be converted by the PZT. A switching capacitor network for storing electricity was also included, as more capacitors can be employed in the capacitor network to further raise the output voltage in discharging (Pedro Martins & Lanceros-Méndez, 2013). This prototype of vibration energy harvester (Terfenol-D/PZT sandwich structure) can generate a load power, that may be compared to piezoelectric or electromagnetic harvesters(S. X. Dong, Li, & Viehland, 2006). The energy harvesting in the Terfenol-D/PZT/Terfenol-D laminate composites has also been reported (Shashank Priya, Islam, Dong, & Viehland, 2007), as well as ceramic based laminates energy harvesting materials constituted by $PZT/CoFe_2O_4$(P. Li et al., 2010; Moss, McLeod, Powlesland, & Galea, 2012; C. L. Zhang, Yang, & Chen, 2009). In this case, magnetically forced extensional vibrations of laminated plates with piezoelectric and piezomagnetic layers were analysed theoretically, showing that such a structure can be used to harvest magnetic energy and convert it to electric energy. In experimental studies, ME Terfenol-D/PZT laminates were placed between an oscillating spherical steel bearing and a rare-earth magnet (NdFeB) to produce power, approach that may be useful in the future for kinetic energy harvesting for applications where the host accelerations are multiaxial (Pedro Martins & Lanceros-Méndez, 2013; Moss et al., 2012). Finally, as next generation of energy-harvesting applications demand, there will be required for piezoelectric materials to be flexible, lightweight, and even biocompatible (Qi et al., 2010), therefore ME materials based on piezoelectric polymers may lead to interesting approaches to meeting these requirements (Ducharme, Reece, Othon, & Rannow, 2005; Pedro Martins & Lanceros-Méndez, 2013).

1.3.3. Biomedical applications

Functionalized surfaces magnetic nanoparticles have shown applications in biology, medicine and biotechnology, as magnetic tweezers and magnetic separation of proteins and DNA molecules, target delivery drugs and radioactive isotopes for chemotherapy and radiotherapy, between others (Andrä, Häfeli, Hergt, & Misri, 2007; Coey, 2010; Kargol, Malkinski, & Caruntu, 2012).

Guduru *et al.* (Guduru et al., 2013) reported high-specificity targeted delivery of anti-neoplastic drugs through ME nanoparticles that acted as nanosized converters of remote magnetic field energy, triggering high–specificity uptake of paclitaxel loaded on 30nm $CoFe_2O_4/BaTiO_3$ ME nanoparticles when a 30Oe DC magnetic field is applied. After the drug penetrated through the membrane, within 24 hours the ovarian carcinoma was completely eradicated without affecting the normal cells (Guduru et al., 2013).

Kargol *et al.* (Kargol et al., 2012) proposed a new mechanism in which multiferroic nanoparticles in form of spherical core-shell, magnetic rods, (both with ferromagnetic core and ferroelectric shell) or composite piezoelectric spheres with embedded magnetic nanoparticles, relies on localized (nanoscale) electric fields produced in the vicinity of the cells to control the voltage-gating in ion channels.

According to Kargol *et al.* (Kargol et al., 2012), ion channels are membrane proteins that form pores for controlled exchange of ions through cellular membranes (Hille, 1992).Their principal characteristics are on selecting the type of ions they flux and their gating, process of opening and closing in response to the gating variable, being the most common the voltage-gate ion channels that triggers in response to the trans-membrane electric field. The voltage-gated ion channel may be functionalized as a voltage sensor, a pore and a gate acting together on the movement of the "gating charge" that causes the conformational changes of the molecule, with the result of the channel opening or closing (Hille, 1992). Ion channels are crucial to shape electrical properties of various types of cells and regulate a host of cellular processes (as action potentials in neurons or muscle contraction), ion channel defects have also been identified as causes of a number of diseases (such as cystic fibrosis, diabetes, cardiac arrhythmias, neurological disorders, hypertension, etc.) (Ashcroft, 2000).

The proposed mechanism (Kargol et al., 2012) bases on the response of multiferroic nanoparticles, placed in extracellular medium or introduced internally, when exposed to an

applied external magnetic field, converting it to localized electric fields. For particles located near cell membranes containing ion channels this will lead to local membrane depolarization or hyperpolarization, conducting to ion channel opening or closing, accordingly. By modifying the properties of the stimulating magnetic field (its strength, duration, and spectral properties), as well as by controlling the delivery locations for the nanoparticles, a tight control over the localized electric fields may be achieved, which would lead to very localized changes in ion channel gating. Individual or selected group of cells can be targeted, rather than whole tissues, and also, because of the remote way of the performed stimulation, the functions of the cells in the internal organs can be controlled. This selectivity of stimulation can be achieved by functionalizing the surface of the nanoparticles and binding them to cells through antigens, allowing the nano-electro-stimulation to target only specific types of cells or even certain parts of cell membranes.

1.3.4. Other applications

Other multifunctional devices based on ME composites were designed.

- Four-state memory(Pedro Martins & Lanceros-Méndez, 2013):   In the traditional two state (0 and 1) memories, the memory element is a magnetic tunnel junction that consists on an insulating tunnel barrier sandwiched by two magnetic electrodes (Burrell et al., 2001; Karedla, Love, & B. G. Wherry, 1994; Zhu, 2008). The resistance of such junctions depends on the relative orientation of the magnetic moments, which determines the memory state (0 or 1) from the two magnetic electrodes (Julliere, 1975). The coded magnetic bits can then be read out non-destructively by detecting such resistance changes, however the writing process is led by the use of high magnetic fields, being relatively slow and energetically expensive process(Eerenstein et al., 2006). Taking advantage of the ME effect, the magnetization direction can be manipulated by the use of an electric field (Bibes & Barthelemy, 2008; Hambe et al., 2010; Hu, Li, Wang, & Nan, 2010). For this kind of multi-state memory the multiferroicity is the essential factor for the information storage while the ME or the magnetodielectric effect (Y. Guo et al., 2010) is the mechanism for the reading and writing procedure. A four-state memory cell based on the ME Co/PZT bi-layer composite has been already proposed (Shi, Wang, Liu, & Nan, n.d.). The polarization/magnetization of such composite can be controlled by the application of

magnetic and electric fields and the combination of the remanent ferroelectric polarization and magnetization in the Co/PZT bi-layer memory cell exhibits the desired four physical states. With the reduction of size, densities up to 40 Gbits cm 2 per layer can be expected for low energy, non-volatile memory devices. Given the very low expected power, such a device is a strong contender for vertical integration of several layers, quickly increasing the memory density (Tiercelin, Dusch, Preobrazhensky, & P. Pernod, 2011; Tiercelin, Dusch, Klimov, et al., 2011). As the current electronic market demands are intimately related to the use of flexible materials, (Coufal, Dhar, & Mee, 2006) not only the magnetic/dielectric properties of materials will play a key role in the future but also their mechanical properties. In this way, the substitution of PZT by a polymer in bi-layer four-state ME memories will meet these new challenges (Dee, 2006).

- ME transformers or gyrators: Those devices have important application as voltage gain devices, current sensors, and other power conversion devices (C. Nan et al., 2008). It is a passive, two-port electric network (J. Zhai et al., 2009). It can achieve the impedance inversion function, therefore it can convert an inductor (capacitor) to a capacitor (inductor) (Gao, 2013). A long-type ME laminate consisting of Terfenol-D and PZT layers reported an extremely high voltage gain effect (S. X. Dong et al., 2004), offering potential for high voltage miniature transformer applications (C. Nan et al., 2008).

- ME-based frequency multiplier: It has been proposed made up of FeBSiC and PZT, and wrapped with a coil by Ma *et al.* (Ma, Li, Lin, & Nan, 2011). It shows a steady frequency doubling behaviour at various frequencies. Moreover, the small DC bias can switch device on or off. Zhang *et al.* designed one resonance frequency multiplier(W. Zhang, Yin, Cao, Bai, & Wei, 2012). The multiplying signal can be generated when the input frequency of AC magnetic field is around $1/n$ (n denotes integer) of mechanical resonance frequency of device. Such frequency multiplying behaviour can be tuned by using external DC bias. Compared to traditional frequency multipliers, these devices are passive components and can be used in broad frequency range (Gao, 2013).

1.4. Models and simulations of magnetoelectric composites

Theoretical and numerical investigation research has become increasingly important (H.-L. Wang, Liu, & Fang, 2013). In 1993, Harshe *et al.* developed a theoretical model that dealt with linear behaviour of ME composites (G. Harshe et al., 1993). They calculated the ME voltage coefficient by using a cube model with 3–0 or 0–3 connectivity of phases., concluding that for best ME effect, both of the phases should have comparable elastic and dielectric properties (Jungho Ryu et al., 2002). Later, in 2001, Nan *et al.* predicted a giant magnetoelectric effect of Terfenol-D and P(VDF-TrFE) composites by modelling the strain-mediated coupling through Green's function technique (C. W. Nan et al., 2001; C.-W. Nan et al., 2001), considering the influence of the composites microstructure (phase volume fraction, phase connectivity, among others) on the effective properties of the composite (C. W. Nan, 2012). The shear-lag and demagnetization effects in laminated ME composites were considered by Chang and Carman (Chang & Carman, 2007) and the influence of interfacial bonding on the ME coefficient was discussed by Nan *et al.* (C. W. Nan, Liu, & Lin, 2003). Recently, the resonance behaviour of ME composite has also being investigated (Bichurin, Petrov, Averkin, & Filippov, 2010; Filippov, Laletsin, & Srinivasan, 2007; J.Wu, Zhang, Li, & Zhang, 2011).

According to Pan and Wang (E. Pan et al., 2009), representative analytical studies on the ME effect include, among others:

- Green's function and perturbation method (C.-W. Nan, 1994): As the magnetoelectric effect is absent in the piezoelectric and piezomagnetic, it is a new property of the composites. This statement allows a strain-mediated coupling simulation by a generalized theoretical framework based on a Green's function method and perturbation theory. Explicit relations are derived for the effective magnetoelectric effect in the composite, and the different approximate expressions for the magnetoelectric coefficient of the fibrous composites with 1-3 or 3-1 connectivity of phases are given.

- Micromechanics-based method (Bichurin, Petrov, & Srinivasan, 2002; Bichurin, Filippov, et al., 2003a): This theoretical model is presented for low-frequency magnetoelectric effect in bi-layers of magnetostrictive and piezoelectric phases. The model introduces an interface coupling parameter k for the consideration of actual boundary conditions at the interface.

An averaging method is used to estimate effective material parameters. Expressions for ME voltage coefficients are obtained by solving elasto- and electro-static equations. Both unclamped and rigidly clamped bi-layers are considered and there are three different field orientations of importance: (i) longitudinal fields, (ii) transverse fields, and (iii) in-plane longitudinal fields. Estimates of the magnetoelectric coefficient are carried out as a function of the interface coupling k and volume fraction, f, for the piezoelectric phase.

- Equivalent circuit method (S. Dong, Li, & Viehland, 2003; Shuxiang Dong, Zhai, et al., 2006b; C. Nan et al., 2008): Using piezoelectric and magnetostrictive constitutive equations, coupling both phases through elastic interaction, via an equation of motion that is excited by a magnetic field, a magneto-elasto-electric bi-effect equivalent circuit is developed. The circuit is used to predict the longitudinal and transverse ME voltage coefficients. These constitutive equations are linear relationships, which do not account for loss components, although a mechanical quality factor may be introduce to these ends.

- Continuum mechanics method with consideration of the grading composition effect (Petrov & Srinivasan, 2008; X. Wang, Pan, Albrecht, & Feng, 2009):it is a micromechanics approach to derive the effective properties (including thermal properties) of a multi-layered functionally graded multiferroic composite. Concise matrix expressions of the effective properties of the layered composite are used to derive formulas that are then applied to find the explicit expressions of the effective properties for three practical cases of ME composites: (a) one composed of an orthotropic piezoelectric phase and an orthotropic magnetostrictive phase; (b) one composed of an orthotropic piezoelectric phase, an orthotropic magnetostrictive phase and an orthotropic elastic substrate; (c) one composed of a functionally graded orthotropic piezoelectric phase and a functionally graded orthotropic magnetostrictive phase. Results show that i) the magnetoelectric coupling effect for case (b) dramatically drops as the volume of the elastic substrate increases; and ii) the magnetoelectric coupling effect for case (c) can be significantly enhanced or reduced depending on the material gradient manner for the functionally graded piezoelectric and magnetostrictive phases

As progress was achieved in nonlinear magnetic–mechanical coupling (Y. P. Wan, Fand, & Wang, 2003; X. J. Zheng & Liu, 2005), the nonlinear characteristics of magnetostrictive phase in the ME composite began to receive attention. Guo *et al.* (Y. Y. Guo, Zhou, & Liu, 2010) used the nonlinear magnetic–mechanical coupling theory of giant magnetostrictive materials to explain the changes with bias magnetic field in the ME conversion coefficient. Wong and Shin (C. K. K. Wong & Shin, 2008) introduced the nonlinear magnetization and magnetostrictive strain when studying the ME characteristics in laminated piezoelectric/magnetostrictive particulate composite. Kukhar *et al.* (Kukhar, Pertsev, & Kholkin, 2010) considered the nonlinear magnetization in ferromagnetic phase and developed a nonlinear thermodynamic theory for the ME effect of ferroelectric–ferromagnetic nanostructures. The magnetization and magnetostrictive strain are highly influenced by the pre-stress and bias magnetic field, due to the nonlinear magnetic–mechanical coupling characteristics in magnetostrictive materials. Therefore, the only way to capture the magnetic–electric coupling of laminated ME composites is to consider the nonlinear magnetization and magnetostrictive strains, which means, the full complex magnetic–mechanical–electric coupling characteristics (Hao-Miao Zhou, Li-Ming Xuan, Chao Li, Zhou, Xuan, Li, & Wei, 2011).

Numerically, Liu *et al.* (Gang Liu, Nan, Cai, & Lin, 2004) and Zhou *et al.* (Hao-Miao Zhou, Li-Ming Xuan, Chao Li et al., 2011) calculated the magnetoelectric effect using finite element method (FEM). In their models, the nonlinear behaviour of magnetostrictive material is considered. Linnemann *et al.* (Linnemann, Klinkel, & Wagner, 2009) proposed a constitutive model for magnetostrictive and piezoelectric materials and gave FEM examples, while Nguyen *et al.*(Nguyen, Bouillault, Daniel, & Mininger, 2011) modelled the nonlinear behaviour of magnetic sensor using FEM(H.-L. Wang et al., 2013). Compared to analytical models, the finite element method (FEM) has two advantages (H.-L. Wang et al., 2013):

i. it is able to simulate the magnetic, electric and mechanical field distribution in the composite for any geometry and/or configuration, while analytical models simplify the field distribution under certain assumptions which are only valid in certain cases.

ii. it can adopt nonlinear constitutive relations more conveniently, which is crucial for modelling ME composite because the magnetostriction of most magnetostrictive materials

are nonlinear. Therefore, the magneto-mechanical coupling, that is, the magnetostriction depends both on the magnetic field and stresses.

In most existing works, FEM is usually used to predict only the ME coefficient. Although it is also desirable to get knowledge of the non-uniform magnetic, electric, and mechanical field distribution in this composite material (H.-L. Wang et al., 2013). In order to obtain all these variables, a multiphysics simulator (Finite Element software) can provide the computation of the magnetodielectric effect in the ME composites, as already performed by Rasoanoavy *et al.* (Rasoanoavy, Laur, Smaali, & Queffelec, 2010), and by Zadov *et al.* (Zadov et al., 2012).

Zadov *et al.* (Zadov et al., 2012)consider a ME laminate which comprises two magnetostrictive (Ni) layers and an in-between piezoelectric layer (PZT). Using the finite-element method-based software COMSOL, they calculated numerically the induced voltage between the two faces of the PZT piezoelectric layer, by an external homogeneous small-signal magnetic field threading the three-layer Ni/PZT/Ni laminate structure. For approaching the real material´s properties and to avoid solving the nonlinear micromagnetic problem, a measured magnetization curve of the Ni plate, an explicit *H-B curve*, is used in the computations. The reported results take into account the finite-size effects of the structure, such as the fringing electric field effect and the demagnetization, as well as the effect of the finite conductivity of the Ni layers on the output voltage.

1.4.1. Simulations of piezoelectric materials

Early work of Eer Nisse (Eer Nisse, 1967) and Tiersten (Tiersten, 1967) established variational principles for piezoelectric media. In 1970, Allik and Hughes (Allik & Hughes, 1970) proposed a tetrahedral volumic element accounting for the piezoelectricity. Starting from Hamilton's principle and the constitutive equations for piezoelectric media, a simple volumetric element (tetrahedron), taking into account the piezoelectric coupling, was presented. Twenty years later, Lerch (Lerch, 1990) developed a general formulation accounting for the piezoelectric coupling for two and three-dimensional finite element modelling of piezoelectric devices. A higher order tetrahedral element was proposed by Moetakef *et al.* (Moetakef, Lawrence, Joshi, & Shiakolas, 1995), where interpolation functions of higher orders were used and the number of degrees of freedom reduced by assembling tetrahedrons using a Guyan condensation of the

resulting internal nodes, obtaining brick elements, which were used to model a bimorph pointer (actuation) (Piefort, 2001).

Tzou & Tseng (Tzou & Tseng, 1990, 1991) and Ha *et al.* (Ha, Keilers, & Chang, 1992) used a similar brick element, where the multi-layer structure was taken into account; the element matrices were integrated over the thickness of each layer. Such element was used to simulate the cantilever plate described in (Crawley & Lazarus, 1991) (static case), determine the step-response of a cantilever beam and to design the active damping of the first mode of sensor/actuator composite cantilever plate. Rao & Sunar (Rao & Sunar, 1993) established a finite element formulation of thermo-piezoelectric problems starting from the linear thermo-piezoelectric constitutive equations established by Mindlin (Mindlin, 1974) and the Hamilton's principle. In (Sunar & Rao, 1996, 1997) were used the quasistatic equations of thermo-piezoelectricity to develop heat, sensor and actuator equations; a finite element formulation was presented (Piefort, 2001).

Lee & Saravanos (H.-J. Lee & Saravanos, 1996) derived a thermo-piezoelectric multi-layer beam element which uses linear shape functions along the beam and through the thickness of each layer (layerwise linear). A reduced integration scheme for the transverse shear stiffness was used where the element takes into account the effect of constant thermal load (constant gradient of temperature). Additionally a cantilever beam under thermal load was modelled. Heyliger *et al.* (Heyliger, Pei, & Saravanos, 1996) extended the layerwise linear formulation to a piezoelectric shell element and applied it to static and dynamic modelling of a simply supported plate and a cylindrical shell. Later, Saravanos (Saravanos, 1997) presented a multi-layer piezoelectric thin plate using the Kirchhoff-Love assumption (linear displacement field through the thickness) and bilinear shape functions; assuming a constant electric field through the thickness for each layer (layerwise linear transverse shape function for the electric potential) (Piefort, 2001; Saravanos, 2000).

A pure bending (Kirchhoff assumption) plane rectangular plate element was proposed by Hwan & Park in 1993 (Hwang & Park, 1993); their main idea was to neglect the transverse shear by using a multi-layered plate element with a single electrical degree of freedom per piezoelectric layer, obtaining an electric potential across the layer thickness (that was uniform on each surface element). Six years later, Chattopadhyay *et al.* (Chattopadhyay, Li, & Haozhong, 1999) developed a quasi-static coupled thermo-piezoelectric model for a smart composite plate

40

structure, with surface bonded piezoelectric materials, by using a variational FEM model of piezoelectric active structures approach. In such model a linear piezoelectric response was assumed and a higher order transverse shear strain distribution was used (third order). After that, a shell finite element formulation was obtained (X. Zhou, Chattopadhyay, & Haozhong, 2000)with the same transverse shear strain distribution and a higher order thermal field. A rectangular fibre-reinforced laminated plate with surface bonded piezoelectric patches was modelled and the influence of the couplings on the dynamics of piezo- and thermo- actuated structures was obtained (Piefort, 2001).

1.4.2. Piezoelectric and magnetoelectric simulations for micro and nanostructures

In the field of piezoelectric fibres, in 1993, Bent *et al.* (Bent & Hagood, 1993; Bent, 1997) studied the use of piezoelectric composite actuators for structural applications by constructing piezoceramic fibres that were embedded into a composite helicopter rotor blade. In 2000, Wilkie *et al.*(Wilkie et al., 2000) demonstrated the use of the macro fibre composite actuator to counteract the bending and torsional stresses applied to the vertical tail of a fighter aircraft as a result of buffeting loads (Y. Lin & Sodano, 2008). In 2006, Berger *et al.* (Berger et al., 2006) established unit cell models of 1-3 periodic piezoelectric (PZT) unidirectional cylindrical fibre composites (embedded in a soft non-piezoelectric matrix) for numerical and analytical calculation of effective properties. The numerical approach was based on the finite element method and it allows extension to composites with arbitrary geometrical inclusion configurations. In 2008, Lin *et al.*(Y. Lin & Sodano, 2008) presented a one dimensional micromechanics model of a structural fibre coated with a piezoceramic interphase layer (PZT) in order to evaluate the piezoelectric coupling that could be achieved through this design. In order to understand the effect of the active fibre parameters such as the fibre geometry, core fibre material and piezoceramic coating thickness on the fibre coupling, micromechanics models were derived to predict the material properties of the active structure fibre. All these prior efforts have characterized and developed models for Lead Zirconate Titanate (PZT) as the piezoelectric ceramic, with one or two phases (Y. Lin & Sodano, 2008). But none of those efforts considered a 3D fibre model with PVDF as the piezoelectric composite integrand. Pu *et al.* (Pu et al., 2010) simulated the piezoelectric responses of a suspended one-phase PVDF fibre to the applied electric field along the x-direction are calculated using FEM.

As presented in 1.4, the theory and modelling of ME effect has being widely studied by Harshe and co-workers (Avellaneda & Harshé, 1994; G. Harshe, 1991; Girish Harshe, Dougherty, & Newnham, 1993), Srinivasan *et al.*(Srinivasan, Rasmussen, & Hayes, 2003; Srinivasan et al., 2001; Srinivasan, Hayes, Devreugd, Laletsin, & Paddubnaya, 2005; Srinivasan, Rasmussen, Gallegos, et al., 2002), Nan and co-workers (G. Liu, Nan, Cai, & Lin, 2004; C. W. Nan et al., 2001; C. W. Nan, Lin, & Huang, 2002; C.-W. Nan et al., 2001), Bichurin *et al.*(Bichurin, Petrov, & Srinivasan, 2003; Bichurin, Filippov, et al., 2003b; Filippov et al., 2004), although the major part of these theoretical investigations of magnetoelectric effect are mostly focused on layered ME structures than particulate composites (Y. Zhou & Shin, 2006). In 2008, Wong and Shin developed a model that allows the quantification of the ME effect on a ME nanocomposite as function of the magnetic bias (J. X. Zhang et al., 2009b). The model combines the piezoelectric model developed by Wong in 2001 (C. K. Wong, Poon, & Shin, 2001)of particulate composites with the magnetostrictive model of particulate composites developed by Zhou and Shin (Y. Zhou & Shin, 2005), leading to expressions for the ME effects on the ME nanoparticles (C. K. K. Wong & Shin, 2008). The model, originally developed to study the magnetoelectric effect of magnetostrictive/piezoelectric dilute particulate composites (C. K. K. Wong & Shin, 2008), bases on treating the inclusion/matrix as mildly conducting materials, considering the effect of conductivity and therefore describing the influence of the constituent´s electrical conductivity on the ME effect (C. K. K. Wong & Shin, 2008; Y. Zhou & Shin, 2006). Although this model fully describes the nonlinear effect of stress on the strain-stress-magnetization constitutive relation, it introduces an appreciable amount of fitting constants. If the approach is based on a linear strain-stress-magnetization constitutive relation, the ME effect emerges via stress-induced excess magnetic anisotropy energy (Zadov et al., 2012).

In the present framework, solving the full micromagnetic problem is avoided by establishing an explicit (measured) *H-B curve* of the magnetostrictive material (Bozorth, 1951; Lacheisserie, Gignoux, Schlenker, & Eds., 2004) into a multiphysics interface, generating a model that will couple the magnetic field and piezoelectric model via strain on the piezoelectric part when an external magnetic field is applied. Therefore, there is one distinctive feature of the magnetostrictive part compared to the piezoelectric part of the model, because the magnetostrictive constitutive relation is linear in the strain components but nonlinear in the

magnetization distribution, while the piezoelectric constitutive relations are linear overall, as presented in chapter 2 (F. Graham, 2009; Zadov et al., 2012).

1.5. Objectives of the thesis

Taking the above into consideration, the main objective of this work is to optimize ME polymer based composites suitable for new and advanced applications. The composites will be simulated, the origin of the effects investigated and the range of applicability determined.

In particular, the main scientific objectives of the project are:

1. to develop a model to simulate laminated composites based on electroactive polymers and magnetostrictive materials.

2. develop simulation of magnetoelectric composite structures such as spheres and fibres.

3. compare the results to the experimental data from the literature and guide optimization of materials characteristics and design;

4. select the best structures to be studied from the technological and the fundamental points of view;

5. to get a deeper knowledge of the physical origin of the magnetoelectric coupling.

1.6. Structure of the thesis

This thesis was divided into four main parts, which intends to establish an extensive report that progressively integers partial research achievements during the time of the investigation. The *first chapter* is devoted to an introduction on the main concepts and the state of the art on the subject, with special emphasis on magnetoelectric effect, materials and simulations, providing the basis of the theory and literature that will guide the development of the following sections. The *second chapter* presents the optimization of laminated ME composites by the development

of a FEM piezoelectric model for different numbers of layers and configurations, presenting the influence of mechanical properties (such as elasticity) and PVDF polymer structure, on the Vitrovac/PVDF laminate ME behaviour, when compared to the corresponding Vitrovac/PZT (rigid and ceramic) laminate configuration. The interface problem is analysed in terms of a bonding analysis. The *third chapter* is devoted to the optimization of cobalt ferrite/PVDF spherical and ellipsoidal ME structures, fibres and cylindrical ME composites, by FEM simulation of the ME model, that couples previous piezoelectric model with a magnetostrictive model, via strain. For different sizes and concentrations, 3-D simulations of spheres were compared to 2-D axisymmetrical models, then transforming the spheres in ellipsoidal ME structures that eventually become fibre-shaped. The results on those stuctures are compared to actual 2-D axisymmetric fibres simulation. The integration of magnetostrictive spheres into a cylindrical PVDF matrix is also addressed. Finally, in the last chapter, *fourth chapter*, the main conclusions and suggestions for future work are provided.

CHAPTER 2: SIMULATION OF MAGNETOELECTRIC LAMINATED COMPOSITES

Simulations by finite element method(FEM) of ME materials performance is a powerful tool that can contribute to a better selection of the materials and structures before fabrication. In this chapter, a linear piezoelectric model for ME composites was developed from FEM simulations and applied to multi-layered Vitrovac/PVDF and Vitrovac/PZT laminated composites. The ME model consist on a coupled piezoelectric model, where some assumptions are made in order to introduce the magnetoelastic performance of the material into the electromechanical model, as setting the maximal magnetostriction (at saturation magnetization) by a deformation boundary condition of the magnetostrictive material and therefore not being necessary the simulation of the magnetoelastic behaviour of the material.

2.1. Electromechanical model of a linear piezoelectric material

The constitutive relations for piezoelectric materials under small field condition for direct (eq. 2.1) and converse (eq. 2.2) piezoelectric effect, are (IEEE American National Standards Institute, Ultrasonics, Ferroelectrics, Committee., & Engineers., 1988):

$$\Gamma_i = \overline{\varepsilon_{ij}^T} E_j + d_{im}^d T_m \qquad (2.1)$$

$$S_k = d_{jk}^c E_j + \overline{s_{km}^E} T_m \qquad (2.2)$$

Where Γ is the displacement vector (3x1) (C/m²), S_k is the second order strain tensor (3x3), E is the applied external electric field vector (3x1) (V/m), T_m is the stress tensor (3x3) (N/m²), $\overline{\varepsilon_{ij}^T}$ (F/m) is the second order dielectric permittivity tensor under constant stress, d_{im}^d (mechanical strain per unit electric field under constant mechanical stress) (C/N) and d_{jk}^c (m/N) (electric displacement per unit stress under constant electric field) are the third order piezoelectric strain coefficient tensors, and $\overline{s_{km}^E}$ (m²/N) is the fourth order elastic compliance tensor under constant electric field. The subscripts T and E stand for measurements at constant stress or constant electric field, respectively; also, the subscript d stands for direct, and the subscript c, stands for the converse piezoelectric effect. Because of the symmetry of the stress

and strain tensors, they can be reduced to equivalent vector forms (from (3x3) to (6x1)) as: $[S]=[S_{11}, S_{22}, S_{33}, S_{23}, S_{31}, S_{12}]^T$ and $[T]=[T_{11}, T_{22}, T_{33}, T_{23}, T_{31}, T_{12}]^T$, respectively. By the same way, the piezoelectric strain coefficients and the compliance tensor can be reduced to second order tensors, as $[d^t]$ (3x6), $[d^t]$(6x3) and $\overline{s^E}$ (6x6), respectively. $[d^t]$ and $[d^t]$ are numerically equal and both depend on the crystal structure of the material and the poling direction. From energy considerations, the compliance matrix is symmetric, leaving therefore 21 independent coefficients (for isotropic materials, there are only three independent coefficients); by those energy arguments, the permittivity tensor ($\overline{\varepsilon_{ij}^T}$) is also symmetric, reducing the number of independent coefficients to 6 (even more simplifications can be achieved by taking advantages of crystal configurations) (Culshaw, 1996).

For linear piezoelectricity and in stress charge form, equations 2.1 ad 2.2 (electromechanical constitutive equations) can be also written by (IRE (The Institute of Radio Engineers), 1958; Nechibvute, Chawanda, & Luhanga, 2012):

$$T_m = c_E S - e_s E$$
$$D = e_s^T S + \varepsilon_S E$$

(2.3)

Where T_m(N/m²) is the stress vector; D (C/m²) is the electric flux density vector; S (N/m²) is the strain vector; E (V/m) is the electric field vector, c_E (Pa) is the elasticity matrix (evaluated at constant electric field), e_s is the piezoelectric stress matrix(C/m²), ε_s is the dielectric matrix (evaluated at constant mechanical strain). These equations represent the behaviour of the material for the FEM software. The discretization establishes nodal solution variables and element shape functions over the elements domain, following:

$$u_c = N_u^T \cdot u$$
$$V_c = N_V^T \cdot V$$

(2.4)

where u_c represents the displacement within the element domain in the x, y, z directions, V_c, the electrical potential within the element domain, N_u, the matrix of displacement shape functions, N_V, the vector of the electrical potential shape function, u, the vector of nodal

displacements, and V, the vector of nodal electrical potential. With these equations, and relating to the strain S and electric field E, they can be re-written as:

$$S = B_u \cdot u$$
$$E = -B_V \cdot V$$

(2.5)

where:

$$B_V = \begin{bmatrix} \dfrac{\partial}{\partial x} & \dfrac{\partial}{\partial y} & \dfrac{\partial}{\partial z} \end{bmatrix}^T \text{ and}$$

$$B_u = \begin{bmatrix} \dfrac{\partial}{\partial x} & 0 & 0 & \dfrac{\partial}{\partial y} & 0 & \dfrac{\partial}{\partial z} \\ 0 & \dfrac{\partial}{\partial y} & 0 & \dfrac{\partial}{\partial x} & \dfrac{\partial}{\partial z} & 0 \\ 0 & 0 & \dfrac{\partial}{\partial z} & 0 & \dfrac{\partial}{\partial y} & \dfrac{\partial}{\partial x} \end{bmatrix}^T .$$

Finally, after application of the variational principle and finite element discretization, the coupled finite element time-dependent matrix equation is given by:

$$\begin{bmatrix} M_0 & 0 \\ 0 & 0 \end{bmatrix} \cdot \begin{bmatrix} \dfrac{\partial^2 u}{\partial t^2} \\ \dfrac{\partial^2 V}{\partial t^2} \end{bmatrix} + \begin{bmatrix} C & 0 \\ 0 & 0 \end{bmatrix} \cdot \begin{bmatrix} \dfrac{\partial u}{\partial t} \\ \dfrac{\partial V}{\partial t} \end{bmatrix} + \begin{bmatrix} K & K_z \\ K_z^T & K_d \end{bmatrix} \cdot \begin{bmatrix} u \\ V \end{bmatrix} = \begin{bmatrix} F_0 \\ L_0 \end{bmatrix}$$

,

(2.6)

where the structural mass is $M_0 = \int \rho N_u N_u^T dv$ (with ρ being the mass density); the structural stiffness is $K = \int B_u^T c B_u dv$; the piezoelectric coupling matrix is $K_z = -\int B_u^T e_s B_V dv$; the dielectric conductivity is $K_d = \int B_V^T \varepsilon B_V dv$; C is the structural damping matrix, F_0 is the structural load vector and L_0 is the electrical load vector.

For the stationary case, the coupling represented in equation 2.6, may be given by:

$$\nabla \cdot D = \rho_V \text{ (Gauss Law, t=0)}$$

,

(2.7)

$$\nabla \cdot \sigma = f_V \text{ (Cauchy Momentum Equation, t=0)} \qquad , \qquad (2.8)$$

where $"\nabla \cdot"$ represents the divergence, D the electrical displacement field, ρ_v, the free electric charge density, σ, the stress tensor and f_v the force per unit volume.

2.2. Two dimensional piezoelectric simulations for magnetoelectric laminates

The essential step before numerical simulation of the composites was the construction of a computer model and the assumption of initial conditions (H. Wang, 2009). A wide amount of numerical approaches have been used to determine the ME response of piezoelectric/magnetostrictive composites, namely the Green's function technique (N. Cai et al., 2003; C.-W. Nan et al., 2001; C.-W. Nan, 1994), the finite element method (G. Liu et al., 2004; Gang Liu et al., 2004), the constitutive equations (Bao & Luo, 2011), the numerical statistical analysis (Chiolerio et al., 2012)and the effective medium approximation(S. Srinivas & Li, 2005). Regardless, considering that both magnetostrictive and piezoelectric behaviours are anisotropic and that the model incorporates specific mechanical coupling factors into the final ME response, the approach that best fit the evaluation of the macroscopic experimental response was the FEM (M. Silva et al., 2013). By these means, magnetoelectric responses of laminates were simulated by FEM, using an electromechanical model and assuming linear piezoelectricity and magnetostriction range, as described in 2.1.

A two-dimensional approximation was considered, establishing that the ME response of the structure would be constant along the width of the structure. Based on the constitutive equations (H. Wang, 2009), the calculations were performed on each nodal point with specific boundary conditions and holding into two essential principles, energy conservation and continuity at the nodal interface (Gauss Law and Cauchy Momentum Equation, for stationary case, t=0), as described in the previous section. Structural design parameters such as geometry effects and configurations and materials structural properties are subsequently analysed and discussed.

The simulation analyses were performed in order to conceive the structural influence of the magnetostrictive and piezoelectric layers properties on the ME performance of the material. Assuming linear range of magnetostriction, the electro-mechanical coupling of each ME structure was modelled by FEM in order to obtain the numerical ME response. Each model additionally

48

considered the ME structure as composed by flexible films - magnetostrictive layer of Vitrovac, piezoelectric layer of PVDF (and epoxy layer for experiment 2.2.2) - and properly glued to each other. The electromechanical simulation consisted in applying a deformation on the lateral ends of the magnetostrictive layer taking into account the magnetostrictive response of the material (Fonteyn, Belahcen, Kouhia, Rasilo, & Arkkio, 2010; Grunwald & Olabi, 2008; M. Silva et al., 2013) and evaluating the electric potential obtained across the piezoelectric layer. The input parameter for the calculations was S=λ(H), which is the magnetically induced magnetostrictive strain from the magnetic field, the magnetostriction curve of the material. In all cases it was chosen the strain corresponding to the maximum deformation experienced by the magnetostrictive layer. Structurally, as the layers were perfectly bonded and assuming linear range of magnetostriction, the deformation on the magnetostrictive layer would produce a deformation on the other layers that will depend directly of their mechanical properties. Boundary conditions as lateral polarization of the piezoelectric material, grounds, and fixing the ME structure only to deform in longitudinal direction were also set, in order to diminish the degrees of freedom.

The simplest model of ME laminate (experiment 2.2.1) consisted of a biphasic laminated structure with one magnetostrictive and one piezoelectric layer. Analyses were performed in order to conceive the structural influence of the magnetostrictive and piezoelectric layer´s width on the ME performance of the material. Despite the high values of ME response on polymer based ME laminates, proper description, characterization and optimization of both piezoelectric and magnetostrictive phases, the optimization of the element responsible for the coupling between the phases (usually an epoxy) remains poorly studied (G. Liu et al., 2004; C. W. Nan, Liu, et al., 2003). Trying to solve this limitation, in the second simulation experiment, 2.2.2, PVDF was bonded to the magnetostrictive material with epoxy. The influence of the mechanical properties of the epoxy over the ME performance of the material were then tested and compared with experimental measurements of ME materials glued with three different epoxies.

Three-phasic and multi-phasic ideal models were established in order to perceive the influence of the structural symmetries on the piezoelectric and magnetostrictive width dimensions. Different configurations were then evaluated: For the tri-phasic composite, the cases of two magnetostrictive layers sandwiching a piezoelectric layer - from now on MPM ME

structure- and two piezoelectric layers sandwiching a magnetostrictive layer - from now on PMP ME structure; for multi-layered laminate composites, the cases of even number of layers -from now on MP ME configurations, and odd number of layers, with top and bottom magnetostrictive layers configurations -named M-M ME configurations- and top and bottom piezoelectric layers configurations - from now on P-P ME multi-layered configurations. Simulations were performed with PVDF and PZT in order to establish the influence of the mechanical properties of the amorphous semi-crystalline polymer (softer and more flexible than piezoceramics) on the ME response of the structure.

To simulate the elastic behaviour of the magnetostrictive and epoxy (for experiment 2.2.2) domains, a linear elastic material model was used with the boundary condition of a prescribed displacement on each lateral end of the magnetostrictive layer of $\lambda_{max}/2$ (=0.4μm)). Piezoelectric domains employed linear model, as previously described by the constitutive equations, with the boundary condition of electrical ground on one of its surfaces or interfaces, in front of the other electrically isolated surface (interface) where the electric potential was evaluated. Obtained values for electric potential distribution were integrated over the electric potential interface line and the ME coefficient was obtained by the following equation:

$$\alpha_{ME} = \left| \frac{dE}{dH} \right| = \left| \frac{\delta V}{d_{pzo}} \right| = \left| \frac{\int_{int\,erface} \varphi \cdot dL}{d_{pzo}(cm) \cdot L} \right| \left(\frac{V}{cm} \right) \qquad , \qquad (2.9)$$

where α_{ME} is the magnetoelectric coefficient, δV is the induced magnetoelectric voltage, d_{pzo} is the piezoelectric thickness (in centimetres), φ is the electric potential, and L is the interface length.

In cases of experiments with more than one piezoelectric layer, the composite was treated as a device where piezoelectric layers are connected in series. By this way, the final ME coefficient (α_{ME}) is obtained by the sum of each ME coefficient, over each interface, as:

$$\alpha_{ME} = \sum_{INTERFACE} \alpha_{ME-INTERFACE} \qquad (2.10)$$

50

FEM was used to simulate the performance of the ME structure according to the piezoelectric material properties (PZT/PVDF), the thickness of magnetostrictive material and the thickness of piezoelectric material. For ideal tri-layered and multi-layered ME structures, cases of free and clamped composites were analysed. In clamped configurations the laminated structure was set to deform only along longitudinal direction in both bottom and top piezoelectric surfaces, as can be when the material is fixed into a device.

For all purposes, the length of the ME structure was set to 30 mm with an increase of 1mm at each end of each piezoelectric layer, with a width of 6 mm and the piezoelectric material polarization established to be lateral. Vitrovac 4040 ($Fe_{39}Ni_{39}Mo_4Si_6B_{12}$) (Grunwald & Olabi, 2008) was used as magnetostrictive component, not for its magnetostriction value (λ_{max}=8 ppm), actually modest, but for its high piezomagnetic coefficient (1.3 ppm/Oe) at low magnetic fields ($\approx$15 Oe), and low cost (Gutierrez et al., 2012). PVDF was chosen as the polymeric piezoelectric component since it is the overall best piezoelectric polymer (P. Martins, Lopes, & Lanceros-Mendez, 2013; P. Martins, Lasheras, et al., 2011). Lead zirconate titanate (PZT-5H) was selected to compare the obtained results with a ceramic based ME structure. Materials properties of PVDF, PZT and Vitrovac are shown in Tables 2.1 and 2.2.

Table 2.1: Electromechanical properties of PVDF (Esterly, 2002) and PZT (COMSOLMultiphysics, 1998; CTSElectronichsComponents, 2014)

Property/Name	PVDF	PZT	Unit
Density	1470	7500	kg/m³
Elasticity matrix, c_E (Ordering: xx, yy, zz, yz, xz, xy)	{{2.74e+09, 5.21e+09, 4.78e+09, 0, 0, 0}, {5.21e+09, 2.36e+09, 5.21e+09, 0, 0, 0}, {4.78e+09, 5.21e+09, 2.12e+09, 0, 0, 0}, {0, 0, 0, 2.74e+09, 0, 0}, {0, 0, 0, 0, 2.74e+09, 0}, {0, 0, 0, 0, 0, 2.74e+09}}	{{1.27e+11, 8.02e+10, 8.47e+10, 0, 0, 0}, {8.02e+10, 1.27e+11, 8.47e+10, 0, 0, 0}, {8.47e+10, 8.47e+10, 1.17e+11, 0, 0, 0}, {0, 0, 0, 2.30e+10, 0, 0}, {0, 0, 0, 0, 2.30e+10, 0}, {0, 0, 0, 0, 0, 2.35e+10}}	Pa
Compliance matrix, c_E^{-1} (Ordering: xx, yy, zz, yz, xz, xy)	{3.65e-10,-1.92e-10, 4.24e-10, -2.09e-10, -1.92e-10, 4.72e-10, 0, 0, 0, 3.65e-10, 0, 0, 0, 0, 3.65e-10, 0, 0, 0, 0, 0, 3.65e-10}	{1.65e-11, -4.78e-12, 1.65e-11, -8.45e-12, -8.45e-12, 2.07e-11, 0, 0, 0, 4.35e-11, 0, 0, 0, 0, 4.35e-11, 0, 0, 0, 0, 0, 4.26e-11}	1/Pa
Coupling matrix, e	{{0, 0, -4.761, 0, 0, -33.33}, {0, 0, 3.703, 0, 1.703, 0}, {1.703, 0, 0, 0, 0, 0}}	{{0, 0, -6.62281, 0, 0, -6.62281}, {0, 0, 23.2403, 0, 17.0345, 0}, {17.0345, 0, 0, 0, 0, 0}}	C/m²
Relative permittivity, ε_S	{{13, 0, 0}, {0, 13, 0}, {0, 0, 13}}	{{1704.4, 0, 0}, {0, 1704.4, 0}, {0, 0, 1433.6}}	1

Table 2.2: Mechanical Properties of Vitrovac 4040

Property/Name	VITROVAC 4040	Unit
Density, ρ	7900	kg/m^3
Poisson´s Ratio, ν	0.27	1
Young´s Modulus, Y	1500	MPa

2.2.1. Ideal bi-layer two dimensional laminate simulation

As reported before, experiment 2.2.1. consisted on the simulation of an ideal bi-layer, where the deformation of the magnetostrictive material produces a deformation on the piezoelectric material, generating via strain, an electric potential distribution on the interface between the piezoelectric and the magnetostrictive material, as pictured in Figure 2.1.
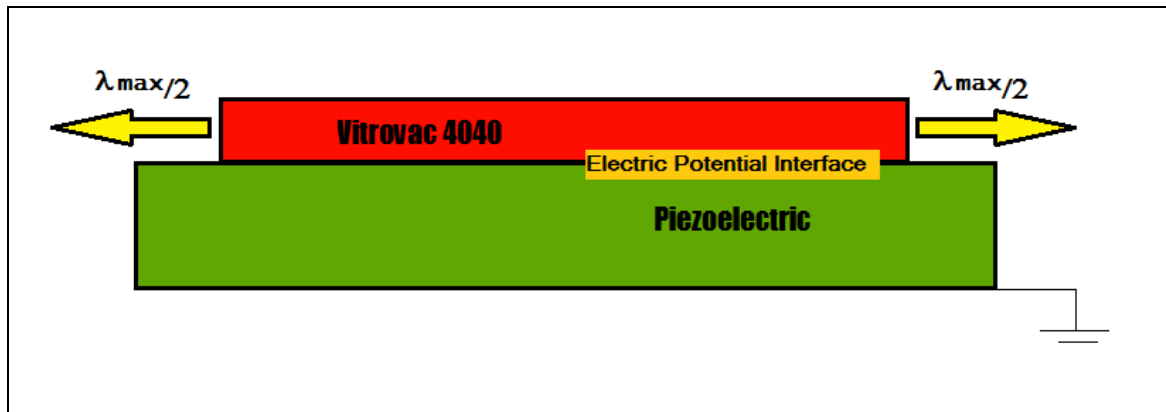
Figure 2.1: Representation of the bi-layer magnetoelectric simulation experiment

Figure 2.1 represents the experiment of the bi-phasic laminate composite, establishing deformation direction (of $\lambda_{max}/2$) on each side of the magnetostrictive (Vitrovac 4040) ends, and electric potential and ground on the top and bottom interfaces, respectively.

According to the piezoelectric material properties (PZT/PVDF), the thickness of the magnetostrictive material and the thickness of piezoelectric material, the ME performance of the structure was obtained. Thickness values were swept, including values for thickness between 1μm and 1mm. When the Vitrovac thickness was swept, the piezoelectric material held a constant value of 110 μm; likewise, when the piezoelectric material was being simulated, the held value for the magnetostrictive thickness was of 25 μm.

52

2.2.2. Epoxy properties on bi-layer two dimensional laminate simulation

In the second simulation experiment (2.2.2), PVDF was bonded to the magnetostrictive material with epoxy. The influence of the mechanical properties of the epoxy on the ME performance of the material were then tested and compared with experimental measurements of ME materials glued with three different epoxies. The model considered the ME structure as composed by three flexible films - magnetostrictive layer of Vitrovac, epoxy layer and piezoelectric layer of PVDF- properly glued to each other with an appropriate coupling, as presented in Figure 2.2.
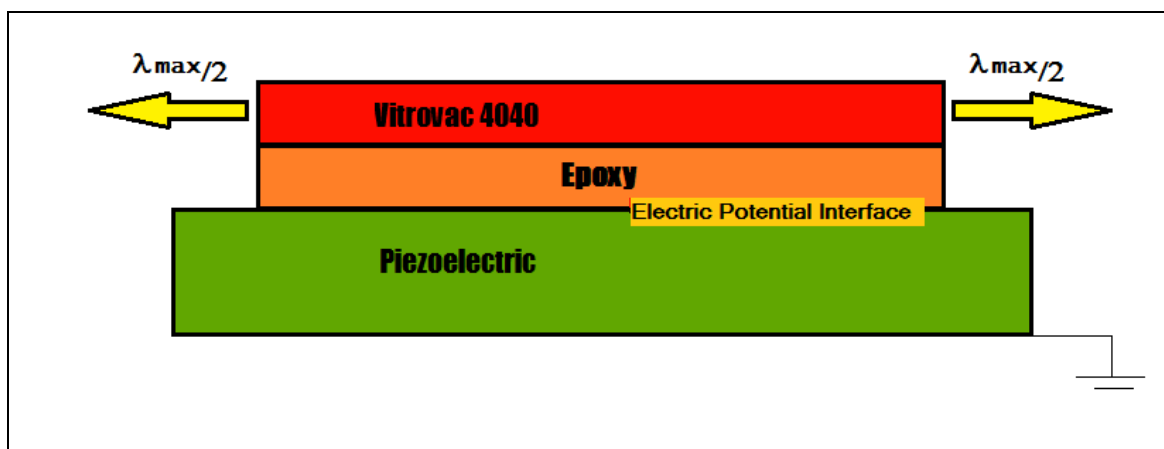
Figure 2.2: Representation of the tri-layer piezoelectric-epoxy-magnetostrictive magnetoelectric simulation experiment

Figure 2.2 represents the experiment of the tri-phasic laminate composite (magnetostrictive/glue/piezoelectric phase), establishing deformation direction (of $\lambda_{max}/2$) on each side of the magnetostrictive (Vitrovac 4040) ends, and electric potential and ground on the top and bottom interfaces, respectively.

Structurally, when the three layers are perfectly bonded, the deformation on the magnetostrictive layer will produce a deformation on the other 2 layers, which will depend on their mechanical properties. The influence of the bonding layer Young modulus on the ME performance of the structure was thus simulated together with the ME response of the laminate with varying piezoelectric and bonding layer thickness, in order to optimize the ME response of the fabricated multi-layer structures.

Finally, the comparison between numerical and experimental data allowed to select the appropriate epoxy characteristics and to optimize the piezoelectric PVDF layer width to maximize

the induced magnetoelectric voltage. A coupling coefficient (k) was included to the simulated values, representing the mechanical coupling between the epoxy and both Vitrovac and PVDF layers. Such coefficient was set to be between 0 (not coupled) and 1 (ideal coupling).

For experimental evaluation and comparison, laminated composites were prepared by gluing the piezoelectric layer to the magnetostrictive layer with three different epoxy resins, chosen due to their distinct mechanical properties (Young Modulus given in the brackets): ITW Devcon 5 Minute® Epoxy (0.7 GPa), Strain Gage Adhesive M-Bond 600 - Vishay Precision Group (0.3 GPa) and Stycast 2850 FT blue (9 GPa). The Young modulus of the epoxy resins were determined from the initial slope of strain–stress curves measured using a Shimadzu AG-IS universal testing machine in tensile mode, with a 2 mm min−1 loading rate (data not shown).Commercial poled β-PVDF with thicknesses of 28, 52 and 110 μm with Cu-Ni electrodes deposited on both sides was purchased from Measurement Specialties, USA, and used as provided (d_{33}=-33×10 and d_{31}=23×10 pC/N). Vitrovac 4040® ($Fe_{39}Ni_{39}Mo_4Si_6B_{12}$), 30 mm x 6 mm x 25 μm magnetostrictive ribbons were used as magnetostrictive components. The ME measurements were performed simultaneously applying a H_{DC} magnetic field ranging from 0 to 50 Oe and a superimposed H_{AC} field equal to 0.13 Oe at resonance frequencies ranging from 30 to 45 kHz. The ME response of these laminates were determined with the following equation(M. Silva et al., 2013):

$$\alpha_{ME} = \frac{dE}{dH} = \frac{1}{d_{pzo}(cm)}\left(\frac{\delta V}{\delta H_{AC}}\right) \qquad , \tag{2.11}$$

where α_{ME} is the ME coefficient, δH_{AC} is the AC magnetic field amplitude (for these cases, of 0.13 Oe), δV is the induced magnetoelectric voltage, d_{pzo} is the piezoelectric thickness (in centimetres) and L is the interface length.

The measurement of δV was performed with a SR830 DSP lock-in amplifier. In order to compare simulated and measured data, simulated results have to be divided by the AC magnetic field amplitude (δH_{AC}), in order to analyse data with same magnitudes (V/cm)(M. Silva et al., 2013).

2.2.3.Ideal tri-layer two dimensional laminate simulation

Ideal ME 3-layered laminated structures were simulated for PVDF and PZT piezoelectric phase and Vitrovac magnetostrictive phase, for the case where the piezoelectric phase is sandwiched by the magnetostrictive phase (MPM configuration, 2.2.3.1) and the case where the magnetostrictive phase is sandwiched by the piezoelectric phase (PMP configuration, 2.2.3.2).

2.2.3.1. Magnetostrictive-piezo-magnetostrictive laminate simulations (MPM)

Following the bi-layer experiment (2.2.1), a tri-layer laminate structure was analysed, in which the piezoelectric material is sandwiched by magnetostrictive material (Figure 2.3).
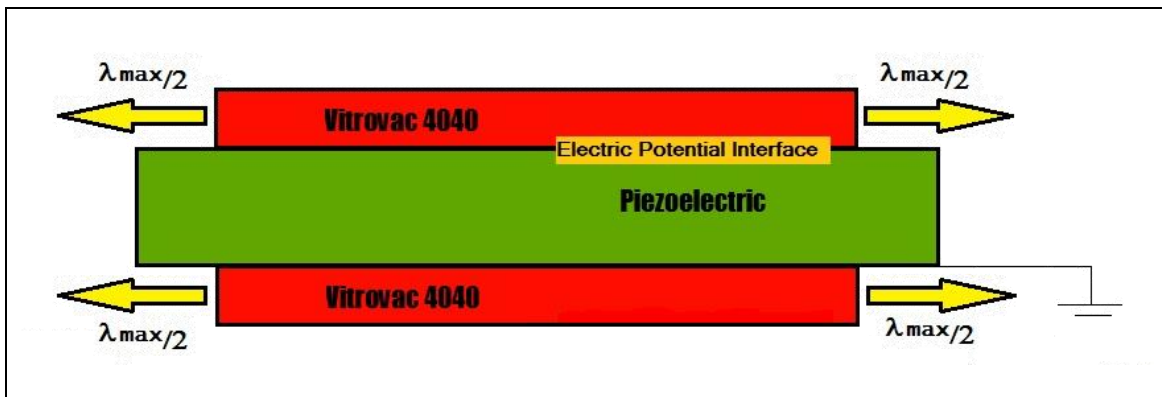
Figure 2.3: Representation of the tri-layer magnetostrictive-piezoelectric-magnetostrictive (MPM) magnetoelectric simulation experiment

Figure 2.3 represents the experiment of the tri-phasic laminate magnetostrictive-piezoelectric-magnetostrictive (MPM) composite, establishing deformation direction (of $\lambda_{max}/2$) on each side of the magnetostrictive (Vitrovac 4040) ends, and electric potential and ground on the top and bottom interfaces of the piezoelectric material, respectively.

FEM was used to simulate the performance of the ME structure according to the piezoelectric material properties (PZT/PVDF) and different configurations of piezoelectric and magnetostrictive material´s thickness for free and clamped configurations, the former referring to a configuration that was not allowed to move in the vertical direction for bottom and top surfaces. A sweep was made, including values for thickness between 10 μm and 600 μm. First, piezoelectric thickness was tested when both magnetostrictive layers have a 25 μm width. Following, symmetric and asymmetric configurations for the magnetostrictive and piezoelectric thicknesses were tested, including studies with sweep parameters presented in Table 2.3, where

d_ms represents magnetostrictive thickness, and d_pzo represents piezoelectric thickness. The numbers 1 and 2 establish the case where the thickness may take 2 different values for the same configuration. Obtained values for electrical potential distribution were integrated over each interface and the ME coefficient (α_{ME}) is obtained by equation (2.9).

Table 2.3: Configurations for tri-layer magnetostrictive-piezoelectric-magnetostrictive (MPM) simulations and sweep parameters, according to the piezoelectric thickness (d_pzo) and magnetostrictive thickness (d_ms) of the configuration

Configuration	Sweep Parameter	Sweep parameter range	Fixed Parameters	Fixed Parameter Values
Symmetric	d_pzo	10-600 µm	d_ms1=d_ms2	25 µm
Symmetric	d_ms1	10-600 µm	d_ms2	25 µm
			d_pzo	110 µm
Asymmetric	d_pzo	10-600 µm	d_ms1	25 µm
			d_ms2	12 µm
Asymmetric	d_ms1	10-600 µm	d_ms2	25 µm
			d_pzo	110 µm

2.2.3.2. Piezoelectric-magnetostrictive-piezoelectric laminate simulations (PMP)

This experiment consisted of a tri-layer laminate, where the magnetostrictive material was sandwiched by the piezoelectric material of the ME composite, piezoelectric-magnetostrictive-piezoelectric (PMP) configuration. The experiment included free and clamped configurations, the last referring to a configuration that was not allowed to move in the vertical direction for bottom and top surfaces.

Figure 2.4 (a) pictures the free PMP experiment, while Figure 2.4 (b) shows the clamped PMP configuration.
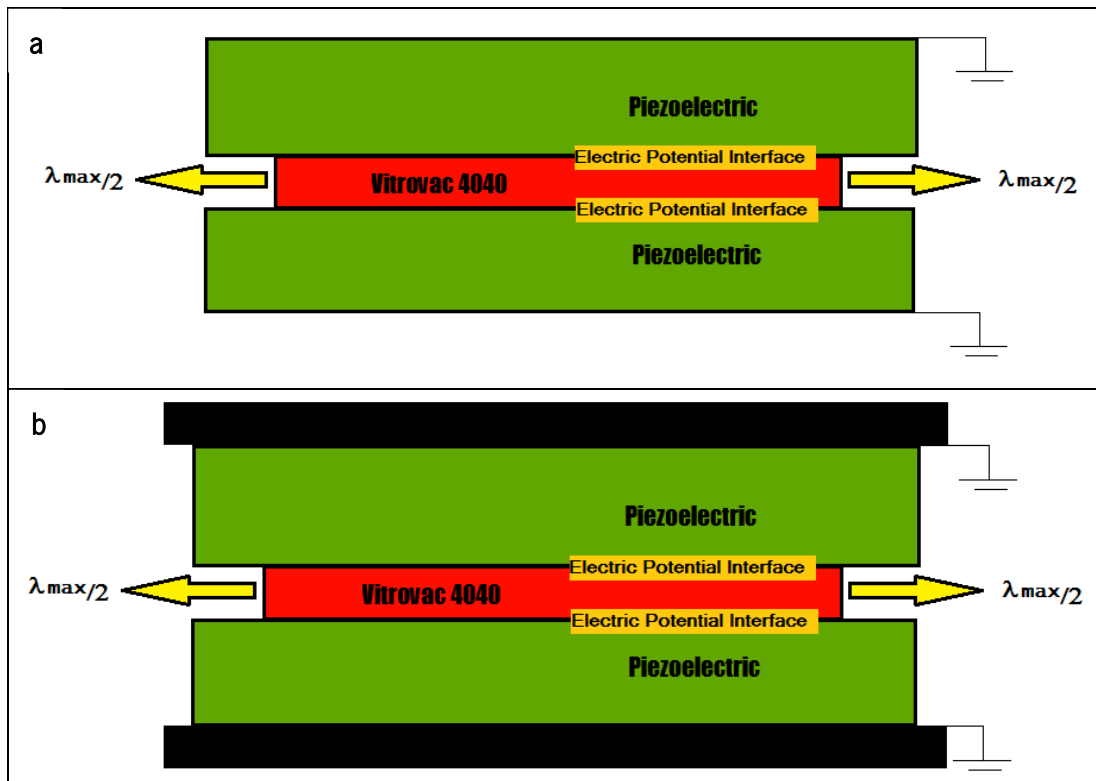
Figure 2.4: Representation of the tri-layer piezoelectric-magnetostrictive-piezoelectric (PMP) magnetoelectric simulation experiment, for free (a) and clamped (b) experiments

Figure 2.4 represents the experiment of the tri-phasic laminate piezoelectric-magnetostrictive-piezoelectric (PMP) composite, establishing deformation direction (of $\lambda_{max}/2$) on each side of the magnetostrictive (Vitrovac 4040) ends, electric potential on each magnetostrictive/piezoelectric interface, and ground on the top and bottom interfaces of the composite, respectively.

Likewise, the deformation of the magnetostrictive material produced a deformation on both piezoelectric layers, generating via strain, an electric potential distribution on the interfaces between the piezoelectric and the magnetostrictive material. FEM was used to simulate the performance of the ME structure according to the polymer/ceramic piezoelectric material properties (PVDF/PZT) and different configurations of piezoelectric material´s thickness for clamped and free cases. A sweep was made, including symmetric and asymmetric configurations for piezoelectric and magnetostrictive thickness values. Sweep parameters and fixed values for every simulation are established in Table 2.4, where d_ms represents magnetostrictive thickness, and d_pzo represents piezoelectric thickness. The numbers 1 and 2 establish the case where the thickness may take 2 different values for the same configuration.

Table 2.4: Configurations for tri-layer piezoelectric-magnetostrictive-piezoelectric (PMP) simulations and sweep parameters, according to the piezoelectric thickness (d_pzo) and magnetostrictive thickness (d_ms) of the configuration

Configuration	Sweep Parameter	Sweep parameter range	Fixed Parameters	Fixed Parameter Values
Symmetric	d_ms	10-600 µm	d_pzo1=d_pzo2	110 µm
Symmetric	d_pzo1	10-600 µm	d_pzo2	110 µm
			d_ms	25 µm
Asymmetric	d_ms	10-600 µm	d_pzo1	110 µm
			d_pzo2	25 µm
Asymmetric	d_pzo1	10-600 µm	d_pzo2	110 µm
			d_ms	25 µm

In order to obtain the ME coefficient of the structure and as the magnetoelectric laminate was composed of two piezoelectric parts, the composite had to be treated as a device where obtained values for electric potential distribution were integrated over each interface and the ME coefficient is obtained by equation (2.9), applied on each interface and then treated as a device where both piezoelectric layers were connected in series. Therefore, the final ME coefficient (α_{ME}) was obtained by the sum of each ME coefficient, over each interface, as presented in equation (2.10).

2.2.4. Ideal multi-layer two dimensional laminate simulation

As established for the tri-layer experiments, and in order to improve understanding on the systems, multi-layer 2D laminate experiments were subdivided by the top and bottom material type (magnetostrictive/piezoelectric) of the multi-layered layered composite. They were subdivided into a) magnetostrictive-piezoelectric (M-P) multi-layer configurations (2.2.4.1), for composites with even number of layers, where the bottom layer is magnetostrictive and the top layer is piezoelectric, b) magnetostrictive-magnetostrictive (M-M) multi-layer configurations (2.2.4.2), for composites with odd number of layers, where bottom and top layers are magnetostrictive and c) piezoelectric-piezoelectric (P-P) multi-layer configurations (2.2.4.3), for composites with odd number of layers, where bottom and top layers are composed of piezoelectric material.

2.2.4.1. Magnetostrictive-piezoelectric multi-layer simulations (M-P)

This experiment consisted of 5 different configurations with equal number of piezoelectric and magnetostrictive layers (between 2 and 10 layers of Vitrovac and PZT or Vitrovac and PVDF), where the total thickness of the ME composite remains the same, as depictured in Figure 2.5.
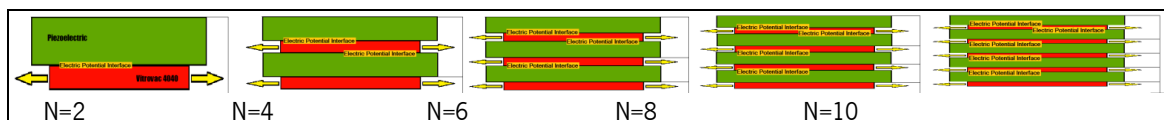
Figure 2.5: Representation of magnetostrictive-piezoelectric (M-P) multi-layer magnetoelectric simulation experiment, where N is the number of layers.

Figure 2.5 shows a schematic representation of M-P multi-layer simulation experiments, for number of layers (N) between 2 and 10. The piezoelectric material is colour green, while the magnetostrictive material is red. Yellow arrows represent deformation boundary conditions, while yellow interfaces include a floating potential condition.

M-P multi-layer of Vitrovac/PZT and Vitrovac/PVDF were modelled, for composites with a total thickness (D_c) of 600 and 300 μm (for n=2, 300 μm piezoelectric/300 μm magnetostrictive, or 150 μm piezoelectric/150 μm magnetostrictive, and so on) and a number of layers, N, between 2 and 10. Likewise, the deformation of the magnetostrictive material produced a deformation on both piezoelectric layers, generating via strain, an electric potential distribution on the interfaces between the piezoelectric and the magnetostrictive material. FEM was used to simulate the performance of the ME structure according to the polymer/ceramic piezoelectric material properties (PVDF/PZT). In order to assess the limitations of this structural analysis, results were compared with those obtained by Srinivasan *et al.*(Srinivasan, Rasmussen, Levin, et al., 2002), that compiled an experimental analysis with a 400 μm thick bi-layer and multi-layer on thick-film structures of $La_{0.7}Sr_{0.3}MnO_3$ (LSMO)-PZT and $La_{0.7}Ca_{0.3}MnO_3$ (LCMO)-PZT. Their samples were made with an equal number of manganite and PZT layers, between 2 and 8 layers.

As presented by Srinivasan *et al.*, α was not calculated by equation 2.11, but from the total electric potential (by the sum of all partial electric potential between magnetostrictive and piezoelectric layers) divided by the total piezoelectric length (in cm), called unitary α, or $\boldsymbol{\alpha_{unit}}$ (equation (2.12)):
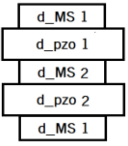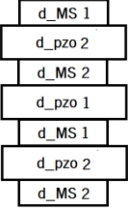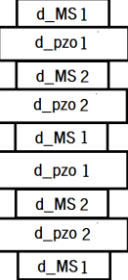
$$\alpha_{unit} = \left|\frac{dE}{dH}\right| = \left|\frac{\delta V}{d_{pzo}}\right| = \frac{\sum\limits_{INTERFACE}\left|\int\limits_{interface}\varphi \cdot dL\right|_{INTERFACE}}{d_{pzo}(cm)\cdot L}\left(\frac{V}{cm}\right) \qquad , \qquad (2.12)$$

where $\boldsymbol{\alpha_{unit}}$ is the unitary ME coefficient for the multi-layer, δV is the induced magnetoelectric voltage, d_{pzo} is the total piezoelectric thickness (sum of all individual piezoelectric thicknesses, in centimetres),φ is the electric potential and L is the interface length. For symmetric cases, $\boldsymbol{\alpha_{unit}}$ corresponds also to the average $\boldsymbol{\alpha_{ME}}$, or the sum of all α-values (equation 2.10) divided by the number of piezoelectric layers (N_pzo).

2.2.4.2. Magnetostrictive-magnetostrictive multi-layer simulations (M-M)

FEM was used to simulate the performance of multi-layered ME structures according to the polymer/ceramic piezoelectric material properties (PVDF/PZT) and different configurations of piezoelectric material´s thickness, for free and clamped configurations. Multi-layers included were composed of 5 to 9 layers of magnetostrictive/piezoelectric phases, where the layers were sandwiched by magnetostrictive material: 5-layered structure MPMPM, 7-layered structure MPMPMPM, and the9-layered structure MPMPMPMPM, where M represents the magnetostrictive material and P represents the piezoelectric material. Configurations, sweep parameters and fixed values are established in Table 2.5, where d_ms represents magnetostrictive thickness, and d_pzo represents piezoelectric thickness. The numbers 1 and 2 establish the case where the thickness may take 2 different values for the same configuration.

Table 2.5: Configuration, sweep parameters and fixed values for all simulated magnetostrictive-magnetostrictive (M-M) multi-layers configurations, where d_ms represents magnetostrictive thickness and d_pzo represents piezoelectric thickness.

Configuration			Sweep Parameter	Sweep Parameter Range	Fixed Parameters	Fixed Par. Values
	MPMPM	Symmetric (d_ms1=d_ms2; d_pzo1=d_pzo2)	d_ms	10-600 µm	d_pzo	110 µm
		Symmetric (d_ms1=d_ms2; d_pzo1=d_pzo2)	d_pzo	10-600 µm	d_ms	25 µm
		Asymmetric	d_ms1	10-600 µm	d_pzo1=d_pzo2	110 µm
					d_ms2	25 µm
		Asymmetric	d_pzo1	10-600 µm	d_pzo2	110 µm
					d_ms1=d_ms2	25 µm
	MPMPMPM	Symmetric (d_ms1=d_ms2; d_pzo1=d_pzo2)	d_ms	10-600 µm	d_pzo	110 µm
		Symmetric (d_ms1=d_ms2; d_pzo1=d_pzo2)	d_pzo	10-600 µm	d_ms	25 µm
		Asymmetric	d_ms1	10-600 µm	d_pzo1=d_pzo2	110 µm
					d_ms2	25 µm
		Asymmetric	d_pzo2	10-600 µm	d_pzo1	110 µm
					d_ms1=d_ms2	25 µm
	MPMPMPMPM	Symmetric (d_ms1=d_ms2; d_pzo1=d_pzo2)	d_ms	10-600 µm	d_pzo	110 µm
		Symmetric (d_ms1=d_ms2; d_pzo1=d_pzo2)	d_pzo	10-600 µm	d_ms	25 µm
		Asymmetric	d_ms1	10-600 µm	d_pzo1=d_pzo2	110 µm
					d_ms2	25 µm
		Asymmetric	d_pzo1	10-600 µm	d_pzo2	110 µm
					d_ms1=d_ms2	25 µm
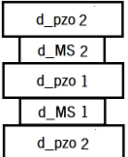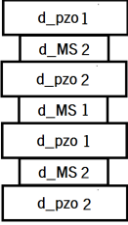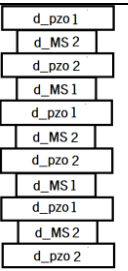
As well as other experiments with more than one piezoelectric layer, the magnetoelectric coefficient was obtained by equation (2.9), applied on each interface and then treated as device where both piezoelectric layers are connected in series. Therefore, the final ME coefficient (α_{ME}) was obtained by the sum of each ME coefficient, over each interface, as presented in equation - (2.10).

2.2.4.3. Piezoelectric-piezoelectric multi-layer simulations (P-P)

FEM was used to simulate the performance of multi-layered ME structures according to the polymer/ceramic piezoelectric material properties (PVDF/PZT) and different configurations of piezoelectric material´s thickness, for free and clamped configurations. Multi-layers included were composed of 5 to 11 layers of magnetostrictive/piezoelectric phases, where the layers were sandwiched by piezoelectric material: 5-layered PMPMP, 7-lyered PMPMPMP and the 11-layered PMPMPMPMPMP structure. Configurations, sweep parameters and fixed values are established in Table 2.6, where d_ms represents magnetostrictive thickness, and d_pzo represents piezoelectric thickness. The numbers 1 and 2 establish the case where the thickness may take 2 different values for the same configuration.

As well as other experiments of more than one piezoelectric layer, the magnetoelectric coefficient was obtained by equation (2.9), applied on each interface and then treated as device where both piezoelectric layers were connected in series. Therefore, obtaining the final ME coefficient (α_{ME}) was obtained by the sum of each ME coefficient, over each interface, as presented in equation (2.10).

Table 2.6: Configuration, sweep parameters and fixed values for all simulated piezoelectric-piezoelectric (P-P) multi-layer configurations, where d_ms represents magnetostrictive thickness, and d_pzo represents piezoelectric thickness.

Configuration			Sweep Parameter	Sweep Parameter Range	Fixed Parameters	Fixed Par. Values
	PMPMP	Symmetric (d_ms1=d_ms2; d_pzo1=d_pzo2)	d_ms	10-600 µm	d_pzo	110 µm
		Symmetric (d_ms1=d_ms2; d_pzo1=d_pzo2)	d_pzo	10-600 µm	d_ms	25 µm
		Asymmetric	d_ms1	10-600 µm	d_pzo1=d_pzo2	110 µm
					d_ms2	25 µm
		Asymmetric	d_pzo2	10-600 µm	d_pzo1	110 µm
					d_ms1=d_ms2	25 µm
	PMPMPMP	Symmetric (d_ms1=d_ms2; d_pzo1=d_pzo2)	d_ms	10-600 µm	d_pzo	110 µm
		Symmetric (d_ms1=d_ms2; d_pzo1=d_pzo2)	d_pzo	10-600 µm	d_ms	25 µm
		Asymmetric	d_ms2	10-600 µm	d_pzo1=d_pzo2	110 µm
					d_ms1	25 µm
		Asymmetric	d_pzo1	10-600 µm	d_pzo2	110 µm
					d_ms1=d_ms2	25 µm
	PMPMPMPMP	Symmetric (d_ms1=d_ms2; d_pzo1=d_pzo2)	d_ms	10-600 µm	d_pzo	110 µm
		Symmetric (d_ms1=d_ms2; d_pzo1=d_pzo2)	d_pzo	10-600 µm	d_ms	25 µm
		Asymmetric	d_ms2	10-600 µm	d_pzo1=d_pzo2	110 µm
					d_ms1	25 µm
		Asymmetric	d_pzo1	10-600 µm	d_pzo2	110 µm
					d_ms1=d_ms2	25 µm

2.3. Results and discussion

FEM Simulation results are displayed by graphs of the simulated magnetoelectric coefficient of the structure versus the sweep parameter, as PVDF/PZT thickness or Vitrovac thickness, according to the simulation experiment. Also, in some cases, images of electric potential distribution and/or displacement field on the vertical (y) plane are used to establish the influence of the mechanical properties (elasticity) and morphological features of the materials over the obtained ME performance of the structure. These images use a rainbow colour range (from minimal, negative blue to maximal, positive red) that establishes the intensity of the electric potential value (V)/displacement field value (m) at each point of the piezoelectric/structure surface.

2.3.1. Ideal bi-layer 2D laminate simulation

ME performance of bi-layer laminates have been widely studied for piezoelectric ceramics and magnetostrictive metals (Babu, Bhimasankaram, & Suryanarayana, 2005; C. Nan et al., 2008; Jungho Ryu et al., 2001, 2002), but variations on the mechanical properties in the piezoelectric component (when including an electrostrictive polymer as PVDF, more flexible and with an amorphous semi-crystalline structure) may lead to variations in the ME performance of the composite. FEM structural simulations of the ME performance for bi-layer ME composites of Vitrovac and PVDF and Vitrovac and PZT are presented in order to establish these differences.

Figure 2.6 establishes the simulated ME performance (ME coefficient, α_{ME}) of the bi-layer laminate structure for both cases, PVDF and PZT, including magnetostrictive (a) and piezoelectric (c) thickness sweep from 10 μm to 1mm.

64
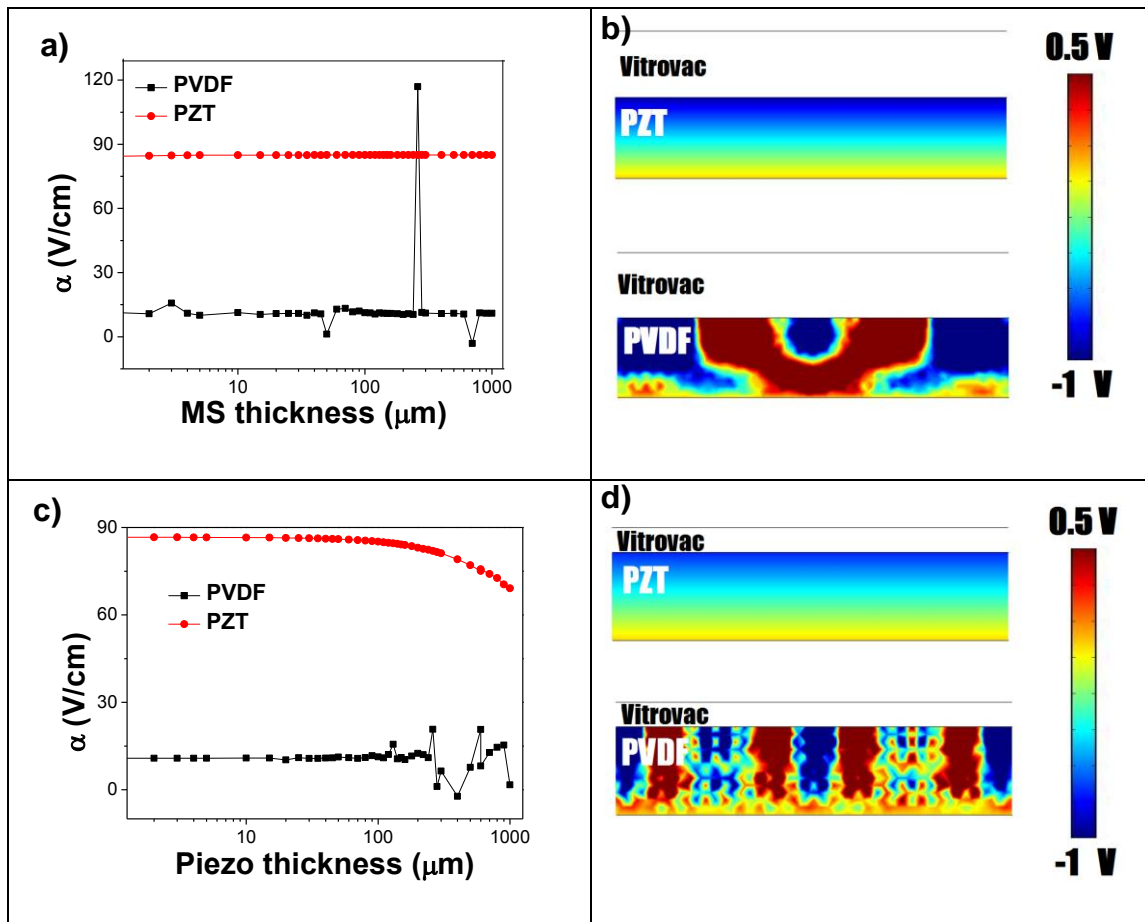
Figure 2.6: Bi-layered ideal laminate simulation results. Figure (a) shows the magnetoelectric response-α (V/cm)- of structures with constant piezoelectric thickness of 110 μm, over a range of 1μm to 1 mm of magnetostrictive material thickness (Vitrovac 4040). Figure (c) shows the magnetoelectric response of structures with constant magnetostrictive material thickness of 25 μm, over a range of 1μm to 1 mm of piezoelectric thickness (PVDF/PZT). Figure (c) shows the electric potential distribution for the case of a structure with a magnetostrictive (Vitrovac 4040) thickness of 90 μm, for 110 μm PZT (up)- and PVDF (down)- piezoelectric thickness. Likewise, Figure (d) shows the electric potential distribution for a 25 μm-width Vitrovac and 90 μm PZT (up) and PVDF (down) magnetoelectric structures. The electric potential scale can be found on the right side.

By establishing magnetostriction as a deformation, it may be expected the independence of the magnetostrictive thickness on the ME performance of the composite, which is confirmed by the results obtained for the magnetostrictive thickness sweep presented in Figure 2.6 (a) for PZT bi-layer composite. PVDF-bi-layered composite curves showed a relatively stronger dependence of the ME response on the magnetostrictive thickness for specific values of magnetostrictive thickness, rising above average α value for Vitrovac thicknesses of 20 μm and 300 μm, and shrinking to average α values for magnetostrictive thicknesses of 50 μm and 700

μm. As these values are isolated, and show no clear trend, they represent isolated values governed by PVDF´s semicrystalline constitution and are not considered as conclusive results.

As presented in chapter 1, Ryu *et al.* (Jungho Ryu et al., 2002) reported a constant ME coefficient for higher Terfenol-D/PZT thickness ratio, that decays for thicknesses ratio below 10, establishing values for 0.5, 0.4 and 0.3 mm of PZT. The same results are established by the FEM simulations, presenting a constant value for the ME coefficient for small piezoceramic thicknesses and a decaying α for PZT-thicknesses above 200 μm, as shown in Figure 2.6 (c). For PVDF-thicknesses below 100 μm, it also achieves a constant ME performance, getting irregular for thicknesses above 200 μm, as shown also in Figures 2.6 (c).

Figures 2.6 (b) and (d) show the electric potential distribution for two particular cases of PVDF and PZT. Figure 2.6 (b) shows the case of a piezoelectric thickness of 110 μm and a Vitrovac thickness of 90 μm; Figure 2.6 (d) shows the case of Vitrovac of 25 μm and PVDF/PZT of 90 μm, revealing a strong influence of the PVDF´s semi-crystalline constitution. While the piezoceramic establishes a laminar pattern of electric potential distribution in the polarization direction, the formation of clusters of heterogeneous regions with an irregular electric potential distribution are observed in the PVDF´s simulation result, therefore establishing one of the main differences between the piezoelectric ceramic and the polymer, related to the more irregular ordering in which dipoles generate the piezoelectric response in the PVDF´s samples.

For constant piezoelectric thickness, it can be observed that the performance of the PVDF-bi-layered composite is lower than the PZT-composite, establishing an α_{ME} of approximately the 12% of the α_{ME} of PZT-composite, by taking into account the average of both relation values (α_{ME} of PVDF/α_{ME} PZT bi-layer, with the exception of the special cases of 20, 50, 300 and 700 μm of magnetostrictive thickness). On the other hand, for equal piezoelectric thickness below 200 μm and constant Vitrovac thickness of 25 μm, the performance of the PVDF-composite has a mean value of 7.7% the α_{ME} valueof the PZT-composite.

2.3.2. Epoxy properties on a bi-layer 2D laminate simulation

The comparison between measured and simulated results reveal the strong influence of the epoxy layer on the ME response of the composite, although the difference of the ME performance between ideal and epoxy-glued ME bi-layer structures only presents itself for PVDF thicknesses above 100 μm, as can be realized in Figure 2.7, which show simulation results for an ideal bi-layer and a glued bi-layer, with an epoxy of 12μm thickness and a Young modulus of 270 MPa.
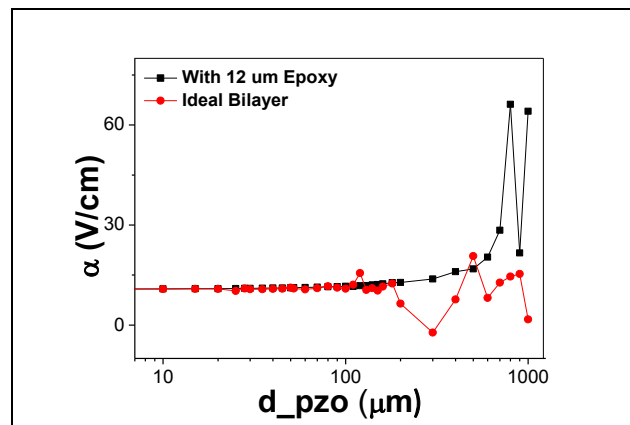
Figure 2.7: Magnetoelectric coefficient for ideal bi-layer structure and epoxy-glued bi-layer magnetoelectric structure

For both cases (ideal and glued MP bi-layers), the ME performance of the structure tends to increase until 100 μm of piezoelectric thickness, reaching for larger values a region where elasticity and morphology govern an irregular behaviour. Anyhow, theory claims that increasing the PVDF layer thickness gives as a first consequence that a larger number of dipolar moments suffer variation under the applied stress, resulting in a higher ME response, nevertheless above 700 μm thick layers, inhomogeneous deformations of the material are obtained, with larger deformations at the boundary layer with the binder and lower deformation far from that layer, thus decreasing the ME response (M. Li, Hasanyan, et al., 2012). Figure 2.8 also shows an increased ME response with increasing PVDF layer thickness of the epoxy-bi-layer structure until it reaches the value of 700 μm.

With increasing PVDF layer thickness a larger number of dipolar moments suffer variation under the applied stress, resulting in a higher ME response(M. Li, Hasanyan, et al., 2012). However it should be noted that it must exist a maximum value for the PVDF thickness at which the ME response is maximized as shown in the simulation represented in Figure 2.8.
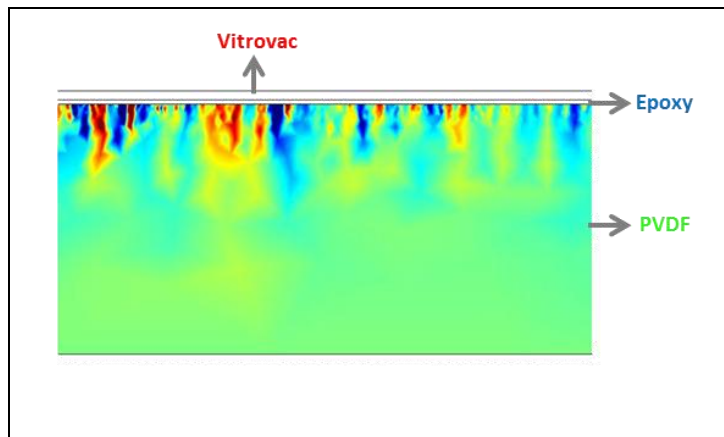
Figure 2.8: Numerical simulation of a thick PVDF layer (750 µm) bonded to a Vitrovac layer with 12µm M-Bond epoxy

Figure 2.8 shows that for a very thick layer of PVDF (750 µm) the deformation generated by Vitrovac is only transmitted to a volume fraction of the PVDF layer close to the epoxy layer, causing the observed decrease of the magnitude of the ME effect. Figure 2.9 presents the ME coefficient for different epoxy's elastic modulus.
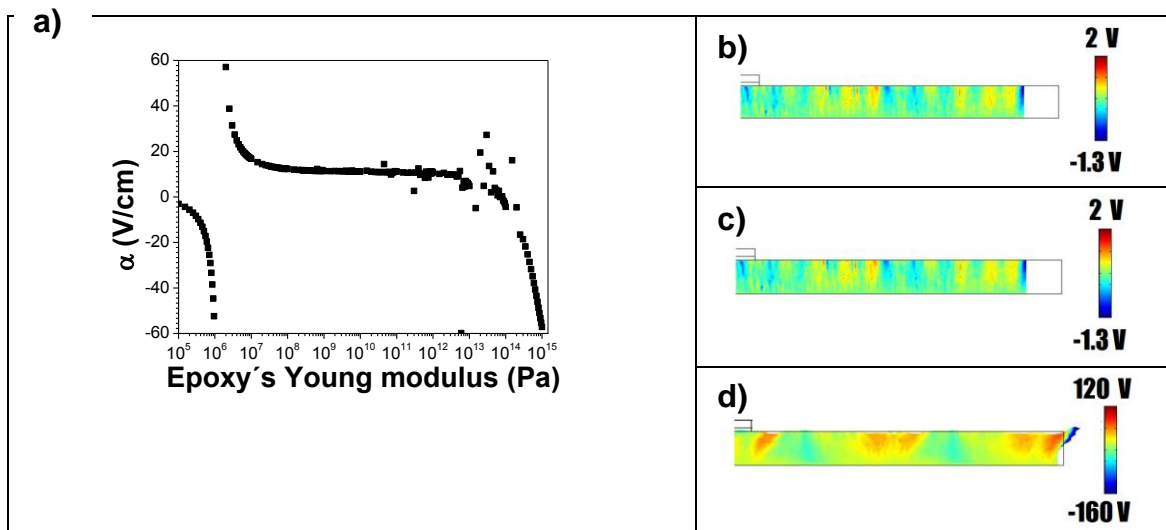
Figure 2.9: Epoxy´s Young modulus influence on the magnetoelectric performance of the epoxy bi-layer structure. Figure (a) shows the curve of the magnetoelectric coefficient versus the swept Young modulus parameter. Figures (b), (c), and (d) display the deformed (in a 1:100 scale) electric potential distribution for three particular cases: (b) very low values of epoxy's Young modulus (1x106 Pa), (c) middle values of Young modulus (2.5x107 Pa), (d) very hard epoxy (high values of Young modulus, case 1x1014Pa).

At Young modulus values of 10^6 Pa, an abrupt change in the epoxy behaviour occurs. For lower values the epoxy stretches in the vicinity of the magnetostrictive material and cringing in

the vicinity of the PVDF layer. The epoxy leads the PVDF to compress, as can be seeing in Figure 2.9(b). For middle values of epoxy´s Young modulus, the piezoelectric material stretches homogeneously, as presented in Figure 2.9(c). For higher values of the Young modulus, the epoxy loses its ability to transmit the deformation from the magnetostrictive layer to the piezoelectric layer due to the increased rigidity, having as a consequence a decrease in the ME response. The deformation of the piezoelectric domain is not homogeneous, comprising in the bottom of the domain, and stretching in the top side of the structure, at the interface with the epoxy (Figure 2.9(d)).

Figure 2.10 shows the influence of the epoxy´s thickness on the ME performance of the bi-layered structure.
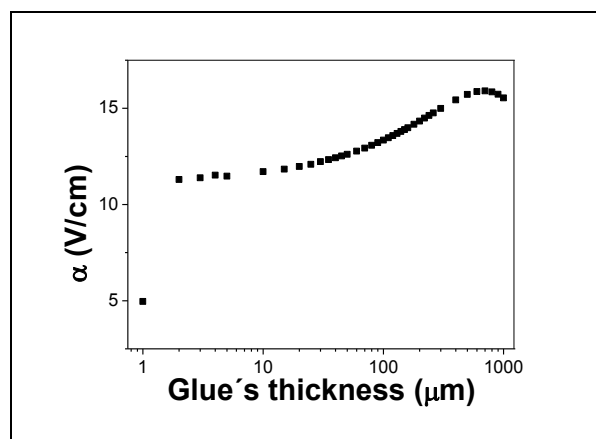
Figure 2.10: Epoxy´s thickness influence on the magnetoelectric performance of a bi-layer structure

Increasing the epoxy thickness leads to an increase of the ME voltage coefficient explained by a better coupling between the epoxy layer and the other two layers, as represented on Figure 2.10. From a certain value of epoxy thickness, the glue loses the ability to transmit the deformation between the layers, the decrease is explained by the high distance between the layer in which the deformation occurs (Vitrovac) and the layer on which the deformation has to be transmitted (PVDF), as a consequence part of the deformation was damped along the thick epoxy layer. Thicker epoxy layers would also limit the ME response due to low mechanical strength and contribute towards increasing noise level and aging (Yan, Zhou, & Priya, 2013).

2.3.2.1. Simulated versus constructed me laminates and epoxy properties

Figure 2.11 shows the ME response of laminate composites of 110 µm thick PVDF films bonded with Devcon, M-Bond and Stycast to Vitrovac magnetostrictive substrates. The highest ME response was obtained for the M-Bond bonded composites, the epoxy with the lowest Young modulus; on the opposite, the lowest response was obtained for Stycast bonded composites, which is the epoxy with the highest Young modulus and for which a lower k value was used (M. Li, Hasanyan, et al., 2012; G. Liu et al., 2004; C. W. Nan, Liu, et al., 2003).
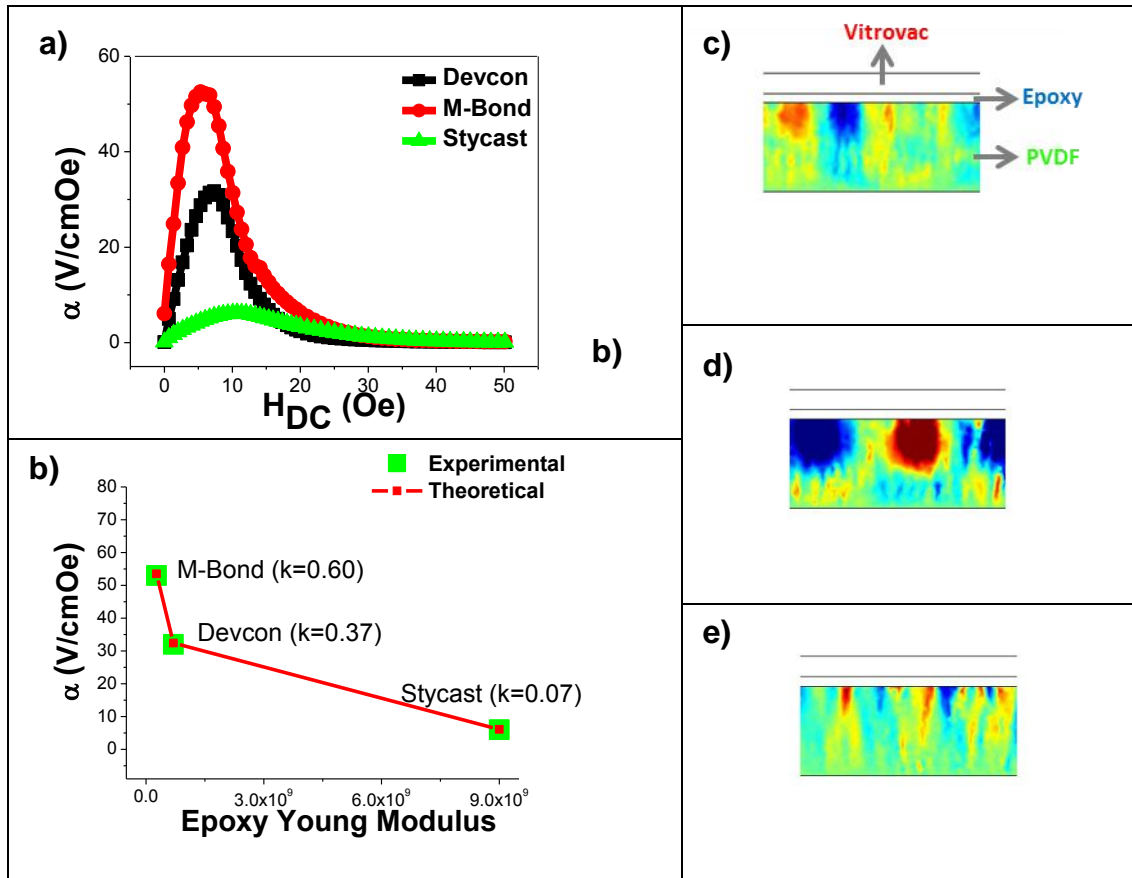
Figure 2.11: (a) Magnetoelectric response, α, at resonance obtained for the PVDF/epoxy/Vitrovac composites for a 110 µm PVDF layer and different epoxy binders; (b) Relation between α and the epoxy Young modulus. Images from the numerical simulation of the magnetoelectric effect in the laminates bonded with: (c) Devcon; (d) M-Bond and (e) Stycast.

It is observed that with higher Young modulus the epoxy loses its ability to transmit the deformation from the magnetostrictive layer to the piezoelectric layer due to the increased rigidity, leading to a decreasing in the coupling factor from 0.6 to 0.07. This values can be

interpreted as an interface detachment between the active layers (magnetostrictive and piezoelectric) and the epoxy layer. Further, the highest ME response was also obtained at the lowest applied H_{DC} filed by using M-Bond; in correspondence, Stycast shows the lowest ME response at the highest applied H_{DC} field. Devcon containing composites showed an intermediate behaviour. This relation between the ME response and the Young modulus show the relevance of the latter parameter for the fabrication of devices and indicates the best choice for ME performance optimization. These results are supported by the simulations as the images obtained by FEM (Figure 2.11 (c),(d) and (e)), where red colours indicate minimum electric potential values and the blue colours indicate the maximum potential in the static analysis electric potential distribution.

As the M-Bond bonded laminates showed the highest ME response, this epoxy was used in the study of the effect of the thickness of the PVDF layer on the ME response of PVDF/M-Bond/Vitrovac laminates.

PVDF layers with 28, 52 and 110 μm were used and it was evaluated, both experimentally and through theoretical FEM simulations, the effect of the piezoelectric layer thicknesses on the ME response of the composites. Figure 2.12(a) shows the magnetoelectric coefficient as a function of the DC applied field and Figure 2.12(b) the comparison of experimentally and theoretically obtained values of the ME coefficient for the different piezoelectric layer thickness.

As previously reported, Figure 2.12 shows that the ME response of PVDF based ME laminated composites increases with increasing thickness of PVDF layer (Carvell, Cheng, & Yang, 2013). Nevertheless, an increase of 300% in the thickness of PVDF (from 28μm to 110μm) has, as a consequence, just an increase of 20% in the ME response (from 45 $V.cm^{-1}.Oe^{-1}$ to 53 $V.cm^{-1}.Oe^{-1}$).In the images obtained by the FEM simulations (Figure 12(c), (d) and (e)) it can be observed that the intensity of the red and blue colours increases with increasing thickness of PVDF.
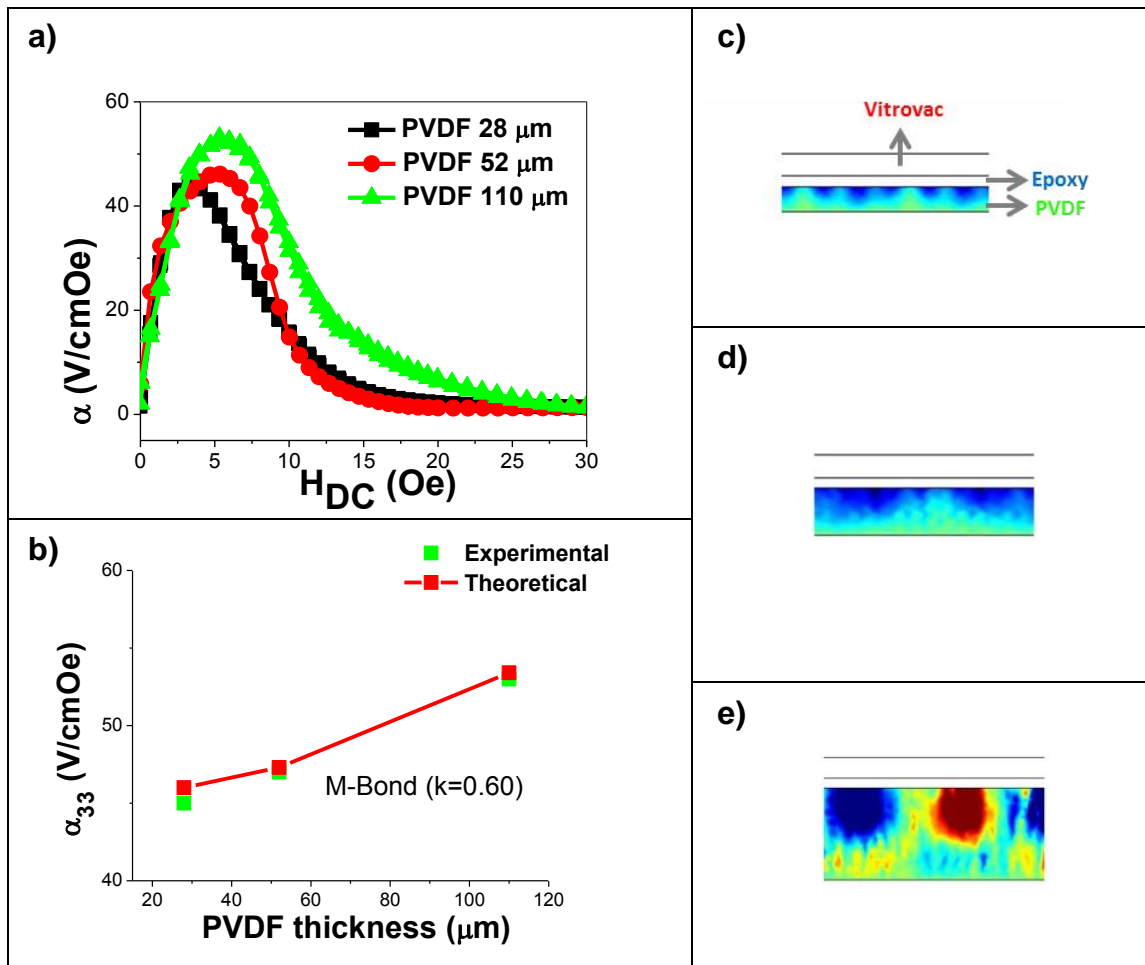
Figure 2.12: (a) Magnetoelectric coefficient, α, measured at the resonance frequency as a function of the DC magnetic field for piezoelectric layer of different thickness and (b) comparison between the experimental and theoretical results. Images from the FEM simulation of the magnetoelectric effect in laminates bonded with M-Bond epoxy with PVDF thickness of: (c) 28 μm; (d) 52 μm; (e) 110 μm.

Another important parameter for practical applications is the thermal stability of the device. Figure 2.13 shows the variation of the ME response with temperature in the temperature range 20-85 °C for a PVDF 110μm/M-Bond/Vitrovac laminate. The maximum temperature of 85 °C was chosen as around that temperature PVDF undergoes the α-relaxation leading to strong shrinking of the material (Sencadas, Lanceros-Méndez, Sabater I Serra, Andrio Balado, & Gómez Ribelles, 2011).
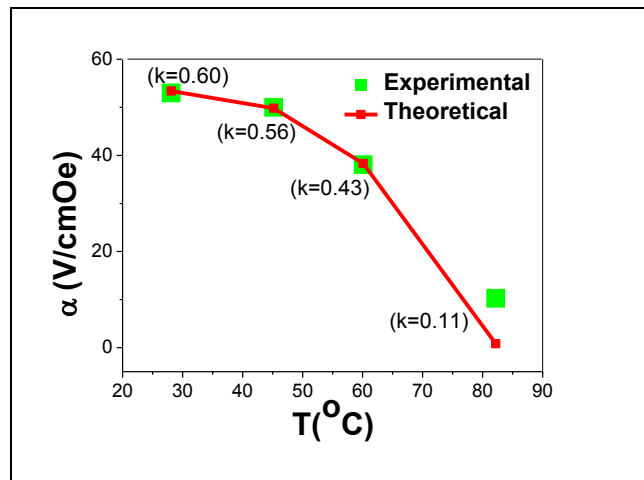
Figure 2.13: Temperature dependence of the ME coefficient, α, measured at the resonance frequency for the composites PVDF (110 μm)/M-Bond/Vitrovac.

As previously reported(Gutierrez et al., 2012) the ME response of PVDF based materials decreases with increasing temperature. This decrease is not mainly explained by the depoling effects (related to increased molecular mobility with increasing temperature) which leads to a decreased piezoelectric response, since it was reported just a decrease of 20% in the PVDF piezoelectric coefficient when the temperature increased until 100°C(M. P. Silva, Costa, Sencadas, Paleo, & Lanceros-Méndez, 2011). Figure 2.13demonstrates a decrease of more than 80% in the ME response of the laminate which is related with a decrease of the coupling, defined as k, between the epoxy and the active layers of the laminate. The coupling factor k varies from 0.6 at room temperature to 0.11 at 80°C, and reflects a weaker coupling between the layers due to a softening of the materials leading to a smaller k. Results on Figure 2.11 suggest that softer materials have higher k value. In this way, the decrease of the k values shown in Figure 2.13 should be related with the temperature dependent deformations that lead to interface detachment (due to the different thermal expansion coefficients of the material) and therefore reduced transduction capability.

Despite the temperature effect on the ME response, the ME coupling coefficient still remains at suitable values up to temperatures of 80 °C, which allows widespread use for sensor and actuator applications. In a similar way, it was reported that PVDF still retained stable piezoelectric response after temperature annealing at 140 °C, with a value of -4 pC/N, which is still high for polymer systems (M. P. Silva et al., 2011), making this polymer an appropriate

choice for the development of the flexible, low cost and easy shaping ME materials with large potential for device fabrication (Pedro Martins & Lanceros-Méndez, 2013).

2.3.3. Two dimensional ideal tri-layer laminate simulation results

Tri-layer ME laminates may be composed of one piezoelectric layer sandwiched by two magnetostrictive layers (MPM configuration) or by one magnetostrictive layer intercalated between two piezoelectric layers(PMP configuration). When two piezoelectric layers were included, two sources of electric potential were involved which required considering the ME composite as a device, obtaining α-values by equation (2.9 and 2.10). When configurations are to be compared, it is desirable to establish one single value that gives information about the performance of the material per unit piezoelectric length, which can be obtained by equation (2.12), called unitary ME coefficient, $\alpha_{unit.}$, and can only be applied to symmetric configurations.

2.3.3.1. Magnetostrictive-piezo-magnetostrictive laminate simulation results

Figure 2.14 displays the ME response of symmetric MPM configurations, for magnetostrictive thickness sweep. In Figure 2.14 (a), simulated α_{ME} of PVDF bi-layer and MPM configurations are presented over the magnetostrictive thickness range, and Figure 2.14 (b) shows the ME performance of the respective PZT configurations. Figure 2.14 (c) shows the electric potential distribution for PZT and PVDF clamped and free –MPM configurations, and Figure 2.14 (d) presents the vertical displacement field (y-displacement field) for both configurations and both piezoelectric materials.

74
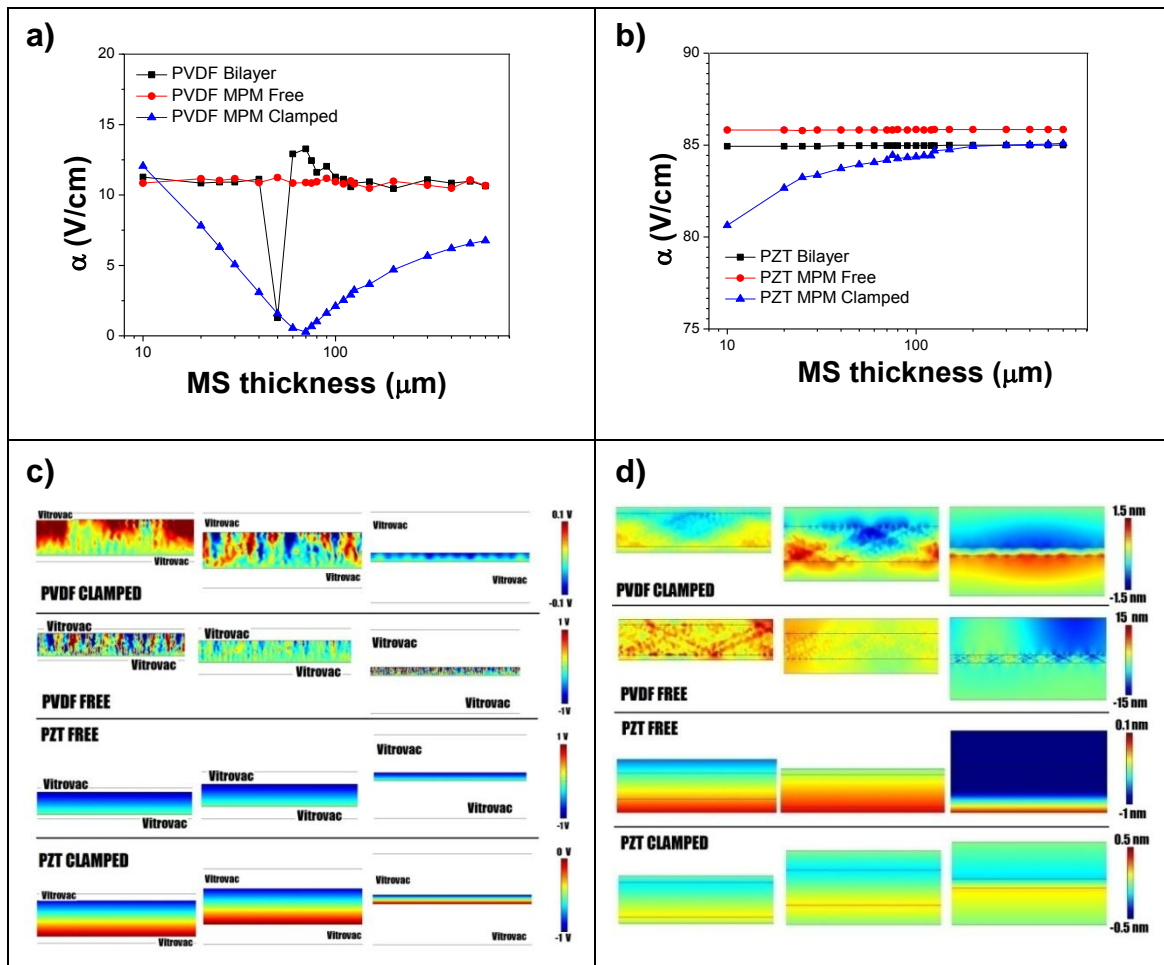
Figure 2.14: Magnetostrictive-piezoelectric-magnetostrictive (MPM) tri-layered symmetric laminate results for magnetostrictive thickness sweep. In Figures (a) and (b), the magnetoelectric coefficient is presented for symmetric PVDF-MPM (a) and PZT-MPM (b) over a range of 10-600 μm of magnetostrictive thickness, when the piezoelectric thickness holds a value of 110 μm. Magnetoelectric coefficients are compared between MPM free case, clamped case and the bi-layer. Figure (c) presents the electric potential distribution for MPM free and clamped case. Figure (d) shows the vertical displacement field (y) for the free and clamped case. Vitrovac thicknesses of 20 μm, 60 μm and 500 μm are the particular cases shown. Specific scales are established on the right side of the images.

Figure 2.14 (b) shows PZT-symmetric-MPM and bi-layer simulation results. It can be seeing, that the additional layer of Vitrovac increases α_{ME} in about 1 V/cm in comparison to the ME performance of the bi-layered configuration (for all range of magnetostrictive thickness). Clamping the structure has the effect of decreasing the ME performance of the composite for thinner ME thicknesses (between 10-100 μm), reaching its maximal performance above 150 μm -with the same order of values of the α_{ME} of the bi-layered structure.

For clamped MPM PVDF tri-layers, these differences are even stronger, reaching near zero ME effect around a magnetostrictive thickness of 70 μm, but having a smaller value of α_{ME} around all other magnetostrictive thickness, except for the case of 10 μm of Vitrovac, where all values for clamped MPM, free MPM and bi-layered configuration, meet (Figure 2.14 (a)). As PVDF is a more elastic material than PZT, and there is no structural damping considered, simulation results of the bi-layer and the MPM free configuration do not show significant differences. It appears just that the extra magnetostrictive layer has an effect of comprising (fixing, homogenizing) the ME coefficient in about 11 V/cm, the same as it was for the thinnest and thickest magnetostrictive thicknesses in the bi-layer configuration.

In Figure 2.14 (c), while PZT laminates show an homogeneous electric potential distribution and vertical displacement field, both for the free and clamped cases, in the case of PVDF laminates, the polymer morphology influences these patterns and shows an inhomogeneous electric potential distribution, which is more disperse for the clamped configuration than for the free configuration. In this way, a more disordered pattern is also found for the vertical displacement in Figure 2.14 (d).

Figure 2.15 (a) and (b) shows the ME coefficient for a symmetric-MPM configuration of PVDF (a) and PZT (b) as function of the piezoelectric thickness of the laminated composite. Figure 2.15 (c) and (d) show the respective potential distribution (c) and vertical displacement field (d) for PZT and PVDF clamped and free MPM configurations.
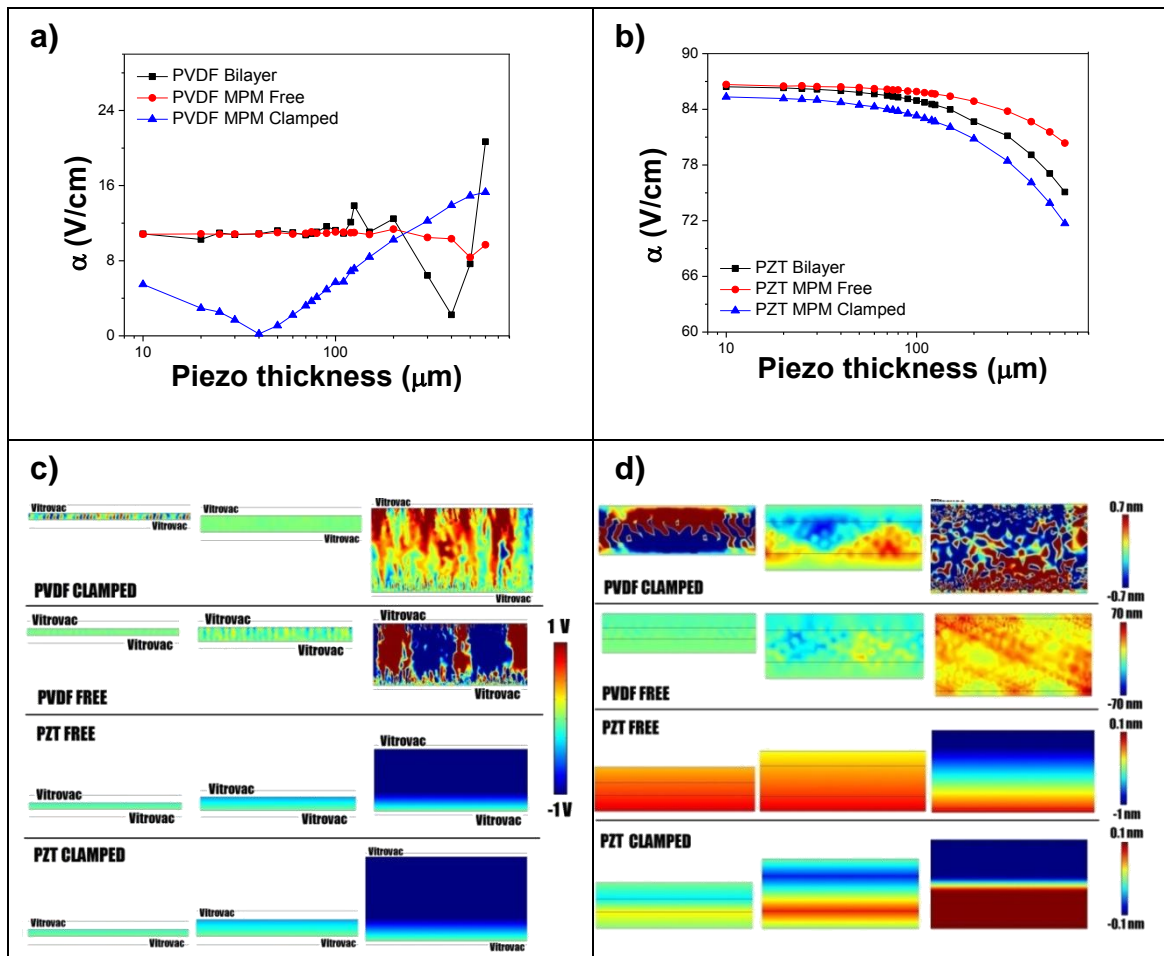
Figure 2.15: Magnetostrictive-piezoelectric-magnetostrictive (MPM) tri-layered symmetric laminate results for piezoelectric thickness sweep. In Figures (a) and (b), the magnetoelectric coefficient is presented for symmetric PVDF-MPM (a) and PZT-MPM (b) over a range of 10-600 μm of piezoelectric thickness, when the magnetostrictive thickness holds a value of 25 μm. Magnetoelectric coefficients are compared between MPM free case, clamped case and the bi-layer. Figure (c) presents the electric potential distribution for MPM free and clamped case. Figure (d) shows the vertical displacement field (y) for the free and clamped case. Piezoelectric thicknesses of 20 μm, 50 μm and 400 μm are the particular cases shown. Particular scales are established on the right side of the images.

Similar to all other experiments, PZT laminates show a clearer trend than PVDF laminates. PZT-free, clamped and bi-layered- configurations present a constant value of α_{ME} below a piezoelectric thicknesses of 60 μm, which decreases when increasing piezoelectric thickness. Although the general trends are similar for the 3 configurations, the clamped configuration shows the lowest ME performance, followed by the bi-layered one, thus showing the free configuration the highest ME performance.

Simulations of PVDF -bi-layer and free- configuration display similar ME performances for piezoelectric thickness below 200 μm, establishing that the free configuration has a more stable trend than the bi-layered one. The free configuration shows a stable α_{ME} of approximately 11 V/cm for the range of piezoelectric thickness below 200 μm, decreasing for increasing piezoelectric thickness above 200 μm. The clamped configuration presents a decaying value of α_{ME} for the range of PVDF-thickness 10-40 μm, then rising for thicker PVDF layers, obtaining better ME performance than the bi-layered and free configurations for piezoelectric thicknesses above 200 μm.

As presented in chapter 1, Ryu *et al.* (Jungho Ryu et al., 2001) established the theoretical expectation for the ME voltage coefficient (dE/dH) as a function of the thickness ratio (d_ms/d_pzo) between Terfenol-D and PZT, presenting that the output voltage increases with increasing the thickness ratio, saturating above d_ms/d_pzo=10 (Figure 2.16 (b)). Also, Fang (F. Fang et al., 2011) presented peak values of α_{ME} as a function of n-ratio (2*d_ms/(2*d_ms+d_pzo)) for Metglas/PZT/Metglas. Calculations (lines) and measured data (dots+lines) are presented in Figure 2.16 (g). These results were also confirmed by the measured trends for α_{ME} by Ryu *et al.* (Jungho Ryu et al., 2001)for Terfenol-D/PZT/Terfenol-D laminates (Figure 2.16 (c)), Stognij *et al.*(Stognij et al., 2013)for Co/PZT/Co Heterostructures (Figure 2.16 (d)) and by Wong (W. Wong, 2007) for the ME performance of different thickness ratio values of Terfenol-D/PMN-PT/Terfenol-D laminates (Figure 2.16 (e)). It is worth noticing, that the data established in Figures (c), (d) and (e) is normalized with respect to their higher value.

Figures 2.16 (a) and 2.16 (f) show the FEM simulation values for the ME coefficient as a function of the thickness ratio (d_ms/d_pzo) (2.16(a)) and n-ratio (2*d_ms/(2*d_ms+d_pzo)) (2.16(f)) for comparison with the simulated values of α_{ME}, established in Figures 2.16 (b) and (g), with respect to the thickness ratio (tm/tp) and n-ratio, respectively.
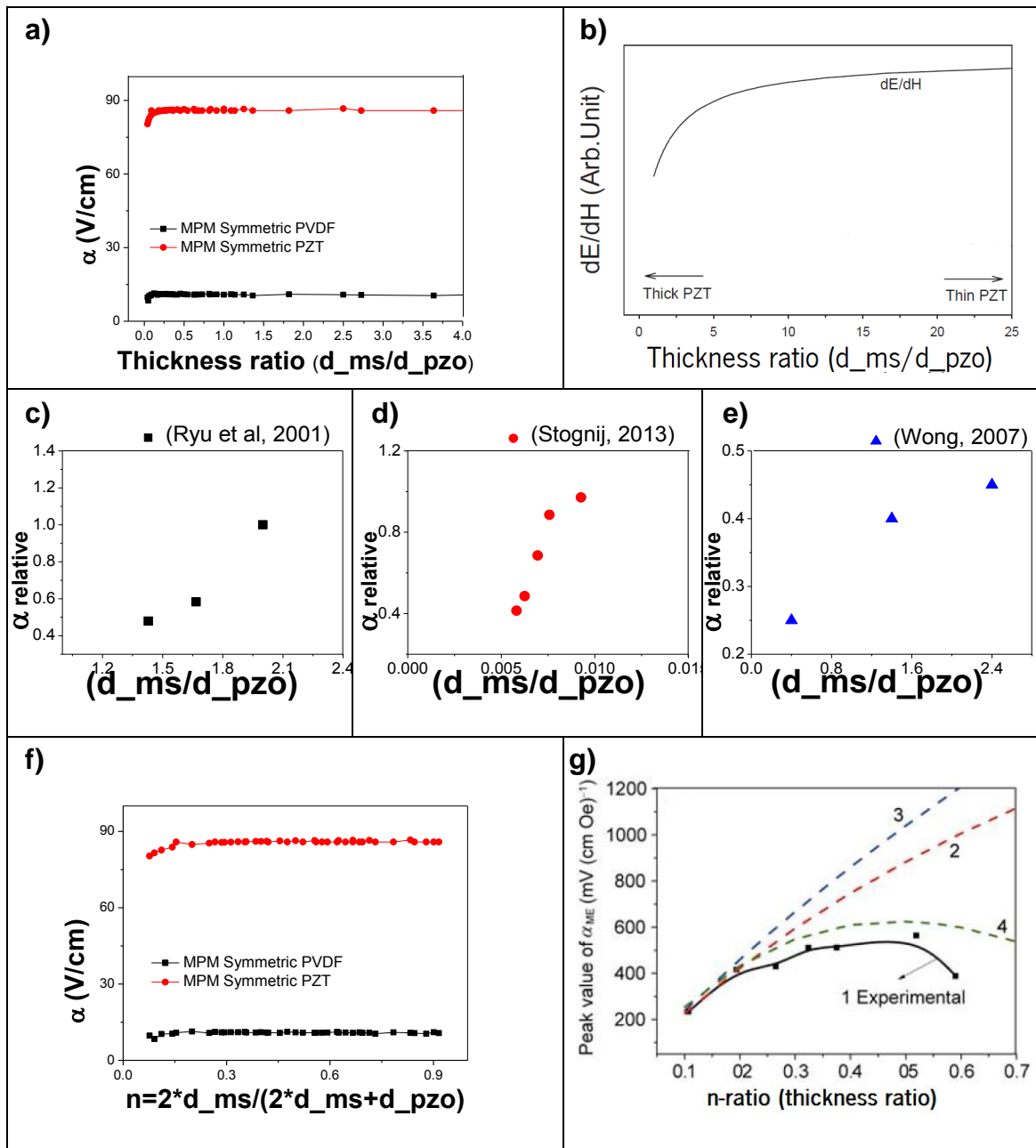
Figure 2.16: Simulated magnetoelectric coefficient as a function of the thickness ratio (d_ms/d_pzo) of magnetostrictive and piezoelectric thicknesses (a) and for n-ratio (n=2*d_ms/(2*d_ms+d_pzo) (f), for both PZT and PVDF MPM free configurations, where d_ms and d_pzo represent magnetostrictive and piezoelectric thickness, respectively. Results are compared with the trends established in the literature and data used in references (Jungho Ryu et al., 2001) (b,c), (Stognij et al., 2013) (d), (W. Wong, 2007) (e) and (F. Fang et al., 2011) (g).

In Figure 2.16 (a) and (b), good agreement can be established for small thickness ratio, where the ME performance diminishes with increasing the piezoelectric thickness, but not confirming the performance established for higher values of n-ratio (Figures 2.16 (f) and (g)), where for smaller piezoelectric thicknesses the ME coefficient should decrease its values, as can be seeing from Fang *et al.* 's experiment in Figure 2.16 (g). It is worth to mention that epoxy bonding on Terfenol-D phases and damping effects on Fang *et al.* (F. Fang et al., 2011)measurements might also have some influence on this performance, as established in chapter 2.3.2 for the bonding effects on bi-layer experiments.

Asymmetric MPM configurations where also simulated, for magnetostrictive and piezoelectric thickness sweep experiments. For magnetostrictive thickness sweep, the piezoelectric thickness held a value of 110 μm, the bottom magnetostrictive thickness held a value of 25 μm and the top magnetostrictive thickness was varied between 10 and 600 μm. The simulated ME performance is shown in Figure 2.17.
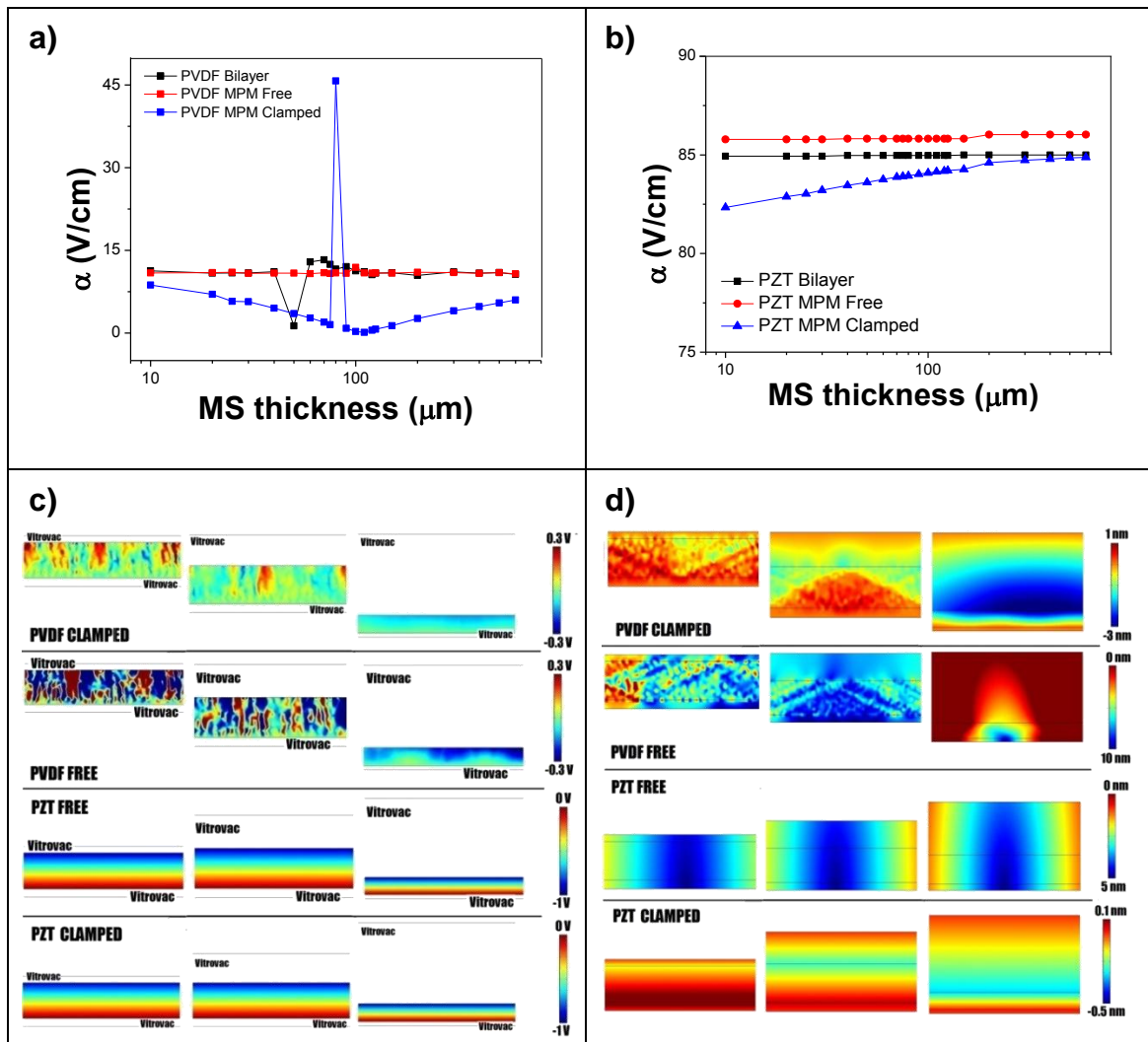
Figure 2.17: Magnetostrictive-piezoelectric-magnetostrictive (MPM) asymmetric tri-layered laminate results for magnetostrictive thickness sweep. In Figures (a) and (b), the magnetoelectric coefficient is presented for symmetric PVDF-MPM (a) and PZT-MPM (b) over a range of 10 -600 µm of magnetostrictive thickness, where the piezoelectric thickness holds a value of 110 µm and the bottom magnetostrictive thickness holds a value of 25 µm. Magnetoelectric coefficients are compared between MPM free and clamped case, and the bi-layer. Figure (c) shows the electric potential distribution for MPM free and clamped case. Figure (d) shows the vertical displacement field (y) for the free and clamped case. Piezoelectric thicknesses of 20 µm, 90 µm and 500 µm are the particular cases shown. Particular scales are established on the right side of the images.

As former experiments show no dependence of the ME performance over the magnetostrictive thickness, it can be predicted that the inclusion of asymmetries on the magnetostrictive thicknesses of the composite will not have a large impact on the performance of

the MPM structure, at least when the model is based on a structural analysis that does not incorporate the nonlinear magnetostrictive effect.

The only difference between symmetric and asymmetric configurations is obtained for clamped configurations, as can be observed in Figure 2.17. The PZT clamped configuration shows higher α_{ME} values for Vitrovac thicknesses in the range 10 to 100 µm for the asymmetric when compared to the symmetric configuration. In the PVDF clamped configuration, the relation of α with the magnetostrictive thickness also holds. On the other hand, the values of α are slightly lower and with a drift of the minimum ME coefficient to 100 µm of magnetostrictive thickness, whereas for the symmetric MPM configuration the minimum ME coefficient was obtained for a Vitrovac thickness of 70 µm (as shown in Figure 2.14 (a)).

Figure 2.17 (c) shows the electric potential distribution for asymmetric free and camped configurations, presenting for PVDF a more homogeneous distribution for clamped than for free configurations. A more laminar behaviour for microstructure variations is observed for very thick magnetostrictive thickness (as can be also seeing in Figure 2.17 (d), for y-field displacement), similar to the pattern produced in the piezoceramic.

Accordingly, for piezoelectric thickness sweep of asymmetric MPM configurations, the bottom magnetostrictive thickness holds a value of 25 µm, the top magnetostrictive thickness holds a value of 12 µm and the piezoelectric thickness is varied between 10 and 600 µm. The ME performance is established in Figure 2.18.

82
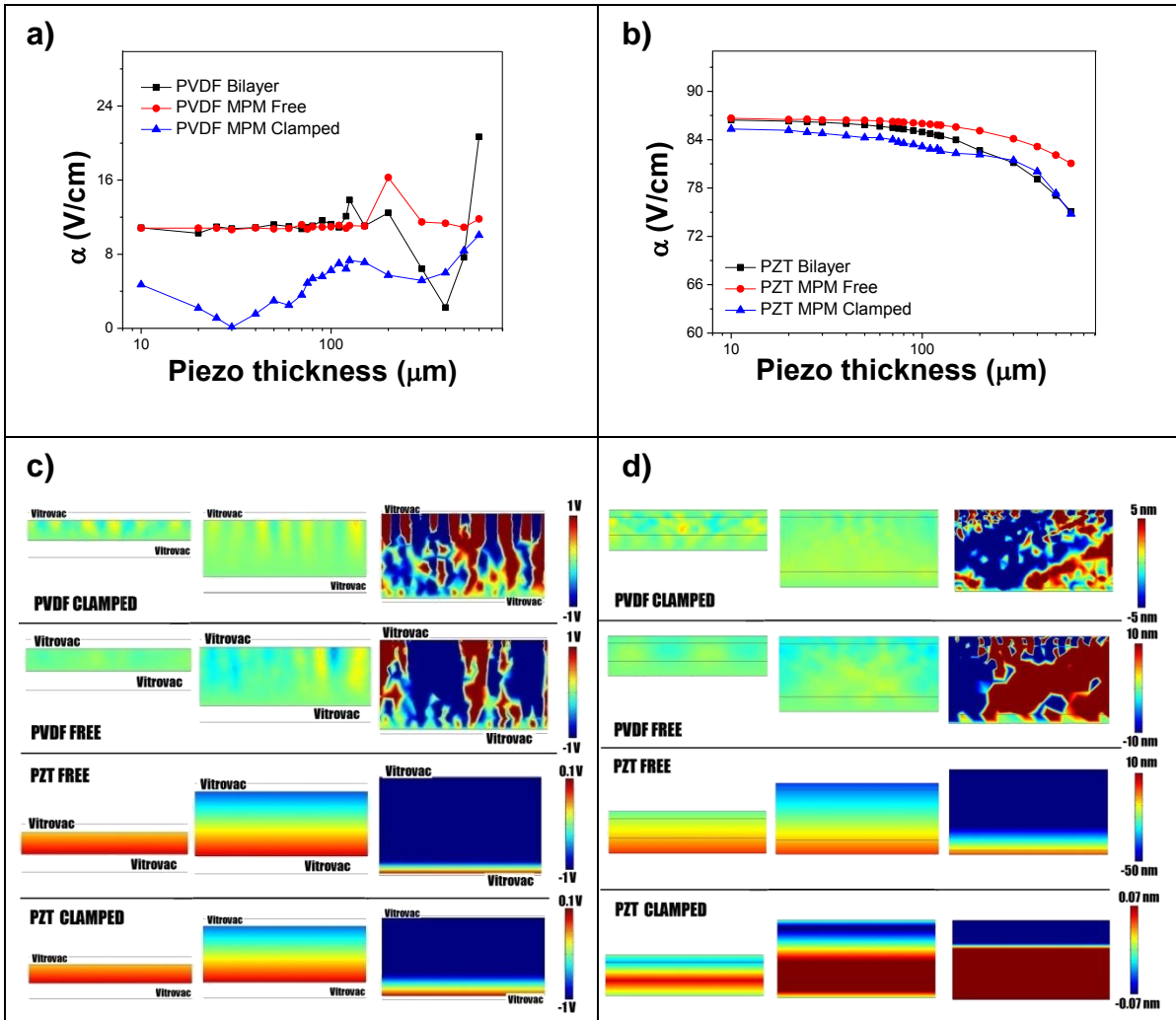
Figure 2.18: Magnetostrictive-piezoelectric-magnetostrictive (MPM) asymmetric tri-layered laminate results for piezoelectric thickness sweep. In Figures (a) and (b) the magnetoelectric coefficient is presented for asymmetric PVDF-MPM (a) and PZT-MPM (b) over a range from 10 to 600 μm of piezoelectric thickness, while the magnetostrictive thicknesses holds values of 25 and 12 μm. Magnetoelectric coefficients are compared between the MPM free case, clamped case and the bi-layer. Figure (c) presents the electric potential distribution for the MPM free and the clamped case. Figures (d) shows the vertical displacement field (y) for the free and clamped cases. Piezoelectric thicknesses of 30 μm, 90 μm and 500 μm are the particular cases shown. Particular scales are established on the right side of the images.

For free configurations, the inclusion of a magnetostrictive asymmetry resulted in a very low influence on the ME performance of the laminated structure (or even no influence for PZT), establishing a main single difference: a higher α_{ME} for 200 μm thick PVDF. Clamped configurations do show differences with respect to symmetric ones. The PZT clamped

configuration increased its ME performance above 200 μm of piezoelectric thicknesses, showing the behaviour of the bi-layered structure. The asymmetric PVDF clamped configuration shows a minimal value at a piezoelectric thickness of 30 μm, then increasing again its ME performance until a piezoelectric thickness of 150 μm, decreasing again up to 300 μm of piezoelectric thickness and, finally, increasing again, almost reaching the free MPM performance at 600 μm of piezoelectric thickness.

2.3.3.2. Piezoelectric-magnetostrictive-piezoelectric laminates

Piezoelectric-magnetostrictive-piezoelectric laminates are those composites where the magnetostrictive material is sandwiched between two piezoelectric layers. Figure 2.19shows the simulated ME coefficient, α_{ME}, for PVDF(a) and PZT (b) symmetric PMP and the PZT bi-layer (a,b) configurations, for magnetostrictive thickness sweep between 10 and 600 μm. The respective electric potential distribution and y-displacement field (vertical) are shown below in (c) and (d), respectively.
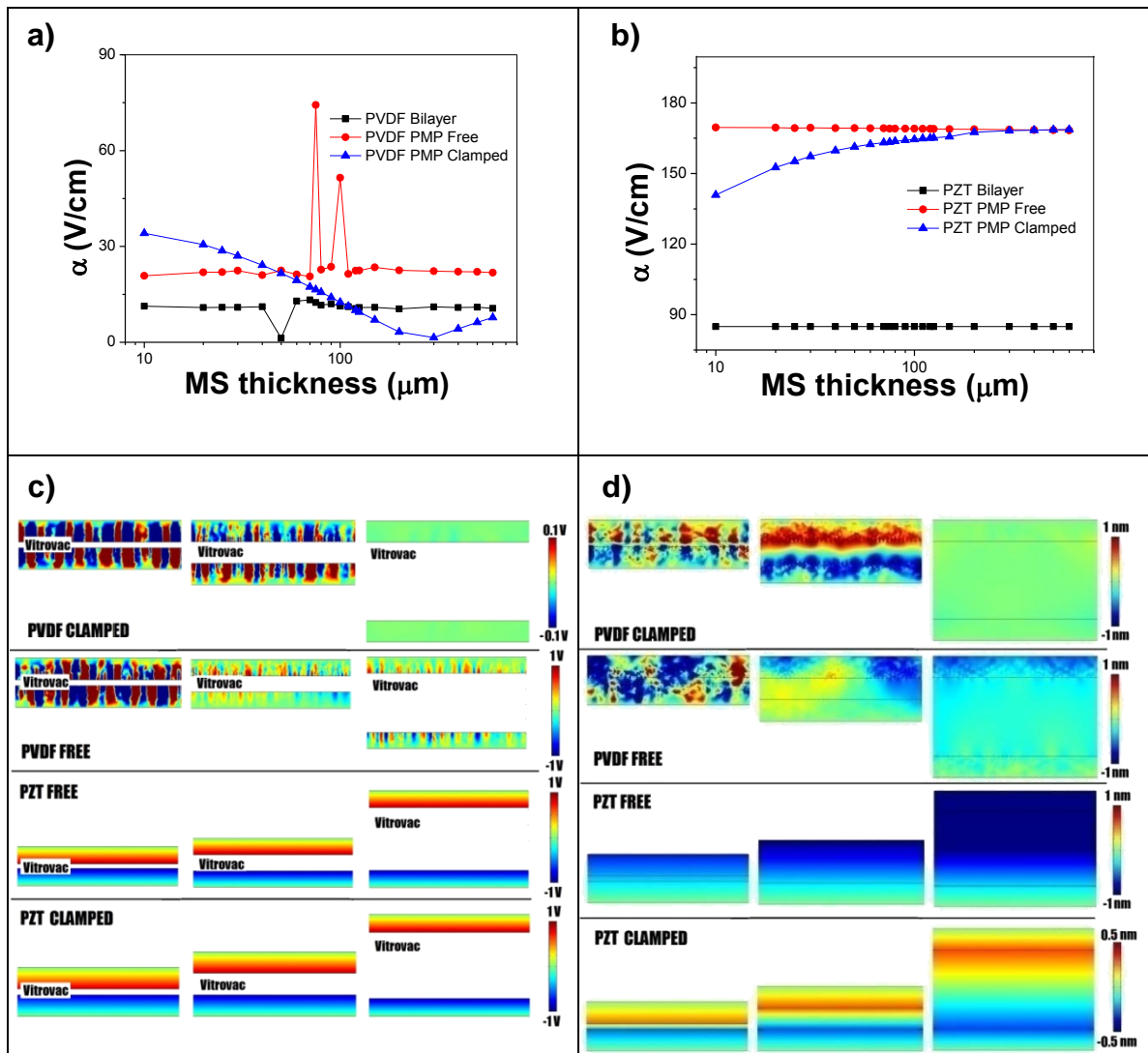
Figure 2.19: Piezoelectric-magnetostrictive-piezoelectric tri-layered (PMP) symmetric laminate simulation results for magnetostrictive thickness sweep. In Figures (a) and (b), the magnetoelectric coefficient is presented for symmetric PVDFMPM (a) and PZTMPM (b) over a range of 10 to 600 μm of magnetostrictive thickness, where the piezoelectric thickness holds a value of 110 μm. Magnetoelectric coefficients are compared between MPM free case, clamped case and the bi-layer. Figure (c) presents the electric potential distribution for MPM free and clamped case. Figure (d) shows the vertical displacement field (y) for the free and clamped case. Vitrovac thicknesses of 30 μm, 110 μm and 400 μm are the particular cases shown. Particular scales are established on the right side of the images.

As already established, it can be expected that the inclusion of a piezoelectric layer into the former bi-layer will double the ME coefficients (by treating the composite as a device, obtaining α_{ME} by eq. 2.10), as can be seen in figure 2.19 (a,b) for PVDF and PZT PMP symmetric configurations. The independence of α_{ME} over the magnetostrictive thickness remains present for PMP free configurations, with the only isolated exceptions of PVDF laminates with

magnetostrictive thicknesses of 90 and 75 µm, where the PVDF´s semicrystalline composition play a role in establishing isolated peaks on the ME performance. For PZT configurations, clamping the structure has the effect of decreasing the ME performance of the composite for thinner ME thicknesses between 10 and 200 µm, reaching its maximal performance for values of the same order than the free structure above 200 µm (Figure 2.19 (b)).

As PVDF is a viscoelastic material, the behaviour of the clamped PMP configuration for very low thicknesses of Vitrovac surpassed the standard improvement of duplicating the ME performance of the bi-layer (PMP configuration with a magnetostritive thickness of 10 µm triples the ME response of the bi-layer), decreasing α-values for higher magnetostrictive thicknesses. The minimal performance is obtained for the particular case of Vitrovac of 200 µm, then raising its ME performance for thicker magnetostrictive layers. For thinner magnetostrictive thicknesses, the PVDF clamped configuration shows higher α-values than the free one, decreasing their performance for higher thicknesses and matching the free configuration performance at magnetostrictive thickness of 50 µm and later the bi-layer performance for 100 µm of magnetostrictive thickness. This lead to conclude that clamping will only be useful for thickness below 50 µm of magnetostrictive thickness.

Figure 2.19 (c) shows the electric potential distribution for PZT and PVDF clamped and free PMP configurations. As expected, PZT shows a homogeneous electric potential distribution for the free and clamped cases, while in the case of PVDF, and its inhomogeneous electric potential distribution, the free case shows a more disperse electric potential distribution than the clamped one. Figure 2.19 (d) shows the y-displacement field, where PVDF displays a more inhomogeneous pattern than for PZT.

The results of the ME performance of the bi-layer, PMP -PVDF and PZT symmetric-configurations for different piezoelectric thickness are shown in Figure 2.20.
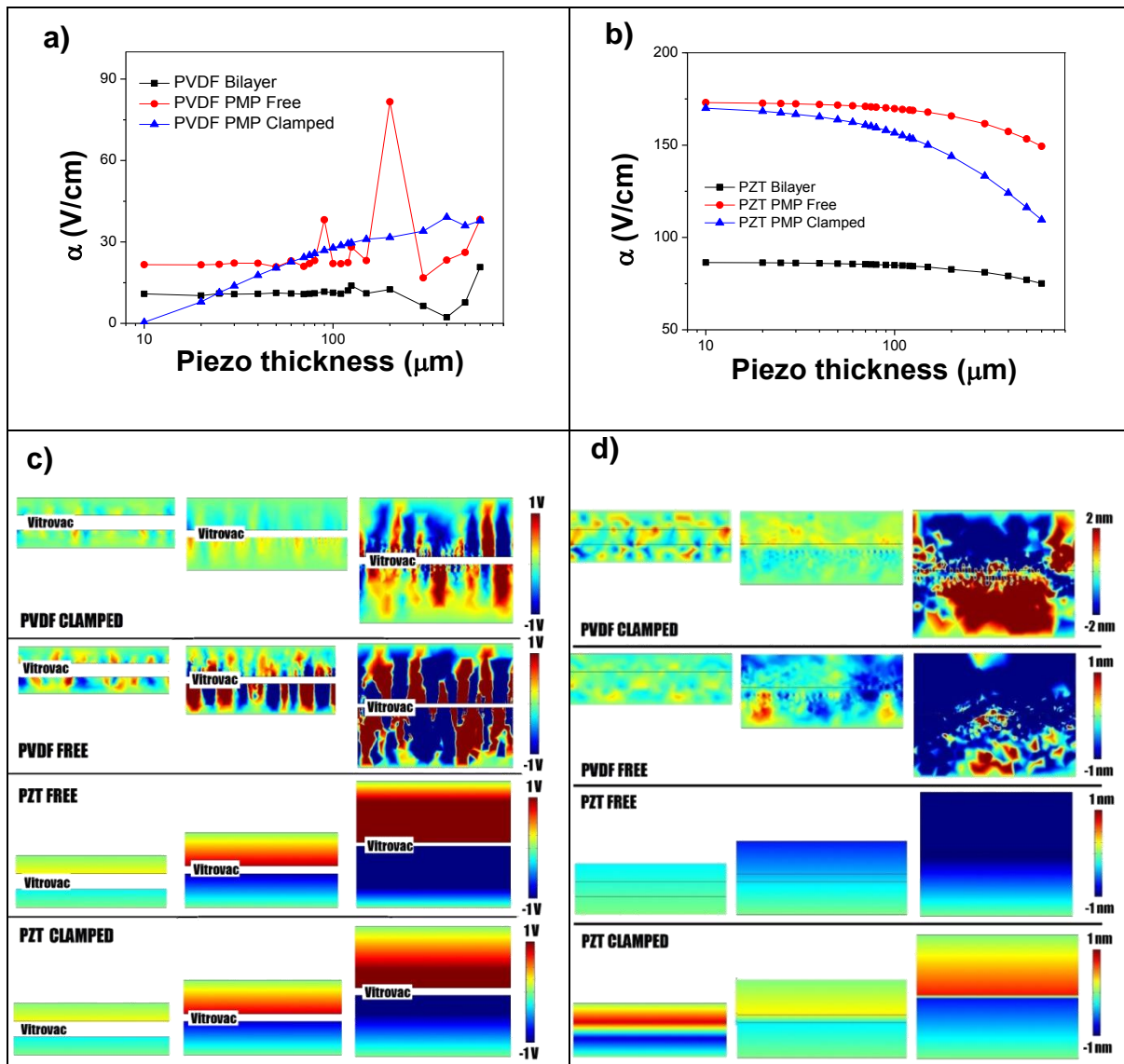
Figure 2.20: Piezoelectric-magnetostrictive-piezoelectrictri-layered (PMP) symmetric laminate simulation results for piezoelectric thickness sweep. In Figures (a) and (b), the ME coefficient is presented for symmetric PVDF-MPM (a) and PZT-MPM (b) over a range of 10 to 600 μm of magnetostrictive thickness, where the magnetostrictive thickness holds a value of 25 μm. ME coefficients are compared between the MPM free case, clamped case and the bi-layer. Figure (c) shows the electric potential distribution for MPM free and clamped case. Figure (d) shows the vertical displacement field (y) for the free and clamped case. Piezoelectric thicknesses of 30 μm, 110 μm and 400 μm are the particular cases shown. Particular scales are established on the right side of the images.

As both, PZT and PVDF free PMP configurations double the bi-layer-α for all piezoelectric thickness range, the clamped configuration introduce some differences. While clamped the PZTPMP configuration reduces its ME performance when increasing the piezoelectric thickness, as shown in Figure 2.20 (b), on the contrary, PVDF clamped configuration increases the ME performance with increasing the piezoelectric thickness, starting with a near-to zero performance

at 10 μm, but improving the bi-layer performance above 20 μm of piezoelectric thickness and even improving the free configuration above 50 μm of piezoelectric thickness on each side of the Vitrovac layer.

As established in chapter 1, Wong (W. Wong, 2007)also measured α_{ME} as function of bias magnetic field for PMP laminates (PMN-PT/Terfenol-D/PMN-PT) with three different thickness ratios, of 0.4, 1.4 and 2.4. These results are established with α relative to the highest value obtained for the measurements and presented in Figure 2.21 (b) in order to allow a comparison with the FEM simulated trends of symmetric PMP -PVDF and PZT- configurations, established in Figure 2.21 (a).
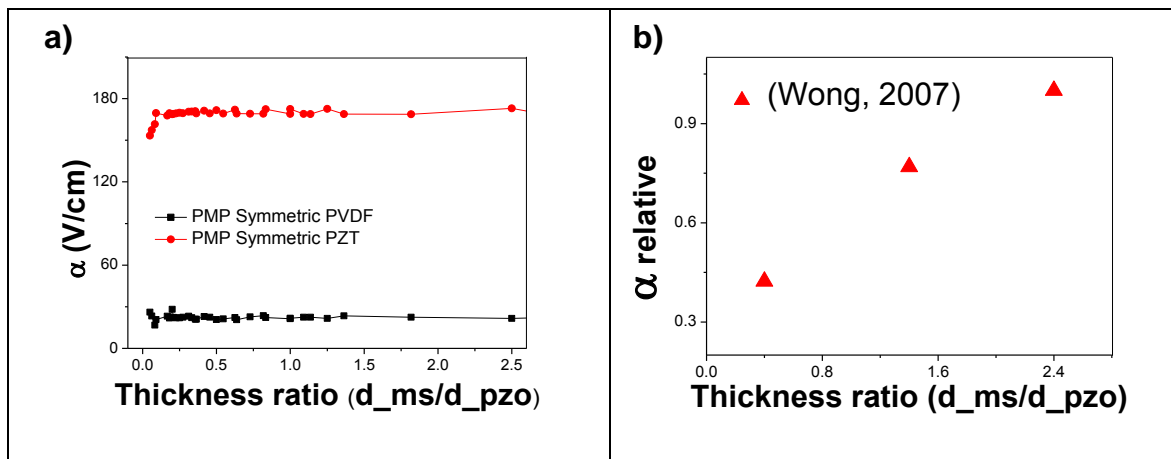
Figure 2.21: Magnetoelectric coefficient FEM simulation for PMP symmetric -PZT and PVDF- configurations as a function of thickness ratio (d_ms/d_pzo) of magnetostrictive (d_ms) and piezoelectric (d_pzo) thicknesses (a). Results are compared with measured data established in reference(W. Wong, 2007) (b).

The results in (W. Wong, 2007) show that the ME performance of the PMP configurations increase when increasing the thickness ratio (Figure 2.21(b)). This trend is confirmed by FEM simulation results. The PZT-PMP laminate thickness ratio curve shows an increasing ME performance for thickness ratios below 0.3, saturating above this thickness ratio value. PVDFPMP laminate simulations show a more disordered trend, with decreasing α for thickness ratios below 0.1, then increasing until reaching saturation at the thickness ratio of 0.3. This difference is described by the mechanical properties of PVDF, that do not allow to completely transmit deformations when the piezoelectric thickness is too large, therefore decreasing the ME performance, as shown in Figure 2.21 (a).

The inclusion of asymmetry in the PMP configurations was also studied for magnetostrictive thickness sweep between 10 and 600 μm, with holding piezoelectric thickness values at 110 μm (at the bottom of the laminate) and 25 μm at the top layer piezoelectric thickness. Simulation results are presented in Figure 2.22.
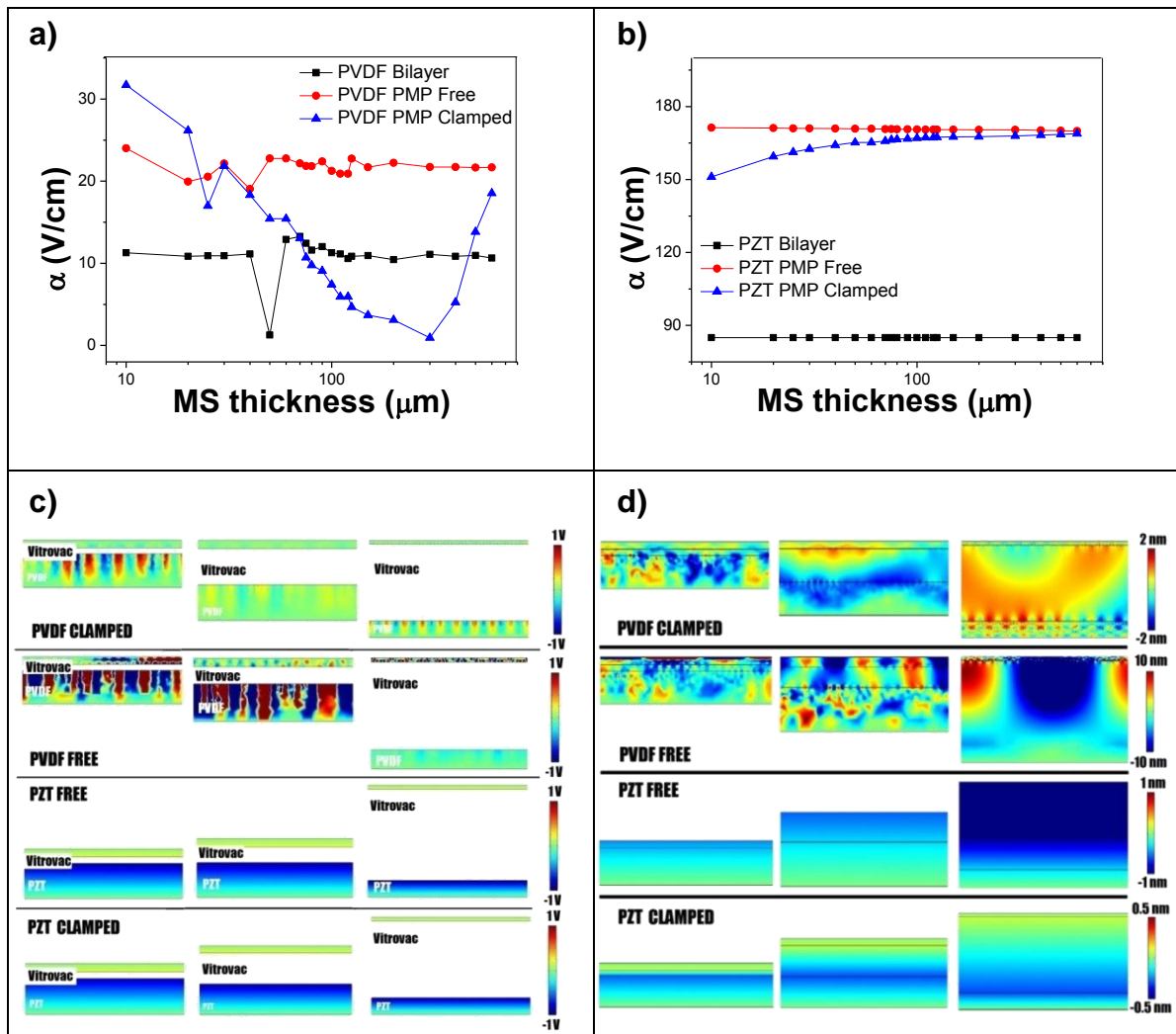
Figure 2.22: Piezoelectric-magnetostrictive-piezoelectric tri-layered (PMP) asymmetric laminate results for magnetostrictive thickness´s sweep. In figures (a) and (b), the ME coefficient curve is presented for PVDF-PMP (a) and PZT-PMP (b) for piezoelectric thicknesses of 110 μm (bottom) and 25 μm (top) in the range of magnetostrictive thicknesses from 10 to 600 μm. Figure (c) presents the electric potential distribution for the PMP free and clamped cases. Figure (d) shows the vertical displacement field (y) for the free and clamped cases. Piezoelectric thicknesses of 20 μm, 50 μm and 500 μm are the particular cases shown. Particular scales are established on the right side of the images.

When compared to symmetric PMP configurations, the introduction of an asymmetry slightly improves the ME performance of the composite. For PZT free configurations (Figure 2.22 (b)) α_{ME} still shows to be independent of the magnetostrictive thickness, but with a slightly higher value (of 2 V/cm, approx.) than the symmetric case. The clamped case shows the same trends as the symmetric case, increasing α_{ME} until reaching saturation for a magnetostrictive thickness of about 100 µm, but with higher ME performance than the symmetric PMP configuration in the whole magnetostrictive thickness range under consideration. The PVDF free asymmetric configurations also show a slight improvement over the symmetric PMP configuration (in the order of 2 to 3 V/cm), but also an enhanced performance for small magnetostrictive thicknesses. The clamped case of asymmetric PVDF laminates show an improvement over all configurations for magnetostrictive thicknesses below 20 µm, but decreasing its behaviour for increasing thicknesses and reaching a minimum for a magnetostrictive thickness of 250 µm, then increasing again, but never reaching the performance of the free configuration.

The asymmetric PMP piezoelectric thickness sweep configuration consisted of sweeping the top piezoelectric thickness when the magnetostrictive -Vitrovac-thickness held a value of 25 µm and the bottom piezoelectric PVDF thickness was held at 110 µm. Simulation results are displayed in Figure 2.23.

90
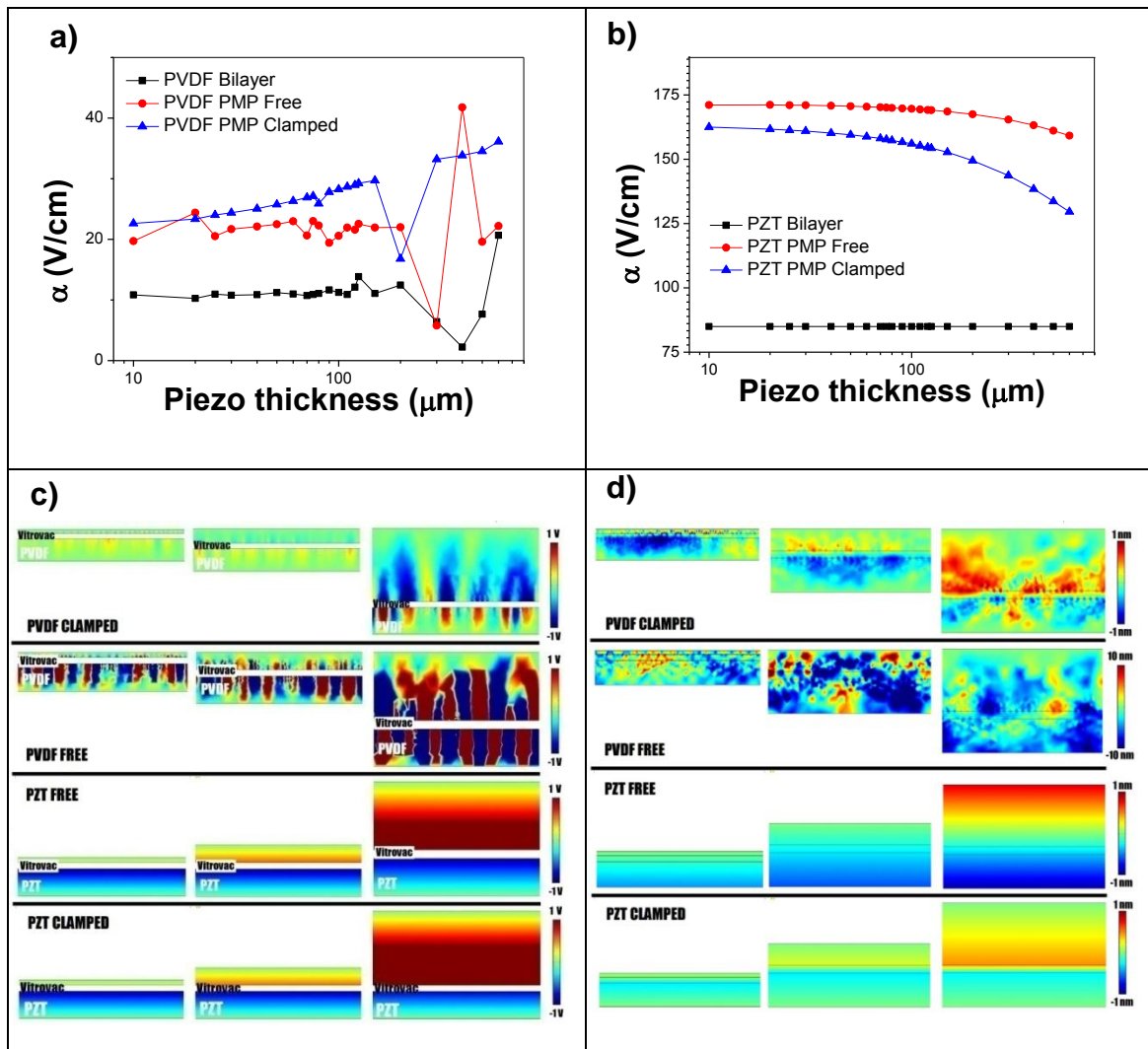
Figure 2.23: Piezoelectric-magnetostrictive-piezoelectric tri-layered (PMP) asymmetric laminate results for piezoelectric thickness´s sweep. In figures (a) and (b), the ME coefficient curve is presented for PVDF-PMP (a) and PZT-PMP (b) composites with 25 μm-Vitrovac thickness and 110 μm piezoelectric thickness, while the other piezoelectric thickness is varied in the range of 10 μm to 600 μm. Figure (c) presents the electric potential distribution for the PMP free and clamped cases. Figure (d) shows the vertical displacement field (y) for the PMP free and clamped cases. Piezoelectric thicknesses of 20/110 μm, 70/110 μm and 200/110 μm are the particular cases shown. Particular scales are established on the right side of the images.

For PZT free asymmetric configurations the enhanced ME performance show to be stable for piezoelectric thicknesses below 100 μm, then decaying for higher piezoelectric thickness values. Clamped configuration show the same results, with lower ME performance than the one

presented for the free configuration and diminishing the ME performance for piezoelectric thicknesses above 60 μm.

The PVDF asymmetric configurations present a relatively stable enhanced performance for all piezoelectric thicknesses, but not for those piezoelectric thickness values in the symmetric range (for piezoelectric thicknesses between 60 and 150 μm). The effect of clamping the PVDF composite has the effect of enhancing the ME performance when increasing the piezoelectric thickness.

2.3.3.3. Comparison between tri-layer symmetric configurations: MPM and PMP

As presented in chapter 1, Wong (W. Wong, 2007) established a comparison between the ME performance of MPM and PMP composites, where both configurations rapidly increased their unitary ME behaviour (α_{unit}) with increasing thickness ratio, until reaching saturation. The main observed difference was that the MPM configurations reached saturation with a higher slope than the PMP configurations, leading also to a higher ME coefficient (PMP-α in saturation is approximately an 85% of MPM-α). In order to verify if the trends are held for the simulations results, Figure 2.24 (a)shows the ME ratio for PVDF- MPM and PMP- configurations, while Figure 2.24 (b) displays ME ratio for PZT -MPM and PMP- configurations.
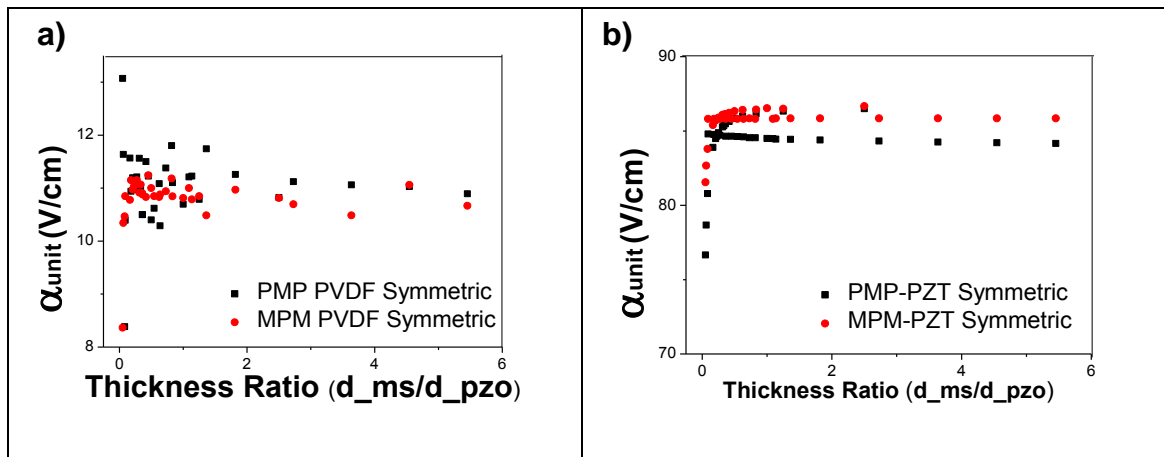
Figure 2.24: Expected magnetoelectric performance for PMP and MPM configurations over the magnetostrictive/piezoelectric thickness ratio (d_ms/d_pzo)for FEM simulation results for PZT(a) and PVDF (b)tri-layers.

While the trends presented by Wong (W. Wong, 2007)are confirmed by PZT MPM and PMP composite simulation results, PVDF MPM and PMP simulations results do not present as a clear trend. Results reported by Wong, and PZT MPM and PMP simulation results display high-sloped increase of the ME performance with increasing thickness ratio, the MPM configuration reaching saturation for a smaller thickness ratio than the PMP configuration, with a higher ME coefficient (in about 2 V/cm), as presented in Figure 2.24(b).

On the other hand, PVDF MPM and PMP configurations show curves that match the high-sloped increase of the ME performance with increasing thickness ratio and saturating afterwards, but the higher viscoelasticity of PVDF plays a fundamental role and, after unity of thickness ratio is reached, PMP configurations establish a better ME performance than MPM configurations, as can be seeing in Figure 2.24 (a).

2.3.4. Ideal two dimensional multi-layer laminate simulations

FEM simulation results are displayed by graphs of the simulated ME coefficient (obtained by equations 2.9 and 2.10, or 2.12) of the structure versus the sweep parameter, including PVDF/PZT thickness or Vitrovac thickness, according to the simulation experiment. Images of electric potential distribution are also used to establish the influence of the mechanical properties of the material over the obtained ME performance of the multi-layered structure.

2.3.4.1. Magnetostrictive-piezoelectric multi-layer simulations (M-P)

As presented in chapter 1, Srinivasan *et al.*(Srinivasan, Rasmussen, Levin, et al., 2002)evaluated the ME effect in bi-layers and multi-layers on thick-film structures of (LSMO)-PZT and (LCMO)-PZT, in which samples were fabricated with an equal number of piezoelectric and magnetostrictive layers, between 2 and 8 layers, maintaining the total thickness, D_c, and the thickness of both magnetostrictive and piezoelectric phases. Their study concluded that the transverse ME voltage is weaker in multi-layers when compared to bi-layers and that the relation is linear and proportional to the number of layers, n, as shown before in Figure 1.5.

In order to compare FEM simulations with these results, multi-layered Vitrovac/PZT and Vitrovac/PVDF configurations were modelled with similar conditions for composites with a total thickness of 600 and 300 μm and a number of layers, n, between 2 and 10. As presented by Srinivasan *et al.*(Srinivasan, Rasmussen, Levin, et al., 2002), α was not calculated by equation 2.9/2.10, but from unitary α, or $\boldsymbol{\alpha_{unit}}$ (Eq. 2.12). The ME coefficient is compared to the transversal ME peak value in Figure 1.5.

Simulation results for PZT and PVDF laminates are shown in Figure 2.25 (a) and (b), respectively, with the corresponding electric potential distribution, in Figure 2.25 (c).
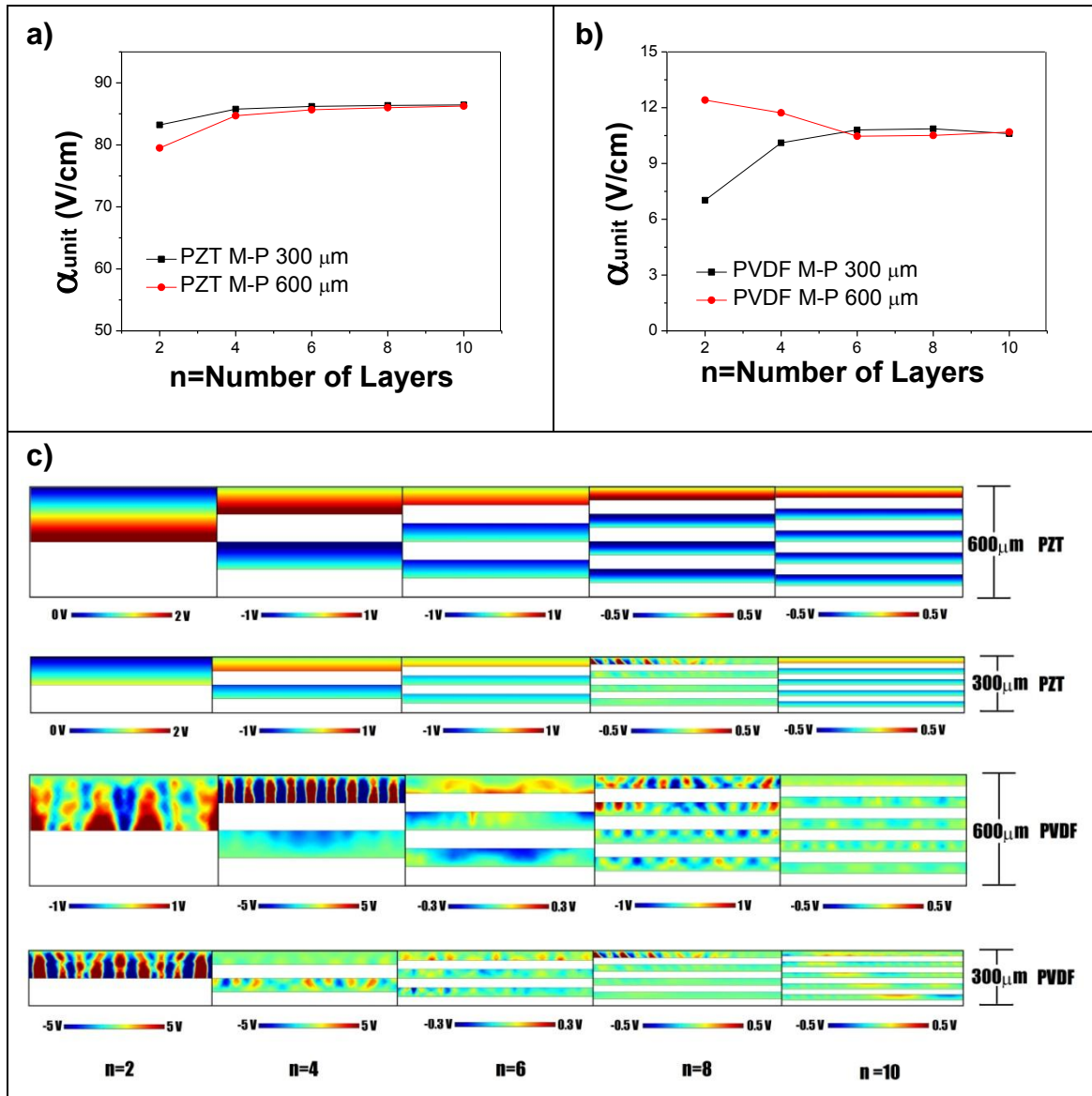
Figure 2.25: Simulations of the peak magnetoelectric voltage coefficient for Vitrovac/PZT (a) and Vitrovac/PVDF (b)M-P multi-layers and the corresponding trend with increasing numbers of layers, n, of the multi-layer. In figure (c) the electric potential distribution is displayed for FEM simulations of PZT (up) and PVDF (down) M-P multi-layers with 2 to 10 layers with f 600μmand 300μm of total thickness in both cases.

PZT M-P laminates show an increase in the ME performance when divided into multi-layers for both total thicknesses, D_c, of 300 and 600μm, presenting discrepancy with the results from Srinivasan *et al.*(Srinivasan, Rasmussen, Levin, et al., 2002). As Srinivasan *et al.* and two of the present multi-layer simulations configurations are based on PZT, it leads to conclude that the variations are due to the lack of consideration, in the simulations, of structural damping and

magnetic losses (that play a relevant role when more layers are introduced), triggering errors on the simulated multi-layer trends. Although the 300μm-thickness PVDF M-P laminate shows the same results as the PZT M-P simulations, the PVDF multi-layer of total thickness of 600μm followed Srinivasan *et al.* results, establishing a slightly improved ME unitary performance as less number of layers are involved. From Figure 2.25 (c), it can be observed that the electric potential for the 300μm-thickness PVDF M-P laminate shows already in the bi-layer simulation a dipolar inhomogeneous pattern, while the case of total thickness of 600μm-until a number of 6layers-, the poles appeared to be bigger and therefore the ME performance is enhanced, even showing an approximately homogeneous electric potential distribution pattern for at least one of the piezoelectric layers (internal) for n=4 and n=6.

2.3.4.2. Magnetostrictive-magnetostrictive multi-layer simulations (M-M)

As for MPM configurations, M-M multi-layer laminate simulations consisted in similar experiments, with composites with a larger number of layers. Laminates of 5 , 7 and 9 layers were simulated, therefore including 2,3, and 4 piezoelectric layers, respectively, with the simulated ME coefficient obtained by equations 2.9 and 2.10.

The first simulations consisted in the magnetostrictive thickness sweep for the symmetric case, in which all magnetostrictive thicknesses are equal and swept between 10 and 600μm, with all piezoelectric thicknesses held constant at 110μm. Results for PVDF and PZT free configurations are shown in Figure 2.26 (a) and (b), respectively. Clamped results are presented in Figures (c), for PVDF, and (d), for PZT, respectively, and the electric potential distribution is presented in (e).
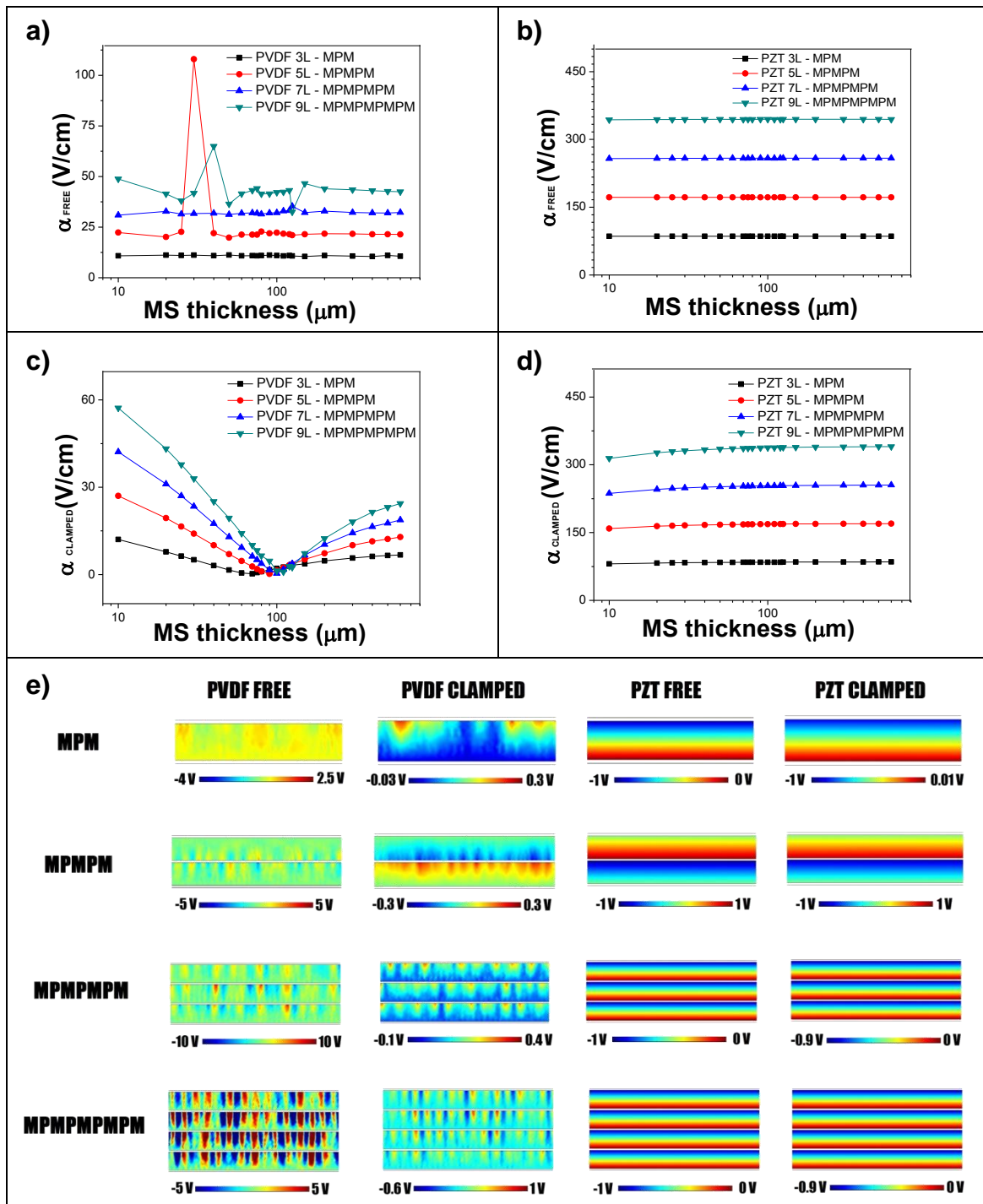
Figure 2.26: Magnetostrictive-magnetostrictive (M-M) symmetric multi-layer FEM simulation results for magnetostrictive thickness sweep, in the range of 10 μm to 600 μm, and for piezoelectric thicknesses of 110 μm. In Figures (a) and (b), the magnetoelectric coefficient curve is presented for PVDF M-M free multi-layers (a), PZT M-M free multi-layers (b), PVDF M-M clamped multi-layers (c) and PZT M-M clamped multi-layers (d). Figure (e) displays the electric potential distribution for each case, where the piezoelectric thickness is 110 μm and the magnetostrictive thickness is 10 μm.

The free M-M multi-layered configuration shows no magnetoelectric response dependence with varying magnetostrictive thickness for PZT and low-layered PVDFM-M multi-layer configurations, as presented in Figure 2.26 (a) for PVDF laminates, and 2.26 (b) for PZT laminates. It is shown that the ME coefficient obtained by applying equation 2.10 is the result of multiplying the ME coefficient, $\boldsymbol{\alpha_{ME}}$, of the bi-layered structure by the number of piezoelectric layers of the composite. The high-layered -9M-MPVDF free laminate (MPMPMPMPM)-shows a non-linear dependence due to the large number of viscoelastic piezoelectric layers of PVDF. It is to notice again, that no damping is considered in this evaluation.

For clamped configurations, on the other hand, clear trends can be established, as shown in Figure 2.26 (c) and (d). The PZT results show a lower ME behaviour with magnetostrictive thicknesses around 10-20 μm and a stable behaviour for higher Vitrovac thickness values. On the other hand, the PVDF configuration show an optimal performance with thinner magnetostrictive layers, decaying until reaching a minimal performance for magnetostrictive thickness around 90-100 μm. Further increasing thickness leads to higher ME performance but without reaching the ME performance obtained by the thinner magnetostrictive thickness values. Electric potential distribution for magnetostrictive sweeps are presented in Figure 2.26 (e).

Further simulation results consisted in the piezoelectric thickness sweep for the symmetric case, in which all piezoelectric thicknesses equal and swept 10 and 600 μm, with all magnetostrictive thicknesses held constant at 25 μm. Results for PVDF and PZT free configurations are shown in Figure 2.27 (a) and (b), respectively. Clamped results are presented in Figures (c) for PVDF, and (d) for PZT, respectively. Electric potential distributions are presented in (e).

98

Figure 2.27: Magnetostrictive-magnetostrictive (M-M) symmetric multi-layer FEM simulation results for piezoelectric thickness´s sweep. Magnetostrictive thicknesses is held at 25 µm, with the piezoelectric thickness varying in the range of 10 µm to 600 µm. In Figures (a) and (b), the magnetoelectric coefficient curve is presented for PVDF M-M free multi-layers (a), PZT M-M free multi-layers (b), PVDF M-M clamped multi-layers (c) and PZT M-M clamped multi-layers (d). Figure (e) displays the electric potential distribution for each case, when the piezoelectric thickness is 10 µm and the magnetostrictive thickness is 25 µm.

As presented in Figure 2.27 (b), PZT free M-M multi-layered structures present a constant ME performance with a small decay for piezoelectric thicknesses above 200 μm. These results are more evident when a larger number of piezoelectric layers are involved in the ME composite configuration. PVDF free M-M multi-layers also show a constant ME performance until 70 μm of piezoelectric thickness, decreasing their ME performance in a non-linear way-as shown in Figure 2.27 (a)- for larger thickness values.

The clamped PZT M-M configuration maintains its trend of constant performance over all the piezoelectric thickness range and then decaying for higher thicknesses, the decay appears around a thickness of 100 μm of PZT, showing a higher slope than the free configuration performance as can be seeing in Figure 2.27 (d)-. PVDF clamped M-M multi-layered structures show a divergent ME performance that reduces its value between 10 to 20 μm of piezoelectric thickness, reaching a minimum for 20-30 μm and then increasing performance along with the piezoelectric thickness of the structure, including the 7-layered MPMPMPM configuration that shows a nonlinear zone between piezoelectric thicknesses of 90 and 200 μm, as shown in Figure 2.27 (c).

Electric potential distributions for all configurations in the case of piezoelectric thickness of 10 μm are presented in Figure 2.27 (e). It can be noticed that the PVDF electric potential distributions showed a more distributed path for free configurations than for clamped configurations, where saturated poles are observed.

Figure 2.28 shows simulation results for particular cases of symmetric M-M multi-layered configurations with equal magnetostrictive and piezoelectric thicknesses. The first case is related to symmetric multi-layered laminates with thickness ratio of 1 (25 μm magnetostrictive/25 μm piezoelectric thickness and 110 μm magnetostrictive/110 μm piezoelectric thickness, for Vitrovac/PVDF -in Figure 2.28 (a)- and Vitrovac/PZT -in Figure 2.28 (b)-, the second case is related to symmetric multi-layered laminates with a thickness ratio of 1 and constant total thickness of 300 μm/600 μm (independent of the number of layers), also for Vitrovac/PVDF in Figure 2.28 (c)- and Vitrovac/PZT -in Figure 2.28 (d)-.

100

Figure 2.28: Magnetostrictive-magnetostrictive (M-M) symmetric multi-layer laminate FEM simulation results as a function of the number of layers, n, when the magnetostrictive and piezoelectric layers have the same thickness, of 25 and 110 μm, for Vitrovac/PVDF (a) and Vitrovac/PZT (b) M-M laminates, and when layers have the same thickness in a constant total thickness of 300 and 600 μm, for Vitrovac/PVDF (c) and Vitrovac/PZT (d) M-M laminates.

For both PZT symmetric M-M experiments, the ME performance increase with the number of layers, with a higher α_{ME} for thinner layers and lower amount of layers, but reaching similar results for more than 7 layers composites. Those results are similar than for the MPM laminates, but also establishing that higher number of layers include other effects as coupling parameters for bonding properties, magnetic losses, etc.

PVDF configurations appear to be influenced by the elasticity and morphology of the electroactive polymer, presenting better α-values for low-layered composites with higher thickness. For 5 or more layers, PVDF experiments show to have a clear trend of maintaining α-

values independently of the total thickness of the composite. As obtained by M-P multi-layered composites, symmetric laminates of Vitrovac/PVDF M-M multi-layered laminates perform better as a bulk bi-layered composite than in a thinner multi-layered one, as represented in Figure 2.28 (a) and (c). Also considering results obtained by Srinivasan *et al.* (Srinivasan, Rasmussen, Levin, et al., 2002) and considering damping, bonding and magnetic losses, it may be concluded that thicker bi-layered PVDF composites will have an enhanced performance over multi-layered thinner ones.

Figure 2.29 establishes simulations results for M-M configurations ME performance as function of the thickness ratio (d_ms/d_pzo) for PVDF simulations (Figure 2.29 (a) and PZT simulations (Figure 2.29 (b).
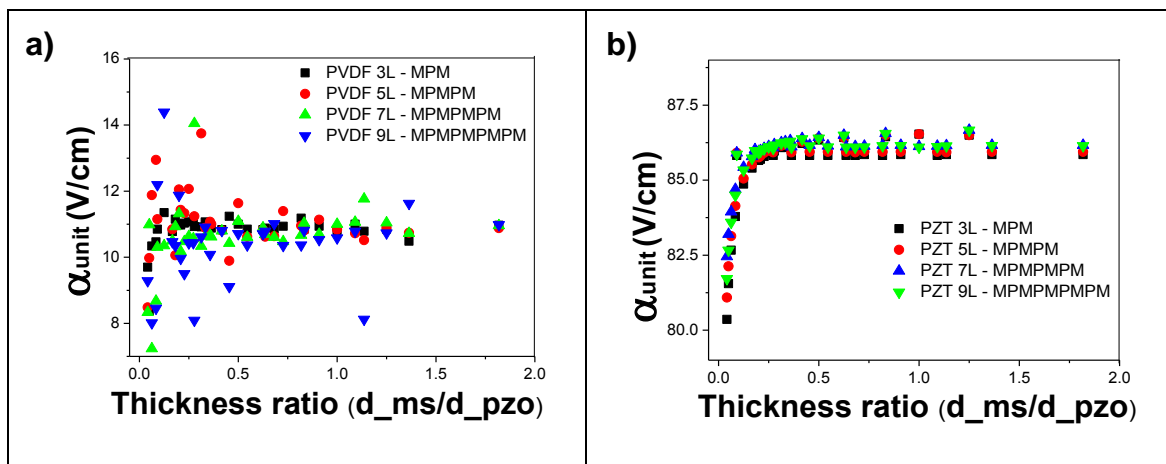
Figure 2.29: Magnetostrictive-magnetostrictive (M-M) symmetric multi-layered configurations simulation results as a function of the thickness ratio (d_ms/d_pzo), for PVDFM-M configurations (a) and PZT M-M configurations (b).

PZTM-M-symmetric laminates show an enhanced performance for either undersized magnetostrictive thicknesses or bulky piezoelectric thicknesses, as presented in Figure 2.29 (b), where the ME performance (α_{unit}) increases rapidly while increasing thickness ratio for all M-M configurations, saturating around a thickness ratio of 0.5 and showing therefore a constant performance for higher thickness ratios. While maintaining the trend of rapidly increasing their magnetic performance with increasing the thickness ratio and saturating above thickness ratio of 0.5, PVDFM-M symmetric-multi-layered composites (Figure 2.29 (a) show some particular peak

values of unitary ME coefficient for low thickness ratio values, especially for composites with high number of layers.

Asymmetric multi-layered M-M configurations were also simulated. The first experiment results are presented for magnetostrictive thickness sweep, in which all piezoelectric thickness are 110 µm thickness and the other magnetostrictive are fixed at 25 µm thicknesses, as presented in chapter 2.2.4.2. Magnetostrictive thickness sweep results (in the range of 10 µm to 600 µm) are shown in Figure 2.30: (a) for PVDF free case, (b) PZT free case, (c) PVDF clamped case, (d) PZT clamped case. The electric potential distribution for all cases is shown in (e).

For PZT and in the conditions in which the materials were evaluated (no nonlinear magnetostriction simulation model), it can be predicted that asymmetric configurations will not show different performance when compared with the symmetric configurations. Furthermore, it can be observed in Figures 2.26(b) and (d) -PZT simulations for symmetric configurations- and 2.30 (b),(d) -PZT simulations for asymmetric configurations- that asymmetric configurations show the same behaviour as the symmetric ones, for free and clamped cases.

On the contrary to the PZT configurations, PVDFM-M multi-layered asymmetric configurations change their ME performance when asymmetries are introduced. First, the introduction of intercalated magnetostrictive thickness of 25 µm and the when other thickness finds itself below 20 µm, the ME performance of high-ordered M-M free multi-layered laminates increase, as shown in Figure 2.30 (a). Clamped PVDFM-M multi-layered configurations maintain their performance to the symmetric ones, but displacing the minimal thickness value and diminishing their ME performance in the whole range.
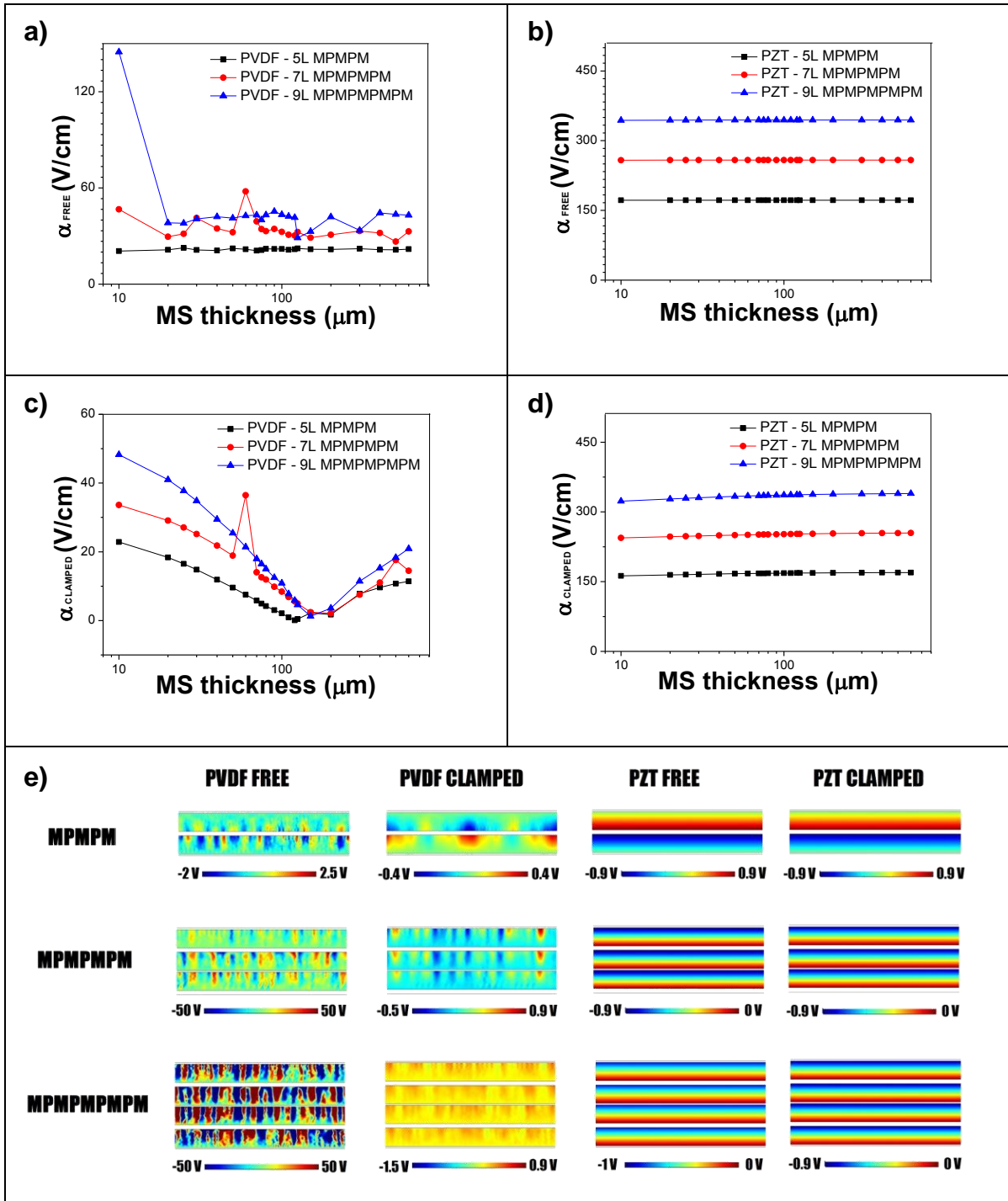
Figure 2.30: Magnetostrictive-magnetostrictive (M-M) asymmetric multi-layered FEM simulation results for magnetostrictive thickness´s sweep. The magnetoelectric coefficient curve is presented for PZT M-M free (a), PVDF M-M free (b), PZT M-M clamped (c) and PVDF M-M clamped configurations (d). Piezoelectric thickness for composites was held at110 μm, the fixed magnetostrictive value at 25 μm, and the variable magnetostrictive thickness is swept in the range of 10 μm to 600 μm. Electric potential distribution for all cases of asymmetric configurations when variable magnetostrictive thickness hold a value of 10 μm are shown in (e).

The second asymmetric M-M experiment results are presented for piezoelectric thickness sweep, in which all magnetostrictive thicknesses were 25 μm, and there were intercalated swept and fixed piezoelectric (of 110 μm) thicknesses, as presented in chapter 2.2.3.5. Piezoelectric thickness sweep (in the range 10 μm to 600 μm) results are shown in Figure 2.31: (a) for PVDF free case, (b) PZT free case, (c) PVDF clamped case, (d) PZT clamped case, and (e) electric potential distribution for all cases.

The results for piezoelectric thickness sweep are similar to the results obtained for magnetostrictive thickness sweep. PZTM-M asymmetric configurations show the same behaviour as the symmetric ones, for free and clamped cases, (Figures 2.31 (b), (d) and 2.27 (b),(d)). For PVDF M-M configurations, the introduction of a piezoelectric thickness asymmetry increased the ME behaviour of high ordered M-M free and clamped multi-layered configurations (Figure 2.31 (a),(c)), keeping the reduction of ME performance for variable piezoelectric thicknesses above 150 μm for the free case, and starting with near-zero performance in the clamped case, establishing improvement just above 25 μm when introducing piezoelectric asymmetry on the piezoelectric thickness for the M-MPVDF-clamped case.
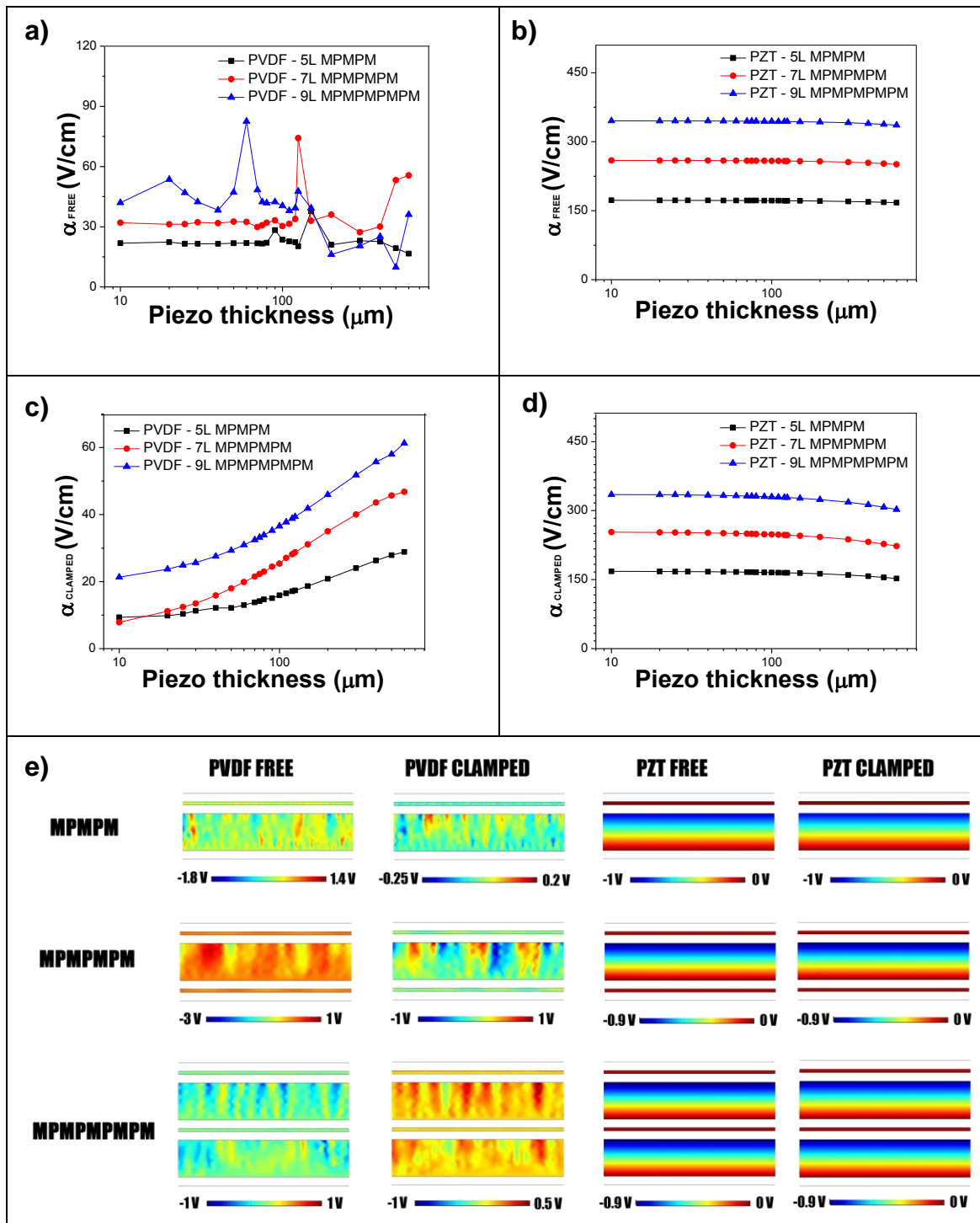
Figure 2.31: Magnetostrictive-magnetostrictive (M-M) asymmetric multi-layered FEM simulation results for piezoelectric thickness sweep. In Figures (a) and (b), the magnetoelectric coefficient curve is presented for PZTM-M free multi-layers (a), PVDF M-M free multi-layers (b), PZT M-M clamped multi-layers (c) and PVDF M-M clamped multi-layers (d). Magnetostrictive thickness is held at 25 μm, with intercalated piezoelectric thickness of 110 μm and others varying in the range 10 to 600 μm. Electric potential distribution for all cases of asymmetric M-M multi-layer simulations when variable piezoelectric thickness hold a value of 10 μm is shown in (e).

106

2.3.4.3. Piezoelectric-piezoelectric multi-layer simulations (P-P)

As for PMP configurations, P-P multi-layer laminates simulations consisted in similar experiments, with composites with a larger number of layers. Laminates of 5, 7 and 11 layers were simulated, therefore including 3, 4, and 6 piezoelectric layers, respectively, with the simulated ME coefficient obtained by equations 2.9 and 2.10.

The first simulations consisted in the magnetostrictive thickness sweep for the symmetric case, in which all magnetostrictive thicknesses are equal and swept between 10 and 600 μm, with all piezoelectric thicknesses held constant at 110 μm. Results for PVDF and PZT free configurations are shown in Figure 2.32 (a) and (b), respectively. Clamped results are presented in Figures (c), for PVDF, and (d), for PZT, respectively, and electric potential distribution is presented in (e).

The trends presented in Figure 2.32 (b) and (d), for the P-P PZT multi-layered FEM simulations are similar to those presented in Figure 2.26 (b) and (d) for M-M PZT multi-layered FEM simulations, in which there was no interdependency between magnetostrictive thickness and α_{ME} for the free case, while for the clamped case the thinnest magnetostrictive thicknesses - below 30 μm in the P-P multi-layered configurations and below 20 μm in the M-M multi-layered configurations- showed a slight decrease of the ME performance. The main difference appears to be in the dependence of the ME performance on the number of piezoelectric layers, thereby increasing its general behaviour in approximately the α-value of one bi-layer for each different configuration (difference introduced by treating the material as a device, by equation 2.10).
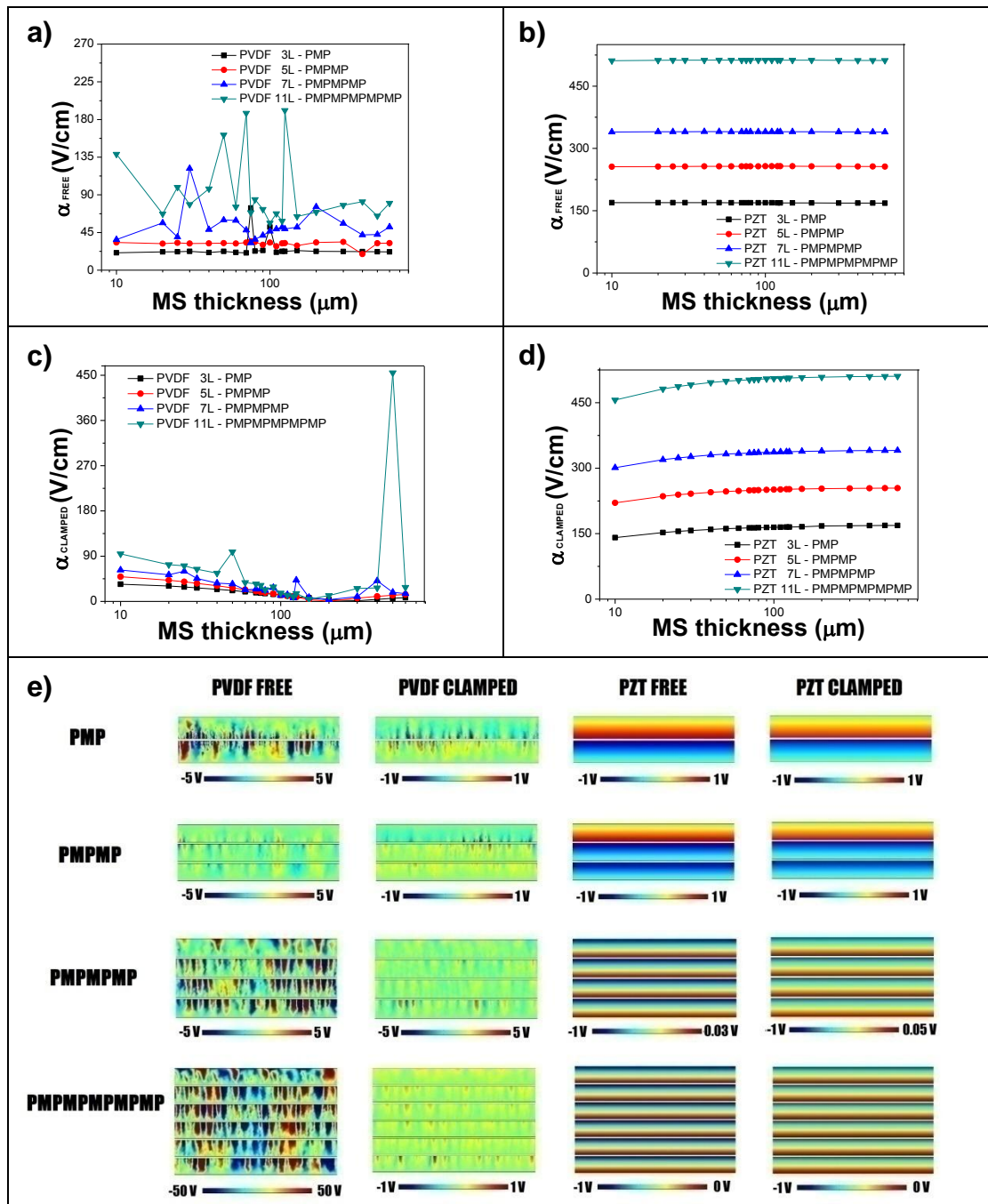
Figure 2.32: Piezoelectric-piezoelectric (P-P) multi-layered symmetric FEM simulation results for magnetostrictive thickness´s sweep. Piezoelectric thickness for composites is established as 110 μm, when the magnetostrictive thickness is varied in the range of 10 μm to 600 μm. In Figures (a) and (b), the magnetoelectric coefficient curve is presented for PVDF P-P free multi-layers (a), PZT P-P free multi-layers (b), PVDF P-P clamped multi-layers (c) and PZT P-P clamped multi-layers (d). Figure (e) displays the electric potential distribution for each case, when the piezoelectric thickness is 110 μm and the magnetostrictive thickness is 10 μm.

As can be observed by comparing Figure 2.32 (a) and (c) to the PVDF M-M multi-layer trends in Figure 2.26 (a) and (c), PVDF P-P multi-layer configurations also preserve ME drifts over magnetostrictive thicknesses, in particular for low-ordered multi-layered configurations. For higher number of layers, the ME performance is governed by its malleability and semicrystalline behaviour, therefore including high number of nonlinearities (peaks). This could indicate a better performance when avoiding damping and magnetic losses in the coupling factor. When considering clamped configurations, trends of decreasing α_{ME} with increasing the magnetostrictive thickness are preserved, reaching to a slightly drifted minimum (at approximately 200 μm of magnetostrictive thickness), then slowly increasing the ME performance for higher magnetostrictive thicknesses values.

Accordingly, following simulations results consisted on the piezoelectric thickness sweep for the symmetric case of multi-layered P-P configurations, in which all piezoelectric thicknesses are equal and swept between 10 and 600 μm, with the magnetostrictive thicknesses held constant at 25 μm. Results for PVDF and PZT free configurations are shown in Figure 2.33 (a) and (b), respectively. Clamped results are presented in Figures (c) for PVDF, and (d) for PZT, respectively, and electric potential distribution is presented in (e).
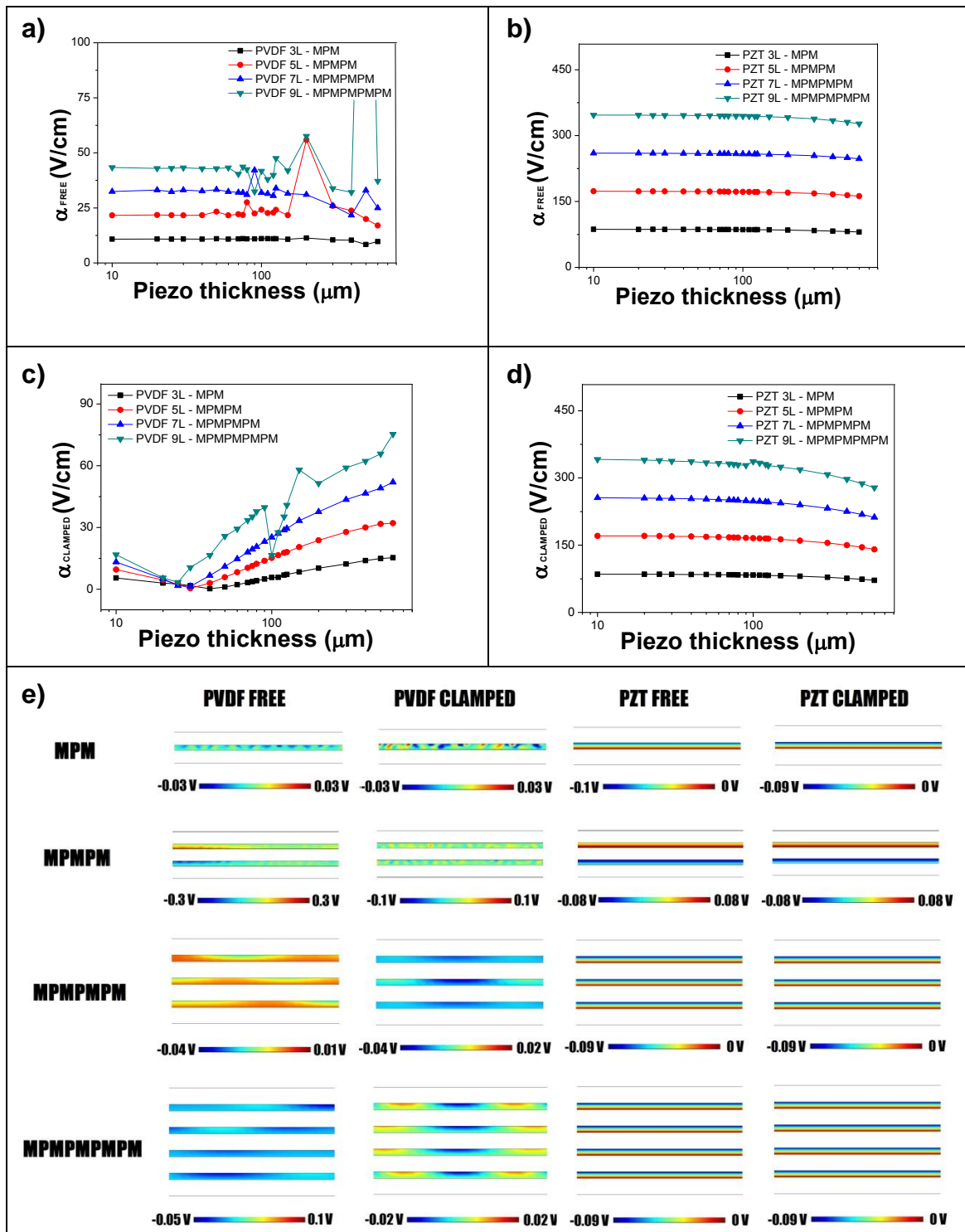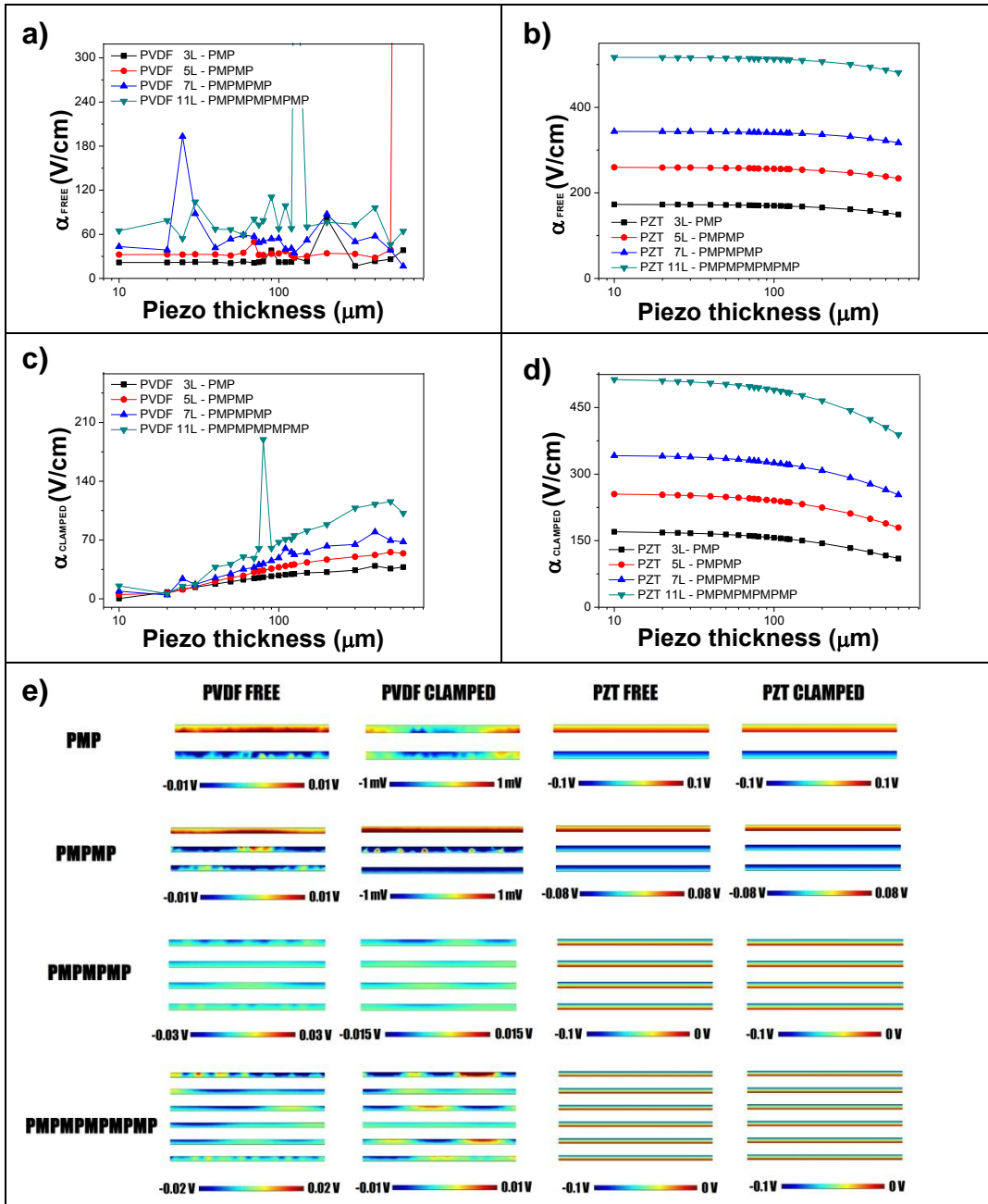
Figure 2.33: Piezoelectric-piezoelectric (P-P) multi-layered symmetric FEM simulation results for piezoelectric thickness´s sweep. Magnetostrictive thickness for composites is established as 25 μm, with the piezoelectric thickness varying in the range of 10 μm to 600 μm. In Figures (a) and (b), the magnetoelectric coefficient curve is presented for PVDF P-P free multi-layers (a), PZT P-P free multi-layers (b), PVDF P-P clamped multi-layers (c) and PZT P-P clamped multi-layers (d). Figure (e) displays the electric potential distribution for each case, with the piezoelectric thickness at 10 μm.

PZT P-P multi-layer simulations present a constant behaviour for lower piezoelectric thicknesses, decreasing slightly for thicker piezoelectric thicknesses (above 200 μm) for the free case and preserving this behaviour for the clamped case, with larger slope in the decrease of the performance for thicker piezoelectric layers (above 150 μm) in the clamped structure, as can be seen in Figure 2.33 (b) and (d).

As shown in Figure 2.33 (a),PVDF free P-P multi-layered configurations present nonlinear trends for high-layered laminates, although it appears to have a general and stable increase of its magnetoelectric performance over the region of piezoelectric thicknesses between 60 and 150 μm of PVDF. Clamped PVDFP-P multi-layered configurations-displayed in Figure 2.33 (b)- on the other hand, show explicit trends in increasing the magnetoelectric performance when increasing the piezoelectric thickness of the composite.

Figure 2.34shows simulation results for particular cases of symmetric multi-layered P-P configurations with equal magnetostrictive and piezoelectric thicknesses. The first case is related to symmetric multi-layered laminates with thickness ratio of 1 (25 μm magnetostrictive/25 μm piezoelectric thickness and 110 μm magnetostrictive/110 μm piezoelectric thickness, for Vitrovac/PVDF -in Figure 2.34 (a)- and Vitrovac/PZT -in Figure 2.34 (b)-,the second case is related to symmetric multi-layered laminates with a thickness ratio of 1 and constant total thickness of 300 μm/600 μm (independent of the number of layers), also for Vitrovac/PVDF in Figure 2.34 (c)- and Vitrovac/PZT -in Figure 2.34 (d)-.
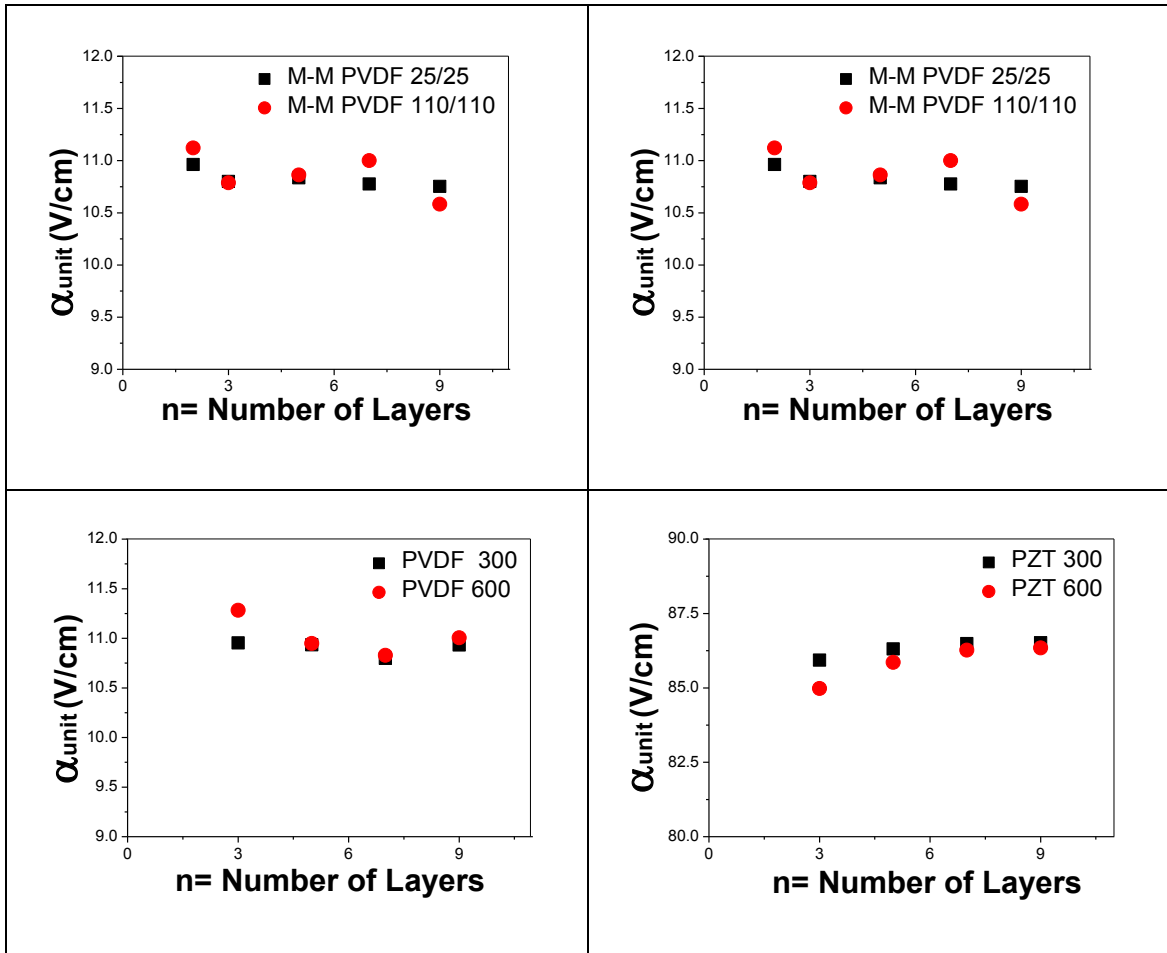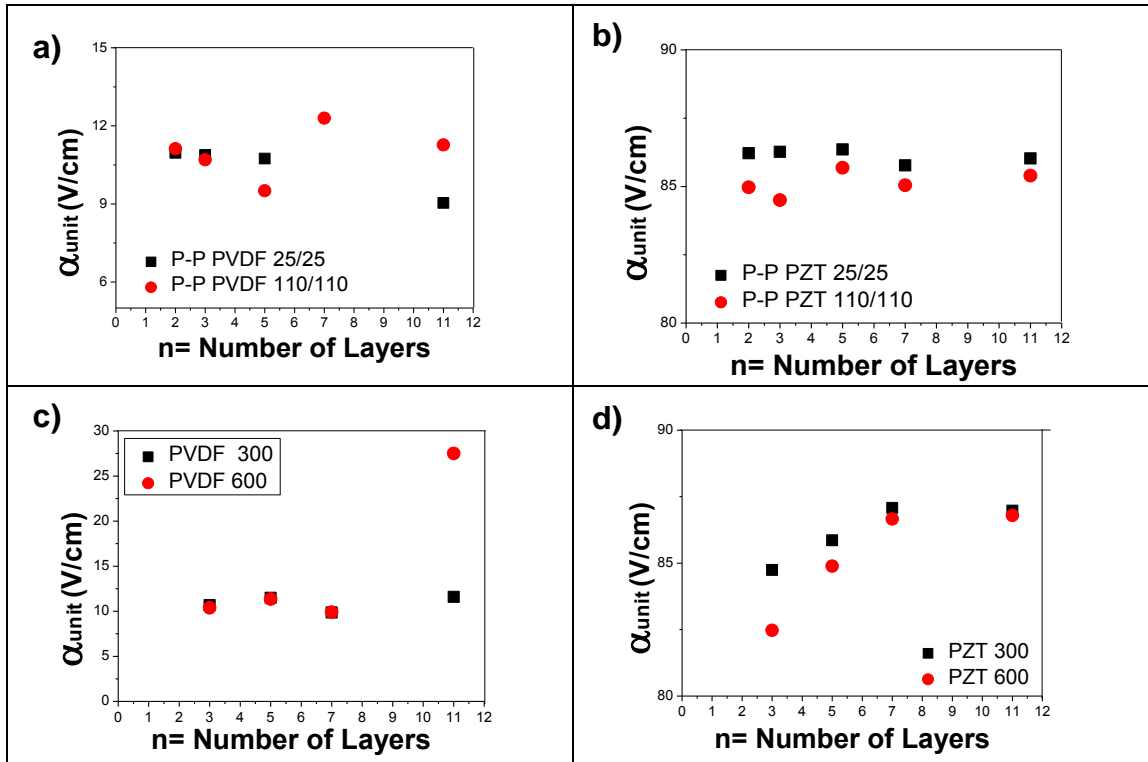
Figure 2.34: Piezoelectric-piezoelectric (P-P) multi-layered FEM simulation results for symmetric configurations as a function of the number of layers, n, when magnetostrictive and piezoelectric layers have the same thickness, of 25 and 110 μm, for Vitrovac/PVDF (a) and Vitrovac/PZT (b) P-P laminates, and when layers have the same thickness in a constant total thickness of 300 and 600 μm, for Vitrovac/PVDF (c) and Vitrovac/PZT (d) P-P laminates.

PZT symmetric P-P experiments present also higher α_{ME} for thinner layers in both experiments (2.34 (b) and (d)). In the experiment for fixed thicknesses, α-values takes an approximately constant value, with the only exception of cases with 2-3 layers on the 110 μm thickness case, where α_{ME} seems to decrease from 2 to 3 layers, then increasing again for 5 layers. The constant total thickness experiment gives coherent values that indicates that the ME performance increases with the number of layers, with a perceivable higher α_{ME} for thinner layers in low amount of layers, but reaching similar results for composites with more than 7 layers. It should be noticed, that these higher values for high number of layers can be minimized when considering other effects as coupling parameters for bonding properties, magnetic losses, etc.

Due to the elasticity and morphology of the piezoelectric polymer, PVDF symmetric P-P experiments do not present as stable values and tendencies as PZT. Although for low number (for 3, 5 and 7 layers) of layers -constant total thickness experiment- presents an approximately

112

constant value, maintained later for the thinner experiment (the case of 300 µm of total thickness), ME performance is doubled for the 11-layers thicker experiment (of total thickness 600 µm), as presented in Figure 3.34 (c). These trends are also preserved in the 25 µm and 110 µm layered experiment, whose results are shown in Figure 3.34 (a), that also display a constant value for low-layered composites, and a difference in the ME performance on the 11-layered composites, in which case the constant value is preserved for the experiment of 110 µm but decreases by the 25-layered composite. After these results it may be established that low-layered composites with thickness ratio of 1 show a constant performance when composed of low number of layers, reaching a better performance when including thicker layers in composites with a larger number of layers.

Figure 3.35 shows the simulations results of the ME performance for P-P configurations as function of the thickness ratio (d_ms/d_pzo) for PVDF simulations -in Figure 2.35 (a)- and PZT simulations -in Figure 2.35 (b)-.
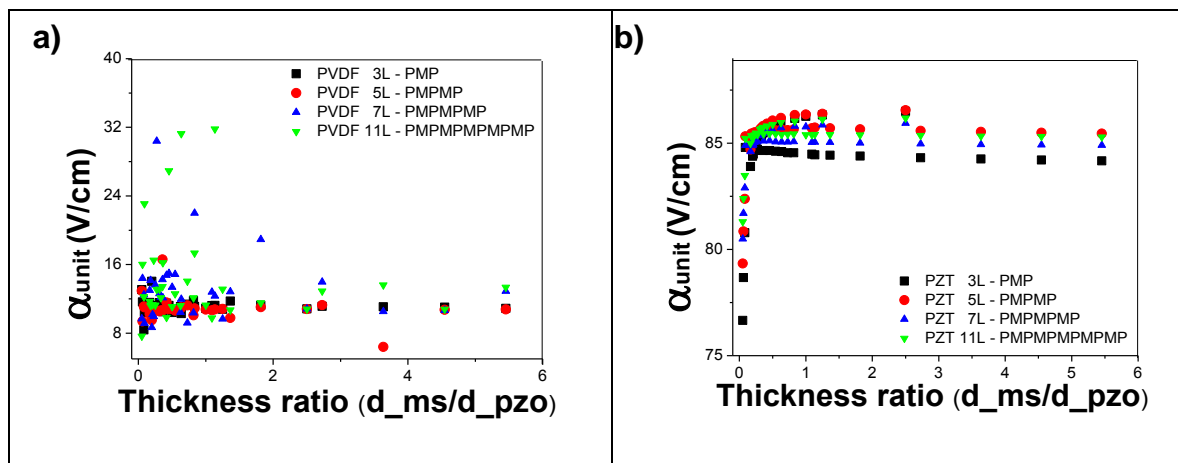
**Figure 2.35:** Piezoelectric-piezoelectric (P-P) multi-layered FEM simulation results for symmetric configurations as a function of their thickness ratio for PVDF(a) and PZT (b).

The trend of rapidly increasing the ME performance with increasing thickness ratio until saturation for thickness ratio around 0.5 is maintained for PZTP-P multi-layers, as presented by (W. Wong, 2007), and saturation values of ME performance seem to be higher when a larger amount of layers are involved in the P-P composite, with the exception of the 5-layered PMPMP composite, that presents the highest saturation α_{ME}, proving to be the optimal configuration, as can be seeing in Figure 2.35 (b).

As established before for PMP and P-P configurations, as a larger number of layers are involved in the composition of the laminate, mechanical effects (elasticity and semicrystalline composition of PVDF) lead to more disordered patterns of α_{ME}, as shown in Figure 2.35 (a). Although preserving Wong´s(W. Wong, 2007) trend for low layer number PVDF P-P multi-layered configurations, the introduction of higher number of PVDF layers in the composite induces a nonlinear behaviour. Those nonlinearities present themselves as peak values for particular thickness ratios, establishing improvements when damping or magnetic losses introduced for high number of layers in the composite are not considered, as established before. It can be also noticed, that the trend of PMPPVDF α_{ME} versus thickness ratio is preserved for the 5-layered PMPMP configuration, obtaining high values of the thickness ratio below 0.1, then decreasing quickly to increase again and saturating for thickness ratios above 0.5, even achieving similar ME performance values.

In asymmetric multi-layered P-P configurations, for magnetostrictive thickness sweep experiments in the range 10 μm to 600 μm, all piezoelectric thickness were of 110 μm thickness, and there were intercalated swept and fixed magnetostrictive (of 25 μm) thicknesses. Results are shown in Figure 2.36: (a) for PVDF free case, (b) PZT free case, (c) PVDF clamped case, (d) PZT clamped case, and (e) electric potential distributions for all cases.

114
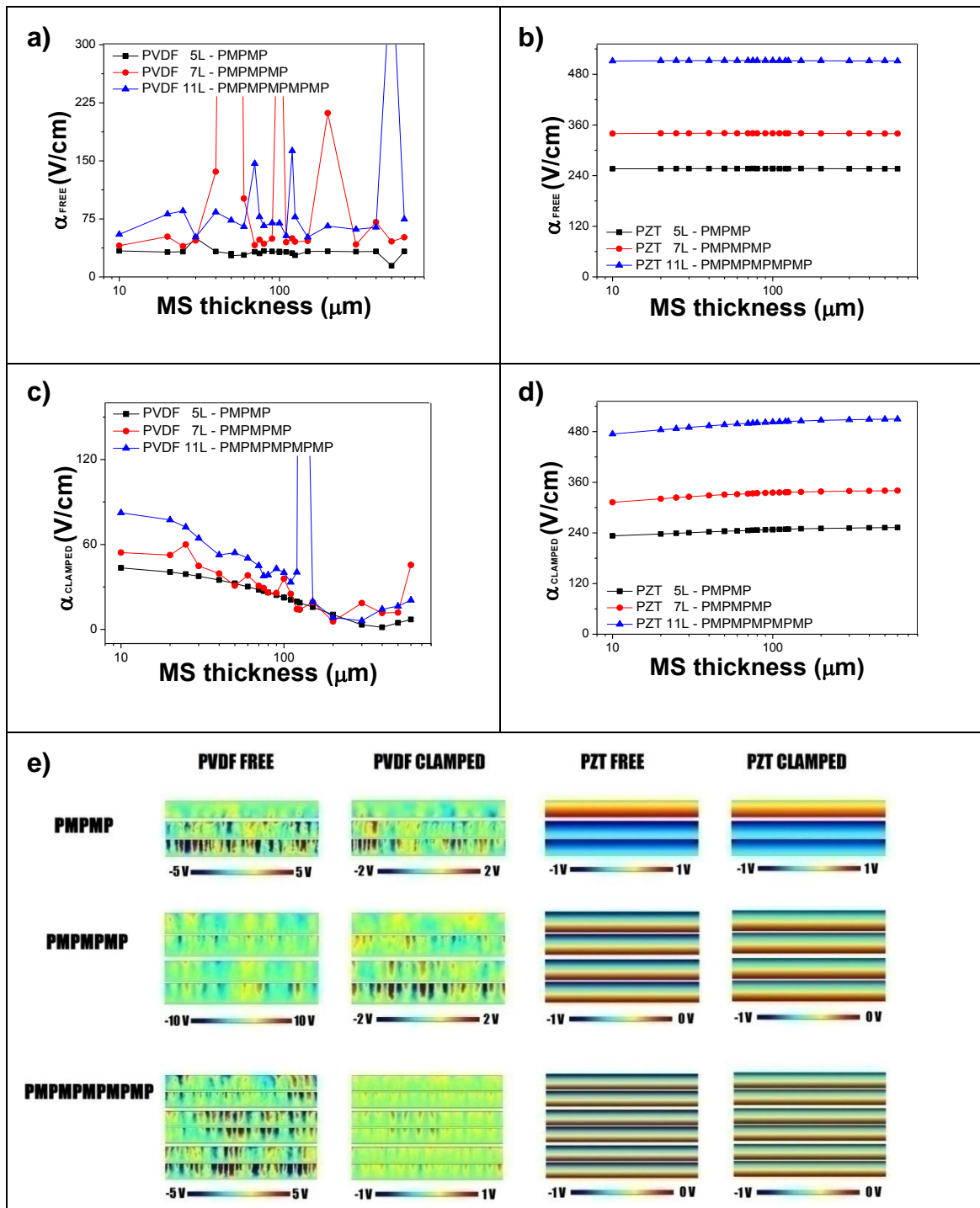
Figure 2.36: Piezoelectric-piezoelectric (P-P) asymmetric results for magnetostrictive thickness´s sweep in the range 10 μm to 600 μm. The magnetoelectric coefficient curve is presented for PZT P-P free (a), PVDF P-P free (b), PZT P-P clamped (c) and PVDF P-P clamped multi-layers (d). Piezoelectric thickness for composites is 110 μm, the fixed magnetostrictive value is 25 μm. Electric potential distribution when variable magnetostrictive thickness holds a value of 10 μm is shown in (e).

As for M-M configurations, PZT asymmetric P-P configurations do not vary their performance when compared with the one of the symmetric configurations. Furthermore, it can be observed in Figures 2.36 (b) and(d), and 2.32 (b) and (d) - for symmetric P-P configurations- that asymmetric configurations have the same behaviour as the symmetric ones, for free and clamped cases for magnetostrictive sweep.

When free and clamped asymmetric PVDF P-P configurations ME performances (Figure 2.36 (a) and (c), respectively) are compared to their respective symmetric α_{ME} (Figure 2.32 (a)and (c)), trends are preserved, with the introduction of some differences in the value of the nonlinear peaked behaviour that becomes more intense with the inclusion of asymmetries, particularly for the case of 7-P-P layered configuration, that increased in number and value of peaks, reaching for this case higher peak performances in the asymmetric configuration for magnetostrictive thicknesses of 50, 100, 200 and 400μm. On the other hand, clamped PVDF P-P multi-layered configurations present a displaced minimum ME value over thickness for thicknesses around 400 μm of magnetostrictive thickness, which leads to the conclusion that the introduction of magnetostrictive asymmetries would improve the performance when lower values of magnetostrictive thickness are introduced.

In the following, results for piezoelectric thickness sweep in the range 10 μm to 600 μm of asymmetric P-P multi-layered configurations are shown in Figure 2.37. All magnetostrictive thicknesses were 25 μm and the configuration had intercalated swept and fixed piezoelectric (110 μm) thicknesses. Results are shown in Figure 2.37: (a) for PVDF free case, (b) PZT free case, (c) PVDF clamped case, (d) PZT clamped case, and (e) electric potential distribution for all cases.

116
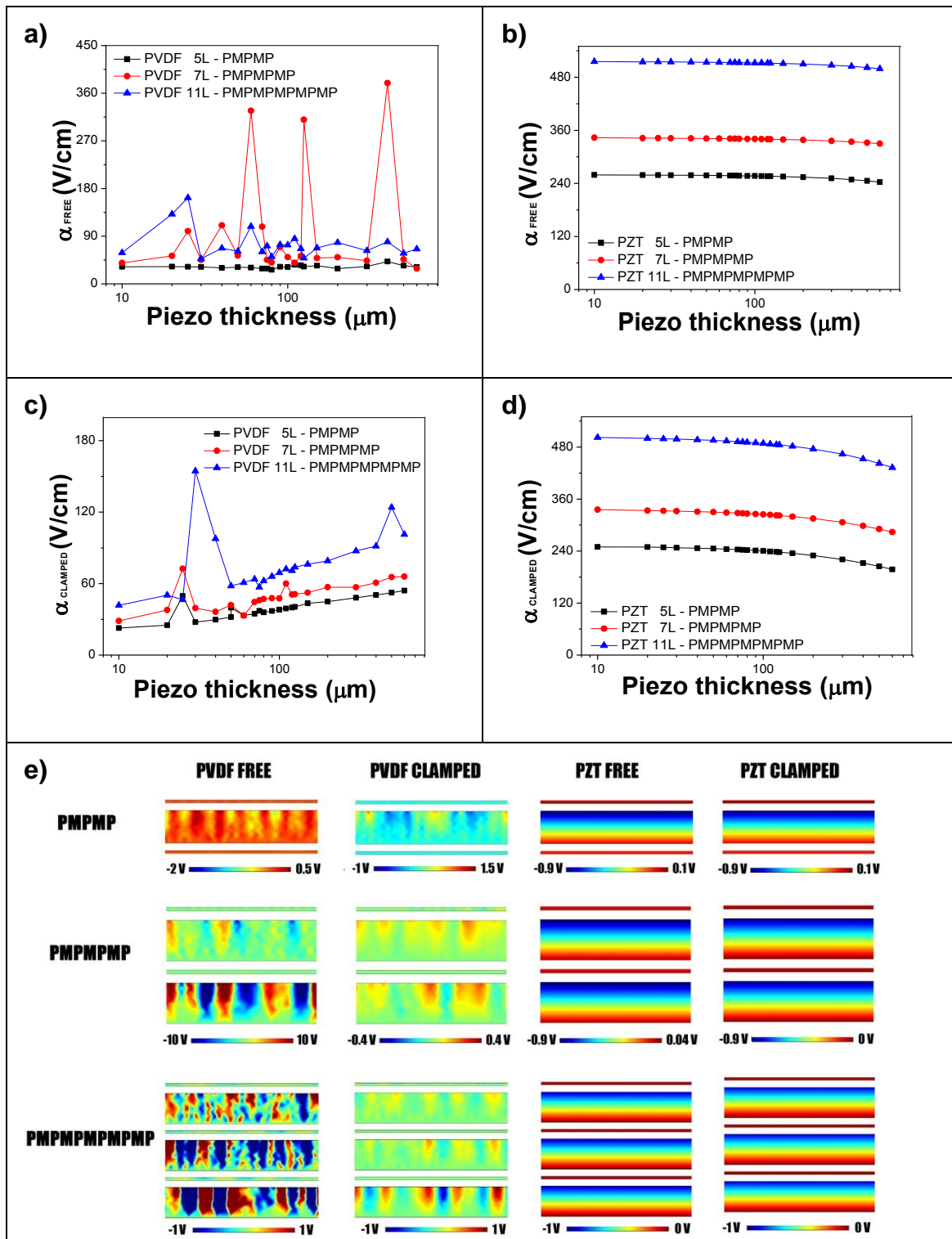
Figure 2.37: Piezoelectric-piezoelectric (P-P) multi-layered asymmetric results for piezoelectric thickness´s sweep in the range 10 μm to 600 μm. The magnetoelectric coefficient curve is presented for PZT P-P free (a), PVDF P-P free (b), PZT P-P clamped (c) and PVDF P-P clamped multi-layers (d). Magnetostrictive thickness for composites is 25 μm, the fixed piezoelectric value is 110 μm. Electric potential distribution when variable piezoelectric thickness holds a value of 10 μm is shown in (e).

As for M-M configurations, for magnetostrictive and piezoelectric thickness sweep experiments, PZT asymmetric P-P configurations do not vary their performance when compared with the one of the symmetric configurations. Furthermore, it can be observed in Figures 2.37 (b)and(d) and 2.33 (b) and (d) -for P-P symmetric configurations- that asymmetric configurations show the exact same behaviour as the symmetric ones, for free and clamped cases for magnetostrictive and piezoelectric sweep.

As presented for PVDF M-M configurations, the introduction of a piezoelectric thickness asymmetry increases the ME behaviour of high ordered PVDFP-P –free and clamped-multi-layered configurations, while decreasing its normal performance for intercalating piezoelectric thicknesses of 110 μm and thicker ones -Figure 2.48 (a) and (c)-.

When free and clamped asymmetric PVDFP-P configurations ME performances(Figure 2.37 (a) and (c), respectively) are compared to their respective symmetric α_{ME} (Figure 2.33 (a) and (c), respectively), it is observed that the general trends are preserved, with some differences in the value of the nonlinear peaked behaviour that becomes more intense with the inclusion of asymmetries, particularly for the case of 7-P-P layered configuration. Clamped PVDF P-P multi-layered configurations present a displaced minimal ME value over piezoelectric thickness to the left, which leads to the trend of a rising α_{ME} with piezoelectric thickness, which leads also to the conclusion that the inclusion of asymmetries on P-P configurations improve slightly their ME performance.

2.3.5. Global Analysis of multi-layers: PZT and PVDF laminates

In order to obtain a deeper understanding on the configuration differences and to enable the possibility of a better data analysis, multi-layered simulations are reorganized by material, as follows. PZT and PVDF multi-layered simulations results are now presented according to the experiment variable (magnetostrictive thickness/piezoelectric thickness sweep) and boundary conditions (clamped/free) and organized by the number of piezoelectric phases involved in the configuration. Furthermore, according to the piezoelectric material component, one graph containing unitary ME coefficients for M-P, M-M and P-P symmetric configurations with a total thickness of 300 μm and 600 μm as function of the number of the composite layers is presented.

118

2.3.5.1. PZT multi-layer configurations

Simulation results for all PZT configurations consisting of 1 to 4 piezoelectric phases (2-9 layers) are presented in Figure 2.38 (a) for magnetostrictive thickness sweep of free configurations, (b) for piezoelectric thickness sweep of free configurations, (c) for magnetostrictive thickness sweep of clamped configurations and (d) for piezoelectric thickness sweep of clamped configurations.
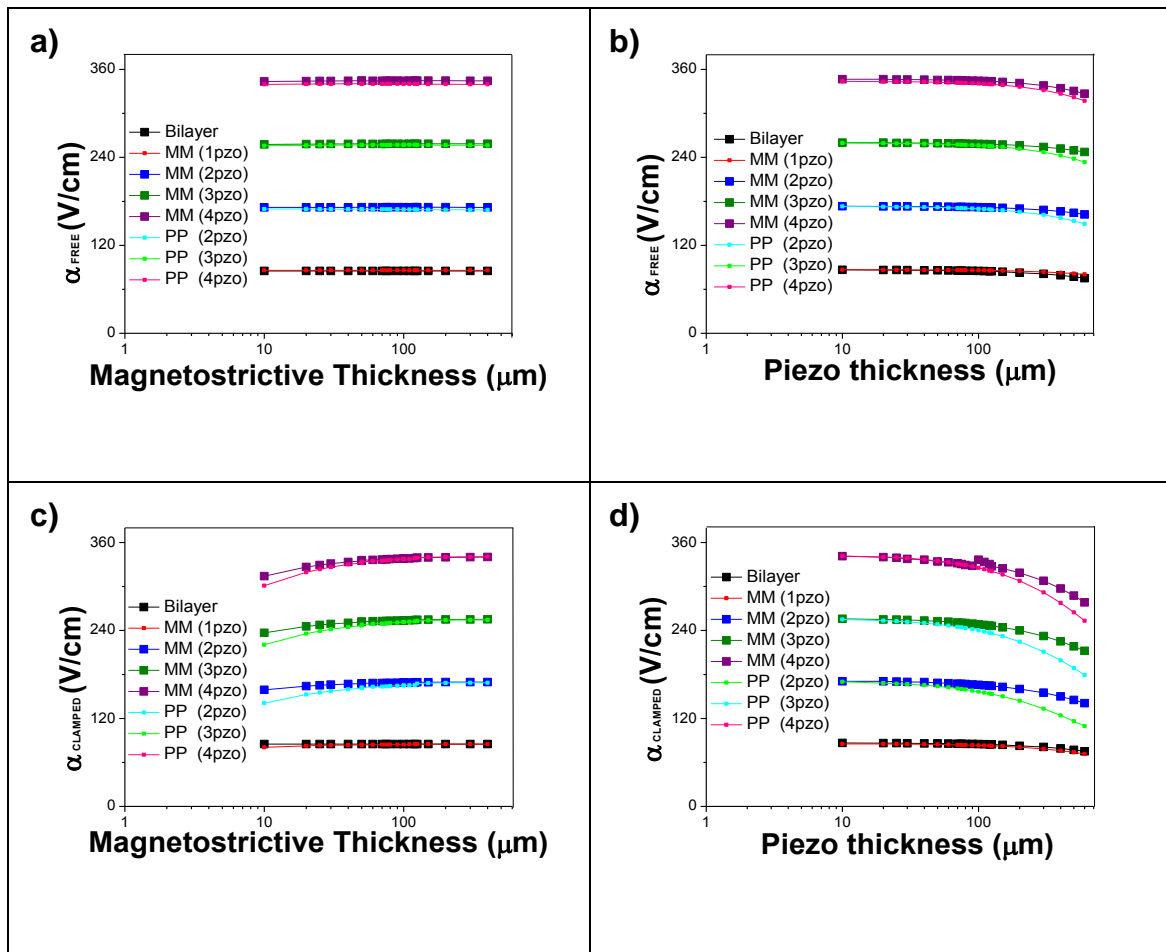
Figure 2.38: Magnetoelectriccoefficients for all symmetric configurations of PZT magnetoelectric laminates as a function of the magnetostrictive thickness of the free configuration (a) and clamped configuration (c), and as function of the piezoelectric thickness of the free configuration (b) and clamped configuration (d).

As expected from previous results, free PZT multi-layer configurations present independence over magnetostrictive thickness in the ME behavior, with a slightly lower value of

α_{ME} for P-P configurations, when compared with M-M configurations with the same number of piezoelectric layers as shown in Figure 2.38 (a)-. Clamped configurations, on the other hand, present the trend of having a lower ME performance for thinner magnetostrictive layers until 50-60 μm of Vitrovac thickness and holding the same value of α_{ME} above it as can be seeing in Figure 2.38 (c)-.

Piezoelectric thickness has influence on the ME response of PZT composites, maintaining a constant behaviour for the lower piezoelectric thicknesses (these constant values of ME performances for PZT configurations are displayed as α_{ME} and α_{unit} in Table 2.7), decreasing slightly for thicker piezoelectric thicknesses (above 200 μm) for the free case -in Figure 2.38 (b)- and preserving this behaviour for the clamped case in Figure 2.38 (d)-, with a higher slope.

Table 2.7: Constant magnetoelectric coefficient -α_{ME} (V/cm)- and unitary magnetoelectric coefficient -α_{unit} (V/cm)- according to configuration and number of piezoelectric phases.

	Bi-layer	M-M (1pzo)	M-M (2pzo)	P-P (2pzo)	M-M (3pzo)	P-P (3pzo)	M-M (4pzo)	P-P (4pzo)
α_{ME} (V/cm)	85.81	84.9	172.06	169.31	257.36	255.86	342.65	339.91
α_{unit} (V/cm)	85.81	84.9	86.03	84.66	85.79	85.29	85.66	84.78

It is also noticed that P-P configurations present slightly lower ME coefficient than the respective M-M configurations with the same number of piezoelectric phases as shown in Figure 2.38 (a)- and furthermore, show a more pronounced slope of decrease in Figures 2.38 (b) and (d), and a more pronounced increase in 2.38 (c).

Figure 2.39 shows the results of FEM ME unitary coefficient, α_{unit}, as a function of the configuration (M-M, P-P or M-P) and the number of piezoelectric phases included in the composite, when the total thickness is held constant at 300 and 600μm. Colour difference establishes each configuration (wine-red are for M-P configurations, blue-cyran for M-M configurations and olive-green for P-P configurations), square shape indicates a total thickness of 300 μm, while circles express total thickness of 600 μm. The size difference of the dots is only established in order to perceive both symbols when they are placed in the same coordinates.

120
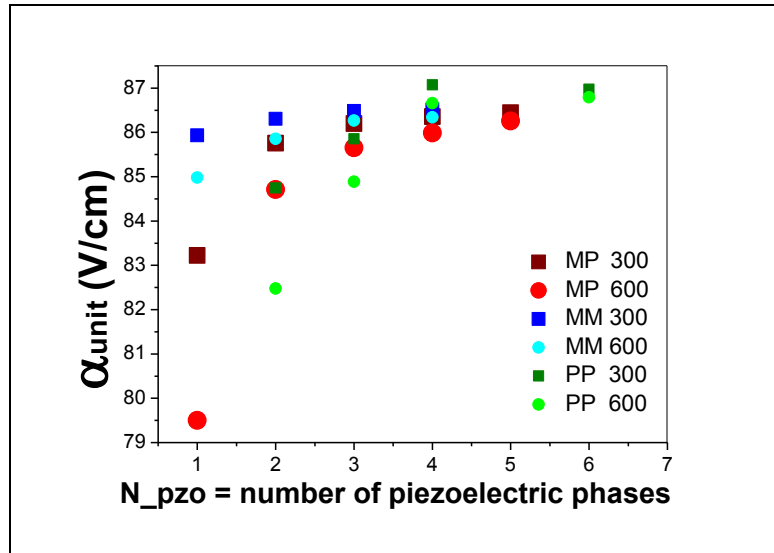
Figure 2.39: Unitary magnetoelectric coefficient for PZT magnetostrictive-piezoelectric (M-P), magnetostrictive-magnetostrictive (M-M) and piezoelectric-piezoelectric (P-P) symmetric configurations with a total thickness of 300 µm and 600 µm as function of the number of piezoelectric layers, N_pzo.

While all configurations for both total thicknesses establish the same trend of increasing α_{unit} with increasing number of layers, with higher ME performance for the case of total thickness of 300µm, presenting for more number of piezoelectric layers a more homogeneous unitary $\boldsymbol{\alpha}$ (above 4 piezoelectric layers, as shown in Figure 2.39), some differences are observed for different configurations: M-P and P-P configurations are more influenced by the total thickness value than M-M configurations, which have a maximal difference on α_{unit} of 1V/cm for 1 piezoelectric layer between both M-M configurations of 300 and 600 µm of total thickness. For high number of piezoelectric layers, P-P configurations have an enhanced performance over M-P and M-M configurations, leading finally to conclude that for low number of piezoelectric layers, M-M is the optimal configuration.

2.3.5.2. PVDF multi-layer configuration

Simulation results for all PVDF configurations consisting of 1 to 4 piezoelectric phases (2-9 layers) are presented in Figure 2.40 (a) for magnetostrictive thickness sweep of free configurations, (b) for piezoelectric thickness sweep of free configurations, (c) for

magnetostrictive thickness sweep of clamped configurations, and (d) for piezoelectric thickness sweep of clamped configurations.
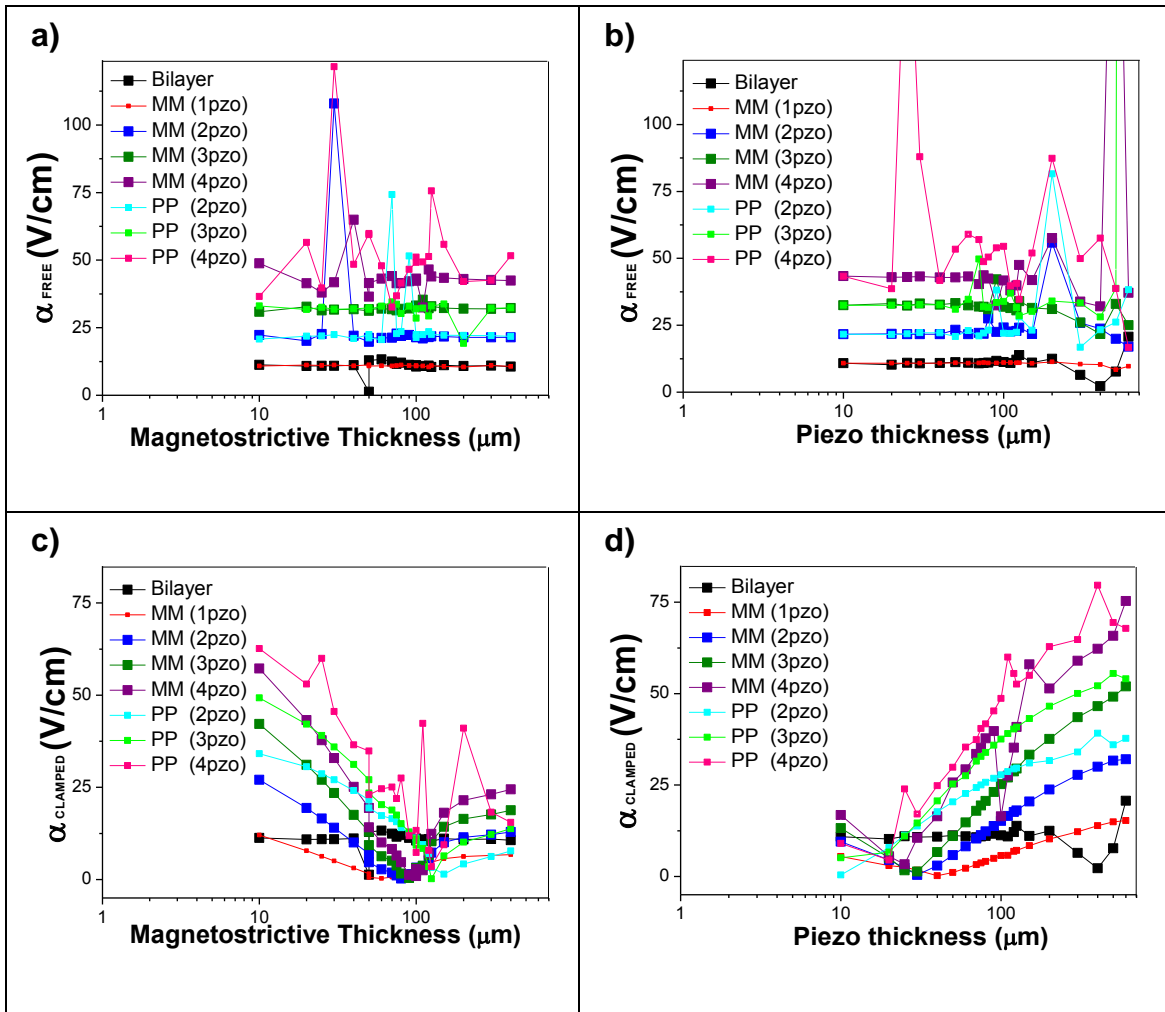
Figure 2.40: Magnetoelectric coefficients for all symmetric configurations of PVDF laminates as function of the magnetostrictive thickness of the free configuration (a) and clamped configuration (c), and as function of the piezoelectric thickness of the free configuration (b) and clamped configuration (d).

As free PZT multi-layer configurations present independence of magnetostrictive thickness, with a slightly lower value of α_{ME} for P-P configurations, from Figure 2.40 (a) it can be concluded that elasticity and morphology of PVDF is a fundamental issue in governing its response, that governs ME composites. This influence increases when the composite is composed by a larger number of layers, and also, when P-P configurations are used. Free M-M configurations show a more stable behaviour and trends over different number of layers, while P-P configurations present regions with peaks that go off any expected trend.

122

PVDF clamped configurations present clearer trends, decreasing ME coefficient, reaching a minimal value and then increasing their ME performance until reaching a minimal α-value, then increasing their ME performance again, for magnetostrictive and piezoelectric thickness sweep. The main difference between the different conditions is the position of the minimal value as shown in Figure 2.40 (c) and (d). Table 2.8 displays the piezoelectric and magnetostrictive thickness at which minimal values of ME performance are established for each configuration.

Table 2.8: Piezoelectric (d_pzo) and magnetostrictive thickness (d_ms) for minimal magnetoelectric performance in clamped PVDF magnetostrictive-magnetostrictive (M-M) and piezoelectric-piezoelectric (P-P) configurations, for cases of magnetostrictive thickness sweep (d_ms sweep) and piezoelectric thickness sweep (d_pzo sweep)

		configuration	1 pzo	2 pzo	3 pzo	4 pzo	
d_ms sweep	d_ms (μm)	M-M	60	80	90	100	α_{ME}(min)
	d_ms (μm)	P-P		150	125	60	α_{ME}(min)
d_pzo sweep	d_pzo (μm)	M-M	40	30	30	25	α_{ME}(min)
	d_pzo (μm)	P-P		10	10	20	α_{ME}(min)

As shown in Table 2.8, magnetostrictive thickness for minimal α_{ME} increases with the number of piezoelectric layers for M-M configuration and diminishes for P-P configuration. While for piezoelectric thickness sweep, piezoelectric thickness for minimal α_{ME} diminishes with increasing the number of piezoelectric layers, for M-M configurations and increases for P-P configurations.

For all clamped experiments, P-P configurations appear to have a slightly better ME performance than M-M configurations, for different magnetostrictive thicknesses -in Figure 2.40 (c)- and piezoelectric thicknesses in Figure 2.40 (d)-.

Figure 2.41 presents the results of FEM ME unitary coefficient of PVDF symmetric multi-layered configuration, α_{unit}, as a function of the configuration (M-M, P-P or M-P) and de number of piezoelectric phases in the composite, when the total thickness is held constant at 300 and 600μm. Colour difference establishes each configuration (wine-red are for M-P configurations, blue-cyran for M-M configurations and olive-green for P-P configurations), square shape indicates a total thickness of 300 μm, while circles express total thickness of 600 μm. The size difference

of the dots is only established in order to perceive both symbols when they are placed in the same coordinates.
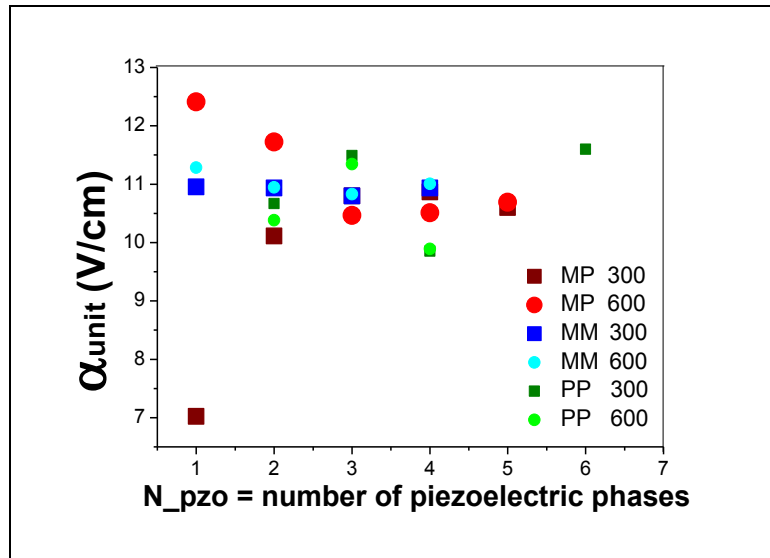
Figure 2.41: Unitary magnetoelectric coefficient for PVDF magnetostrictive-piezoelectric (M-P), magnetostrictive-magnetostrictive (M-M) and piezoelectric-piezoelectric (P-P) symmetric configurations with a total thickness of 300 μm and 600 μm as function of the number of piezoelectric layers, N_pzo.

Constant composite thickness of 300 and 600 μm experiments-in Figure 2.41-showed that M-M configurations present a more stable unitary α over different number of layers (with an almost constant value of unitary α, of approx. 10.7-10.9 V/cm), while M-P configurations of total thickness of 600 μm present the best performance for low number of layers, and M-P configurations of total thickness of 300 μm presented the lower performance for low number of layers. This experiment confirmed also that P-P configurations may not presented clear trends and that the elasticity and morphology of PVDF have a larger influence over this configuration, as already established.

CHAPTER 3: SIMULATIONS OF MAGNETOELECTRIC RESPONSE OF SPHERES AND FIBRE COMPOSITES

3.1. Magnetoelectric model for finite element method (FEM) simulations

The functional principle of the model is based on that magnetostrictive and piezoelectric parts are in a stressed state as a result of bonding, where the stressed state is induced by the application of an external magnetic field that produces changes in the characteristics of the magnetostrictive part of the composite. In order to solve this problem, the coupled magnetic-elastic-electric fields are coupled to be computed into two steps. First, the magnetic field source, driven by coil(s) carrying DC current density, has to be computed (establishing an almost homogeneous magnetic potential). Second, the coupled mechanical-magnetical-electric fields are to be computed in terms of variables as the components of the mechanical displacement vector (u), magnetic vector potential (Ψ), magnetization (M), electric polarization (P), and electric potential (ϕ).

3.1.1. Magnetic field model for magnetostatics

From Maxwell´s equations and by the assumption that charge move as a steady current J_e, the coil(s) will induce a magnetic field (*H*) given by Ampere´s Law:

$$\nabla \times H = J_e \tag{3.1}$$

Then, by Gauss´s Law for magnetism, the magnetic flux density, *B*, will remain as:

$$\nabla \cdot B = 0, \text{ which implies } B = \nabla \times \psi \tag{3.2}$$

Where Ψ represents the magnetic vector potential, and where $\nabla \cdot$ and $\nabla \times$ represent the mathematical operators divergence and rotor.

There exist symmetry in the magnetic field with respect to the zx, zy, and zz planes; these planes, therefore, may serve as exterior boundary to the geometry. Also, the air box surrounding the coil(s) and structure has to be sufficiently large in order to establish little influence of the boundary conditions of the outer border of the model on the vicinity of the magnetic system.

Establishing a condition of magnetic insulation ($\Psi = 0$) on all exterior boundaries of the air box domain (Zadov et al., 2012).

Inside the magnetostrictive material, the magnetic induction (*B*) in terms of the applied magnetic field (*H*) and the magnetization (*M*) is given by (equation 3.3):

$$B = \mu_0 \cdot \left(H + M \right),$$ (3.3)

where μ_0 represents the vacuum permeability, and can be also described in terms of Ampere´s Law, as:

$$\nabla \times \left(\frac{B}{\mu_0 \mu_r} \right) = J_e,$$ (3.4)

where μ_r describes the relative permeability of the material.

As the magnetic permeability and magnetostrictive strains in the magnetostrictive materials are nonlinearly dependent on magnetic flux density and mechanical strains and stresses, the nonlinear magnetization will be given by an explicit (measured) *H-B curve*, given by (Zadov et al., 2012):

$$H + M\left(H \right) = \frac{1}{\mu_0} B$$ (3.5)

Outside the magnetostrictive material, permeability of air ($\mu_r=1$) and PVDF ($\mu_r \cong 1$) are constant, allowing to establish magnetostatics conditions of continuity of normal component *B* and tangential components of *H*.

3.1.2. Hysteretic behaviour: H-B curve

Figure 3.1 shows a typical hysteretic process (Hysteresis curve). Hysteresis causes the permeability of ferromagnetic materials, and correspondingly its susceptibility, to be multi-valued (David C. Jiles, 1991; Ralph C Smith, 2005).
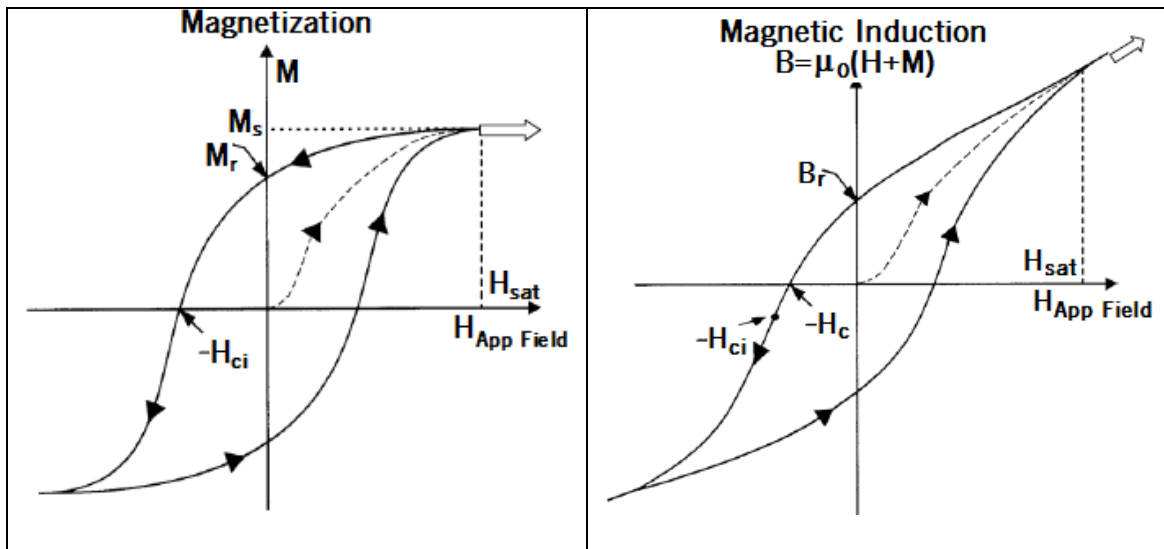
Figure 3.1: Hysteresis process as function of magnetization (a) and magnetic induction, H-B curve (b) of ferromagnetic materials (Ralph C Smith, 2005). Magnetization curve (a) can be defined by parameters as saturation magnetization (M_s), remanent magnetization (M_r) and coercivity (H_c), while H-B curve can be defined by parameters as saturation magnetic field (H_s), saturation induction (B_s), remanent induction (B_r) and coercivity (H_c).

As shown in Figure 3.1, in ferromagnetic materials, domain wall movements and domain rotation is the process that characterizes this behaviour, resulting in a hysteretic applied magnetic field-magnetization (H-M) relation, as can be seeing in Figure 3.1 (a), or in a hysteretic applied magnetic field-induction (H-B) relation, known as H-B curve of the material, shown in figure 3.1 (b). This process can be explained in 4 processes (David C. Jiles, 1991; Ralph C Smith, 2005):

i.   In a demagnetized state, the material is composed of spontaneously magnetized domains, arranged in random configuration. As the magnetization in each domain differs from the next one, the bulk magnetization of the material will be null.

ii. Low magnetic field levels produce reversible domain wall movement and moment rotation, which produce small changes in the magnetization.

iii. With higher magnetic field levels, domain wall movement allow the increase of domains with magnetization components in the magnetic field direction and also, domain moments rotate to those easy axis, which are closest to the field direction. Although those two former processes are reversible, combined together in the

127

hysteretic process produce an irreversible region in the H-M curve where small magnetic field changes lead to large strain or magnetization variations.

iv. At the final state, the magnetization reaches its saturation value (**M$_s$** in the magnetization curve, and **B$_s$** and **H$_s$** in the induction hysteretic relation), acting as a single domain. Magnetization moments rotate together to align with the applied magnetic field direction from the easy axis.

If the magnetic field is reverted after saturation is achieved, a reversible process of moment rotation and wall movement is produced and followed by an irreversible reorientation and wall displacement of the domains. Magnetic remanence (remanent magnetization -**M$_r$**- and induction -**B$_r$**-) occurs when the material is magnetized to saturation and the magnetic field is null, which provides an upper bound for all remanent values, as presented in Figure 3.1.On the other hand, coercivity (**H$_c$**) is the required magnetic field in order to drive the magnetization to zero starting at an arbitrary level. This is the final step of the ferromagnetic hysteresis curve(Ralph C Smith, 2005).

3.1.3. Magnetostriction model

Magnetostriction component (magnetostrictive strains) along any direction are defined as a nonlinear function of the magnetostriction by the expression of Becker and Döring (Bozorth, 1951; Chikazumi, 1997), as:

$$\lambda_i = \frac{3}{2}\lambda_S\left(\overline{m_i}^2 - \frac{1}{3}\right) = \frac{3}{2}\lambda_S\left(\left(\frac{M_i}{M_S}\right)^2 - \frac{1}{3}\right) \tag{3.6}$$

where λ_i represents the i-th component of the relative magnetostrictive deformation along the i-th direction, λ_s is the polycrystalline magnetostriction constant, and $\boldsymbol{m_i}$ is the magnetization direction cosine. $\boldsymbol{m_i}$ is also the ratio of magnetization along the required direction (**M$_i$**) and the saturation magnetization (**M$_s$**) of the material, corresponding to the ratio of local magnetization in a grain/domain to the saturation magnetization (the upper bar, establishing the average value over grains/domains) (Comsol Multiphysics Library & Multiphysics, 2011; Zadov et al., 2012).

128

The term 1/3 establishes that the magnetic moments are randomly oriented in the material in the absence of any magnetic field, which means that by the assumption that the material is sufficiently pre-stressed in a manner that all magnetic moments are perpendicular to the direction of magnetization at the beginning of the process, the term 1/3 should be neglected.

When the sufficiently pre-stressed magnetostrictive material has no preferential crystallographic orientation, magnetostriction on every direction will be represented by:

$$\lambda_i = \frac{3}{2} \lambda_s \overline{m_i^2} = \frac{3}{2} \lambda_s \left(\frac{M_i}{M_S} \right)^2 , \tag{3.7}$$

expression that will only depend on the local magnetization of every direction. Furthermore, when cubic anisotropy is assumed and magnetic saturation is reached, the magnetostriction that is parallel ($\lambda_\parallel$) and perpendicular ($\lambda_\perp$) to the magnetization is be given by the relation (F. C. Graham, Mudivarthi, Datta, & Flatau, 2009; Zadov et al., 2012):

$$\lambda_\parallel = \lambda_S \left(\frac{M}{M_S} \right)^2$$
$$\lambda_\perp = -\frac{1}{2} \lambda_S \left(\frac{M}{M_S} \right)^2 \tag{3.8}$$

3.1.4. Mechanical model for magnetostrictive material

The mechanical model for magnetostrictive material is given by a linear elastic model, described by the following constitutive equations (Zadov et al., 2012):

Strain-Displacement Equation

$$S = \frac{1}{2} \left[(\nabla u)^T + (\nabla u) \right] \tag{3.9}$$

Hooke´s Law

$$\sigma - \sigma_0 = C_E \cdot (S - S_0) \tag{3.10}$$

Newton´s Second Law for stationary case, motion equation:

$$\nabla \sigma = 0 \tag{3.11}$$

Where u is the displacement tensor, S is the strain tensor (and S_0 an initial strain), σ is the Cauchy stress tensor (and σ_0 an initial stress), and C_E is the elasticity matrix (calculated by Young´s modulus and Poisson´s ratio (F. Graham, 2009)). The non-linear magnetostriction is implemented and included in this model by the introduction of a pre-strain that is equal to the magnetostrictive strain (Equations 3.7 or 3.8, according to the magnetic material anisotropy) and a null initial strain. The model also considers traction-free boundary conditions at outer surfaces and perfect bonding at all the interfaces of the structure (continuity equations of displacement and normal stress).

3.1.5. Mechanical model for piezoelectric material

As established in Chapter 2.1.2, linear piezoelectric model is governed by equations 2.1 and 2.3, respectively:

$$\varepsilon - \varepsilon_0 = S_E \cdot (\sigma - \sigma_0) + d^T \cdot E \tag{2.1}$$

$$D = P_r + d_{3n} \cdot (\sigma - \sigma_0) + \kappa_\sigma \cdot E \tag{2.3}$$

Where E is the electric field, D is the electric displacement, P_r is the remanent polarization, S_E is the compliance coefficients matrix, d_{3n} is the piezoelectric coefficients matrix, and K_σ is the dielectric permittivity matrix.

Similarly to the model in 2.1.2 the electro-mechanical coupling is then driven by:

$$\nabla \cdot D = \rho_V \text{ (Gauss Law, t=0)} \tag{2.7}$$

$$\nabla \cdot \sigma = f_V \text{ (Cauchy momentum equation, t=0)} \tag{2.8}$$

Where "$\nabla \cdot$" represents the divergence, D the electrical displacement field, ρ_V, the free electric charge density, σ, the stress tensor and f_V the force per unit volume.

In order to obtain the electric potential (φ), the assumption of an electrode on the external surface of the ME structure is made, as an electrically floating electrode condition (where zero charge is held), therefore given by:

$$E = -\nabla \varphi \qquad\qquad\qquad (3.12)$$

where E is the local electric field strength.

3.1.6. Magnetostrictive material properties

For the present study, mechanical, electrical and most of magnetic properties of cobalt ferrite ($CoFe_2O_4$, CFO) are those presented by Zhang *et al.* (J. X. Zhang et al., 2009a) on their investigation on the effect of magnetic nanoparticles over the morphology, ferroelectric and magnetic behaviour of CFO/P(VDF-TrFE) 0-3 nanocomposites. Their study suggested that CFO nanoparticles embedded in P(VDF-TrFE) responses are strongly influenced by the CFO concentration and that the magnetoelectric nanoparticles have no preferential crystallographic orientations. Those properties of CFO and its hysteresis curve -that was obtained experimentally[2] - are presented in Table 3.1.

---

[2] Cobalt ferrite measurements were provided by Jon Gutiérrez (Departamento de Electricidad y Electrónica, Facultad de Ciencia y Tecnología, Universidad del País Vasco UPV/EHU, P. Box 644, E-48080-Bilbao, Spain).

Table 3.1: Mechanical, magnetic and electrical properties of cobalt ferrite ($CoFe_2O_4$) (J. X. Zhang et al., 2009a)

Material Property					CFO
Structural	Density	**P**	(kg/m³)		5300
	Young modulus	**Y**	(GPa)		1.39
	Poisson´s ratio	**ν**	1		0.37
Electrical	dielectric constant	**ε**	1		10
Magnetic	Permeability	**μ_r**	1		2
	Susceptibility	**χ**	1		0.03
	Curie Temperature	**τ**	K		Above 700
	sat. magnetization	**M_s**	(emu/gr)		59
	sat. magnetization	**M_s**	(kA/m)		312.7
	H-B curve[3]	sat. induction	**B_s**	(kA/m)	315.3
		sat. magnetic field	**H_s**	(T)	1.8
		remanent induction	**B_r**	(kA/m)	153.5
		coercivity	**H_c**	(T)	0.2±0.012
Magnetostrictive	strain ratio	**β**	1		0.5
	Magnetostriction	**λ_s**	1		10⁴

3.2. Spheres and fibres magnetoelectric simulations

Simulation analyses were performed in order to conceive the ME performance of magnetostrictive CFO and piezoelectric PVDF composites. Spherical and ellipsoidal structures and fibres of different radii and concentrations were modelled for a series of magnetic fields by a multiphysics simulator in order to obtain their magnetoelectric performance by FEM calculations.

ME spheres were modelled by a tri-dimensional (3-D) model and results were corroborated and expanded by an axisymmetric bi-dimensional (2-D) model of spheres. Bi-dimensional axisymmetric models have also been established for ellipsoidal structures, fibres and a cylindrical piezoelectric matrix embedding magnetostrictive spheres. Both, 3-D and 2-D-axisymmetrical models couple electric, magnetic and mechanical fields, where the external magnetic field is generated by a DC current density (J_0) running on coil(s) (1 large coil for the 2-D axisymmetric model and 2 coils -Helmholtz coils- for the 3-D model). The magnetoelectric composite was situated on the geometrical centre of the model and therefore establishing within a homogeneous magnetic field induced by the coil(s).

---

[3] Cobalt ferrite measurements were provided by Jon Gutiérrez (Departamento de Electricidad y Electrónica, Facultad de Ciencia y Tecnología, Universidad del País Vasco UPV/EHU, P. Box 644, E-48080-Bilbao, Spain).

The coupling between the magnetic, electrical and mechanical field was established as follows:

a. The magnetic field generated by the coils magnetized the magnetostrictive material, generating nonlinear magnetostriction (obtained from the explicit *H-B curve*). Isotropic magnetostriction (with no preferred crystallographic orientation, by equation 3.7) and cubic anisotropy magnetostriction (by equation 3.8) were analysed.

b. This magnetostriction introduced an initial strain into the piezoelectric material, which caused the appearance of an electric polarization perpendicular to the direction of the deformation induced by the initial strain, generating an electrical charge distribution.

c. As the magnetostrictive-piezoelectric surface was electrically grounded and the outside surface of the composite was considered as an electrically floating electrode (EFE), an electric potential was generated between both interfaces. By the assumption of EFE (zero net charge held on the electrode), this electric potential was constant along the outer surface of the composite.

d. As the ME coefficient is defined by equation 2.10 and the present study is stationary, including only DC magnetic Bias, α_{ME} was defined as:

$$\alpha_{ME} = \left| \frac{\partial E}{\partial H_{AC}} \right| = \left| \frac{dE}{dH_{AC}} \right| = \left| \frac{\varphi}{\Delta r_{piezo}} \right|, \qquad (3.13)$$

where Δr_{piezo} expresses the thickness between ground and the electrode (EFE), where the electric potential (φ) may be obtained. As some of the geometries included in this study have radial symmetry, Δr_{piezo} represents the piezoelectric thickness.

3.2.1. Ideal three dimensional magnetoelectric sphere simulations

The 3-D experiment consisted in an air box cube of width, height and length of 12.5 μm, a Helmholtz coil, that is composed of two identical circular magnetic coils, placed symmetrically along a common axis, and separated by a distance equal to the radius of the coil, of 5 μm, and a rectangular transversal coil section of 0.5 μm x 0.5 μm. Each coil carried an equal electrical current density J_0 (A/m²) flowing in the same direction, producing a region of nearly uniform magnetic field between them.

Current density was varied between $5 \times 10^{11} A/m^2$ and $1 \times 10^{13} A/m^2$, which produced a nearly homogeneous magnetic field along the x-axis between 11Oe and 222Oe, respectively. The magnetic field distribution along the x direction is shown in Figure 3.2 within Table 3.2, where relationship between electric current density and magnetic field in x direction is displayed, in both magnetic field units, A/m and Oe.

Table 3.2: Magnetic field along x-direction, H_x, (in A/m and Oe) and their relation with the current density input (J_0) in the Helmholtz coils for the 3-D magnetoelectric sphere model

J_0 (A/m²)	H_x (A/m)	H_x (Oe)
1×10^{11}	1772.51	22.27
5×10^{11}	8862.26	111.37
1×10^{12}	17725.12	222.74
5×10^{12}	88625.59	1113.7
1×10^{13}	177251.18	2227.4
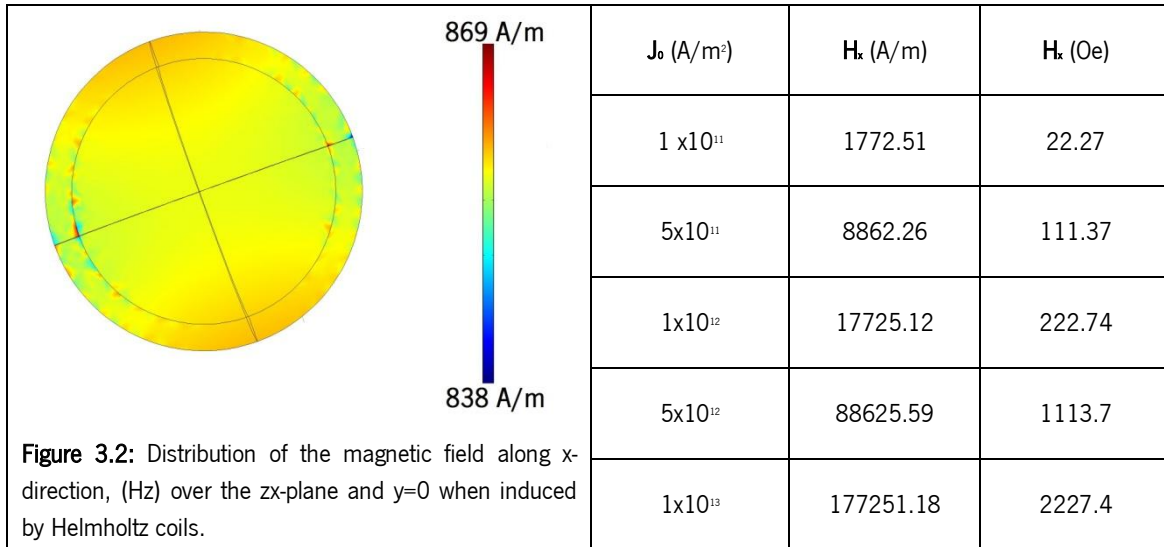
Figure 3.2: Distribution of the magnetic field along x-direction, (Hz) over the zx-plane and y=0 when induced by Helmholtz coils.

The spherical ME structure was surrounded by a larger air sphere (for discretization reasons) and located in the centre between the two coils, as can be seen in Figure 3.3.
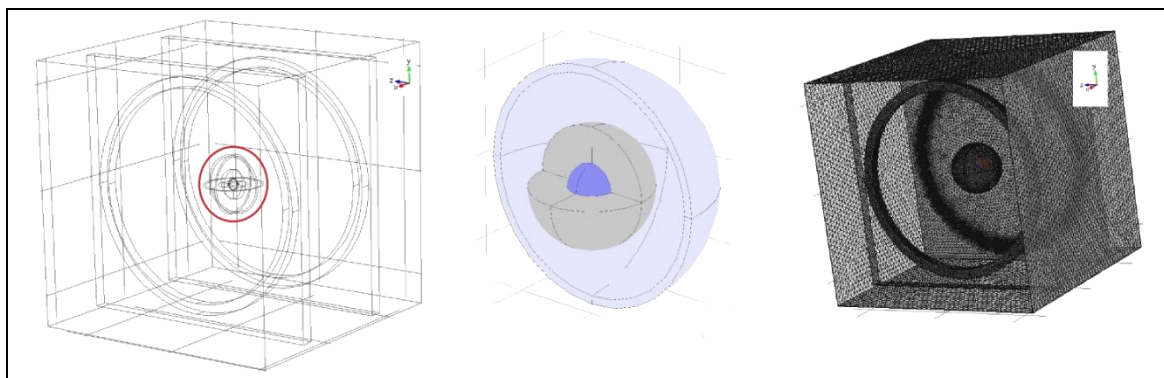
Figure 3.3: Representation of the sphere simulation. On the left, the whole experimental configuration is shown. In the middle, a zoom to the magnetoelectric structure is shown, including the air ball surrounding it. On the right, the discretization process of the experiment is shown.

The experiment was composed by two concentrically located spheres (of radios **R** and **r**), the smallest sphere (of radius **r**) being the CFO/magnetostrictive part and the external spherical shell (of thickness **Δr=R-r**) being the PVDF/magnetostrictive component of the spherical composite. The polarization of the piezoelectric material was established radial in the boundary conditions of the problem, as the magnetization was fixed parallel to the x-axis. The study focused in analyzing the influence of size and concentration of the composite over the ME coefficient. ME structures of diameters of 1.4μm, 0.6μm and 0.1μm were analysed for concentrations of 90 wt.% of CFO, 50wt.%and 15wt.%, with no preferred crystallographic orientation. The relationship between concentration (**wt.%**), sphere radius (**R**), magnetostrictive radius (**r**) and piezoelectric thickness (**Δr**) for all simulations is established in Table 3.3.

Table 3.3: Sphere geometrical conditions according to the concentration (wt.%) of cobalt ferrite ($CoFe_2O_4$, CFO): the external sphere radius (R), the internal magnetostrictive sphere radius (ms radius, r) and the piezoelectric thickness (pzo thickness, Δr).

concentration (wt.%)	sphere radius (R)	ms radius (r)	pzo Thickness (Δr)
15wt.%	700 nm	270 nm	430 nm
50wt.%	700 nm	440 nm	260 nm
50wt.%	300 nm	190 nm	110 nm
50wt.%	50 nm	32 nm	18 nm
90wt.%	700 nm	635 nm	65 nm

3.2.2. From the bi-dimensional axisymmetric sphere to the bi-dimensional axisymmetric fibre
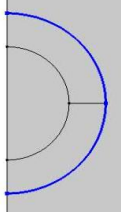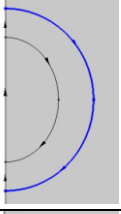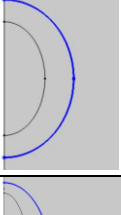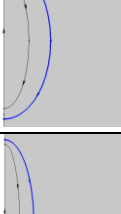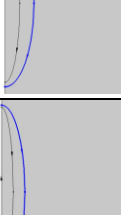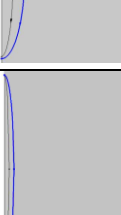
3-D models for micro- and nanostructures require high discretization levels, and in order to produce an homogeneous magnetic field, coils have to be at least five times the longest dimension of the ME structure. Therefore, 3-D models require a high amount of informatics resources and time, which can be reduced by introducing symmetry planes as can be achieved by the 2-D axisymmetric model. To increase the data obtained by 3-D sphere simulation with efficiency of resources, a 2-D axisymmetrical model for the sphere was established. Axisymmetric models are those with the presence of rotational symmetry and therefore are ideal for simulations with cylindrical symmetries, as the ME fibre. In the case of the ME sphere, this

symmetry might not be accurate but anyhow approximate, because of the radial polarization of the sphere that is introduced as radial in cylindrical coordinates. This approximation only affects the amount of magnetostriction that would be transformed in the piezoelectric effect, establishing curves of ME performance that preserved their shape among the magnetic field H.

By these means, this experiment was subdivided in 2 subcategories:

i)   First, the ME spheres were simulated with the same characteristics of the former experiment, in order to validate the axisymmetric model. Sphere dimensions and concentrations were the same as those established in Table 3.3. But also, including the case of cubic magnetic anisotropies.

ii) Then, the ME sphere was transformed into a series of ellipsoidal ME structures maintaining the volume and the concentration of the initial sphere (R=700nm and concentration of 50wt.%) but changing the ellipsoids eccentricity, **e**, until becoming approximately a fibre (images of all ellipsoidal structures are displayed in Table 3.4). For symmetry reasons, the ellipsoids had to be also axisymmetric and therefore, they were only defined by one major axis (a) and one minor axis (b). The ME structure was composed by two ellipsoids: the internal (magnetostrictive ellipsoid) and the external (piezoelectric) ellipsoid, both holding the same eccentricity value. In order to simplify the calculation of the ME coefficient, the piezoelectric thickness (that was not constant over the structure) had to be considered as the simple subtraction of the external and internal ellipsoids minor axis ($\Delta r = a_{piezo} - a_{ms}$). Eccentricity values, dimensions of major and minor axis and shape of the ME structure are presented in Table 3.4.

Table 3.4: Ellipsoids geometrical major and minor axis as function of its eccentricity (e) for every simulation experiment, together with the corresponding values of weight concentration of cobalt ferrite (wt.%), total volume (total volume, constant value), magnetostrictive internal ellipsoid parameters (magnetostrictive ellipsoid (ms ellip.): major axis a_{CFO}, minor axis b_{CFO}) and piezoelectric external ellipsoidal parameters, (piezoelectric ellipsoid (pzo ellip.):: major axis a_{pzo}, minor axis b_{pzo}, piezoelectric thickness $\Delta r = b_{pzo} - b_{CFO}$).

Image	e (nm)	wt.%	total vol. (μm)^3	pzo ellip. a_{PZO} (nm)	pzo ellip. b_{PZO} (nm)	ms ellip. a_{CFO} (nm)	ms ellip. b_{CFO} (nm)	Δr (nm) $b_{PZO} - b_{CFO}$
	0	50	1.44	700	700	440	440	260
	300	50	1.44	743	680	508	410	270
	400	50	1.44	776	665	559	390	275
	800	50	1.44	993	588	860	315	273
	1200	50	1.44	1300	512	1230	263	249
	1600	50	1.44	1660	454	1620	230	224
	3200	50	1.44	3216	326	3204	163	163

The magnetic field generation in the model was induced by a coil with larger extensions in the z-axis than the fibre or any simulated ME structure, carrying a current density J_0 (A/m^2) and therefore producing a homogeneous magnetic field inside the coil. The magnetic field in z-direction distribution was displayed in Figure 3.4 within Table 3.5, where the relationship between the input current density and the magnetic field in z-direction value is also shown.

Table 3.5: Magnetic field in z-direction values, H_z, (in A/m and Oe) and their relation with the current density input (J_0).

	J_0 (A/m^2)	H_z (A/m)	H_z (Oe)
	1×10^7	9.55	0.12
	5×10^7	47.75	0.6
	1×10^8	95.5	1.2
	5×10^8	477.53	6
	1×10^9	955.06	12
	5×10^9	4775.29	60
	1×10^{10}	9550.58	120.02
	5×10^{10}	47752.89	600.08
	1×10^{11}	95505.79	1200.16
	5×10^{11}	477528.92	6000.8

4776 A/m

-901 A/m

Figure 3.4: Distribution of the magnetic field along the z-direction, (Hz) over the axisymmetric plane when induced by one large coil.
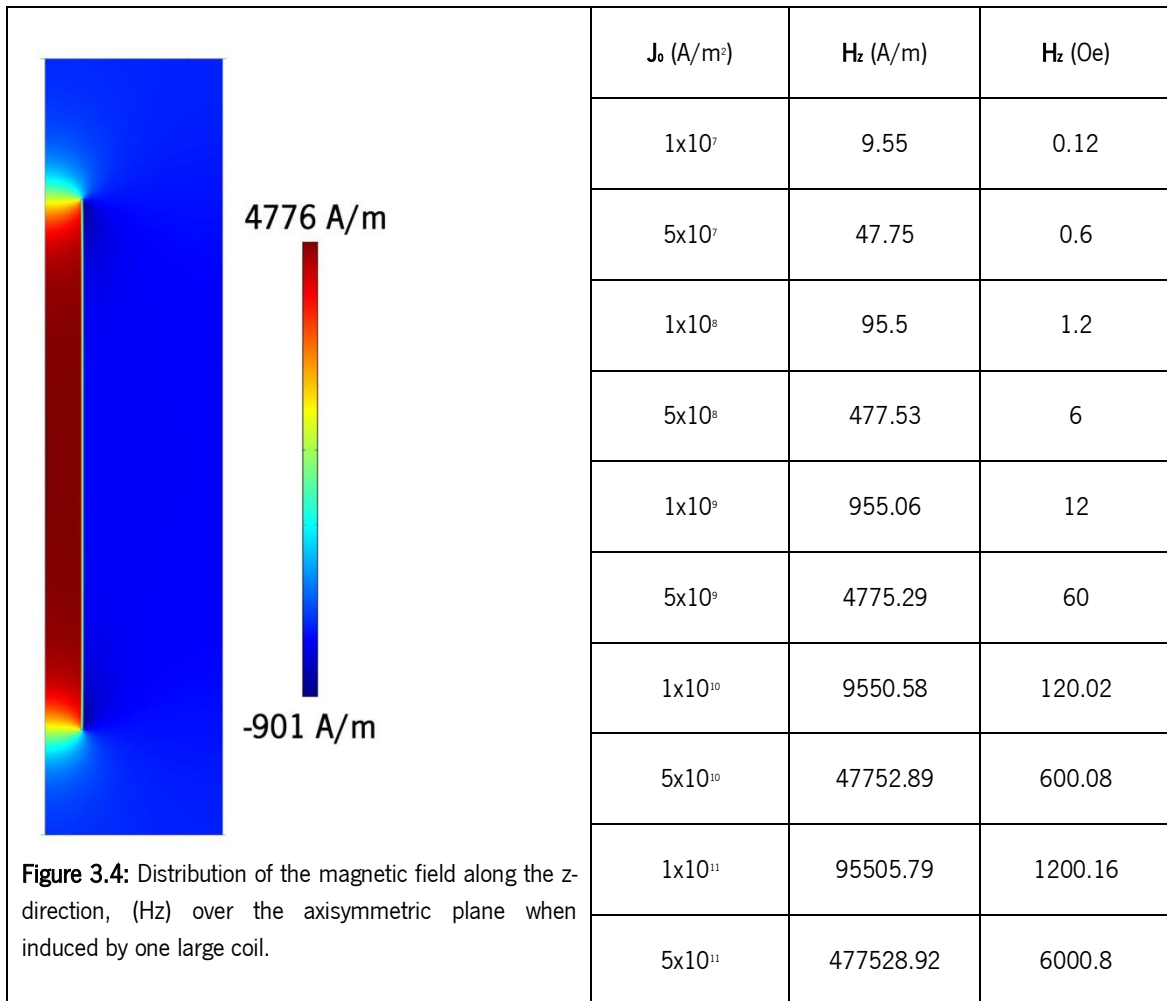
In the axisymmetric model the coils were drawn in the workspace as a rectangle (the transversal area of the coil, which rotated around the z-axis would implement the cylindrical coil that is needed) and were also placed in a much larger air box, also drawn as a rectangular but implying a cylindrical shape. The spheres, modelled as spheres (or ellipsoids), had also
138

axisymmetrical symmetry, only when located in the z-axis (the rotational centre of the symmetry), as shown in Figure 3.4.

The dimension of the air box in the 2-D axisymmetric model was a rectangle of 50 μm width and 300 μm height. The coil had a sectional area of 1μm width and 150 μm height, located 10 μm away from the axis-z, with the rotational symmetry. Therefore, in the 3-D interpolation, this established a cylindrical air box of 50 μm of radius and 300 μm height, a 150 μm long coil of radius 10 μm, and 150 μm height, with 1μm thickness. The ME structure was located at the centre of the geometrical model, where a homogeneous magnetic field was applied (Figure 3.4). Its dimensions depended on the concentration and ellipsoid eccentricity (or radius, for the spherical case).

In Figure 3.5, axisymmetric models are presented in 2-D and 3-D, for the case of the sphere (on the left), an ellipsoids with an intermediate eccentricity e=800nm (on the centre), and an ellipsoid with eccentricity of e=1600nm (on the right), which can be practically considered as a fibre. Every case presents the 2-D axisymmetric model in (A), the mesh 2-D axisymmetric model enlarged to the ME structure (B), the 3-D interpolated system of the whole model (rotated, in (C)), and a zoom of the rotated ME structure in (D).
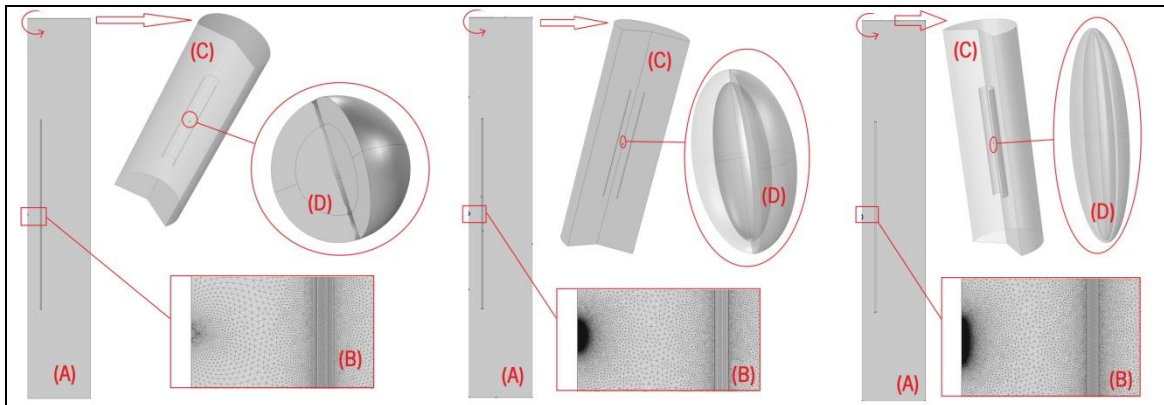
Figure 3.5: Representation of the 2-D axisymmetric sphere to the ideal 2-D axisymmetric fibre simulation experiment. On the left, the axisymmetric spherical case, in the middle, axisymmetric ellipsoid with an eccentricity of e=800nm, and in the right an axisymmetric ellipsoid with e=1600nm are presented. All cases have the complete 2-D axisymmetric model (A), with a zoom to the meshed magnetoelectric structure (B), and representations of the rotation of the model into 3D simulations for the whole system (C) and the enlarged magnetoelectric structure (D).

3.2.3. Ideal bi-dimensional axisymmetric magnetoelectric fibre simulations

As expressed before, axisymmetric models are those with the presence of rotational symmetry and therefore are ideal for simulations with cylindrical symmetries, as the ME fibre. The magnetic field generation in this model was also not created by Helmholtz coils, but by the large and only coil presented in experiment 3.2.2 (Table 3.5), carrying a current density J_0 (A/m^2) and therefore producing a homogeneous magnetic field inside the coil, dependent on the amount of current density. In the axisymmetric model, these coils were drawn in the workspace as a rectangle (the transversal area of the coil, which rotated around the z-axis would implement the cylindrical coil that is needed) and were also inserted in a much bigger air box, also drawn as a rectangular but implying a cylindrical shape (dimensions are established in 3.2.2). The ME structure was composed by two concentrically located cylinders (of radius **R** and **r**), the smallest (of radius **r**) being the CFO/magnetostrictive part and the external cylindrical shell (of thickness **Δr=R-r**) being the PVDF/piezoelectric component of the composite. The magnetostrictive cylinder had a total length of 25 μm and was divided into two symmetrical cylinders of 12.5 μm length each, in order to establish symmetry in the centre of the fibre with respect of the z-axis (therefore reducing computer resources). The piezoelectric shell was located in the middle of the magnetostrictive rod (therefore preserving the symmetry with respect to the z-axis), with a height of 12.5 μm. The polarization of the piezoelectric material was established as radial in the boundary conditions of the problem, as the magnetization was fixed parallel to the z-axis.

In Figure 3.6 axisymmetric models are presented in 2-D and 3-D, for the case of the fibre. The 2-D axisymmetric model is presented in (A), the mesh 2-D axisymmetric model zoomed to the ME structure (B), the 3-D interpolated system of the whole model (rotated, in (C)), and a zoom of the 2-D axisymmetric ME structure in (D), and a zoom of the ME structure in 3-D in (E).

140
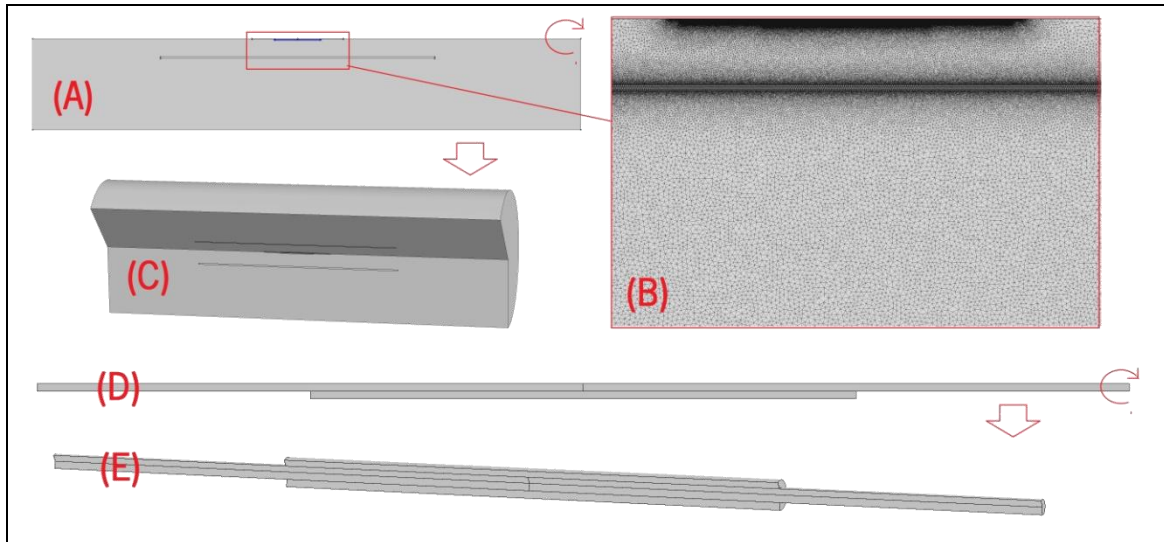
Figure 3.6: Representation of the 2-D axisymmetric fibre simulation experiment. The 2-D axisymmetric model is presented in (A), the meshed 2-D axisymmetric model zoomed to the magnetoelectric structure (B), the 3-D interpolated system of the whole model (rotated, in (C)), and a zoom of the 2-D axisymmetric magnetoelectric structure in (D), and a zoom of the ME structure in 3-D in (E).

ME structures of diameters of 1.4μm, 0.6μm and 0.1μm were analysed for concentrations (wt.% CFO/PVDF) of 90wt.%, 50wt.%and 10wt.%, with cubic magnetic anisotropy. The latter case of 1.4μm of radius with 50wt.%was also simulated with no preferential crystallographic orientation, therefore comparisons may be made.

3.2.4. Ideal bi-dimensional axisymmetric magnetoelectric cylindrical composite simulations

This axisymmetric model was performed in order to establish a comparison between a ME fibre structure and a fibre-shaped ME micro-composite. The magnetic field generation of former experiments was preserved in such manner that current densities induce magnetic fields as displayed in Table 3.5. The model was established to preserve a ME structure of 1.4μm of diameter of 50wt.% of weight concentration. The major difference was presented by the shape of the magnetostrictive component, which was included in the present model as a specific number of CFO micro spheres embedded in a cylindrical PVDF matrix, as presented in Figure 3.7.
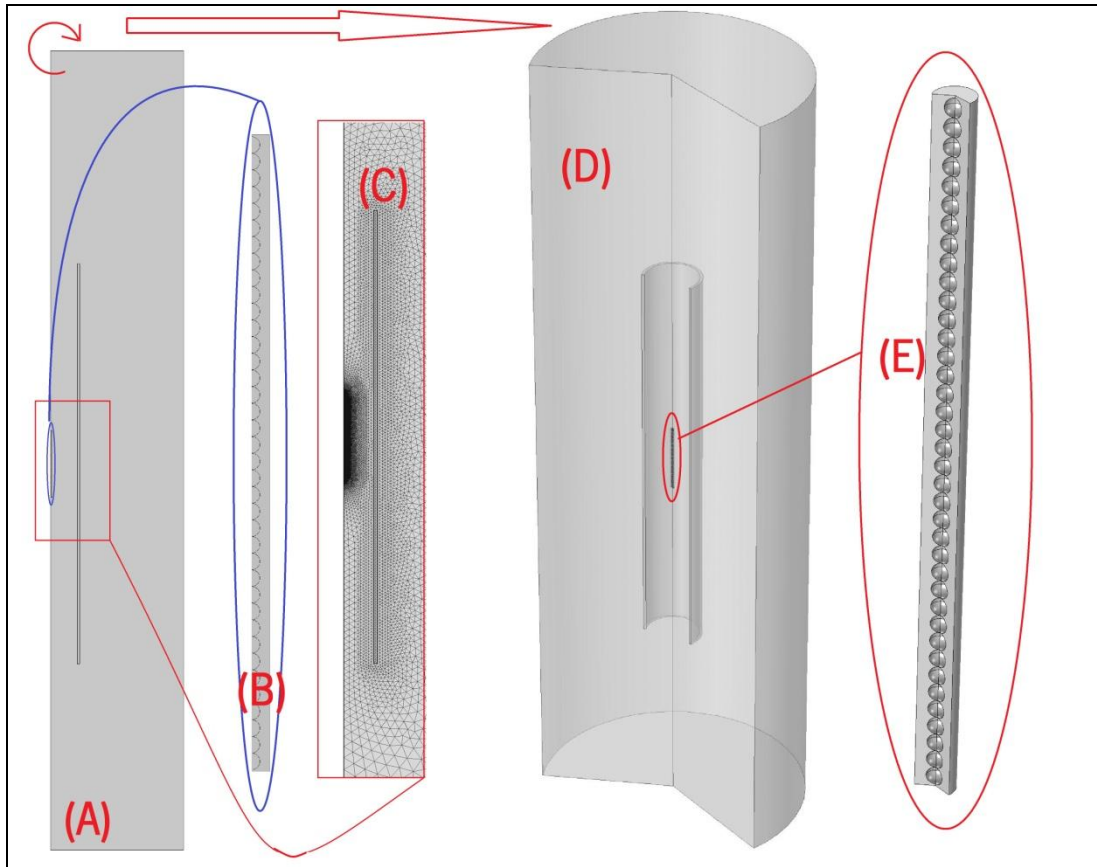
Figure 3.7: Representation of the cylindrical (fibre-formed) micro-composite magnetoelectric structure simulation. The 2-D axisymmetric model is presented in (A), a zoom to the magnetoelectric cylindrical composite 2-D axisymmetric model is presented in (B), the meshed 2-D axisymmetric model zoomed to the magnetoelectric structure and coils in (C), the 3-D interpolated system of the whole model (rotated, in (D)), and a zoom of the 3-D ME composite cylindrical structure in (E).

In order to be compared with the cylindrical fibre, the ME consisted in a piezoelectric cylindrical matrix of 700nm of radius and 25 μm of length. In the centre of the piezoelectric cylinder, 38 spherical spheres of CFO with 325nm of radius were distributed in the z-axis with a separation d_{sp} between each other, as displayed in Figure 3.7. Therefore, the concentration of 50wt.%was preserved for this simulation. Simulations were performed for no preferential crystallographic orientation and cubic magnetic anisotropy, for spheres separations, d_{sp}, of 4nm and 7nm.

142

3.3. Results and Discussion

The idea behind this work is to investigate the influence of the shape and composition of a ME structure in its performance. This work is focused on analyzing ME spherical and ellipsoidal structures, fibres and piezoelectric composites composites embedding magnetostrictive spheres. All simulation experiments were related with each other. First, a 3-D model was used to simulate the ME performance of a ME sphere with radial polarization. This study was emphasized and deeper studied by a 2-D axisymmetric model that simulated the same structure, with the only difference of not being able to establish the radial polarization of the sphere (in the 2-D axisymmetric model), but radial in cylindrical coordinates, that allowed a first approximation to the problem. For comparing with empirical experiences, this might also be a good approximation, because for a material such as PVDF, an accurate radial polarization might be hard to obtain for micro-nanostructures.

Subsequently, one of the former 2-D axisymmetric spheres was transformed gradually into an ellipsoid, becoming gradually a fibre-shaped ME structure. These results allowed to establish some grounds when analyzing the axisymmetric ME fibre.

Finally, all models are joint together into one composite: CFO spheres embedded into a PVDF cylindrical matrix, which was proposed in order to analyse whether a fibre presents different properties to cylindrical ME composites.

3.3.1. Ideal three-dimensional magnetoelectric sphere simulations

When submitted to the magnetic field values presented in Table 3.2, the magnetic field generated by the Helmholtz coils induced a magnetic flux density and magnetization in the ME spheres related to the magnetostrictive properties of the material. Figure 3.8 presents normal magnetic flux density and magnetization for 4 different magnetic fields: 445 Oe, 891 Oe, 1336 Oe, and 1782 Oe.

143

Hx	445 (Oe)	891 (Oe)	1336 (Oe)	1782 (Oe)	Scale
MAGNETIC FLUX DENSITY NORM (B_{norm})					0.25 (T) ... 0 (T)
MAX	0.13 (T)	0.21 (T)	0.23 (T)	0.25 (T)	B_{norm}
MAGNETIZATION NORM (M_{norm})					3.2×10^5 (A/m) ... 0 (A/m)
MAX	103310 (A/m)	145110 (A/m)	120730 (A/m)	92587 (A/m)	M_{norm}
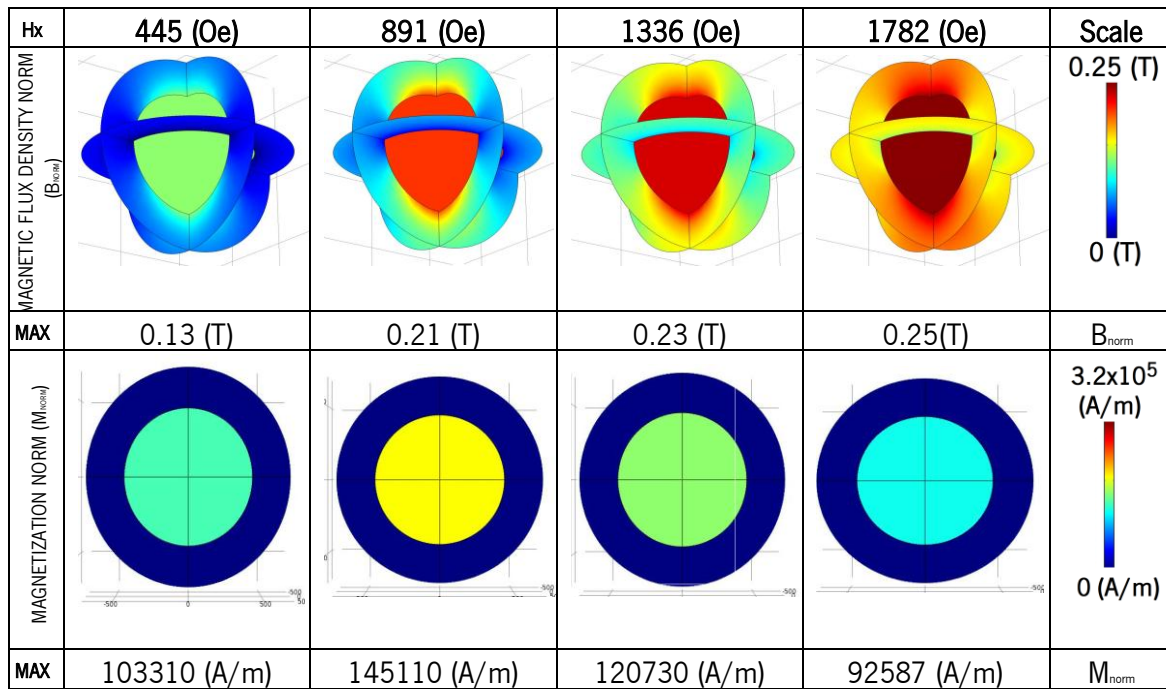
Figure 3.8: Normal magnetic flux density and magnetization of a magnetoelectric sphere (diameter 1.4um, 50wt.%) for different magnetic field values.

It can be observed that the magnetic flux density increases with the magnetic field, and it can be confirmed that the normal magnetic flux density presents a constant value over yz-planes, outside the CFO (implying a homogeneous magnetic field in the x-direction). Therefore, as established by equation (3.3), a maximum is observed for the case of *H*=891 Oe, which implies that around that value the maximal performance of the ME composite should have been reach.

The displacement, although, does not show such symmetries. Even when there are no magnetic anisotropies included on these models, magnetization is predominant in the x-axis (and lower on y- and z-axis's), and further, there are structural anisotropies of the semicrystalline PVDF (Chapter 2).

The total displacement of the ME sphere is presented in Figure 3.9, for xz, xy and zy planes and for concentrations of 15wt.%, 50wt.%and 90wt.%. Besides establishing the displacement field inside the sphere, the deformation is also drawn at the edges of the structure (presented with a scale of 3000x).

	XY-Plane	XZ-Plane	YZ-Plane	Scale
Diameter 1.4μm 15wt.%				0.03 nm · · · 0 nm
MAX	0.0227nm	0.0237nm	0.0245nm	
Diameter 1.4μm 50wt.%				0.03 nm · · · 0 nm
MAX	0.0251nm	0.0327nm	0.0327nm	
Diameter 1.4μm 90wt.%				0.03 nm · · · 0 nm
MAX	0.0391nm	0.0399nm	0.019nm	
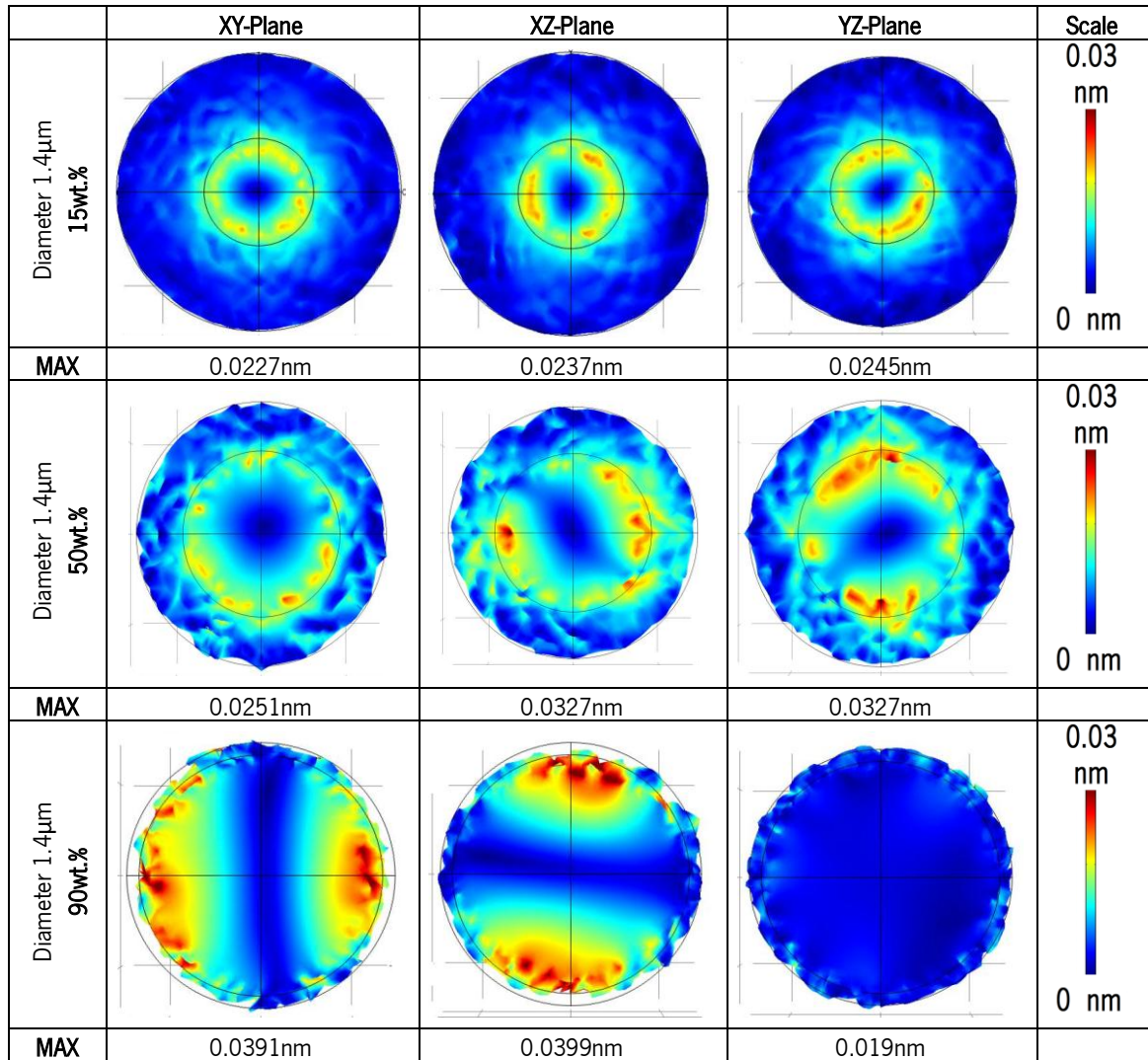
Figure 3.9: Total displacement within 3-D magnetoelectric spheres of 1.4μm of diameter, for 3 weight concentration values (15wt.%, 50wt.%, 90wt.%) when submitted into a magnetic field of 891 Oe.

For spheres of 15wt.%and 50wt.%, the maximum displacement is produced in the interface CFO/PVDF, while for higher concentrations, as the case of 90wt.%of CFO, the deformation is produced in the whole sphere, as presented in Figure 3.9, roughly maintaining its shape on the yz-plane (perpendicular to the magnetic field), but elongating the sphere along the z-axis, with an ellipsoidal shape. In this particular case of 90wt.%CFO, such a displacement in the thin PVDF layer, generates a series of heterogeneous electrical polarity regions in the PVDF, maximizing its transducer properties in converting deformation into electrical charge, as presented in Figure 3.10, that represents the electric potential distribution for all-three concentration values.
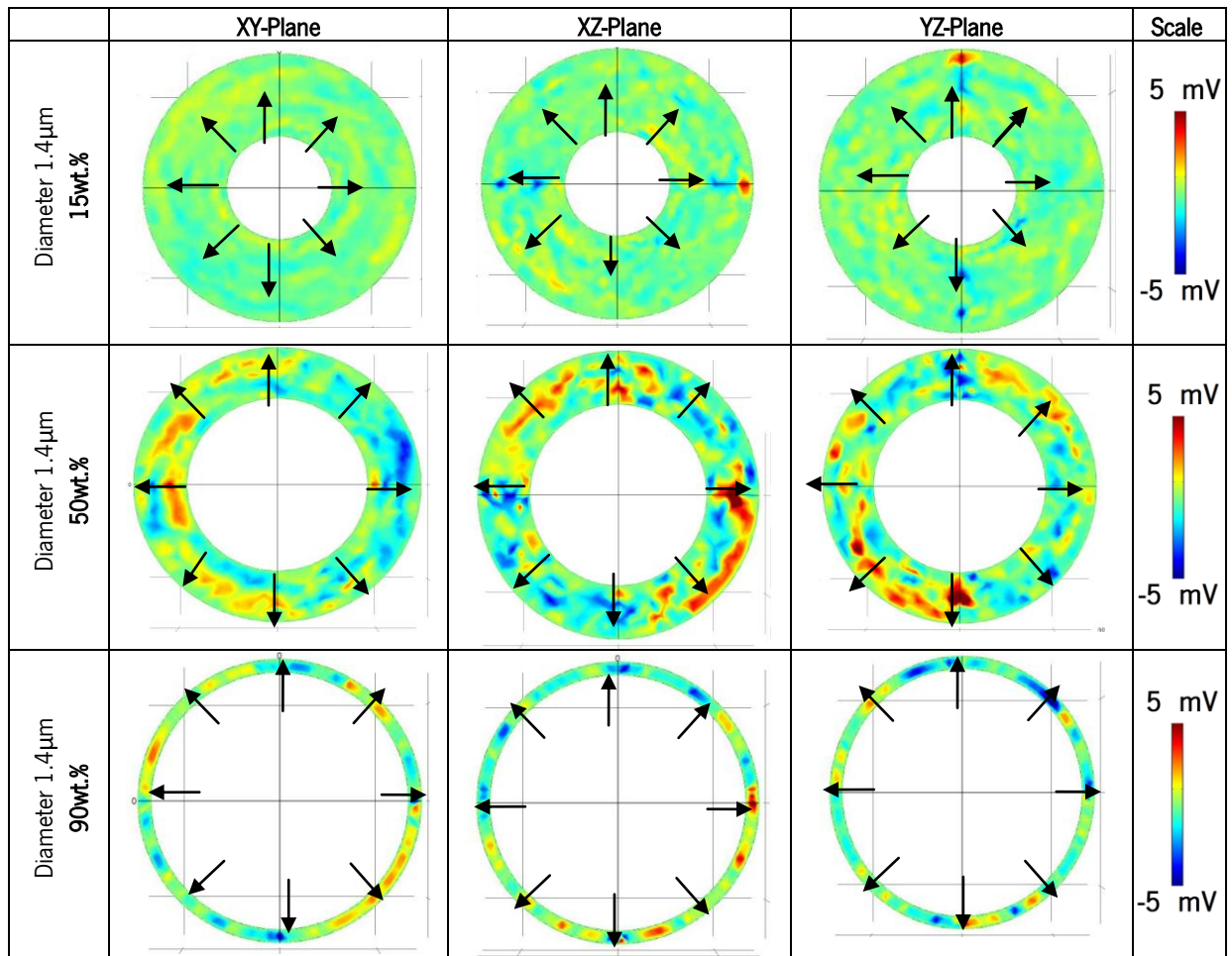
Figure 3.10: Electric potential distribution within the PVDF of the magnetoelectric spheres of 1.4μm of diameter, for 3 weight concentration values (15wt.%, 50wt.%, 90wt.%) when submitted to a magnetic field of 891 Oe. Black arrows indicate polarization orientation (radial on all planes).

In the case of the sphere with filler content of 15wt.%, it can be observed an approximately homogeneous electric potential distribution in the PVDF matrix, with the generation of more electric dipolar regions as the piezoelectric thickness is reduced, as it was found in the case of 50wt.%. By these outcomes, it can already be predicted that the 90wt.%concentration configuration will have an enhanced ME performance over lower CFO concentrations due to two main reasons: on the one hand, the larger quantity of CFO leading to larger overall deformation of the polymer matrix, on the other hand, the large elasticity of PVDF plays a role in the sense that these deformations will not be fully transmitted to the outer surface of the polymer when the thickness in too large. In this situation, a significant amount of elastic energy is not converted into electrical energy. Even more, as PVDF is a semicrystalline and elastic piezoelectric material,

146

small thickness yields to the formation of heterogeneous electrical polarity regions along the piezoelectric thickness (Figure 3.10).

Former arguments lead to the conclusion that the larger the CFO weight concentration, the better performance of the ME sphere will be. This fact is confirmed in Figure 3.11, where the ME performance the of spheres with 15wt.%, 50wt.%and 90wt.%filler concentrations are presented over a DC magnetic field region from 111 Oe to 2227 Oe.
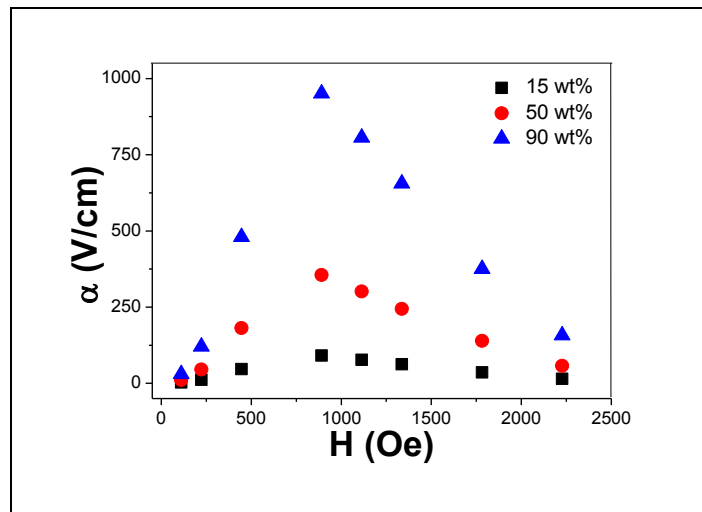
Figure 3.11: Simulated magnetoelectric response of spheres of 1.4μm of diameter as a function of the magnetic field (H) for 3 different CFO weight concentrations (15wt.%, 50wt.%, 90wt.%).

The black dots reflect data obtained for the configuration of spheres with 15wt.%filler content, presenting lower ME coefficients than the ME sphere of 50wt.%and, as expected, a much higher performance is obtained for the configuration with 90wt.%filler content. All maximum α_{ME} are obtained with a magnetic field of approximately 891 Oe, but with the calculated sampling rate it is hard to define whether all the samples show the same maximal operational magnetic field. In any case, it can be concluded that H_{max} is between 445 Oe and 890 Oe for all weight concentrations.

Figure 3.12 displays total displacement simulation results for ME spheres of 50wt.%CFO with diameters of 1.4μm and 0.1μm when submitted to a magnetic field of 891 Oe, in order to analyse the size effect.

147

	XY-Plane	XZ-Plane	YZ-Plane	Scale
Diameter 1.4μm 50wt.%				0.03 nm – 0 nm
MAX	0.0251 nm	0.0327nm	0.0327nm	
Diameter 0.1μm 50wt.%				0.002 nm – 0 nm
MAX	0.0016nm	0.0019nm	0.0021nm	
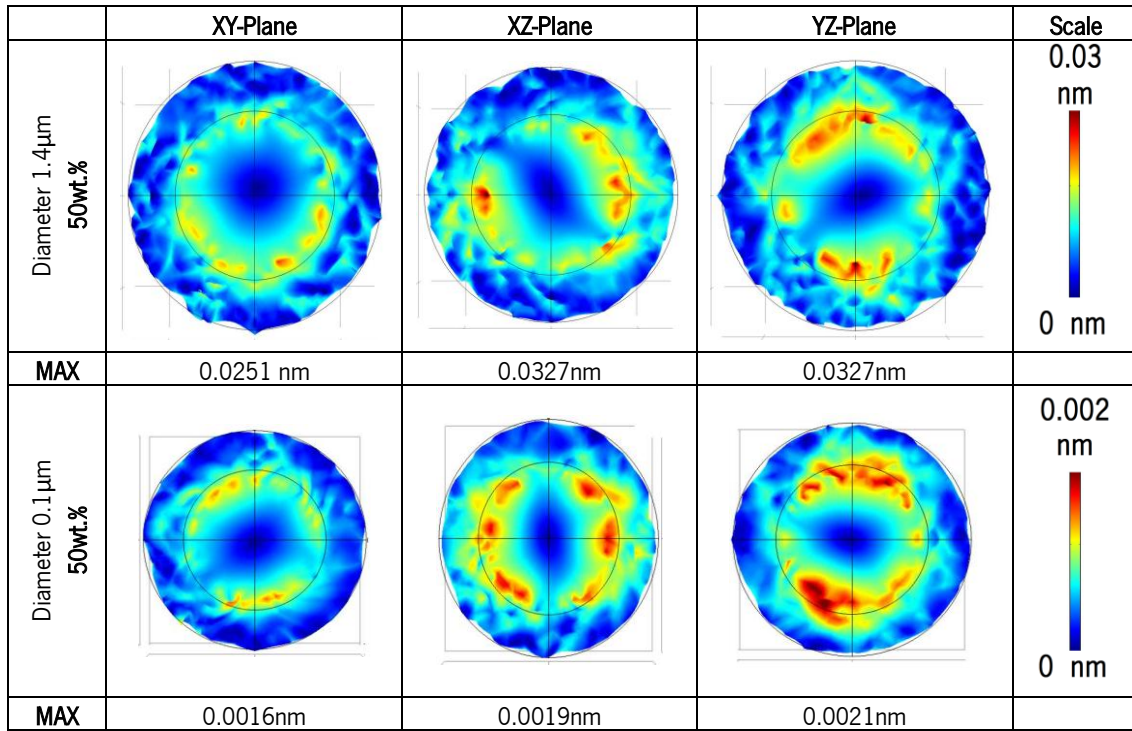
Figure 3.12: Total displacement within the magnetoelectric spheres of 50wt.%CFO with 1.4μm and 0.1μm of diameter when submitted to a magnetic field of 891 Oe.

As presented in the analysis for the 50wt.%case, the total displacement holds maximal values around the CFO/PVDF interface, the deformation being influenced by the semicrystalline nature of PVDF, leading to a heterogeneous deformation. Although the spheres of 1.4μm diameter show ten times the maximal deformations with respect to the spheres with 0.1μm of diameter (proportional to the relation of sizes), there is no significant change in deformation patterns for the different sizes.

Accordingly, and in order to further analyse the size effect, Figure 3.13shows the electric potential distribution results for ME spheres with 50wt.%CFO with diameters of 1.4μm and 0.1μm when submitted to a magnetic field of 891 Oe.
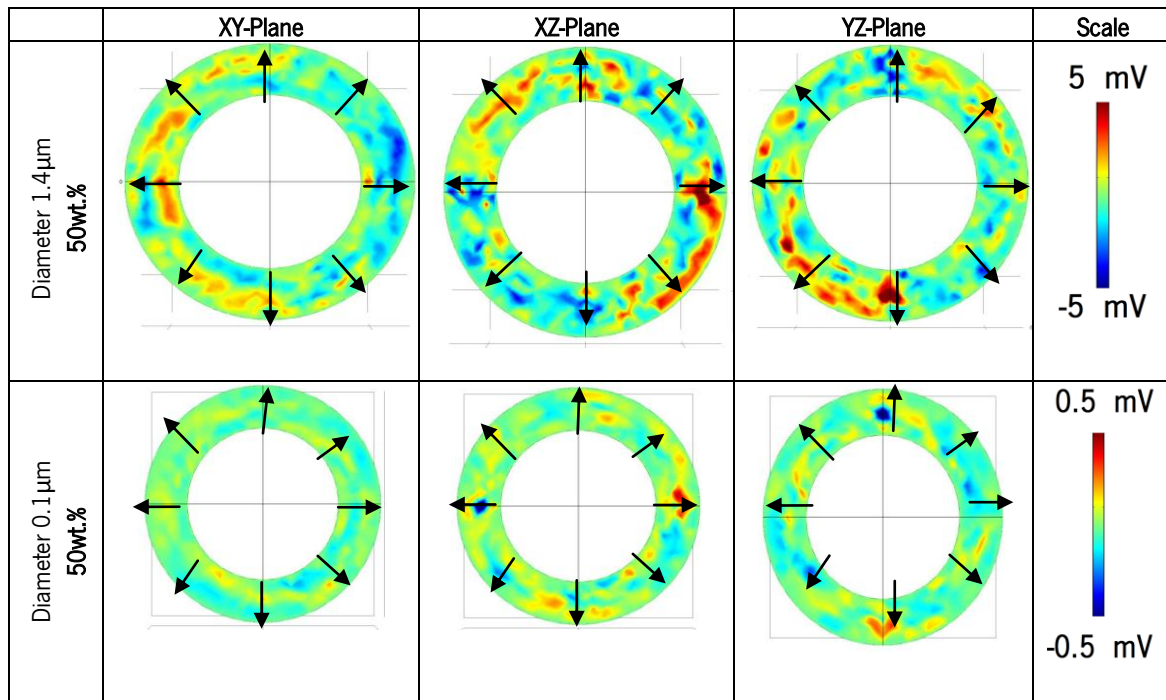
Figure 3.13: Electric potential distribution within the PVDF for the magnetoelectric spheres of 1.4μm and 0.1 μm of diameter, for 50wt.%filler concentration, when submitted to a magnetic field of 891 Oe. Black arrows indicate polarization orientation (radial in all planes).

For the electric potential distribution, the pattern also remains in establishing zones of maximal electrical potential in a circular geometry, but in a disordered way due to the influence of the electroactive polymer semicrystalline morphology. As noticed for the total displacement, also for the electric potential distribution, the only noticeable difference between the two samples is that the electric potential maximal and minimal values are around 10% lower for the smallest sphere radius under consideration, i.e. proportional to the thickness ratio.

Therefore, and as established in Figures 3.12 and 3.13, sphere size influences the ME performance of the sphere just in a quantitative manner, establishing better performances for larger spheres for a given filler concentration. Figure 3.14shows magnetoelectric performance of the spheres with 1.4μm, 0.6 μm and 0.1 μm of diameter for 50wt.%content of CFO.
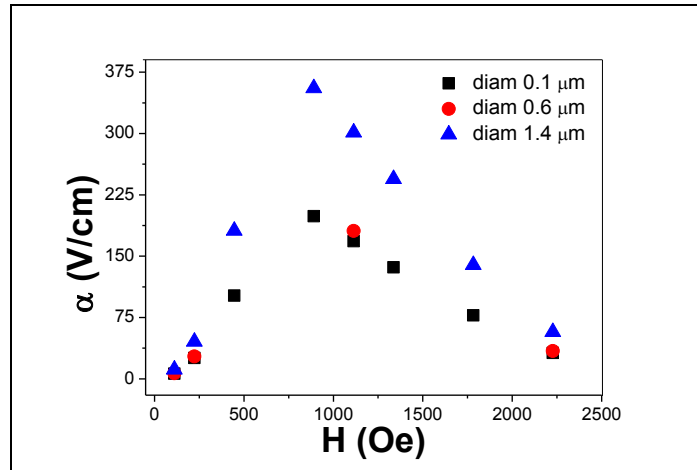
Figure 3.14: Simulated magnetoelectric response of spheres of 50wt.% CFO concentration as a function of the magnetic field for different sphere sizes, including sphere diameters of 0.1, 0.6 and 1.4μm.

As for the effect related to the variation of weight concentration, with respect to the variation of the sphere diameter, the maximal values for ME structures of 0.1 and 1.4μm are obtained for a magnetic field of 891 Oe, and α_{ME} for the configuration with 1.4μm sphere diameter is 1.75 times larger as for of the sphere with a diameter of 0.1μm. This results, together with the results presented in Figures 3.12 and 3.13, lead to the conclusion that size just has a quantitative effect over the ME performance of the spheres, establishing enhanced ME performance for larger ME spheres.

Although experiments show no maximal operational magnetic field dependence of size and weight concentration, a more detailed analysis is needed to conclude that there is no such dependency over the ME performance of the spheres, that includes a more dense evaluation of magnetic field values in the range of 445 Oe to 890 Oe.

3.3.2. From the bi-dimensional axisymmetric sphere to the axisymmetric fibre

The validation of the axisymmetrical model by the 3-D ME sphere simulations is substantial in order to reduce system and time resources that allow not only to improve the quality of the investigation for the ME sphere, but also to expand this research into other ME structures, such as fibres and composites.

150

It is worth noticing that there are 2 assumptions in the 2-D axisymmetric model, which introduce variations in the simulation´s results. First, axisymmetry does not allow a radial polarization along the piezoelectric thickness. In this way, an approximation, being perpendicular to the symmetry axis. As polarization is of large importance in the magnetoelectric effect, with direct influence over on the electrical outcome of the ME structure, some noticeable changes are expected. The second assumption is to establish a structural symmetry (axisymmetry) over a structurally semicrystalline material such as PVDF, with the implications of establishing no displacement along the axisymmetrical axis for this material.

In order to illustrate the behaviour of the axisymmetric model, the 3-D and the axisymmetrical models should be compared by a parameter that in the 3-D model is already axisymmetric: The normal magnetic flux density, presented for both models in Figure 3.15.

Hx 3-D	445 Oe	891 Oe	1336 Oe	1782 Oe	Scale
MAGNETIC FLUX DENSITY NORM (B_{NORM})					0.25 T — 0 T
MAX	0.13 T	0.21 T	0.23 T	0.25T	
MAX	0.12T	0.2 T	0.21T	0.22T	
MAGNETIC FLUX DENSITY NORM (B_{NORM})					0.25 T — 0 T
Hx 2-D	390 Oe	690 Oe	990 Oe	1200 Oe	
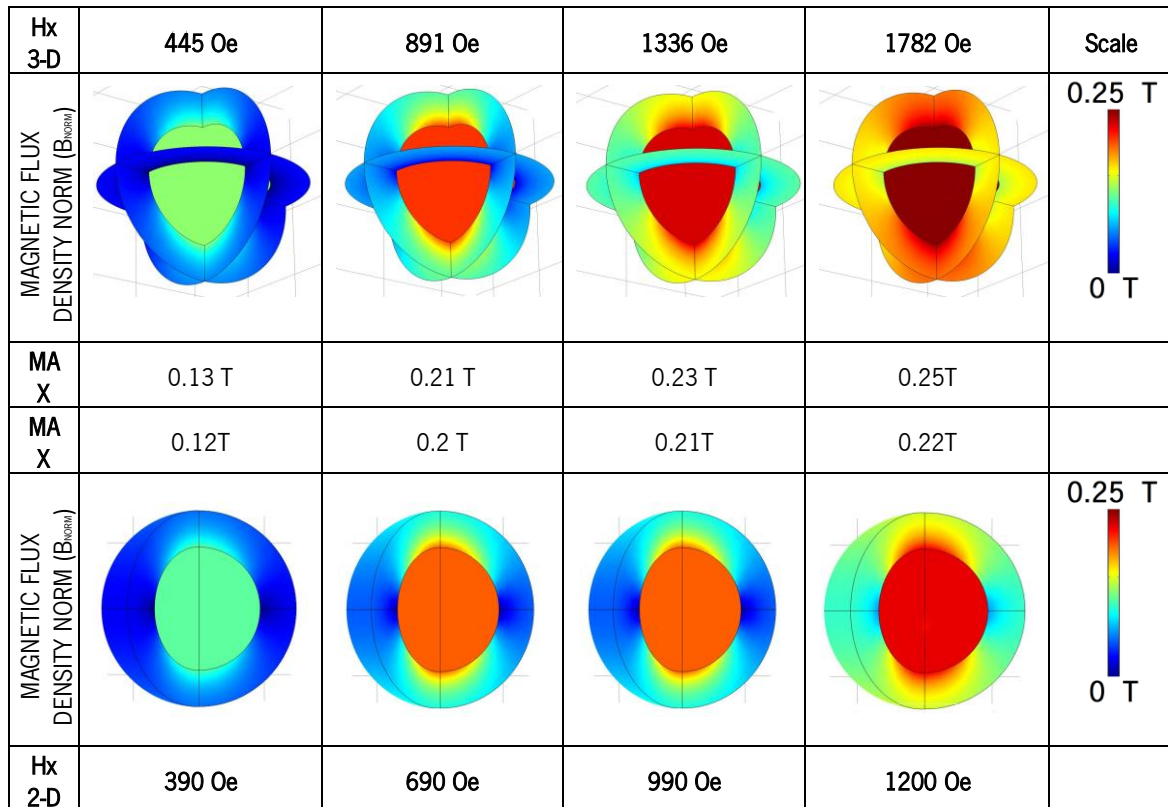
Figure 3.15: Normal magnetic flux density and magnetization of the magnetoelectric sphere with 1.4µm of diameter and 50wt.%filler content for different magnetic field values in the 3-D model(above) and in the 2-D axisymmetric model (below).

As shown in Figure 3.15, for similar magnetic fields not only the general trends are preserved, but also the magnetic flux density values. In this way, the approximations allow the investigation of the system.

151

3.3.2.1. Two-dimensional axisymmetric spheres

Figure 3.16 shows the comparison of the 3-D magnetoelectric simulation and their 2-D axisymmetric counterpart for different weight concentration of CFO (15wt.%, 50wt.% and 90wt.%).
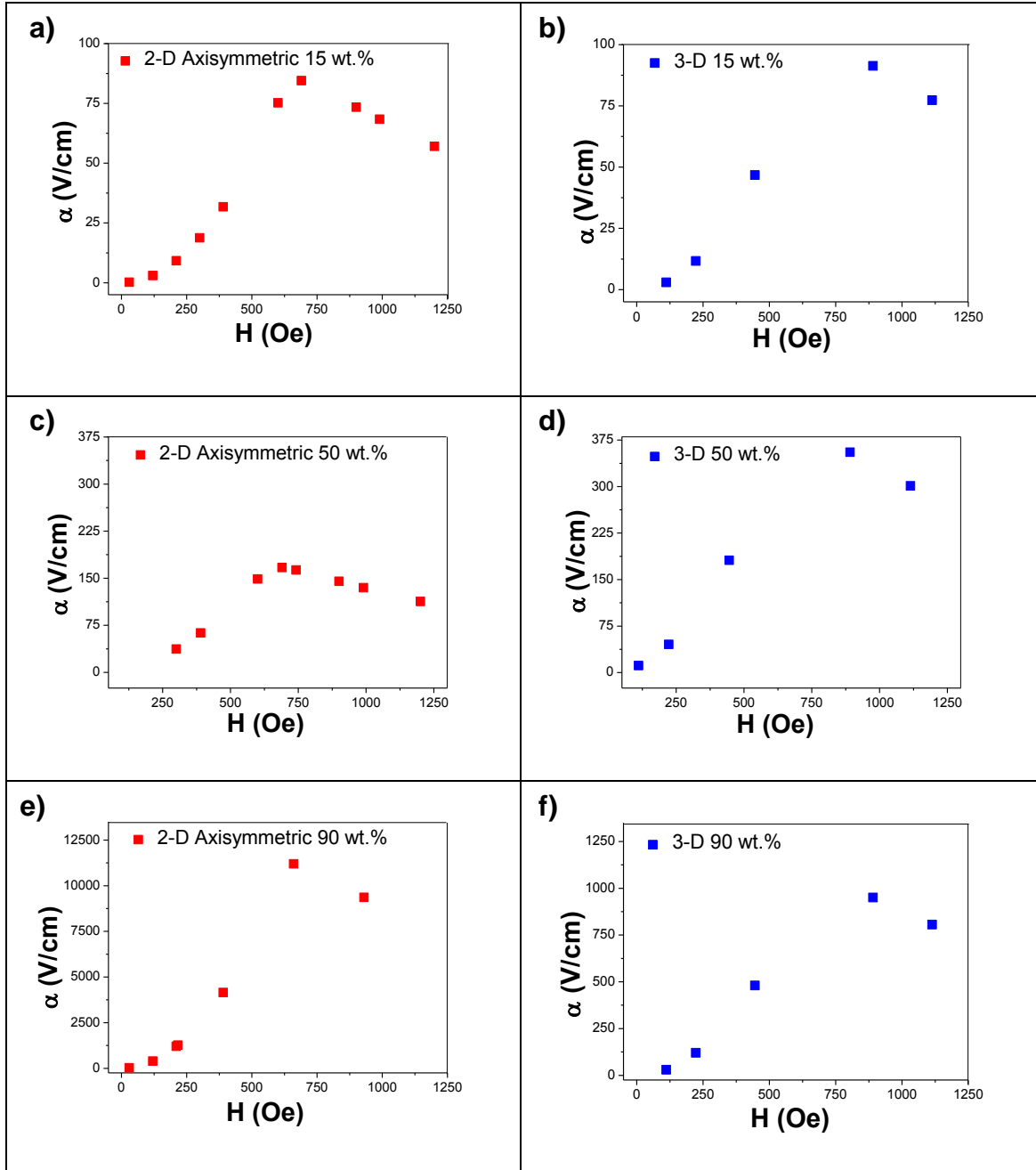
Figure 3.16: Comparison of the α_{ME} dependence over the magnetic field of a 1.4μm diameter magnetoelectric sphere for three different filler concentrations of CFO, for 2-D axisymmetric model (left) and 3-D model (right).

As the magnetic part of the problem shows complete axisymmetry, the characteristic ME response over magnetic field maintained their shape in both 3-D and 2-D models, only establishing differences between their piezoelectric performance, and therefore, only quantitative discrepancies in the value of the ME performance. 2-D axisymmetric model presented again no difference in the magnetostriction curve, holding a maximal performance around 700 Oe.

Although a good agreement between both simulation models can be established from Figure 3.16, there are some issues to be analysed in more detail, as follows:

Between the two models, the difference on the polarization direction should have a direct impact on the simulated ME behaviour for different concentrations and sizes. As the polarization in the axisymmetric model is not spherically radial, but perpendicular to the magnetic field (radial in cylindrical coordinates), there should be maximal polarization for z=0, and minimal near the symmetrical axis, where the maximal deformation should be produced in the magnetostrictive part of the structure. For these reasons, the ME effect should be reduced by the polarization approximation in the 2-D axisymmetric model in most of the cases -as it is presented for the case of the ME spheres with 15 wt.% and 50 wt.% filler content-, with the exception of high concentrations, where this approximation should be more accurate, due to the generation of a thin piezoelectric shell. Geometrically, the axisymmetric model will become more accurate and even may present increased values of α_{ME}, because in most of the CFO/PVDF interface the polarization will be perpendicular to the displacement (in the same direction as the magnetic field), as presented in Figure 3.16 (e, f).In this case (90 wt.% filler content ME spheres), the 2-D axisymmetrical model has a ME performance that is approximately ten times the ME performance of the 3-D model, not only due to the establishment of a more accurate polarization orientation, but also because of the formation of dipolar regions in thin piezoelectric shells. Further, it is also improved due to the lower content of elastic material, which introduces a more efficient transmission of the deformation and therefore a larger contribution to the ME coupling.

Figure 3.17shows the comparison of the 3-D magnetoelectric simulation and their 2-D axisymmetric counterparts for different sizes of the ME sphere, for diameters of 0.1μm, 0.6μm and 1.4μm.
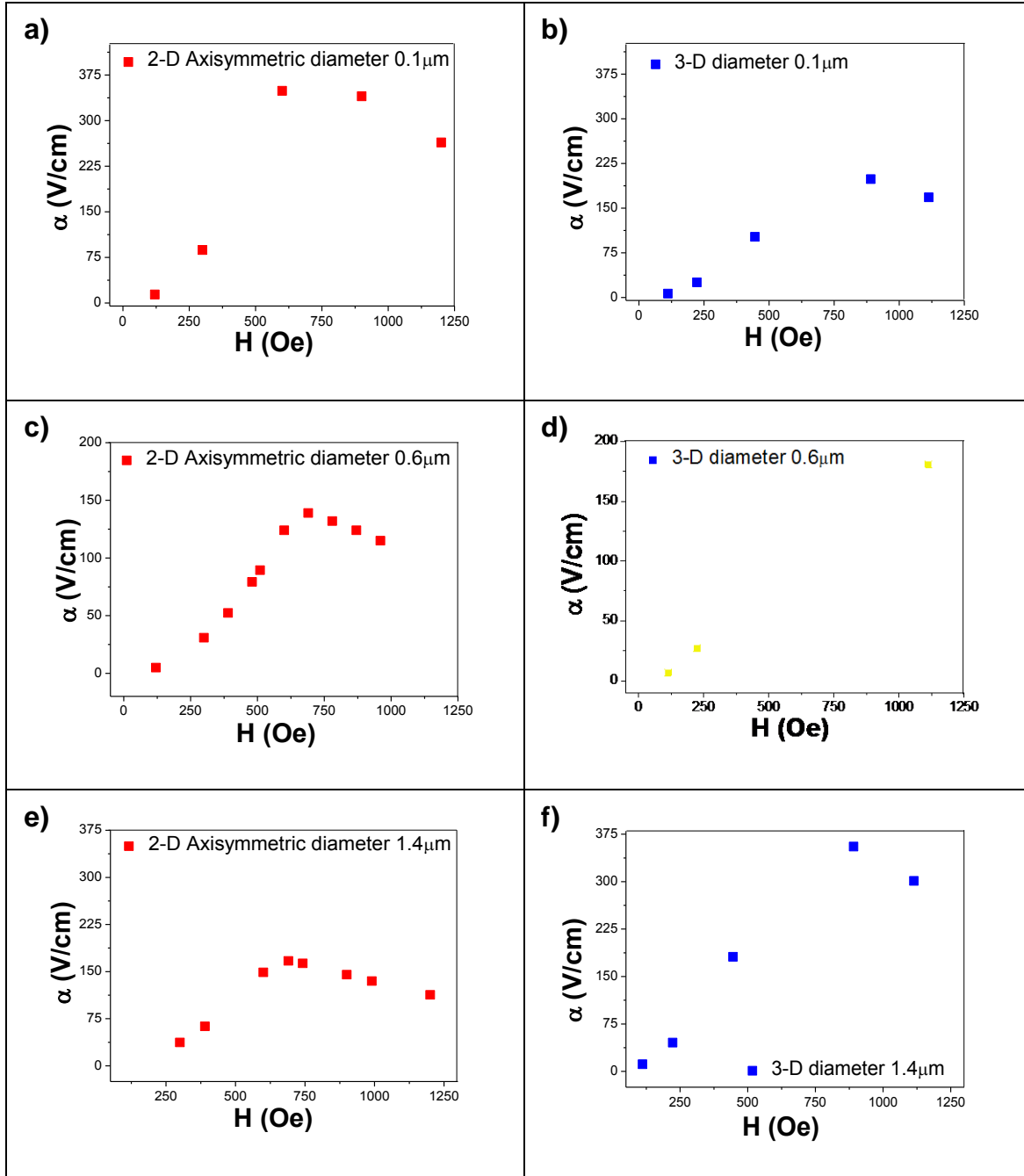
Figure 3.17: Comparison of the α_{ME} dependence over the magnetic field for filler concentration of 50wt.%, for magnetoelectric spheres of 1.4μm, 0.6 μm and 0.1 μm of diameter, for 2-D axisymmetric model (left) and 3-D model (right).

The same geometrical background for higher concentration ME structures applies to smaller spheres. In this way, enhanced values of α_{ME} are observed for smaller spheres than for larger ones for the 2-D axisymmetric simulated case of 0.1 μm of diameter when compared to the 3-D simulation. On the contrary, a lower value is observed for the 2-D axisymmetric approximation in the experiment with 1.4 μm of diameter, as presented in Figure 3.17.

Figure 3.18shows a comparison between simulated ME results of different weight concentration and sphere sizes for isotropic (with no preferential crystallographic orientation) and anisotropic (with cubic magnetic anisotropy)spherical structures.
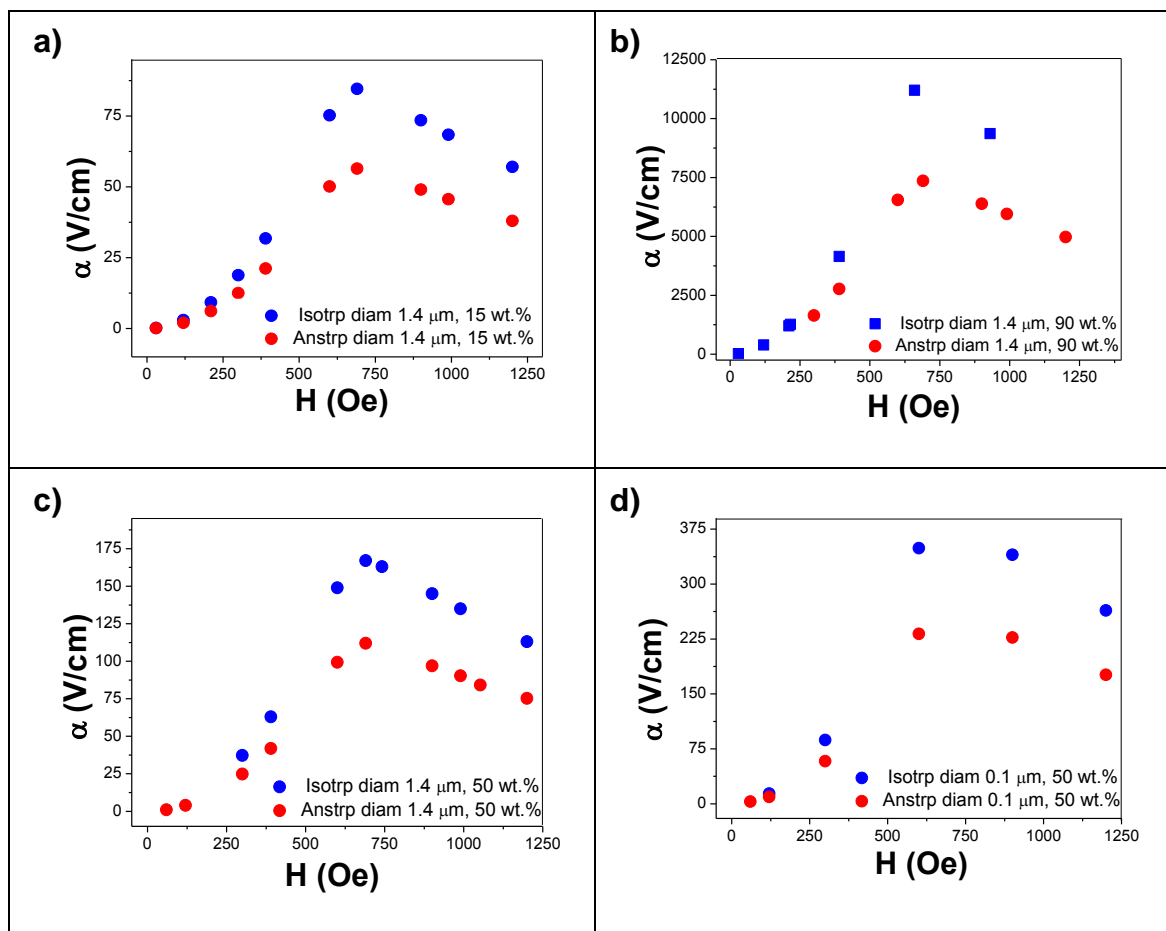
Figure 3.18:Effect of cubic or isotropic crystallographic orientation over the magnetoelectric performance of CFO/PVDF spheres, with different concentration and sizes, magnetoelectric spheres of: (a) 1.4 μm of diameter and 15 wt.% CFO; (b) 1.4 μm of diameter and 90 wt.% CFO; (c) 1.4 μm of diameter and 50 wt.% CFO; (d) 0.1 μm of diameter and 50 wt.% CFO.

As magnetization was established to be along the z-axis direction, and the ME spheres were submitted to an homogeneous magnetic field, the main difference between introducing a cubic crystallographic orientation in the magnetostriction model appears a decrease in the magnetoelectric performance, with the maximal ME performances, α_{ME} of isotropic ME spheres maintaining a relation of 1.5 times the ME performance of the anisotropic ME spheres. These can be explained by the homogeneous field along the z direction (and therefore no net magnetostriction in r-direction) and the difference in the magnetostriction models, established in equations (3.7) for the isotropic model and equation (3.8) for the anisotropic model. If just magnetostriction along the z-axis is to be considered, equations should return those results, therefore implying that there is no important magnetization along the radial direction of the axisymmetric model.

3.3.2.2. From the bi-dimensional axisymmetric sphere to the fibre model

As magnetostriction induces a relative deformation to the initial length of the structure mainly along the direction of the magnetic field, it can be expected that stretching the geometry of the ME sphere into an ellipsoid with the major axis along the magnetic field direction will increase the ME behaviour of the structure. Beside this, by increasing the area of the structure, that is normal to the magnetic field, and from Gauss law on equation (3.2), it can also be expected that magnetization will reach higher values inside the magnetostrictive component with lower magnetic field values, and therefore giving as a result that the eccentricity of the ellipsoidal shape of the ME sphere also displaces the ME curve to the left, presenting maximal behaviour with lower magnetic fields. This effect is shown in Figure 3.19, where simulation results for ME performance are presented for ME structures with eccentricities between 0nm (sphere) and 3200nm (fibre-shaped). The concentration and total volume of the ME structures is preserved from the sphere with diameter of 1.4μm and 50wt.%.

156
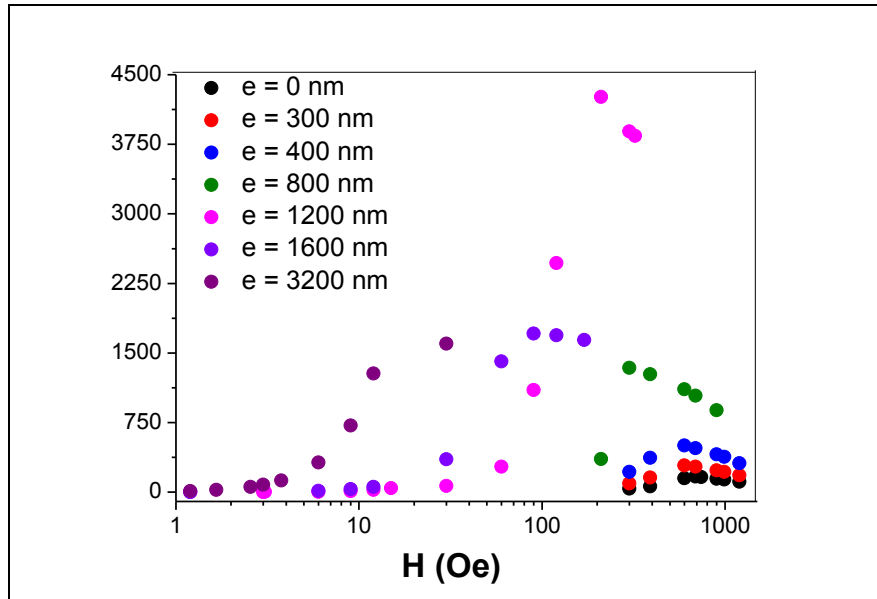
Figure 3.19: Magnetoelectric coefficient for 50wt.%structures with different ellipsoidal eccentricities at constant volume.

Figure 3.19 shows that with increasing eccentricity until 1200 nm, ME performance is enhanced while the maximal operational magnetic field diminishes. The ME structure with eccentricity of 1200nm shows the highest ME performance, reaching more than ten times the α_{ME} of the ME sphere, with the most abrupt curve. Table 3.6 shows the maximal operational magnetic field value and maximal ME coefficient, α_{ME}, for each configuration, according to their eccentricities.

Table 3.6: Maximal operational magnetic field value and maximal magnetoelectric coefficient for each investigated configuration, according to their eccentricities

Configuration eccentricity e (nm)	Maximal operational magnetic field H_{max} (Oe)	Maximal ME coefficient α_{ME} (V/cm)
0	684	182
300	611	290
400	588	508
800	298	1338
1200	208	4241
1600	90	1709
3200	30	1601

While continuing raising the structure eccentricity, maximal operational magnetic fields continues to reduce, and the curves return to a less abrupt shape, but reducing gradually their ME performance, establishing a maximal performance for eccentricity of 1200 nm and showing for fibre-shaped structures a monotone increasing curve (as presented for the configuration with eccentricity of 3200nm).

According to those arguments, three-types of ellipsoidal-shaped ME structures can be established. The first type are the ellipsoidal-spherical ME structures, with eccentricities bellow 800 nm that operate in DC magnetic fields between 200-2000 Oe, with simulated α_{ME} of the order of hundreds and with a ME curve with a similar shape as a spherical structure. The second type of ellipsoidal structures show a giant ME effect and are the ones with eccentricities above 800nm and below 1600 nm. They show a more abrupt curve and operate between 20-200 Oe magnetic DC bias field. It should be noticed the existence of an exceptional ME behaviour of the ME structure of eccentricity of 1200nm, with a ME coefficient of the order of 4000V/cm. The third type is the fibre type. They are structures with eccentricities above 1600 nm, show a lower order of magnitude of α_{ME} than the second group and operating in very low DC bias fields, below 20Oe.

Figure 3.20showsthe normal magnetic flux density distribution for ellipsoidal ME structures of the third group, when exposed to a magnetic field of 12 Oe.

H_z	12 (Oe)	12 (Oe)	12 (Oe)	Scale
MAGNETIC FLUX DENSITY NORM (B_{NORM})				Bm (T) ... 0 T
MAX	0.02 T	0.035 T	0.17 T	Bm
e	1200 nm	1600 nm	3200 nm	e
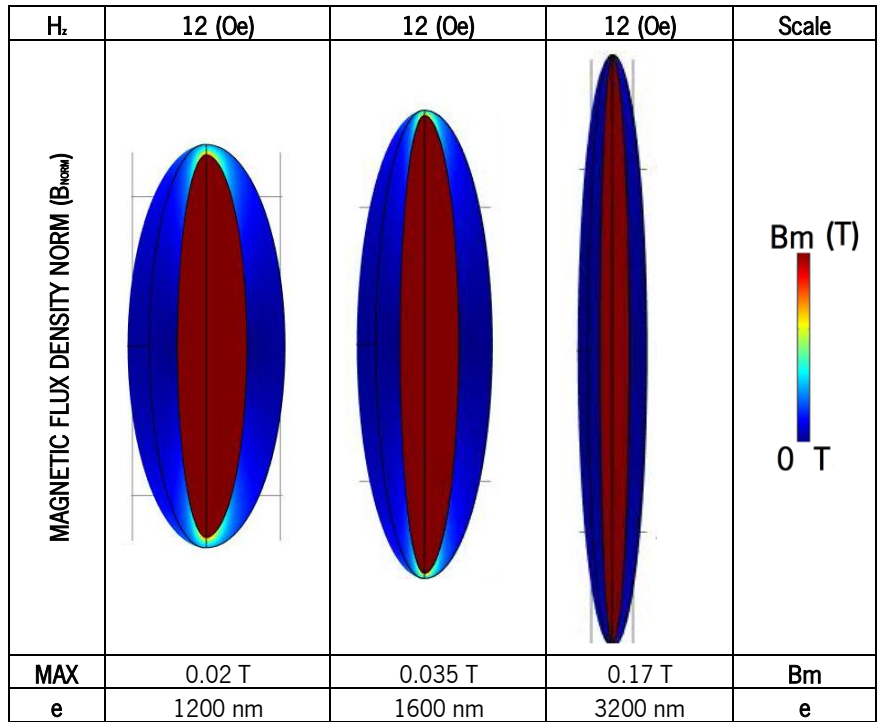
Figure 3.20: Normal magnetic flux density of the more eccentric magnetoelectric ellipsoidal structures when submitted to a magnetic field of 12 Oe (in z-direction).

As expected, with increasing the eccentricity of the fibre-shaped structures, magnetization saturation is reached at lower magnetic fields, therefore, showing a higher and more homogeneous normal magnetic flux density at lower magnetic fields, as shown in Figure 3.20.

The second group of ME ellipsoidal structures show the highest ME performance and a very interesting new area that should be followed by further research. The elaboration of ME structures with such specific geometrical conditions is nowadays limited and therefore these experiments are carried out just in order to present tendencies of ME performances related to geometry optimization. The main objective of this experiment was to obtain the trends of the ME curves and maximal operational magnetic field of ME fibres, therefore establishing the pattern to expect for the fibre simulations, i.e. lower operational magnetic fields, defined by the normal area to the magnetization direction of the fibre, which is larger than the sphere.

159

3.3.3. Ideal bi-dimensional axisymmetric ME fibre simulations

For ellipsoidal structures it can already be established that increasing the magnetostrictive surface perpendicular to the magnetization produces a decrease of the magnetic field for maximal α_{ME}, (H_{max}). Therefore, and as all fibres have the same length, this surface depends only on the magnetostrictive rod radius, which would increase with the diameter of the fibre and with the wt.% content of CFO.

Following, Figure 3.21shows the α_{ME} values for CFO/PVDF fibres of 1.4μm of diameter for weight concentration values of 10wt.%, 50wt.%and 90wt.%.
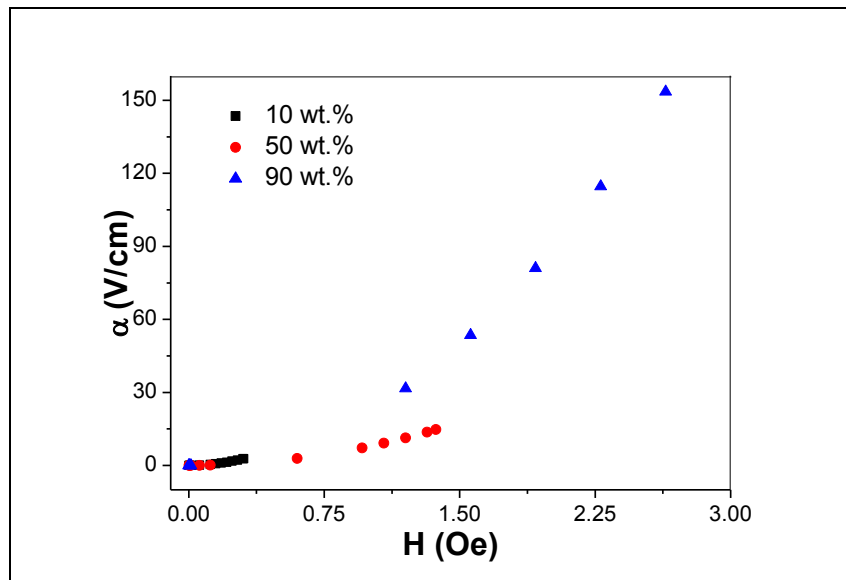
Figure 3.21: Simulations results for magnetoelectric performance of fibre structure with 10wt.%, 50wt.% and 90wt.% CFO.

The 2-D axisymmetric model for ME spheres of 90wt.%CFO content shows an extremely high simulated performance in the order of ten times higher than its 3-D associated model, that also presents more than twice the value α_{ME} of the 50wt.%ME sphere. The case of the ME 90wt.%fibreis not different, presenting not only a ten times higher ME coefficient than 50wt.%and 10wt.%fibre simulations, but also a higher operational DC Magnetic field that arises to 2.63 Oe (with an α_{ME} of 153 V/cm), as shown in Figure 3.21. Maximal operational magnetic field for the 160

fibre with 50wt.%showsa value of 1.38 Oe with an α_{ME} of 15 V/cm, and the fibre 15wt.%presents a maximal ME coefficient value of 3.2 V/cm, for 0.3 Oe.

Figure 3.22 displays the size effect on ME fibres, presenting the simulated ME performance of 50wt.%CFO/PVDF ME fibres with different diameter, of 0.1µm, 0.6µm and 1.4µm.
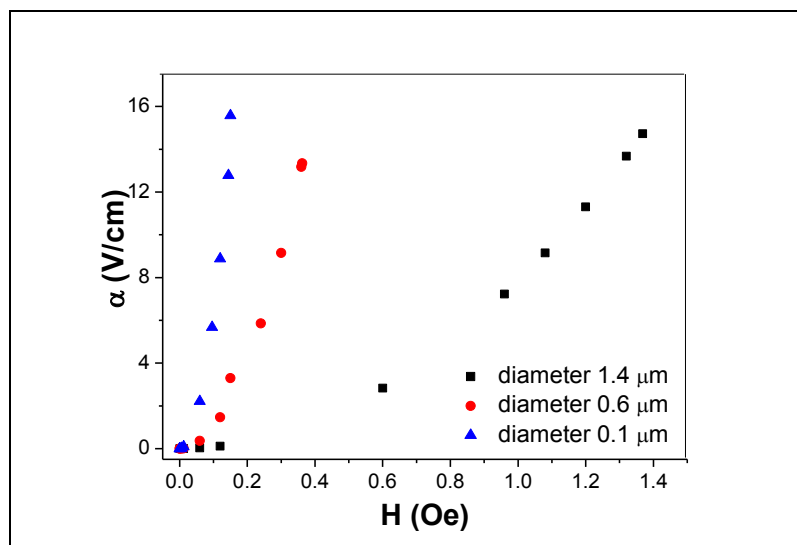
Figure 3.22: Simulation results for magnetoelectric performance of magnetoelectric fibres with diameters of 0.1µm, 0.6µm and 1.4µm.

Decreasing the fibre´s diameter has the consequence of diminishing the maximal operational magnetic field. As presented in Figure 3.22, the fibres with lower diameters, as 0.1 µm and 0.6 µm, presented an operational magnetic field near to zero Oe, having a sharply increasing curve, but reaching, with 0.1-0.3 Oe, the same order of ME coefficient (14-16 V/cm) as the fibre of 1.4µm reaches with magnetic fields of 1.4Oe.

All presented, fibre simulations results were obtained by including cubic magnetic anisotropy on the model. Figure 3.23shows the effect of ME fibres with no preferential crystallographic orientation (magnetically isotropic) on the fibre of 1.4µm diameter with 50wt.% filler content.
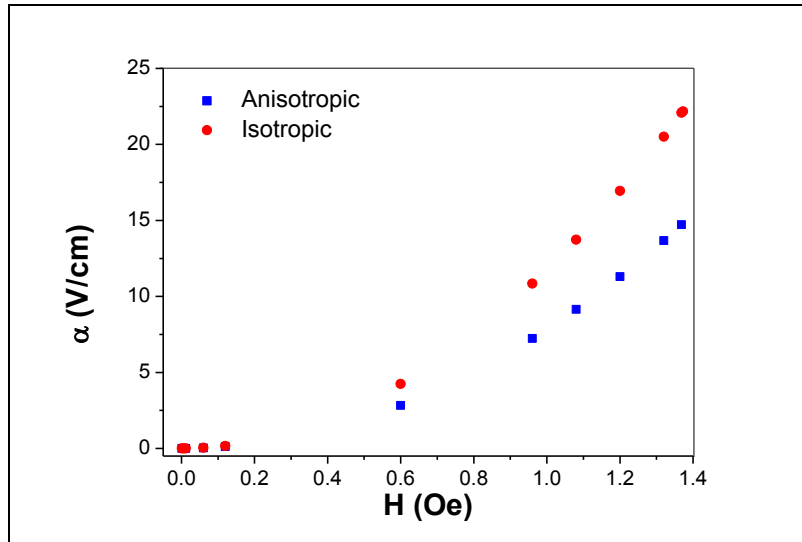
Figure 3.23: Comparison of the effect of a cubic crystallographic orientation or isotropy on the magnetoelectric effect of a 1.4μm diameter fibre with 50wt.% CFO content.

Figure 3.23 shows that the inclusion of magnetic isotropy in the fibre leads to similar results as for ME spheres: no influence on the operational magnetic field over the ME performance of the fibre, H_{max} - α_{ME} relation, but a larger influence on the perpendicular magnetostriction, establishing that α_{ME} for the isotropic configuration takes a value of 22.15 V/cm, with the ME coefficient being 1.47 times higher for the isotropic case that for the anisotropic configuration, with an α_{ME} of 15V/cm for the cubic preferential crystallographic orientation configuration at the magnetic field of 1.4 Oe.

3.3.4. Ideal bi-dimensional axisymmetric magnetoelectric cylindrical micro-composite simulations

The last experiment gathers all former experiments into one. It consisted in multiple magnetostrictive spheres centrally located in the middle of a cylindrical piezoelectric shaped structure, with the generation of a cylindrical ME composite. The concentration was maintained at 50wt.%, as for former experiments, and the variable of separation between spheres was also introduced. Figure 3.24 presents the ME performance for composites with 4nm and 7nm of separation of the magnetostrictive spheres located in the cylindrical ME composite, respectively.
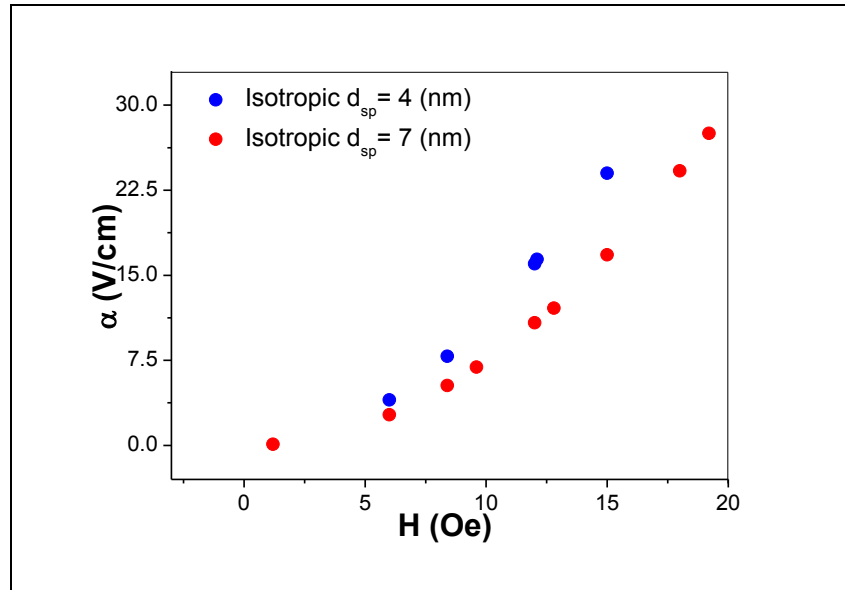
Figure 3.24: Magnetoelectric performance of two CFO/PVDF cylindrical composites of 50wt.% with two different separations between the CFO spheres: of 4nm and 7nm.

Results show that closely located ME CFO spheres embedded into a PVDF polymer matrix preserves the trend of the fibre, but increases not only the ME performance, but also the operational magnetic fields, as can be seen in Figure 3.24, reaching the same range of operational magnetic field as the ellipsoidal sphere of high eccentricity of 3200 nm. The configuration with CFO sphere separation of 4nm reaches an α_{ME} of 15 V/cm, with a magnetic field of 24 Oe, while the configuration with a sphere separation of 7nm shows an α_{ME} of 27.6 V/cm with a magnetic field of 19 Oe, which is closer to the 30-Oe for H_{max} of the ellipsoidal structure (of 3200 nm of eccentricity) than the 3 Oe of H_{max} of the ME fibre.

Figure 3.25shows the ME performance of the CFO/PVDF composite when subjected to a magnetic field of 12 Oe(a), with the electric potential distribution in a rotated 3-D way -Figure 2.25 (a)-, with the total displacement within structure-Figure 2.25 (b)-, the normal magnetic flux density-Figure 2.24 (c)- and the electric potential on the piezoelectric matrix-Figure 2.24 (d)-. Here the fibre areas display the magnetization in the axis direction (z) and the arrows display the polarization of the piezoelectric material.
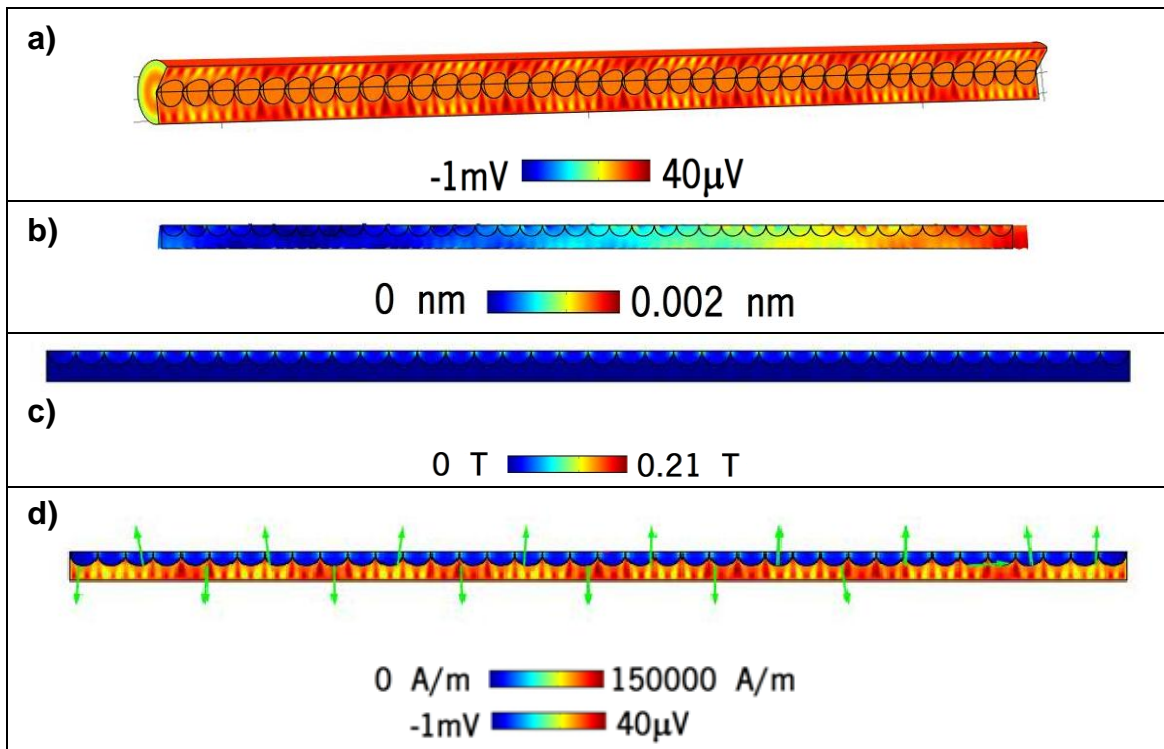
Figure 3.25: Magnetoelectric performance of the CFO/PVDF composite when subjected to a magnetic field of 12 Oe. (a) Shows the electric potential distribution in a rotated 3-D way, (b) shows the deformation of the structure, (c) shows the normal magnetic flux density and (d) shows the electric potential on the piezoelectric matrix. The magnetostrictive areas display the magnetization in the axis direction (z) and the arrows display the polarization of the piezoelectric material.

As shown in Figure 3.25,the electric potential distribution generates a radial pattern within the PVDF with maximum and minimum values along the z-axis, which are produced by the compressions and tensions by the displacements of the magnetostrictive structures along this direction. Normal magnetic flux density shows a nearly homogeneous distribution, with the exception of the areas between the magnetostrictive spheres, that provide for the maximal values and therefore, it can be established that the distance between them is the main component that will determinate the magnetic behaviour of the composite.

Closely located magnetostrictive spheres embedded into a PVDF matrix, perform with more magnetically similitude to a fibre than to a number of ME spheres, acting independently on the ME composite. Furthermore, it behaves even in a more similar way to a ME ellipsoidal structure. Furthermore, the distance between the magnetostrictive spheres allows the magnetic field to interact with the lateral surfaces, and therefore interacting with more perpendicular surface than

164

one sphere alone (as the ellipsoidal ME structure), but less normal surface than a cylinder (that would have all surface perpendicular to the magnetic field). It can be also expected that increasing the distance of the magnetostrictive spheres will also allow them to interact more independently with the piezoelectric material, leading to a better magnetoelectric performance, at higher magnetic fields.

Figure 2.26 introduces the effect of the crystallographic orientation of the CFO spheres, showing for both configurations, separation between magnetostrictive spheres of 4 nm and 7 nm, the ME performance of the configuration with cubic anisotropy and no preferential crystallographic orientation (magnetically isotropic).
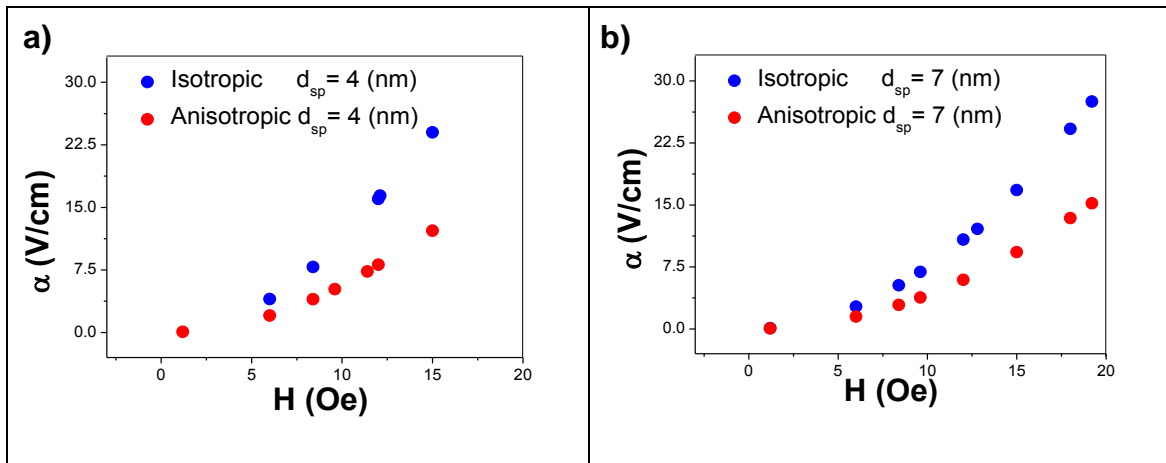
Figure 3.26:α_{ME} for magnetoelectric composites with magnetic isotropy and cubic anisotropy, when CFO spheres are separated in 4nm (a) and 7nm (b).

As for the former results, magnetic anisotropy (or cubic anisotropy) only produces a decrease on the ME performance of the structure, when compared to the composite with CFO spheres with no preferred crystallographic orientation (or magnetically isotropic), displayed in Figure 3.26.Table 3.7 shows the ME coefficients for the isotropic and anisotropic experiments.

Table 3.7: ME coefficient and maximal operational magnetic field for both configurations of cylindrical magnetoelectric composites embedding magnetostrictive spheres according to their crystallographic orientation

configuration	crystallographic orientation	H_{max} (Oe)	α_{ME} (V/cm)
d_{sp} = 4nm	Isotropic	15	24
d_{sp} = 4nm	Anisotropic	15	12.2
d_{sp} = 7nm	Isotropic	19	27
d_{sp} = 7nm	Anisotropic	19	15.33

Results displayed in Table 3.7 lead to conclude more influence of the crystallographic orientation for magnetostrictive rods embedded in piezoelectric matrix than for the fibre. As closely located the particles are, less influence of the inclusion of anisotropies is presented. While for the configuration with 4 nm of separation between magnetostrictive spheres the ME coefficient of the isotropic configuration is approximately twice the ME performance of the anisotropic configuration, the configuration with 7 nm of separation only achieves to have an enhancement of approx. 1.75 times the ME performance of the anisotropic configuration. Therefore, being able to establish more influence of the radial magnetostriction in the present configurations than in ME spheres and fibres.

CHAPTER 4: CONCLUSIONS AND FUTURE WORK

A simulation model based on Finite Element Methods (FEM) for magnetoelectric (ME) composites was developed.

Structural simulation of the ME performance of different laminate ME composites configurations were obtained for poly(vinylidene fluoride) (PVDF) and lead zirconate titanate (PZT; Pb[Zr$_x$Ti$_{1-x}$]O$_3$)as piezoelectric material layer, and Vitrovac, as magnetostrictive layer. Simulations assumed maximal deformation for the magnetostrictive material, obtaining the structural piezoelectric response for the piezoelectric ceramic and the piezoelectric polymer when the magnetostrictive layer was deformed to its maximal value from the magnetostriction curve. This allowed to establish the influence of the mechanical properties and of the materials morphology on the ME performance of different laminate configurations.

Although ceramic PZT based ME composites obtained higher ME responses in all simulated configurations (when compared with the composites with the electroactive polymer), PVDF based ME composites are more suitable for its specific applications in technology devices, where properties such as elasticity, malleability and biocompatibility, are required, among others. Further, for some of those innovative applications(such as biomedical materials), biocompatibility, easy shaping, large area fabrication flexibility and low cost are among the larger advantages of the incorporation of the polymer instead of the piezoceramic material. The inclusion of PZT based ME composites in this study intended to serve as comparison of the ME response of a rigid-crystalline-ceramic-piezoelectric material with the ME response of an elastic-semicrystalline-polymeric-piezoelectric material, such as PVDF. This comparison, allowed to establish the influence of the structural properties of PVDF in the ME coupling, leading to a better understanding of PVDF based composites behaviour.

Thus, the present study focused mainly on the evaluation of the magnetoelectric response of PVDF composites when bonded to a magnetostrictive material. The model did not included structural damping or magnetic losses, and assumed a maximal deformation on the magnetostrictive ends for all experiments. As the structural model did not include the nonlinear magnetostriction effect, PZT simulations were not influenced by magnetostrictive thickness, and

the parameters involved in the observed differences between both simulations (PVDF´s multi-layers performance and the PZT´s multi-layers performance)were morphological and mechanical.

Different ME configurations were simulated, including bi-layers and bonding properties, and multi-layers, including PZT based composites and PVDF based composites. Following, the main conclusions of the simulations of the different configurations are summarized.

a) Bi-layers

FEM simulations for ideal bi-layers show independence on the magnetostrictive thickness for both piezoelectric materials, presenting a ME coefficient, α_{ME}, of 85 V/cm for the PZT bi-layer and 10.9V/cm the PVDF bi-layer. PZT bi-layers with thin piezoelectric layers show slightly higher values of 86.5V/cm, decreasing progressively their ME performance with increasing the piezoelectric thickness, reaching to α_{ME} of 68 V/cm at piezoelectric thickness of 1mm. PVDF bi-layers, on the other hand, show a constant α_{ME} values for polymer layers below 110µm, of 10.71 V/cm, and then some higher and lower α_{ME} values, establishing a clear influence of the semicrystalline composition and elasticity of PVDF in this disordered pattern.

b) Bi-layers and Bonding Properties

The effect of the bonding layer type and piezoelectric layer thickness on the ME response of layered PVDF/epoxy/Vitrovac composites was reported. It is verified an increase of the ME voltage coefficient from 45 V/cmOe to 53 V/cmOe with increasing PVDF thickness from 28 µm to 110 µm and a reduction of the ME voltage coefficient from 53 V/cmOe to 6 V/cmOe with increasing epoxy Young Modulus from 2.7×10^{8} Pa to 9.0×10^{9} Pa.

The k value, indicative of the quality of the bonding between the active layers and the epoxy layer is the highest for the M-Bond laminates (0.60) and the lowest for the Stycast laminates (0.07). Devcon laminates exhibit an intermediate behaviour, with a k value of 0.37. Also regarding the k values, it was found that they decrease with increasing temperatures due to interface detachment and leading to reduced transduction.

Good agreement between the FEM model and the experimental results are obtained for PVDF/epoxy/Vitrovac tri-layer composites allowing the model to be used for optimizing the epoxy

properties (Young modulus and thickness) and the thickness of PVDF in order to obtain the highest ME coupling on the laminates.

The highest ME response of 53.1 V/cmOe obtained for a PVDF (110µm thick)/M-Bond epoxy/Vitrovac laminate. It was also observed the possibility to optimize such value taking into account the Young modulus and thickness of the epoxy and the PVDF thickness, making this laminate an excellent candidate to be used in applications as sensors, actuators, energy harvesting devices and memories.

c) Multi-layer configurations

Multi-layers configurations were simulated for both piezoelectric materials (PZT and PVDF), with different numbers of layers, for free and clamped cases, and according to the external layers material, into:

- M-P multi-layers, in which configuration the composite has one magnetostrictive end and one piezoelectric end (with an even number of layers),
- M-M configuration, in which the composite is sandwiched between to magnetostrictive layers (with an odd number of layers), or
- P-P configuration, where the composite is sandwiched between two piezoelectric materials (also, with an odd number of layers).

In order to establish the influence of the configuration and the ME piezoelectric and magnetostrictive thicknesses on the ME performance, first the multi-layered structure was treated as a device, in which the ME performance of the composite, α_{ME} was the sum of all partial ME coefficients over all piezoelectric layers, and therefore symmetric and asymmetric configurations may be analysed. Later, and in order to establish the relation between piezoelectric thickness, magnetostrictive thickness and configuration performance for symmetric configurations, a unitary ME coefficient was defined, α_{unit}, which could be obtained by the mean value of all partial α_{ME}. Additionally, in order to analyse the efficiency of the materials performance, the ratio of magnetostrictive to piezoelectric thickness is established, d_ms/d_pzo. Particular experiments were analysed in order to establish general trends between configurations, keeping constant the thickness value (of 300µm and 600µm)and divided into multi-layers with different number of

layers (even for M-P configurations, odd number for M-M and P-P configurations). The unitary ME performance of a multi-layer for those particular thickness with different configurations was reported.

i. PZT multi-layer

Due to its mechanical properties as rigid piezoelectric ceramic, free PZT multi-layer configurations show a ME response that is independent of the magnetostrictive thickness, with a slightly lower value of α_{ME} for P-P configurations, when compared with M-M configurations with the same number of piezoelectric layers. Clamped configurations, on the other hand, show a lower ME performance for thinner magnetostrictive layers, below 50-60 μm of Vitrovac thickness and holding the same value of α_{ME} above it.

Piezoelectric thickness show some influence on the ME response of PZT composites, maintaining a constant behaviour for the lower piezoelectric thicknesses (of approx. 86.7 V/cm per piezoelectric layer), decreasing slightly for thicker piezoelectric thicknesses (above 200 μm) for the free case and preserving this behaviour for the clamped case with a greater slope in the decrease of the performance for thicker piezoelectric layers (above 150 μm) in the clamped than in the free structures. It was also noticed that for higher piezoelectric thickness values, P-P configurations have even a faster decrease of their ME performance when compared to M-M configurations with the same number of piezoelectric layers. Asymmetric configurations show no change in the symmetric behaviour of the ME multi-layered composites when compared to the symmetric configurations.

Good agreement was established when comparing trends reported experimentally in the literature for magnetostrictive to piezoelectric thickness ratio, d_ms/d_pzo, for M-M and P-P configurations, with a curve that rapidly increases their α_{unit} with increasing thickness ratio until n=0.3, when saturation is reached. The difference with M-M configurations is that saturation was reached with a higher slope than P-P configurations, to a higher value. Both, M-M and P-P configurations show higher saturation α_{unit} when more layers are included in the configuration with a more homogeneous value for M-M configurations and the exception of the 5-layered P-P

170

configuration, that shows the highest performance of all configurations for thickness ratio above saturation.

Constant composite thicknesses of 300 and 600 μm experiments, show that higher number of piezoelectric layers provide a more homogeneous unitary-α (above 4 piezoelectric layers). All configurations increase their unitary ME performance by increasing their number of piezoelectric layers, with an enhanced performance of M-M configurations over M-P and P-P. The 300 μmcomposites show also a higher performance than 600 μm-composites, below 4 layers of piezoelectric material.

ii. PVDF multi-layer

As mechanical properties of PVDF include high elasticity (when compared to PZT), and its composition is of a semicrystalline material, the structural behaviour of PVDF multi-layered configurations differed largely to the PZT multi-layered ME performance, presenting a more heterogeneous ME behaviour with isolated peak values that introduce difficulties in establishing trends on the influence of thicknesses and configuration to the ME coefficient of the multi-layered composites. Beside mechanical properties of the piezoelectric polymer, there are three variables that favoured this behaviour: the inclusion of more than 3 piezoelectric layers in the multi-layered composite, piezoelectric thicknesses above 150μm, and the configuration in which piezoelectric material (the elastic material) sandwiched the multi-layered composite, the P-P configuration.

For this disordered behaviour it is difficult to establish whether P-P or M-M configurations show a better ME performance, but conclusions may lead to M-M configurations showing a more stable behaviour and trends over different number of layers, while P-P configurations present regions with peaks that went off the expected trend. For configuration with less than 3 piezoelectric layers (and not considering the existence of those isolated peaks) trends show no particular influence of magnetostrictive thickness over the ME performance of free PVDF multi-layered configurations, and a slight decrease of α_{ME} above piezoelectric thicknesses of 150 μm. Clamped configurations, on the other hand, show a ME performance that is dependent of magnetostrictive and piezoelectric thicknesses. Both dependencies, show a curve that decreases from their initial values, reaching a minimal α_{ME}, then presenting increasing curves. The

magnetostrictive thickness curve presents maximal values for low thicknesses, with higher α_{ME} values for P-P configurations than for M-M configurations and, after reaching the minimal α_{ME}, having an increasing curve that never achieves as high ME performances than for low magnetostrictive thicknesses values, with higher values for M-M configurations than for P-P configurations with the same number of piezoelectric layers. Piezoelectric thickness curves for clamped configurations show slightly higher performance for P-P configurations than for M-M configurations for thick piezoelectric layers, with curves that possessed minimal behaviour for thinner piezoelectric layers (10-40µm).

Constant composite thicknesses of 300 and 600 µm experiments revealed that M-M configurations have a more stable unitary α over different number of layers (of about 10.9±0.3 V/cm), while M-P of 600 µm configurations show the best performance for low number of layers, and M-P of 300 µm display the lowest performance for low number of layers. This experiment confirmed also, that P-P configurations do not show clear trends and that the elasticity and semicrystalline composition of PVDF had a large (higher)influence over this configuration, as already established.

Optimization of ME laminate composites was established by the analysis of the structural influence of PVDF´s materials properties when included into different configurations, with a set of different thickness values. Results lead to conclude that for free configurations, thin PVDF thicknesses improve the ME behaviour of the composite, with the possibility of the incorporation of more than one layer to enhance the performance of the structure.

Future work for polymer-based ME laminate composites

Influence of bonding proved to be important in the bi-layer ME performance, and as the piezoelectric polymer is of a highly elastic constitution, and damping effects also modify the response of the ME structure when incorporated into a device. Bonding and damping effects will be enhanced with the incorporation of more layers in the composite and the present structural model should be improved by incorporating these variables into simulations. With the incorporation of damping and bonding effects, multi-layer structural simulation results would be

172

much more approximated and would allow a better understanding of the peak variations presented by P-P configuration.

Resources should be invested into establishing a nonlinear magnetostrictive model that could be coupled to this structural model, in order to obtain more information about the magnetostrictive performance of the material, and to compare different options of magnetostrictive materials.

PVDF´s biocompatibility, elasticity and malleability, makes it suitable for a high number of technological applications. Although laminated composites have been widely studied, there are not enough models that incorporate all the adequate variables that allow to obtain accurate simulations of such piezoelectric material. Therefore, ME models should be improved to obtain better results and be able to predict the performance of those materials before their empirical testing and application into novel devices as sensor, actuators, etc.

ME Model coupling magnetic-elasto-mechanical couple for spheres and fibres

ME spheres, fibres and piezoelectric composites embedding magnetostrictive spheres were simulated by a multiphysics simulation software. All simulation experiments were related to each other. First, 3-D and 2D-axisymmetrical models were used to simulate the ME performance CFO/PVDF spheres according to their size (diameter) and weight concentration (wt.%). Both models show a good agreement in the ME curve over the applied magnetic field leading to conclude that all simulated ME spheres operated in an enhanced behaviour over the same range of applied magnetic field (between 200-2000 Oe), but leading to larger ME effect when sphere size is larger or when higher wt.% of the magnetostrictive CFO is present in the sphere.

Simulation show stable results in all studied structures, leading to establish that the magnetic materials incorporate the most important parameters of the ME curve of the composite, although for thin PVDF´s thicknesses, at high concentration of CFO, PVDF´s morphology and elasticity take more influence on the ME response of the structure, leading to larger ME response. Besides, for lower CFO concentrations and thicker piezoelectric layers, PVDF´s

elasticity diminished the ME response, not being able to transform all deformation into electric potential.

Ellipsoidal shaped ME spheres were analyzed, stretching them and therefore increasing their eccentricity. Results allow to establish that when more normal surface of the magnetostrictive structure is exposed to a magnetic field, lower value of magnetic field is required to increase magnetization and, therefore, smaller magnetic field values for optimal ME coefficient are needed for more eccentrically ellipsoids and fibres. Even more, three particular groups of ME structures are distinguished according to this argument:

i) The spheres (or ellipsoids with low eccentricity) that operate in higher ME fields (200-2000 Oe)show a ME performance in the order of hundreds. By increasing their eccentricity, the ME curve moves slightly to the left and up, obtaining higher ME coefficients, with lower operational magnetic fields.

ii) Medium eccentricity ellipsoidal ME structures, with the highest ME performance, presenting giant ME and operational magnetic fields 20-200 Oe.

iii) Fibre-shaped ellipsoids that operate below 20 Oe, and showing the lowest ME performances.

The result for 50wt.%filler content for the sphere was 182 V/cm at 684 Oe, the medium eccentricity ellipsoidal structure (with eccentricity of 1200) enhanced more than ten times this result, with 4241 V/cm at a magnetic field of 208 Oe. Fibre shaped ellipsoids show higher ME values than the sphere and the axisymmetric fibre: 1601 V/cm at 30 Oe for an ellipsoid with eccentricity of 3200. The axisymmetric fibre, decreases the ME performance and operational magnetic field in a very abrupt way, to 14.7 V/cm at 1.3 Oe.

Finally, the analysis of the cylindrical composite -where CFO spheres were embedded into a PVDF matrix-, led to conclude that the separation of the spheres will determine whether the composed structure will behave as a single structure or as multiple spheres, obtaining higher ME performance at higher magnetic fields when the separation of the spheres is increased. Thus, a value of 27.7 V/cm at 19 Oe is obtained for the case of separation between CFO spheres of 7 nm and 24V/cm at 15 Oe for the experiment with 4 nm separation between CFO spheres.

Future work on polymer based magnetoelectric fibres and spherical structures

Recently discovered biomedical applications for polymer based ME structures is driven large research efforts into this area. There are few investigations on the ME behaviour of such ME structures and their optimization by shape. The present study should be followed by experimental analyses that corroborate the observed results, including the study of filler concentrations and sizes in order to optimize the ME behaviour of ellipsoidal particles and fibres.

A deeper study, with the incorporation of better informatics resources would lead to the design of novel structures with enhanced functionalities for applications in biomedicine and biotechnology, such as drug delivery, ion channelling, etc. besides the improvement of current applications in sensors, actuators and recording devices.

REFERENCES

Allik, H., & Hughes, T. J. R. (1970). Finite element method for piezoelectric vibration. *International Journal for Numerical Methods in Engineering*, *2*, 151–157.

Andrä, W., Häfeli, U., Hergt, R., & Misri, R. (2007). Applications of magnetic particles ion medicine and biology. In H. Kronmüller & S. Parkin (Eds.), *Handbook of Magnetism and Advanced Magnetic Materials, Vol. 4 (Novel Materials)* (pp. 2536–2568). John Wiley & Sons.

Aoyagi, M., Beeby, S., & White, N. (2002). A novel multi-degree-of-freedom thick-film ultrasonic motor. *IEEE Trans Ultrason Ferroelectr Freq Control.*, *49*(2), 151–8.

Ascher, E., Rieder, H., Schmid, H., & Stössel, H. (1966). Some properties of ferromagnetoelectric nickel-iodine boracite, Ni3B7O13I. *J. Appl. Phys.*, *37*, 1404–1405.

Ashcroft, F. M. (2000). *Ion Channels and disease*. San Diego, London: Academic Press.

Astrov, D. N. (1960). The magnetoelectric effect in antiferromagnetics. *Zh. Eksp. Teor. Fiz.*, *38*, 984–985.

Avellaneda, M., & Harshé, G. (1994). Magnetoelectric effect in piezoelectric/magnetostrictive multilayer (2-2) composites. *Journal of Intelligent Material Systems and Structures*, *5*(4), 501–503.

Babu, S. N., Bhimasankaram, T., & Suryanarayana, S. V. (2005). Magnetoelectric effect in metal – PZT laminates. *Bull. Mater. Sci*, *28*(5), 419–422.

Bao, B., & Luo, Y. (2011). Theory of magnetoelectric effect in laminate composites considering two-dimensional internal stresses and equivalent circuit. *J. Appl. Phys.*, *109*(90), 094503. doi:http://dx.doi.org/10.1063/1.3581104

Bar-Cohen, Y., Xue, T., & Lih, S. (1996). Polymer Piezoelectric Transducers for Ultrasonic NDE. *NDTnet*, *1*(9). Retrieved from http://www.ndt.net/article/yosi/yosi.htm

Belouadah, R., Guyomar, D., Guiffard, B., & Zhang, J.-W. (2011). Phase switching phenomenon in magnetoelectric laminate polymer composites: Experiments and modeling. *Physica B: Condensed Matter*, *406*(14), 2821–2826. doi:10.1016/j.physb.2011.04.036

Bent, A. A. (1997). *Active Fiber Composites for Structural Actuation*. Massachusetts Institute of Technology.

Bent, A. A., & Hagood, N. W. (1993). Development of Piezoelectric Fiber Composites for Structural Actuation. In *34th AIAA/ASME/ASCE/AHS Structures, Structural Dynamics and Materials Conference, April, La Jolla, CA, AIAA* (pp. Paper No. 93–1717–CP, 3625–3638).

Berger, H., Kari, S., Gabbert, U., Rodriguez-Ramos, R., Bravo-Castillero, J., Guinovart-Diaz, R., … Maugin, G. a. (2006). Unit cell models of piezoelectric fiber composites for numerical and analytical calculation of effective properties. *Smart Materials and Structures*, *15*(2), 451–458. doi:10.1088/0964-1726/15/2/026

Bibes, M., & Barthelemy, A. (2008). Multiferroics: Towards a magnetoelectric memory. *Nature Materials*, *4*, 425–426.

Bichurin, M. I., Filippov, D. A., Petrov, V. M., Laletsin, V. M., Paddubnaya, N., & Srinivasan, G. (2003a). Resonance magnetoelectric effects in layered magnetostrictive-piezoelectric composites. *Phys. Rev. B*, *68*(13), 132408.

Bichurin, M. I., Filippov, D. A., Petrov, V. M., Laletsin, V. M., Paddubnaya, N., & Srinivasan, G. (2003b). Resonance magnetoelectric effects in layered magnetostrictive-piezoelectric composites. *Physical Review B*, *68*(13), 132408 [4 pages].

Bichurin, M. I., Korneva, I. A., Petrova, V. M., & Lisnevskaya, I. V. (1997). Investigation of magnetoelectric interaction in composite. *Ferroelectrics*, *204*(1), 289–297.

Bichurin, M. I., Petrov, V. M., Averkin, S. V., & Filippov, A. V. (2010). Electromechanical resonance in magnetoelectric layered structures. *Physics of the Solid State*, *52*(10), 2116– 2122.

Bichurin, M. I., Petrov, V. M., Petrov, R. V., Kiliba, Y. V., Bukashev, F. I., Smirnov, A. Y., & Eliseev, D. N. (2002). MAGNETOELECTRIC SENSOR OF MAGNETIC FIELD. *FERROELECTRICS*, *279 and 28*, 199/[365]–202/[368].

Bichurin, M. I., Petrov, V. M., & Srinivasan, G. (2002). Theory of low-frequency magnetoelectric effects in ferromagnetic-ferroelectric layered composites. *Journal of Applied Physics*, *92*(12), 7681. doi:10.1063/1.1522834

Bichurin, M. I., Petrov, V. M., & Srinivasan, G. (2003). Theory of low-frequency magnetoelectric coupling in magnetostrictive-piezoelectric bilayers. *Physical Review B*, *68*(5), 544021–5440213.

Bluhm, H. (2006). *Pulsed Power Systems: Principles and Applications (Google eBook)* (pp. 116–121). Karlsruhe, Germany: Springer-Verlag Berlin Heidelberg New York.

Boomgaard, J. Van Den, Terrell, D. R., Born, R. A. J., & Giller, H. F. J. I. (1974). An in situ grown eutectic magnetoelectric composite material. Part I: Composition and unidirectional solidification. *J. Mater. Sci.*, *9*, 1705–1709.

Bozorth, R. M. (1951). *Ferromagnetism* (p. 279). Princeton, NJ, USA: Van Nostrand Co. Inc., New Jersey.

Brabers, V. A. M. (1995). Progress in spinel ferrite research. In K. H. Buschow (Ed.), *Hand Book of Magnetic Materials, V. 8* (p. 189). Amsterdam: North-Holand.

Bune, A. V., Zhu, C., Ducharme, S., Blinov, L. M., Fridkin, V. M., Palto, S. P., ... G., Y. S. (1999). "Piezoelectric and Pyroelectic Properties of Ferroelectric Langmuir- Blodgett Polymer Films",. *Journal of Applied Physics*, *85*(11), 7869–7873.

Burrell, K. H., Kaplan, D. H., Gohil, P., Nilson, D. G., Groebner, R. J., & Thomas, D. M. (2001). Improved charge coupled device detectors for the edge charge exchange spectroscopy system on the DIII-D tokamak. *Review Sci. Instrum.*, *72*(1), 1028 – 1033.

Cai, N., Nan, C.-W., Zhai, J., & Lin, Y. (2004). Large high-frequency magnetoelectric response in laminated composites of piezoelectric ceramics, rare-earth iron alloys and polymer. *Applied Physics Letters*, *84*(18), 3516. doi:10.1063/1.1739277

Cai, N., Zhai, J., Nan, C. W., Lin, Y., & Z. Shi. (2003). Dielectric, ferroelectric, magnetic, and magnetoelectric properties of multiferroic laminated composites. *Phys. Rev. B*, *68*(22), 224103 [7 pages].

Cammarata, R. C., & K. Sieradzki. (1994). Surface and Interface Stresses. *Annual Review of Materials Science*, *24*, 215–234. doi:10.1146/annurev.ms.24.080194.001243

Caruso, M. J., Bratland, T., Smith, C. H., & Schneider, R. (1998). A new perspective on magnetic field sensing. In *Sensors Expo Proceedings, Detroit, USA* (p. 195).

Carvell, J., Cheng, R., & Yang, Q. (2013). Induced magneto-electric coupling at ferroelectric/ferromagnetic interface. *Journal of Applied Physics*, *113*(17), 17C715–17C715–3.

Chakrabarti, S. (2011). *Modeling of 3D Magnetostrictive Systems with Application to Galfenol and Terfenol-D Transducers*. Graduate School of the Ohio State Uiversity.

Chang, C. M., & Carman, G. P. (2007). Modeling shear lag and demagnetization effects in magneto-electric laminate composites. *Physical Review B*, *76*(13), 134116 [7 pages].

Chattopadhyay, A., Li, J., & Haozhong, G. (1999). Coupled thermo-piezoelectric-mechanical model for smart composite laminate. *AIAA Journal*, *37*(12).

Chau, K. H., Wong, Y. W., & Shin, F. G. (2009). Magnetoelectric effect of polymer electrolyte composites with Terfenol-D and lead zirconate titanate inclusions. *Appl. Phys. Lett.*, *94*(20), 202902.

Chen, H. S. (1980). Glassy metals. *Rep. Prog. Phys.*, *43*, 353. doi:10.1088/0034-4885/43/4/001

Chiang, L. Y., & Chaikin, P. M. (1990). *Advanced Organic Solid State Materials*. Boston: Materials Research Society.

Chiba, H., Atou, T., & Syono, Y. (1997). Magnetic and electrical properties of Bi1-xSrxMnO3. *J. Solid State Chem.*, *132*, 139–143.

Chikazumi, S. (1997). *Physics of Ferromagnetism* (2nd ed.). Oxford: Clarendon Press.

Chiolerio, A., Quaglio, M., Lamberti, A., Celegato, F., Balma, D., & Allia, P. (2012). Magnetoelastic coupling in multilayered ferroelectric/ferromagnetic thin films: A quantitative evaluation. *Applied Surface Science*, *258*(20), 8072–8077.

Clark, A. E., & Belson, H. S. (1972). Giant Room-Temperature magnetostrictions in TbFe2 and dyFe2. *Physical Review B*, *5*, 3642–3644.

Coey, J. M. D. (2010). *Magnetism and Magnetic Materials* (pp. 555–565). Cambridge University Press, USA.

Comsol Multiphysics Library, & Multiphysics, C. (2011). Nonlinear Magnetostrictive Transducer. *http://www.comsol.com/model/download/186793/models.sme.nonlinear_magnetostriction.pdf*, 1–24. Retrieved from http://www.comsol.com/model/download/186793/models.sme.nonlinear_magnetostriction.pdf

COMSOLMultiphysics. (1998). *COMSOL 4.1. COMSOL 4.1* (p. 2010).

Cottinet, P., Guyomar, D., Guiffard, B., Lebrun, L., Putson, C., & Lgef, I. D. L. (2004). Electrostrictive polymers as high-performance electroactive polymers for energy harvesting, 185–209.

Coufal, H., Dhar, L., & Mee, C. D. (2006). Materials for Magnetic Data Storage: The Ongoing Quest for Superior Magnetic Materials. *MRS Bull.*, *31*(5), 374–378.

Crawley, E. F., & Lazarus, K. B. (1991). Induced strain actuation of isotropic and anisotropic plates. *AIAA Journal*, *29*(6), 944–951.

CTSElectronichsComponents, I. (2014). PZT5A & 5H Materials Technical Data (Typical Values).

Culshaw, B. (1996). *Smart structures and materials* (p. 207). Boston, MA: Artech House.

Dee, R. H. (2006). Magnetic Tape: The Challenge of Reaching Hard-Disk-Drive Data Densities on Flexible Media. *MRS Bulletin*, *31*(5), 404–408.

Destruel, P., Rojas, F. S., Tougne, D., & Hoang-The-Giam. (1984). Pressure and Temperature Dependence of the Electromechanical Properties of Polarized Polyvinylidene Fluoride Films. *Journal of Applied Physics*, *56*(11), 3298–3303.

Dong, S., Cheng, J., Li, J.-F., & Viehland, D. (2003). Enhanced magnetoelectric effects in laminate composites of Terfenol-D/Pb(Zr,Ti)O3 under resonant drive. *Appl. Phys. Lett.*, *83*(23), 4812.

Dong, S., Li, J., & Viehland, D. (2003). Longitudinal and transverse magnetoelectric voltage coefficients of magnetostrictive/piezoelectric laminate composite: theory. *IEEE Trans Ultrason Ferroelectr Freq Control.*, *50*(10), 1253–61.

Dong, S., Li, J.-F., & Viehland, D. (2004). Longitudinal and Transverse Magneto-Electric Effect: II. Experiments. *IEEE Trans. On Ultrasonics, Ferroelectrics and Frequency Control*, *51*(7), 794–799.

Dong, S. X., Li, J. F., & Viehland, D. (2004). Vortex Magnetic Field Sensor Based on Ring-type Magnetoelectric Laminate. *Appl. Phys. Lett.*, *85*, 2307–2309.

Dong, S. X., Li, J. F., & Viehland, D. (2006). Magneto-electric coupling, efficiency and voltage gain effect in piezoelectric-piezomagnetic lam- inate composite: Theory and analysis. *J. Mater. Sci.*, *41*(1), 97–106.

Dong, S. X., Zhai, J. Y., Li, J. F., & Viehland, D. (2006). Small dc magnetic field response of magnetoelectric laminate composites. *Applied Physics Letters*, *88*(8), 082907 – 082907–2.

Dong, S. X., Zhai, J. Y., Li, J. F., Viehland, D., & Priya, S. (2008). Multimodal system for harvesting magnetic and mechanical energy. *Appl Phys Lett*, *93*(10), 103511 – 103511–3.

Dong, S. X., Zhai, J. Y., Xing, Z. P., Li, J. F., & D. Viehland. (2005). Extremely low frequency response of magnetoelectric multilayer composites. *Appl. Phys. Lett.*, *86*, 102901.

Dong, S., Zhai, J., Bai, F., Li, J.-F., & Viehland, D. (2005). Push-pull mode magnetostrictive/piezoelectric laminate composite with an enhanced magnetoelectric voltage coefficient. *Applied Physics Letters*, *87*(6).

Dong, S., Zhai, J., Li, J., & Viehland, D. (2006a). Near-ideal magnetoelectricity in high-permeability magnetostrictive/piezofiber laminates with a (2-1) connectivity. *Applied Physics Letters*, *89*(25), 252904. doi:10.1063/1.2420772

Dong, S., Zhai, J., Li, J.-F., & Viehland, D. (2006b). Magneto-electric effect in Terfenol-D/PZT/mu-metal composite. *Applied Physics Letters*, *89*(122903), 122903.

Dong, X. W., Wang, B., Wang, K. F., Wan, J. G., & Liu, J. –M. (2009). Ultra-sensitive detection of magnetic field and its direction using bilayer PVDF/Metglas laminate. *Sensors and Actuators A: Physical*, *153*(1), 64–68. doi:10.1016/j.sna.2009.04.033

Duc, N. H., & Giang, D. T. H. (2008). Magnetic sensors based on piezoelectric- magnetostrictive composites. *J. Alloys Compd. 2*, *449*, 214.

180

Ducharme, S., Reece, T. J., Othon, C. M., & Rannow, R. K. (2005). Ferroelectric polymer Langmuir-Blodgett films for nonvolatile memory applications. *Device and Materials Reliability, IEEE Transactions*, *5*(4), 720–735.

Dzyaloshinskii, I. E. (1959). On the magneto-electrical effects in antiferromagnets. *Zh. Eksp. Teor. Fiz.*, *37*, 881–882.

Eer Nisse, E. P. (1967). Variational method for electroelastic vibration analysis. *IEEE Transactions On Sonics And Ultrasonics*, *14*(4), 153–160.

Eerenstein, W., Mathur, N. D., & Scott, J. F. (2006). Multiferroic and magnetoelectric materials. *Nature*, *442*(7104), 759–65. doi:10.1038/nature05023

Eerenstein, W., Morrison, F. D., Dho, J., Blamire, M. G., Scott, J. F., & Mathur, N. D. (2005a). Comment on "Epitaxial BiFeO3 Multiferroic Thin Film Heterostructures. *Science*, *307*(5713), 1203.

Eerenstein, W., Morrison, F. D., Dho, J., Blamire, M. G., Scott, J. F., & Mathur, N. D. (2005b). Comment on Epitaxial BiFeO3 multiferroic thin film heterostructures. *Science*, *419*(1203a).

Engdahl, G., & Mayergoyz, I. D. (2000). *Handbook of Giant Magnetostrictive Materials*. (G. Engdahl, Ed.). Maryland, USA: Academic Press.

Esterly, D. M. (2002). *Manufacturing of Poly (vinylidene fluoride) and Evaluation of its Mechanical Properties*. Virginia Polytechnic Institute and State University.

Fang, F., Zhao, C., & Yang, W. (2011). Thickness effects on magnetoelectric coupling for Metglas/PZT/Metglas laminates. *Science China: Physics, Mechanics and Astronomy Physics, Mechanics & Astronomy*, *54*(4), 581–585.

Fang, Z., Lu, S. G., Li, F., Datta, S., Zhang, Q. M., & El Tahchi, M. (2009). Enhancing the magnetoelectric response of Metglas/polyvinylidene fluoride laminates by exploiting the flux concentration effect. *Applied Physics Letters*, *95*(11), 112903. doi:10.1063/1.3231614

Fang, Z., Mokhariwale, N., Li, F., Datta, S., & Zhang, Q. M. (2011). Magnetoelectric Sensors With Directly Integrated Charge Sensitive Readout Circuit—Improved Field Sensitivity and Signal-to-Noise Ratio. *IEEE Sens. J.*, *11*(10), 2260 – 2265.

Farea, A. M. M., Kumar, S., Batoo, K. M., Yousef, A., Lee, C., & Alimuddin, G. (2008). Structure and electrical properties of Co0.5CdxFe2.5-xO4 ferrites. *Journal of Alloys and Compounds*, *464*, 361–360.

Filippov, D. A., Bichurin, M. I., Petrov, V. M., Laletin, V. M., Poddubnaya, N. N., & Srinivasan, G. (2004). Giant magnetoelectric effect in composite materials in the region of electromechanical resonance. *Technical Physics Letters*, *30*(1), 6–8.

Filippov, D. A., Laletin, U., & Srinivasan, G. (2007). Resonance magnetoelectric effects inmagnetostrictive-piezoelectric threelayer structures. *Journal of Applied Physics*, *102*(9), 093901 [4 pages].

Folen, V. J., Rado, G. T., & Stalder, E. W. (1961). Anisotropy of the magnetoelectric effect in Cr2O3. *Phys. Rev. Lett.*, *6*, 607–608.

Fonteyn, K., Belahcen, A., Kouhia, R., Rasilo, P., & Arkkio, A. (2010). FEM for directly coupled magneto-mechanical phenomena in electrical machines. *IEEE Transactions on Magnetics*, *46*(8), 2923–2926.

Fuentes, M. E., Fuentes, L., Olivera, R., & García, M. (2007). Meso- and nano- magnetoelectricity : a review. *Revista Mexicana de Física, Enero*, *53*(1), 21–29.

Furukawa, T. (1989). Ferroelectric Properties of Vinylidene Fluoride Copolymers. *Phase Transitions*, *18*, 143–211.

Gandhi, M. V., & Thompson, B. S. (1992). *Smart materials and structures* (p. 310). London: Chapman and Hall.

Gao, J. (2013). *Magnetoelectric (ME) composites and functional devices based on ME effect Magnetoelectric (ME) composites and functional devices based on ME effect.*

George, M., Nair, S. S., Malini, K. A., Joy, P. A., & Anantharaman, M. R. (2007). Finite size effects on the electrical properties of sol–gel synthesized CoFe 2 O 4 powders: deviation from Maxwell–Wagner theory and evidence of surface polarization effects. *Journal of Physics D: Applied Physics*, *40*(6), 1593. Retrieved from http://stacks.iop.org/0022-3727/40/i=6/a=001

Giang, D. T. H., & Duc, N. H. (2009). Magnetoelectric sensor for microtesla magnetic-fields based on (Fe80Co20)78Si12B10/PZT laminates. *Sensors and Actuators A: Physical*, *149*(2), 229–232.

Graham, F. (2009). *Development ad Validation of a Bidirectionally coupled Magnetoelastic FEM Model for current Driven Magnetostrictive Devices*. University of Maryland.

Graham, F. C., Mudivarthi, C., Datta, S., & Flatau, A. B. (2009). Modeling of a Galfenol transducer using the bidirectionally coupled magnetoelastic model. *Smart Materials and Structures*, *18*(10), 104013.

Gregorio, R. J. ., & Ueno, E. M. (1999). Effect of Crystalline Phase, Orientation and Temperature on the Dielectric Properties of PVDF. *Journal of Material Science*, *34*, 4489–4500.

Grunwald, A., & Olabi, A. G. (2008). Design of a magnetostrictive (MS) actuator. *Sensors and Actuators, A: Physical*, *144*, 161–175.

Guduru, R., Liang, P., Runowicz, C., Nair, M., Atluri, V., & Khizroev, S. (2013). Magneto-electric Nanoparticles to Enable Field-controlled High-Specificity Drug Delivery to Eradicate Ovarian Cancer Cells. *Sci. Rep.*, *3*. Retrieved from http://dx.doi.org/10.1038/srep02953

Guo, Y., Liu, Y., Wang, J., Withers, R. L., Chen, H., Jin, L., & Smith, P. (2010). Giant Magnetodielectric Effect in 0–3 Ni0.5Zn0.5Fe2O4-Poly(vinylidene-fluoride) Nanocomposite Films. *J. Phys. Chem. C*, *114*(32), 13861–13866.

Guo, Y. Y., Zhou, J. P., & Liu, P. (2010). Magnetoelectric characteristics around resonance frequency under magnetic field in Pb(Zr,Ti)O3/Terfenol-D laminate composite. *Curr. Appl. Phys.*, *10*(4), 1092–1095.

Gutierrez, J., Lasheras, A., Barandiaran, J. M., Vilas, J. L., Sebastian, M. S., & Leon, L. M. (2012). Temperature Response of Magnetostrictive/Piezoelectric Polymer Magnetoelectric Laminates. In *Materials and Applications for Sensors and Transducers* (Vol. 495, pp. 351–354).

Guyomar, D., Guiffard, B., Belouadah, R., & Petit, L. (2008). Two-phase magnetoelectric nanopowder/polyurethane composites. *J. Appl. Phys.*, *104*(074902). doi:http://dx.doi.org/10.1063/1.2985904

Guyomar, D., Matei, D. F., Guiffard, B., Le, Q., & Belouadah, R. (2009). Magnetoelectricity in polyurethane films loaded with different magnetic particles. *Mater. Lett. 2009 , 63 , 611 .*, *63*(4), 611–613.

Ha, S. K., Keilers, C., & Chang, F. K. (1992). Finite element analysis of composite structures containing distributed piezoceramic sensors and actuators. *AIAA Journal*, *30*(3), 772–780.

Hambe, M., Petraru, A., Pertsev, N. A., Munroe, P., Nagarajan, V., & Kohlstedt, H. (2010). Crossing an Interface: Ferroelectric Control of Tunnel Currents in Magnetic Complex Oxide Heterostructures. *Adv. Funct. Mater.*, *20*, 2436–2441.

Hao-Miao Zhou, Li-Ming Xuan, Chao Li, J. W., Zhou, H.-M., Xuan, L.-M., Li, C., & Wei, J. (2011). Numerical simulation of nonlinear magnetic–mechanical–electric coupling effect in laminated magnetoelectric composites. *Journal of Magnetism and Magnetic Materials*, *323*(22), 2802–2807. doi:10.1016/j.jmmm.2011.06.018

Harshe, G. (1991). *Magnetoelectric effect in piezoelectric- magnetostrictive composites*. The Pennsylvania State University.

Harshe, G., Dougherty, J. P., & Newnham, R. E. (1993). Theoretical modeling of multilayer magnetoelectric composites. *Int. J. Appl. Electromagn. Mater*, *4*(2), 145–159.

Harshe, G., Dougherty, J. P., & Newnham, R. E. (1993). Theoretical Modelling of Multilayer Magnetoelectric Composites. *Int. J. Appl. Electromagn. Mater.*, *4*(145).

Heyliger, P., Pei, K. C., & Saravanos, D. (1996). Layerwise mechanics and finite element model for laminated piezoelectric shells. *AIAA Journal*, *34*(11), 2353–2360.

Hilczer, B., & Malecki, J. (1986). *Electrets*. Amsterdam: Elsevier.

Hilding, J., Grulke, E. A., Zhang, Z. G., & F. Lockwood. (2003). Dispersion of carbon nanotubes in liquids. *J. Dispers. Sci. Technol.*, *24*, 1–41.

Hille, B. (1992). *Ionic Channels of Excitable Membranes*. Sunderland Massachussetts: Sinauer Associates Inc.

Hong, W., Ren-Fa, S., & Xue-Zhong, W. (2005). A theoretical study on symmetrical magnetostrictive/piezoelectric laminated composite. *Acta Phys. Sin.*, *54*(3), 1426. doi:doi: 10.7498/aps.54.1426

Hopfinger, A. J. (1973). *Conformational Properties of Macromolecules*. New York: Academic Press.

Hu, J.-M., Li, Z., Wang, J., & Nan, C. W. (2010). Electric-field control of strain-mediated magnetoelectric random access memory. *J. Appl. Phys.*, *107*(9), 093912 – 093912–10.

Hur, N., Park, S., Sharma, P. A., Ahn, J. S., Guha1, S., & Cheong, S.-W. (2004). Electric polarization reversal and memory in a multiferroic material induced by magnetic fields". *Nature*, *429*, 392–395.

Hwang, W. S., & Park, H. C. (1993). Finite element modeling of piezoelectric sensors and actuators. *AIAA Journal*, *31*(5), 930–937.

IEEE American National Standards Institute, Ultrasonics, Ferroelectrics, and F. C. S., Committee., S., & Engineers., I. of E. and E. (1988). *IEEE Standard on Piezoelectricity* (p. Std. 176 IEEE/ANSI). New York, N.Y.: Institute of Electrical and Electronics Engineers, ©1988.

Inderherbergh, J. (1991). Polyvinylidene Fluoride (PVDF) Appearance, General Properties and Processing. *Ferroelectrics*, *115*, 295–302.

Inoue, A. (2000). Stabilization of metallic supercooled liquid and bulk amorphous alloys. *Acta Materialia*, *48*, 279–306. doi:10.1016/S1359-6454(99)00300-6

Inoue, S., Inoue, K., Koterazawa, K., & Mizuuchi, K. (2003). Shape memory beha v ior of Fe Á Pd alloy thin films prepared by dc magnetron sputtering, *339*, 29–34.

IRE (The Institute of Radio Engineers). (1958). IRE Standards on piezoelectric crystals: Determination of the elastic, piezoelectric and dielectric constant-The electromechanical coupling fctor. *Proceedings of 58 IRE*, *46*(4), 764–778. doi:10.1109/JRPROC.1958.286778

J.Wu, G., Zhang, R., Li, X., & Zhang, N. (2011). Resonance magnetoelectric effects in disk-ring (piezoelectric—magnetostrictive) composite structure. *Journal of Applied Physics*, *110*(12), 124103 [5 pages].

Jiles, D. C. (1991). *Introduction to magnetism and magnetic materials*. New York: Chapman and Hall.

Jiles, D. C., Ostenson, J. E., Owen, C. V., & Chang, T. T. (1988). Barkhausen Effect and Discontinuous Magnetostriction in Terfenol-D. *J. Appl. Phys.*, *64*, 5417.

Jin, J., Lu, S. G., Chanthad, C., Zhang, Q. M., Haque, M. A., & Wang, Q. (2011). Multiferroic Polymer Composites with Greatly Enhanced Magnetoelectric Effect under a Low Magnetic Bias. *Adv. Mater.*, *23*, 3853–3858.

Julliere, M. (1975). Tunneling between ferromagnetic films. *Phys. Lett. A*, *54*(3), 225–226.

Kambale, R. C., Jeong, D.-Y., & Ryu, J. (2012). Current Status of Magnetoelectric Composite Thin/Thick Films. *Advances in Condensed Matter Physics*, *2012*, 1–15. doi:10.1155/2012/824643

Karedla, R., Love, J. S., & B. G. Wherry. (1994). Caching strategies to improve disk system performance. *Computer*, *27*(3), 38–46.

Kargol, A., Malkinski, L., & Caruntu, G. (2012). Biomedical Applications of Multiferroic Nanoparticles. In L. Malkinski (Ed.), *Advanced Magnetic Materials* (pp. 89–118). Retrieved from http://www.intechopen.com/download/books/books_isbn/978-953-51-0637-1#page=101

Kim, H., Tadesse, Y., & Priya, S. (2009). Chapter 1. Piezoelectric Energy Harvesting. In S. Priya & D. J. Inman (Eds.), *Energy Harvesting Technologies* (pp. 3–38). New York, NY, USA: Springer.

Kimura, T., Kawamoto, S., Yamada, I., Azuma, M., Takano, M., & Yokura, Y. (2003). Magnetocapacitance effect in multiferroic BiMnO3. *Phys. Rev. B 67*, *67*(R180401).

Klement, W., Willens, R. H., & Duwez, P. (1960). Non-crystalline Structure in Solidified Gold-Silicon Alloys. *Nature*, *187*(4740), 869–870. doi:10.1038/187869b0

Koon, N. C., Schindler, A. I., & Carter, F. L. (1971). Giat Magetostriction in cubic rare earth-iron compounds of the type RFe2. *Physics Letters A*, *37*, 412–414.

Kukhar, V. G., Pertsev, N. A., & Kholkin, A. L. (2010). Thermodynamic theory of strain-mediated direct magnetoelectric effect in multiferroic film–substrate hybrids. *Nanotechnology*, *21*(26), 265701.

Lacheisserie, E. T., Gignoux, D., Schlenker, M., & Eds. (2004). *Magnetism: Fundamentals, Vol. 1*. (E. T. Lacheisserie, D. Gignoux, & M. Schlenker, Eds.). New York, NY, USA: Springer New York.

Landau, L. D., & Lifshitz, E. M. (1959). *"Electrodynamics of continuous media."* Moscow: Fizmatgiz.

Lee, H.-J., & Saravanos, D. A. (1996). Coupled layerwise analysis of thermopiezoelectric composite beams. *AIAA Journal*, *34*(6), 1231–1237.

184

Lee, M. K., Nath, T. K., Eom, C.-B., Smoak, M. C., & Tsui, F. (2000). Strain modification of epitaxial perovskite oxide thin films using structural transitions of ferroelectric BaTiO3 substrate. *Appl. Phys. Lett.*, *77*, 3547–3549.

Lerch, R. (1990). Simulation of piezoelectric devices by two- and three-dimensional finite elements. *IEEE Transactions on Ultrasonics, Ferroelectrics, and Frequency Control*, *37*(3), 233–247.

Leung, C. M., Or, S. W., Zhang, S., & Ho, S. L. (2010). Ring-type electric current sensor based on ring-shaped magnetoelectric laminate of epoxy-bonded Tb0.3Dy0.7Fe1.92 short-fiber/NdFeB magnet magnetostrictive composite and Pb(Zr, Ti)O3 piezoelectric ceramic. *J. Appl. Phys.*, *107*(9), 09D918 – 09D918–3.

Li, M., Hasanyan, D., Wang, Y., Gao, J., Li, J., & Viehland, D. (2012). Theoretical modelling of magnetoelectric effects in multi-push–pull mode Metglas/piezo-fibre laminates. *Journal of Physics D: Applied Physics*, *45*, 355002.

Li, M., Wang, Y., Gao, J., Gray, D., Li, J., & Viehland, D. (2012). Enhancement in magnetic field sensitivity and reduction in equivalent magnetic noise by magnetoelectric laminate stacks. *J. Appl. Phys.*, *111*(10), 104504.

Li, P., Wen, Y., Liu, P., Li, X., & Jia, C. (2010). A magnetoelectric energy harvester and management circuit for wireless sensor network. *Sensors and Actuators A: Physical*, *157*(1), 100–106. doi:10.1016/j.sna.2009.11.007

Libermann, H., & Graham, C. (1976). Production Of Amorphous Alloy Ribbons And Effects Of Apparatus Parameters On Ribbon Dimensions. *IEEE Transactions on Magnetics*, *12*(6), 921. doi:10.1109/TMAG.1976.1059201

Lin, Y. H., Cai, N., Zhai, J. Y., Liu, G., & Nan, C. W. (2005). Giant magnetoelectric effect in multiferroic laminated composites. *Phys. Rev. B*, *72*(1), 012405 [4 pages].

Lin, Y., & Sodano, H. (2008). Concept and model of a piezoelectric structural fiber for multifunctional composites. *Composites Science and Technology*, *6932*, 1–9. doi:10.1117/12.776524

Linares, A., & Acosta, J. L. (1995). Pyro-piezoelectrics Polymers Materials-I. Effect of Addition of PVA and/or PMMA on the Overall Crystallization Kinetics of PVDF from Isothermal and Non-isothermal Data. *European Polymer Journal*, *31*(7), 615–619.

Linnemann, K., Klinkel, S., & Wagner, W. (2009). A constitutive Model for magnetostrictive and piezoelectric materials. *International Journal of Solids and Structures*, *Volume 46*(5), 1149–1166.

Liu, G., Nan, C. W., Cai, N., & Lin, Y. (2004). Dependence of giant magnetoelectric effect on interfacial bonding for multiferroic laminated composites of rare-earth-iron alloys and lead-zirconate-titanate. *Journal of Applied Physics*, *95*(5), 2660–2664.

Liu, G., Nan, C.-W., Cai, N., & Lin, Y. (2004). Calculations of giant magnetoelectric effect in multiferroic composites of rare-earth-iron alloys and PZT by finite element method. *International Journal of Solids and Structures*, *41*(16-17), 4423–4434. doi:10.1016/j.ijsolstr.2004.03.022

Liu, Y. Y., Xie, S. H., Jin, G., & Li, J. Y. (2009). The effective magnetoelectric coefficients of polycrystalline Cr2O3 annealed in perpendicular electric and magnetic fields. *Journal of Applied Physics*, *105*(7), 073917 – 073917–5.

Lopatin, S., Lopatin, I., & Lisnevskaya, I. (1994). Magnetoelectric PZT/ferrite composite material. *Ferroelectrics*, *162*(1), 63–68.

Lottermoser, T., Lonkai, T., Amann, U., Hohlwein, D., Ihringer, J., & Fiebig, M. (2004). Magnetic phase control by an electric field. *Nature*, *430*, 541–544.

Lovinger, A. J. (1982). *"Poly(vinylidene fluoride)", Developments in Crystalline Polymers. Applied Science Publishers Ltd, Englewood, NJ, 1982.* Englewood, NJ: Applied Science Publishers Ltd.

Lu, S. G., Fang, Z., Furman, E., Wang, Y., Zhang, Q. M., Mudryk, Y., ... Nan, C. W. (2010). Thermally mediated multiferroic composites for the magnetoelectric materials. *Appl. Phys. Lett.*, *96*, 102902. doi:http://dx.doi.org/10.1063/1.3358133

Lu, S., Jin, J., Zhou, X., Fang, Z., Wang, Q., & Zhang, Q. (2011). Large magnetoelectric coupling coefficient in poly (vinylidene fluoride-hexafluoropropylene)/Metglas laminates. *Journal of Applied Physics*, *110*(10), 104103–104105.

Lupeiko, T. G., Lisnevskaya, I. V., Chkheidze, M. D., & Zvyagintsev, B. I. (1995). Laminated magnetoelectric composites based on nickel ferrite and PZT materials. *Inorganic Materials*, *31*(9), 1139–1142.

Ma, J., Hu, J., Li, Z., & Nan, C.-W. (2011). Recent Progress in Multiferroic Magnetoelectric Composites: from Bulk to Thin Films. *Adv. Mater.*, *23*(9), 1062–1087.

Ma, J., Li, Z., Lin, Y. H., & Nan, C. W. (2011). A novel frequency multiplier based on magnetoelectric laminate. *Journal of Magnetism and Magnetic Materials*, *323*(1), 101–103.

Martins, P., & Lanceros-Méndez, S. (2013). Polymer-Based Magnetoelectric Materials. *Advanced Functional Materials*, *23*(27), 3371–3385. doi:10.1002/adfm.201202780

Martins, P., Lasheras, A., Gutierrez, J., Barandiaran, J. M., Orue, I., & Lanceros-Mendez, S. (2011). Optimizing piezoelectric and magnetoelectric responses on CoFe2O4/P(VDF-TrFE) nanocomposites. *J. Phys. D: Appl. Phys.*, *44*(49), 495303.

Martins, P., Lopes, A. C., & Lanceros-Mendez, S. (2013). Electroactive phases of poly(vinylidene fluoride): Determination, processing and applications. *Progress in Polymer Science*, *39*(4), 683–706. doi:http://dx.doi.org/10.1016/j.progpolymsci.2013.07.006.

Martins, P., Moya, X., Phillips, L. C., Kar-Narayan, S., Mathur, N. D., & Lanceros-Mendez, S. (2011). Linear anhysteretic direct magnetoelectric effect in Ni0.5Zn0.5Fe2O4/poly(vinylidene fluoride-trifluoroethylene) 0-3 nanocomposites. *J. Phys. D: Appl. Phys.*, *44*(48), 482001–482005.

Marutake, M. (1995). The Days When Piezoelectric PVDF Was Discovered. *Ferroelectrics,171*, 5–6.

Mielke, A., & Roubícek, T. (2003). A Rate-Independent Model for Inelastic Behavior of Shape-Memory Alloys. *Multiscale Model. Simul.*, *1*(4), 571–597. doi:10.1137/S1540345903422860.

Mindlin, R. D. (1974). Equations of high frequency vibrations of thermopiezoelectric crystal plates. *International Journal of Solids Structure*, *10*, 625–637.

Moetakef, M. A., Lawrence, K. L., Joshi, S. P., & Shiakolas, P. S. (1995). Closed-form expressions for higher order electroelastic tetrahedral Elements. *AIAA Journal*, *33*(1), 136–142.

Moreira dos Santos, A., Parasharb, S., Rajub, A. R., Zhaoc, Y. S., Cheethama, A. K., & Rao, C. N. R. (2002). Evidence for the likely occurrence of magnetoferroelectricity in the simple perovskite, BiMnO3. *Solid State Commun.*, *122*, 49–52.

Moss, S. D., McLeod, J. E., Powlesland, I. G., & Galea, S. C. (2012). A Bi-axial Magnetoelectric Vibration Energy Harvester. *Sens. Act. A: Phys.*, *175*, 165–168.

Muthuselvam, I. P., & Bhowmik, R. N. (2009). Structural phase stability and magnetism in Co2FeO4 spinel oxide. *Solid State Sciences*, *11*(3), 719–725. doi:10.1016/j.solidstatesciences.2008.10.012

Nan, C., Bichurin, M. I., Dong, S., Viehland, D., & Srinivasan, G. (2008). Multiferroic magnetoelectric composites: Historical perspective, status, and future directions. *Journal of Applied Physics*, *103*(031101), 1–35. doi:10.1063/1.2836410

Nan, C. W. (2012). Magnetoelectric Effect and Green´s Function Method. In M. I. Bichurin & D. Viehland (Eds.), *Magnetoelectricity in Composites* (pp. 107–132). Singapore: Pan Stanford Publishing Pte Ltd.

Nan, C. W., Cai, N., Liu, L., Zhai, J., Ye, Y., & Lin, Y. (2003). Coupled magnetic–electric properties and critical behavior in multiferroic particulate composites. *J. Appl. Phys.*, *94*(9), 5930 – 5936.

Nan, C. W., Li, M., Feng, X. Q., & Yu, S. W. (2001). Possible giant magnetoelectric effect of ferromagnetic rare-earth-iron-alloys-filled ferroelectric polymers. *Appl. Phys. Lett.*, *78*(17), 2527–2529.

Nan, C. W., Lin, Y., & Huang, J. H. (2002). Magnetoelectricity of multiferroic composites. *Ferroelectrics*, *280*(1), 153–163.

Nan, C. W., Liu, G., & Lin, Y. H. (2003). "Influence of interfacial bonding on giant magnetoelectric response of multiferroic laminated composites of Tb1–xDyxFe2 and PbZrxTi1–xO3,." *Applied Physics Letters*, *83*(21), 4366–4368.

Nan, C. W., Liu, L., Cai, N., Zhai, J., Ye, Y., Lin, Y. H., … Xiong, C. X. (2002). A three-phase magnetoelectric composite of piezoelectric ceramics, rare-earth iron alloys, and polymer. *Appl. Phys. Lett.*, *81*, 3831–3833.

Nan, C.-W. (1994). Magnetoelectric effect in composites of piezoelectric and piezomagnetic phases. *Physical Review B (Condensed Matter)*, *50*(9), 6082–6088.

Nan, C.-W., Cai, N., Shi, Z., Zhai, J., Liu, G., & Lin, Y. (2005). Large magnetoelectric response in multiferroic polymer-based composites. *Phys. Rev. B*, *71*(1), 014102 – 014107.

Nan, C.-W., Li, M., & Huang, J. H. (2001). Calculations of giant magnetoelectric effects in ferroic composites of rare-earth-iron alloys and ferroelectric polymers. *Physical Review B - Condensed Matter and Materials Physics*, *63*(14), 144415–144424.

Nechibvute, A., Chawanda, A., & Luhanga, P. (2012). Finite Element Modeling of a Piezoelectric Composite Beam and Comparative Performance Study of Piezoelectric Materials for Voltage Generation. *ISRN Materials Science*, *2012*, 1–11. doi:10.5402/2012/921361

Nersessian, N., Or, S. W., & Carman, G. P. (2004). Magnetoelectric Laminates of Terfenol-D. Composite and Lead Zirconate Titanate Ceramic Laminates. *IEEE Trans. Magn.*, *40*(4), 2646–2648.

Nersessian, N., Or, S. W., Member, S., & Carman, G. P. (2004). Magnetoelectric Behavior of Terfenol-D Composite and Lead Zirconate Titanate Ceramic Laminates, *40*(4), 2646–2648.

Newnham, R. E., Skinner, L. E., & Cross, D. P. (1978). Connectivity and Piezoelectric Composites. *Mater. Res. Bull.*, *13*, 525.

Nguyen, T. T., Bouillault, F., Daniel, L., & Mininger, X. (2011). Finite element modeling of magnetic field sensors based on nonlinear magnetoelectric effect. *Journal of Applied Physics*, *109*(8), 084904 [8 pages].

Ojovana, M. I., & Lee, W. (Bill) E. (2010). Connectivity and glass transition in disordered oxide systems. *Journal of Non-Crystalline Solids*, *356*(44–49), 2534–2540.

Okuno, S. N., Hashimoto, S., & Inomata, K. (1992). Preferred crystal orientation of cobalt ferrite thin films induced by ion bombardment during deposition. *Journal of Applied Physics*, *71*(12), 5926. doi:10.1063/1.350442

Pan, D. a, Bai, Y., Chu, W. Y., & Qiao, L. J. (2008). Magnetoelectric effect in a Ni–PZT–Ni cylindrical layered composite synthesized by electro-deposition. *Journal of Physics D: Applied Physics*, *41*(2), 022002. doi:10.1088/0022-3727/41/2/022002

Pan, E., Wang, X., & Wang, R. (2009). Enhancement of magnetoelectric effect in multiferroic fibrous nanocomposites via size-dependent material properties. *Appl. Phys. Lett.*, *95*(18), 181904.

Petrov, V. M., & Srinivasan, G. (2008). Enhancement of magnetoelectric coupling in functionally graded ferroelectric and ferromagnetic bilayers. *Phys. Rev. B*, *78*(18), 184421 [8 pages].

Petrov, V. M., Srinivasan, G., Bichurin, M. I., & Gupta, A. (2007). Theory of magnetoelectric effects in ferrite piezoelectric nanocomposites. *Phys. Rev. B*, *75*(22), 224407 [6 pages].

Piefort, V. (2001). *Finite Element Modelling of Piezoelectric Active Structures*. Université Libre de Bruxelles, Faculty of Applied Sciences.

Prabhakaran, T., & Hemalatha, J. (2008). Synthesis and characterization of magnetoelectric polymer nanocomposites. *Journal of Polymer Science Part B: Polymer Physics*, *46*(22), 2418–2422. doi:DOI: 10.1002/polb.21575

Priya, S., & Inman, D. J. (2009). *Energy Harvesting Technologies*. Virginia, USA: Springer.

Priya, S., Islam, R., Dong, S., & Viehland, D. (2007). Recent advancements in magnetoelectric particulate and laminate composites. *Journal of Electroceramics*, *19*(1), 149–166. doi:10.1007/s10832-007-9042-5

Pu, J., Yan, X., Jiang, Y., Chang, C., Lin, L., & Pu, U. (2010). Piezoelectric actuation of direct-write electrospun fibers. *Sensors & Actuators: A. Physical*, *164*(1-2), 131–136. doi:10.1016/j.sna.2010.09.019

Pyun, J. (2007). Nanocomposite materials from functional polymers and magnetic colloids. *Polym. Rev.*, *47*(2), 231–263.

Qi, Y., Jafferis, N. T., Lyons Jr., K., Lee, C. M., Ahmad, H., & McAlpine, M. C. (2010). Piezoelectric Ribbons Printed onto Rubber for Flexible Energy Conversion. *Nano Lett.*, *10*, 524–528.

Rafferty, A., Bakir, S., Brabazon, D., & Prescott, T. (2009). Calibration and characterization with a new laser-based magnetostriction measurement system. *Materials & Design*, *30*, 1680–1684.

Rahman, A. U., Rafiq, M. A., Hasan, M. U., Khan, M., Karim, S., & Cho, S. O. (2013). Enhancement of electrical conductivity and dielectric constant in Sn-doped nanocrystlline CoFe2O4. *Journal of Nanoparticle Research*, *15*(6), 1703. doi:10.1007/s11051-013-1703-5

Ramadan, K. S., Sameoto, D., & Evoy, S. (2014). A review of piezoelectric polymers as functional materials for electromechanical transducers. *Smart Materials and Structures*, *23*(3), 033001. doi:10.1088/0964-1726/23/3/033001

188

Ramesh, R., & Spaldin, N. A. (2007). Multiferroics: progress and prospects in thin films. *Nature Materials*, *6*(21).

Rao, S. S., & Sunar, M. (1993). Analysis of distributed thermopiezoelectric sensors and actuators in advanced intelligent structures. *AIAA Journal*, *31*(7), 1280–1286.

Rao, S. S., & Sunar, M. (1994). Piezoelectricity and Its Use in Disturbance Sensing and Control of Flexible Structures: A Survey. *Appl. Mech. Rev.*, *47*(4), 113–123. doi:10.1115/1.3111074

Rasoanoavy, F., Laur, V., Smaali, R., & Queffelec, P. (2010). Modeling of Magnetodielectric Effects in Magnetostrictive / Piezoelectric Multi-layers Using a Multiphysics Simulator .

Ren, K., Liu, Y., Hofmann, H., & Zhang, Q. M. (2007). An active energy harvesting scheme with an electroactive polymer. *Applied Physcics Letters*, *91*(13), 132910– 132913.

Riande, E., & Siaz, E. (1992). *Dipole Moments and Birefringence of polymers*. Englewood Cliffs, N.J: Prentice Hall.

Roya, R., & Majumdara, A. K. (1981). Thermomagnetic and transport properties of metglas 2605 SC and 2605. *Journal of Magnetism and Magnetic Materials*, *25*, 83–89.

Russell, A., & Lee, K. L. (2006). *Structure-Property Relations in Nonferrous Metals. J* (p. 92). Hoboken, New Jersey.: John Wiley & Sons.

Ryu, J., Carazo, A. V., Chino, K. U., Kim, H.-E. E., K.Uchino, Yu, J. R., ... Im, H. K. (2001). Magnetoelectric properties in piezoelectric and magnetostrictive laminate composites. *Japanese Journal of Applied Physics 1*, *40*(8), 4948–4951.

Ryu, J., Carazo, A. V., Uchino, K., & Kim, H. E. (2001). Piezoelectric and magnetoelectric properties of lead zirconate titanate/Ni-ferrite particulate composites. *J. Electroceram.*, *7*(1), 17–24.

Ryu, J., Priya, S., Carazo, A. V., Uchino, K., & Kim, H. E. (2001). Effect of the Magnetostrictive Layer on Magnetoelectric Properties in Lead Zirconate Titanate/Terfenol-D Laminate Composites. *Journal of the American Ceramic Society*, *84*(12), 2905–2908.

Ryu, J., Priya, S., Uchino, K., & Kim, H. (2002). Magnetoelectric effect in composites of magnetostrictive and piezoelectric materials. *Journal of Electroceramics*, *8*, 107–119. Retrieved from http://link.springer.com/article/10.1023/A:1020599728432

Saravanos, D. A. (1997). Mixed laminate theory and finite element for smart piezoelectric shell structure. *AIAA Journal*, *35*(8), 1327–1333.

Saravanos, D. A. (2000). Passively damped laminated piezoelectric shell structures with integrated electric networks. *AIAA Journal*, *38*(7).

Scott, J. F. (2012). Applications of magnetoelectrics. *J. Mater. Chem.,22*, 4567–4574. doi:10.1039/C2JM16137K

Seanor, D. A. (ed. (1982). *Electrical Properties of Polymers*. New York: Academic Press.

Sencadas, V., Lanceros-Mendez, S., & Mano, J. F. (2004). Behaviour of the ferroelectric phase transition of P(VDF/TrFE) (75/25) with increasing deformation. *Ferroelectrics*, *304*, 853–856.

Sencadas, V., Lanceros-Méndez, S., Sabater I Serra, R., Andrio Balado, A., & Gómez Ribelles, J. L. (2011). Relaxation dynamics of poly(vinylidene fluoride) studied by dynamical mechanical measurements and

dielectric spectroscopy. *European Physical Journal E Soft Matter.*, *35*(5), 41. doi:doi: 10.1140/epje/i2012-12041-x. Epub 2012 May 30.

Seva V. V. Khikhlovsky. (2010). *The renaissance of multiferroics: bismuth ferrite (BiFeO3)– a candidate multiferroic material in nanoscience*. University of Groningen. Retrieved from http://www.docin.com/p-266540059.html

Shaikh, A., Kanamadi, C., & Chougule, B. (2005). Electrical resistivity and thermoelectric power studies on Zn-substituted Li–Mg ferrites. *Mater Chem Phys*, *93*, 548–551.

Shi, Z., Ma, J., & Nan, C.-W. (2008). A new magnetoelectric resonance mode in bilayer structure composite of PZT layer and Terfenol-D/epoxy layer. *J. Electroceram.*, *21*(1-4), 390–393.

Shi, Z., Nan, C. W., Liu, J. M., Filippov, D. A., & Bichurin, M. I. (2004). Influence of mechanical boundary conditions and microstructural features on magnetoelectric behavior in a three-phase multiferroic particulate composite. *Phys. Rev. BRev. B*, *70*(13), 134417 (6 PAGES).

Shi, Z., Wang, C., Liu, X., & Nan, C. (n.d.). A four-state memory cell based on magnetoelectric composite. *Chinese Science Bulletin*, *53*(14), 2135–2138.

Shinde, S. S., & Jadhav, K. M. (1998). Electrical and dielectric properties of silicon substituted cobalt ferrites. *Materials Letters*, *37*(1-2), 63–67. doi:10.1016/S0167-577X(98)00068-8

Silva, M. P., Costa, C. M., Sencadas, V., Paleo, A. J., & Lanceros-Méndez, S. (2011). Degradation of the dielectric and piezoelectric response of β-poly(vinylidene fluoride) after temperature annealing. *Journal of Polymer Research*, *18*(6), 1451–1457.

Silva, M., Reis, S., Lehmann, C. S., Martins, P., Lanceros-Mendez, S., Lasheras, A., ... Barandiarán, J. M. (2013). Optimization of the Magnetoelectric Response of Poly(vinylidene fluoride)/Epoxy/Vitrovac Laminates. *ACS Applied Materials & Interfaces*, *5*(21), 10912–10919. doi:10.1021/am4031054

Smith, R. C. (1998). Hysteresis Modeling in Magnetostrictive Materials via Preisach Operators. *Journal of Mathematical Systems, Estimation and Control*, *8*(2), 1–23.

Smith, R. C. (1998). Hysteresis Modeling in Magnetostrictive Materials via Presaich Operators. *Journal of Mathematical Systems, Estimation and Control*, *8*(2), 1–23.

Smith, R. C. (2005). *Smart Material Systems. Model Development*. (H. T. Banks, R. Albanese, C. Castillo-Chavez, D. Cioranescu, L. Fauci, P. Hagan, ... A. Tsao, Eds.) (Banks, H.T., pp. 15–21). Raleigh, North Carolina: Frontiers in Applied Mathematics, SIAM.

Smolensky, G. A., Isupov, V. A., & Agronovskaya, A. I. (1959). New ferroelectrics of complex composition of the type A2 2+(BI3+BII5+)O6. *Phys. Solid State*, *1*, 150–151.

Son, J. Y., Kim, B. G., Kim, C. H., & Cho, J. H. (2004). Writing polarization bits on the multiferroic BiMnO3 thin film using Kelvin probe force microscope. *Appl. Phys. Lett.*, *84*(24), 4971.

Srinivas, K., Bhimasankaram, T., & Suryanarayana, S. V. (2000). Electromechanical Coefficients of Magnetoelectric PZT-CoFe2O4 Composite. *Mod. Phys. Lett. B*, *14*(17n18), 663.

Srinivas, S., & Li, J. Y. (2005). The effective magnetoelectric coefficients of polycrystalline multiferroic composites. *Acta Materialia*, *53*, 4135–4142.

Srinivasan, G. (2010). Magnetoelectric Composites. *Annual Review of Materials Research*, *40*(1), 153–178. doi:10.1146/annurev-matsci-070909-104459

Srinivasan, G., Hayes, R., Devreugd, C. P., Laletsin, V. M., & Paddubnaya, N. (2005). Dynamic magnetoelectric effects in bulk and layered composites of cobalt zinc ferrite and lead zirconate titanate. *Applied Physics A*, *80*(4), 891–897.

Srinivasan, G., Rasmussen, E. T., Bush, A. A., Kamentsev, K. E., Meshcheryakov, V. F., & Fetisov, Y. K. (2003). Magnetoelectric response of a multilayer ferrite-piezoelectric structure to magnetic field pulses. *Appl. Phys. A*, *76*, 1–8.

Srinivasan, G., Rasmussen, E. T., Gallegos, J., Srinivasan, R., Bokhan, Y. I., & Laletin, V. M. (2001). Magnetoelectric bilayer and multilayer structures of magnetostrictive and piezoelectric oxides. *Physical Review B*, *64*(21), 214408.

Srinivasan, G., Rasmussen, E. T., Gallegos, J., Srinivasan, R., Bokhan, Y. I., & Laletin, V. M. (2002). Erratum: Magnetoelectric bilayer and multilayer structures of magnetostrictive and piezoelectric oxides [Phys. Rev. B 64, 214408 (2001)]. *Physical Review B*, *66*(2), 029902(E).

Srinivasan, G., Rasmussen, E. T., & Hayes, R. (2003). Magnetoelectric effects in ferrite-lead zirconate titanate layered composites: The influence of zinc substitution in ferrites. *Physical Review B*, *67*, 014418.

Srinivasan, G., Rasmussen, E. T., Levin, B. J., & Hayes, R. (2002). Magnetoelectric effects in bilayers and multilayers of magnetostrictive and piezoelectric perovskite oxides. *Physical Review B - Condensed Matter and Materials Physics*, *65*(134402), 1–7.

Stognij, A. I., Novitskii, N. N., Sharko, S. A., Bespalov, A. V., Golikova, O. L., Sazanovich, A., ... Ketsko, V. A. (2013). Effect of Cobalt Layer Thickness on the Magnetoelectric Properties of Co/PbZr0.45Ti0.55O3/Co Heterostructures. *Inorganic Materials*, *49*(10), 1011–1014.

Sugawara, F., Iiida, S., Syono, Y., & Akimoto, S. (1968). Magnetic Properties and Crystal Distortions of BiMnO3 and BiCrO3. *J. Phys. Soc. Jpn*, *25*, 1553–1558.

Sunar, M., & Rao, S. S. (1996). Distributed modeling and actuator location for piezoelectric control systems. *AIAA Journal*, *34*(10), 2209–2211.

Sunar, M., & Rao, S. S. (1997). Thermopiezoelectric control design and actuator placement. *AIAA Journal*, *35*(3), 534–539.

Tadokoro, H. (1979). *Structures of Crystalline Polymers*. New York, NY: Wiley.

Thomas, S., Mathew, J., Radhakrishnan, P., Nampoori, V. P. N., George, A. K., Al-Harthi, S. H., ... Anantharaman, M. R. (2010). Metglas thin film based magnetostrictive transducers for use in long period fibre grating sensors. *Sensors & Actuators: A. Physical*, *161*(1-2), 83–90. doi:10.1016/j.sna.2010.05.006

Tiercelin, N., Dusch, Y., Klimov, A., Giordano, S., Preobrazhensky, V., & Pernod, P. (2011). Room temperature magnetoelectric memory cell using stress-mediated magnetoelastic switching in nanostructured multilayers. *Appl. Phys. Lett.*, *99*(19), 192507 – 192507–3.

Tiercelin, N., Dusch, Y., Preobrazhensky, V., & P. Pernod. (2011). Magnetoelectric memory using orthogonal magnetization states and magnetoelastic switching. *J. Appl. Phys.*, *109*(7), 07D726 – 07D726–3.

Tiersten, H. F. (1967). Hamilton's principle for linear piezoelectric media. In *Proceedings of the IEEE* (pp. 1523–1524).

Tzou, H. S., & Tseng, C. I. (1990). Distributed piezoelectric sensor/actuator design for dynamic measurement/control of distributed parameter systems: a piezoelectric finite element approach. *Journal of Sound and Vibration*, *138*(1), 17–34.

Tzou, H. S., & Tseng, C. I. (1991). Distributed modal identification and vibration control of continua: Piezoelectric finite element formulation and analysis. *Transactions of the ASME, Journal of Dynamic Systems, Measurement and Control*, *113*, 500–505.

Van den Boomgaard, J., & Born, R. A. J. (1978). A sintered magnetoelectric composite material BaTiO3-Ni(Co, Mn) Fe2O4. *Journal of Materials Science*, *13*(7), 1538–1548.

Van Run, A. M. J. G., Terrell, D. R., & Scholing, J. H. (1974). An in situ grown eutectic magnetoelectric composite material. *J. Mater. Sci.*, *9*, 1710–1714.

Van Suchtelen, J. (1972). Product properties: a new application of composite materials. *Phil. Res. Rep.*, *27*, 28–37.

Vinogradov, A., & Holloway, F. (1999). Electro-Mechanical Properties of the Piezoelectric Polymer PVDF. *Ferroelectrics*, *226*, 169–181.

Vinogradov, A. M., Hao, T., & Filisko, F. (2002). Encyclopedia of Smart Materials. In M. Schwartz (Ed.), *Vol. 1* (p. p. 362.). New York: J. Wiley & Sons.

Vinogradov, A. M., & Holloway, F. (2000). Dynamic Mechanical Testing of the Creep and Relaxation Properties of Polyvinylidene Flouride. *Polymer Testing*, *19*, 131.142.

Vinogradov, A., Su, J., Jenkins, C., & Bar-Cohen, Y. (2005). State-of-the-Art Developments in the Field of Electroactive Polymers. *MRS Proceeding*, *889*, 0889–W02–05. doi:10.1557/PROC-0889-W02-05

Wan, J. G., Liu, J.-M., Chand, H. L. W., Choy, C. L., Wang, G. H., & Nan, C. W. (2003). Giant magnetoelectric effect of a hybrid of magnetostrictive and piezoelectric composites. *J. Appl. Phys.*, *93*(12), 9916–9919.

Wan, J., Zhang, H., Wang, X., Pan, D., Liu, J., & Wang, G. (2006). Magnetoelectric CoFe[sub 2]O[sub 4]-lead zirconate titanate thick films prepared by a polyvinylpyrrolidone-assisted sol-gel method. *Applied Physics Letters*, *89*(12), 122914. doi:10.1063/1.2357589

Wan, Y. P., Fand, D. N., & Wang, K. C. . (2003). Nonlinear constitutive relations for the magnetostrictive materials. *Int. J. Nonlinear Mech.*, *38*, 1053–1065.

Wang, H. (2009). *Simulation and Evaluation of Dielectric and Magnetodielectric Properties of diphasic and layered Ferroic Composites*. The Pennsylvania State University.

Wang, H.-L., Liu, B., & Fang, D.-N. (2013). A Nonlinear Finite Element Method for Magnetoelectric Composite and the Study on the Influence of Interfacial Bonding. *Mathematical Problems in Engineering*, *2013*, 1–14. doi:10.1155/2013/197940

Wang, J., Neaton, J. B., Zheng, H., Nagarajan, V., Ogale, S. B., Liu, B., … Ramesh, R. (2003). Epitaxial BiFeO3 Multiferroic Thin Film Heterostructures. *Science*, *299*(5613), 1719–1722.

Wang, X., Pan, E., Albrecht, J. D., & Feng, W. J. (2009). Effective properties of multilayered functionally graded multiferroic composites. *Compos Struct*, *87*, 206–214.

Wang, Y., Hu, J., Lin, Y., & Nan, C.-W. (2010). Multiferroic magnetoelectric composite nanostructures. *NPG Asia Materials*, *2*(2), 61–68. doi:10.1038/asiamat.2010.32

Wilkie, W. K., Bryant, R. G., High, J. W., Fox, R. L., Hellbaum, R. F., Jalink, A., ... Mirick, P. H. (2000). Low-Cost Piezocomposite Actuator for Structural Control Applications. In *Proceedings of 7th SPIE International Symposium on Smart Structures and Materials, Newport Beach, CA, March 5-9*. Newport Beach, CA,.

Wirsen, A. (1986). *Electroactive Polymer Materials*. Lancaster, PA.: Technomic Publishing.

Wise, D. (ed). (1998). *Electrical and Optical Polymer Systems*. New York: Marcel Dekker Inc.

Wong, C. K., & F. G. Shin, J. (2007). Effect of inclusion deformation on the magnetoelectric effect of particulate magnetostrictive/piezoelectric composites. *Appl. Phys.*, *102*, 063908.

Wong, C. K. K., & Shin, F. G. G. (2008). Magnetoelectric effects of laminated structures with particulate composite layers. *J. Phys. D: Appl. Phys.*, *41*(13), 135002. doi:10.1088/0022-3727/41/13/135002

Wong, C. K., Poon, Y. M., & Shin, F. G. (2001). Explicit formulas for effective piezoelectric coefficients of ferroelectric 0-3 composites. *Journal of Applied Physics*, *90*(9), 4690–4700.

Wong, W. (2007). *Studies on the Direct and Converse Magnetoelectric Effects in Laminated Composites*. The Hong Kong Polytechnic University.

Xing, Z. P., Zhai, J. Y., Dong, S. X., Li, J. F., Viehland, D., & Odendaal, G. W. (2008). Modeling and detection of quasi-static nanotesla magnetic field variations using magnetoelectric laminate sensors. *Measurement Science and Technology*, *19*(1), 015206.

Xu, H., Shanthi, H., Bharti, V., & Zhang, Q. M. (2000). Structural, Conformational, and Polarization Changes of Poly(vinylidene fluoride-trifluoroethylene) Copolymer Induced by High Energy Electron Irradiatio. *Macromolecules*, *33*, 4125–4131.

Yan, Y., Zhou, Y., & Priya, S. (2013). Giant self-biased magnetoelectric coupling in co-fired textured layered composites. *Applied Physics Letters*, *102*, 052907.

Yang, X., Kong, X., Tan, S., Li, G., Ling, W., & Zhou, E. (2000). Spatially-confined Crystallization of Poly(vinylidene Fluoride). *Polymer International*, *49*, 1525–1528.

Yun, K., Ricinschi, D., Noda, M., & Okuyama, M. (2005). Ferroelectric and Magnetic Properties of Multiferroic BiFeO 3 Thin Films Prepared by Pulsed Laser Deposition, *46*(1), 281–284.

Zadov, B., Elmalem, a., Paperno, E., Gluzman, I., Nudelman, a., Levron, D., ... Liverts, E. (2012). Modeling of Small DC Magnetic Field Response in Trilayer Magnetoelectric Laminate Composites. *Advances in Condensed Matter Physics*, *2012*, 1–18. doi:10.1155/2012/383728

Zeng, M., Or, S. W., & Chan, H. L. W. (2010). Large magnetoelectric effect from mechanically mediated magnetic field-induced strain effect in Ni–Mn–Ga single crystal and piezoelectric effect in PVDF polymer. *J. Alloys Compd.*, *490*, Pages L5–L8.

Zhai, J., Dong, S., Xing, Z., Li, J., & Viehland, D. (2006). Giant magnetoelectric effect in Metglas/polyvinylidene-fluoride laminates. *Applied Physics Letters*, *89*(8), 083507. doi:10.1063/1.2337996

Zhai, J., Gao, J., Vreugd, C. De, Li, J., Viehland, D., Filippov, A. V., ... Dong, S. X. (2009). Magnetoelectric gyrator. *The European Physical Journal B*, *71*(3), 383–385.

Zhai, J., Xing, Z., Dong, S., Li, J., & Viehland, D. (2008). Magnetoelectric Laminate Composites: An Overview. *Journal of the American Ceramic Society*, *91*(2), 351–358. doi:10.1111/j.1551-2916.2008.02259.x

Zhai, J. Y., Dong, S. X., Xing, Z. P., Li, J. F., & Viehland, D. (2007). Giant magnetoelectric effect (under a dc magnetic bias of 2 Oe) in laminate composites of FeBSiC alloy ribbons and Pb(Zn1/3,Nb2/3)O3–7%PbTiO3 fibers. *Appl Phys Lett*, *91*(2), 022915 – 022915–3.

Zhan, Q., Yu, R., Crane, S. P., Zheng, H., Kisielowski, C., & Ramesh, R. (2006). Structure and interface chemistry of perovskite-spinel nanocomposite thin films. *Applied Physics Letters*, *89*(17), 172902. doi:10.1063/1.2364692

Zhang, C. L., Yang, J. S., & Chen, W. Q. (2009). Harvesting magnetic energy using extensional vibration of laminated magnetoelectric plates. *Appl. Phys. Lett.*, *95*(1), 013511 – 013511–3.

Zhang, J. X., Dai, J. Y., Lu, W., Chan, H. L. W., Wu, B., & Li, D. X. (2008). A novel nanostructure and multiferroic properties in Pb(Zr0.52Ti0.48)O3/CoFe2O4 nanocomposite films grown by pulsed-laser deposition. *J. Phys. D: Appl. Phys.*, *41*(23), 235405. doi:10.1088/0022-3727/41/23/235405

Zhang, J. X., Dai, J. Y., So, L. C., Sun, C. L., Lo, C. Y., Or, S. W., & Chan, H. L. W. (2009a). The effect of magnetic nanoparticles on the morphology, ferroelectric, and magnetoelectric behaviors of CFO/P(VDF-TrFE) 0–3 nanocomposites. *Journal of Applied Physics*, *105*(5), 054102. doi:10.1063/1.3078111

Zhang, J. X., Dai, J. Y., So, L. C., Sun, C. L., Lo, C. Y., Or, S. W., & Chan, H. L. W. (2009b). The effect of magnetic nanoparticles on the morphology, ferroelectric, and magnetoelectric behaviors of CFO/P(VDF-TrFE) 0–3 nanocomposites. *J. Appl. Phys.*, *105*, 054102. doi:http://dx.doi.org/10.1063/1.3078111

Zhang, W., Yin, G., Cao, J., Bai, J., & Wei, F. (2012). Frequency multiplying behavior in a magnetoelectric unimorph. *Appl Phys Lett*, *100*(3), 032903 – 032903–3.

Zhao, L., Zhang, H., Xing, Y., Song, S., Yu, S., Shi, W., ... Cao, F. (2008). Studies on the magnetism of cobalt ferrite nanocrystals synthesized by hydrothermal method. *J Solid State Chem*, *181*, 245–252.

Zheng, H., Wang, J., Lofland, S. E., Ma, Z., Mohaddes-Ardabili, L., Zhao, T., ... Ramesh, R. (2004). Multiferroic BaTiO3-CoFe2O4 Nanostructures. *Science*, *303*(5658), 661–663.

Zheng, H., Wang, J., Lofland, S. E., Ma, Z., Zhao, T., Shinde, S. R., ... Ramesh, R. (2004). Multiferroic BaTiO3-CoFe2O4 Nanostructures. *Science*, *303*(5658), 661–663.

Zheng, X. J., & Liu, X. E. (2005). A nonlinear constitutive model for Terfenol-D rods. *J. Appl. Phys.*, *97*(5), 053901.

Zhou, X., Chattopadhyay, A., & Haozhong, G. (2000). Dynamic responses of smart composites using a coupled thermo-piezoelectric- mechanical model. *AIAA Journal*, *38*(10).

Zhou, Y., & Shin, F. G. (2005). Modeling of magnetostriction in particulate composite materials. *IEEE Trans. Magn.*, *41*(6), 2071–2076.

Zhou, Y., & Shin, F. G. (2006). Magnetoelectric effect of mildly conducting magnetostrictive/piezoelectric particulate composites. *Journal of Applied Physics*, *100*(4), 043910 (pp. 1–5).

Zhu, J.-G. (2008). Magnetoresistive Random Access Memory: The Path to Competitiveness and Scalability. *Proc. IEEE*, *96*(11), 1786–1798.